VIBRATION TRANSMISSION THROUGH MACHINERY FOUNDATION AND SHIP BOTTOM STRUCTURE

by

Jorge Tratch Junior

B.S., Escola Politecnica Da Universidade De São Paulo, Brasil
(1974)

Submitted to the Department of
Mechanical Engineering
in Partial Fulfillment of the
Requirements for the
Degrees of

MASTER OF SCIENCE in MECHANICAL ENGINEERING
and MECHANICAL ENGINEER

at the

MASSACHUSETTS INSTITUTE OF TECHNOLOGY

June 1985

© Jorge Tratch Junior

The author hereby grants to M.I.T. permission to reproduce and to distribute copies of this thesis document in whole or in part.

Signature of Author _____
Department of Mechanical Engineering
April 10, 1985

Certified by _____
Thesis Supervisor

Accepted by _____
Chairman, Mechanical Engineering Department Committee

MASSACHUSETTS INSTITUTE
OF TECHNOLOGY

JUL 22 1985

LIBRARIES

Archives

VIBRATION TRANSMISSION THROUGH MACHINERY FOUNDATION AND SHIP BOTTOM STRUCTURE

JORGE TRATCH JUNIOR

Submitted to the Department of Mechanical Engineering on April 10, 1985 in partial fulfillment of the requirements for the Degrees of MASTER OF SCIENCE in Mechanical Engineering and MECHANICAL ENGINEER

ABSTRACT

An unstiffened plate-like steel scaled model (1:2.5) is conceived based on a diesel engine foundation and double bottle structure of an actual naval vessel. Statistical Energy (SEA) is applied to study the vibration transmission through it in four steps (two, four, seven and twelve-plate models). The application consists of the identification of the SEA subsystems, the determination of its parameters and the utilization of power balance equations to estimate the energy-ratio levels of each subsystem with respect to the directly excited subsystem. The study is carried out in third octave bands and the frequency interval varies from 0.63 to 20 kHz (0.25 to 8 kHz in full scale). Two analytical models are investigated. One model assumes that the vibration transmission is associated with flexural motions only. In the other model the two in-plane motions are included and the transfer of energy between the three motions is taken into account. The internal loss factor of each plate associated with bending is determined experimentally by using decay method. The in-plane internal loss factors are estimated based on published works. The mode count (N) is determined experimentally when $N > 12$ and by applying the formulations of modal density when $N < 12$. The coupling loss factors (η_{ij}) are determined using a wave description of the vibrational field and the concept of transmission losses. Analytical expressions are derived to determine average transmission coefficients ($\bar{\tau}_{ij}$) between up to four plates at a common joint. Bending, longitudinal and shear incidence are treated individually. From the derived equations, computer programs are developed to calculate $\bar{\tau}_{ij}$ and the related η_{ij}. The predicted flexural energy-ratio levels are compared with those resulting from laboratory measurements. The power balance equations and SEA parameters are also utilized to understand the vibration transmission through the models (especially the twelve-plate model) and to identify the main energy transmission paths. Two basic conclusions result. First, the in-plane motions and the energy conversions at structural discontinuities play an important role in the vibration transmission through the basic model. When only bending is assumed, significant underestimations are verified above 3.15 kHz (1.25 kHz full scale). The most significant differences between the two predicted values goes from 3 dB at 3.15 kHz up to 8 dB at 20 kHz, for the twelve-plate model. Second, the agreement between analytically and experimentally determined energy-ratios is fairly good (generally within $\pm$ 3dB), especially considering that in several bands less than six in-plane and/or flexural modes are excited in some of the plates.

Thesis Supervisor: Richard H. Lyon
Title: Professor of Mechanical Engineering

DEDICATION

This thesis is dedicated to my parents. To the memory of my Father, who died prematurely, at the age of thirty, with a heart filled with dreams and ideals, and with a promising future ahead. Although he is not here, he is very much alive in my heart. I shall always admire my Father, from whom I have learned principles and examples which are more valuable than any material legacy. This work is also dedicated to my Mother who fought with tenacity and dignity to give a good education and an honourable life to me and my sister, supporting us throughout our lives with her love, friendship and strength.

ACKNOWLEDGEMENTS

First, I thank my Lord for the grace He has given me to accomplish this work. He guided me all the way through it; He gave me strength and perseverance, and, through persons of good will, supported me and gave me the necessary encouragement to overcome obstacles that I have had to face.

I wish to express my sincere appreciation to my advisor, Professor R. H. Lyon, for his supervision and guidance throughout the duration of this research. He has made it an invaluable learning experience.

I also gratefully acknowledge the invaluable advice, incentive and support given during this very difficult and long time by Mrs. Sandra Tepper, my friends Germano - Vilma de Freitas, and my friends Eduardo - Sonia Misawa.

My special thanks to:

1. My mother for her patience, very dear company, support and encouragement.

2. My friend, Alfonso Garcia Reynoso whose spontaneous and generous help saved important time by familiarizing me with the Acoustics and Vibration Laboratory equipment and computer work.

3. The AV laboratory members whose suggestions and continuous incentive were very much appreciated: Gregory Chisholm, Hossein Haj Hariri, Richard Lueptow, Peter Meckl, Yoshihiro Shimomura and Veronique Pevtschin.

4. Dr. Richard DeJong of Cambridge Collaborative, Inc., for his information and helpful suggestions, especially at the beginning of the experimental work.

5. Leslie Regan, not only for the excellent typing, but also for her kindness in helping me to finish on time.

6. Dr. Steve Strang, Director of the Writing Center for his patience, text corrections and comments that helped me to produce a document of better quality.

7. Captain Othon Luiz Pinheiro of the Brazilian Navy, who created, in 1979, this professional opportunity and gave support to my first summer term at MIT.

8. Admiral Aloysio Ferreira dos Santos of the Brazilian Navy, for his comprehension, incentive and support, especially with respect to the extension of the initially authorized duration of my stay at MIT.

Finally, I would like to express my deepest appreciation to Captain Edgar Argrives Carvalho of the Brazilian Navy, for his comprehension and generous help in managing to provide me the extra time (beyond the extension) without which the completion of this thesis would not be possible.

TABLE OF CONTENTS

PAGE

LIST OF FIGURES

NOMENCLATURE

a_i	propagating bending wave amplitude in plate i
a'_i	non-propagating bending wave amplitude in plate i
$\langle a_i^2 \rangle$	mean square acceleration level of plate i: time and spatial average
A_i	area of plate i
ABN	airborne noise
b_i	amplitude of longitudinal wave in plate i
b	(subscript) - beam
b	bandwidth
b	rectangular beam thickness
c_i	amplitude of transverse shear wave in plate i
c_B	bending wave speed
c_g	energy velocity
c_L	longitudinal wave speed
c_T	transverse shear wave speed
c_ϕ	phase velocity
c_τ	torsional wave speed
D	bending stiffness
E	vibrational energy level
E	modulus of elasticity of material
E_p	modulus of elasticity for plates
E_p/E_r	ratio between the energy level of a plate p and the energy level of a reference plate r
$(E_p/E_r)_E$	energy-ratio resulting from experimental work
$(E_p/E_p)_F$	predicted energy-ratio resulting from SEA application when bending transmission only is assumed

$(E_p/E_r)_G$	Predicted energy-ratio resulting from SEA application when the three wave fields are considered
f	frequency
$\underline{F}$	force vector
F	(subscript) pertaining to foundation
F_{ij}	dimensionless parameter - equation D.78
G	shear modulus of elasticity
G	conductance, real part of mobility
g	(subscript) pertaining to energy or giration
h	plate thickness
H	Heckl's formulation for heavy and light beams (equation C.2.1)
i	$\sqrt{-1}$
i	(subscript) - pertaining to subsystem or plate i
j	(subscript) - pertaining to subsystem or plate j
J	moment of rigidity for a cross section
k	bending wave number
kg	radius of giration
k_ϕ	radius of giration about the center of gravity of a cross section
K	mounting stiffness
ℓ	longitudinal wave number
L	linear dimension
L_{ij}	length of joint between plates i and j
m_b	mass per unit length of a beam
m_p	mass per unit area of a plate
M	mass
M	moment

M	(subscript) pertaining to mounting or moment
n	modal density
N_i	number of resonant modes in excitation bandwidth in subsystem i
p	(subscript) pertaining to plate
P_{ab}	Swift's parameter -- Appendix C
Q	shear force
r	(subscript) pertaining to reference
s	convenient form for $\sin\alpha_1$
S	(subscript) pertaining to source
S	reactance - imaginary part of mobility
SEA	statistical energy analysis
SBN	sturctureborne noise
SPL	sound pressure level
t	transverse shear wave number
T	(subscript) pertaining to test
u_i	displacement in x_i direction
U_i	average energy of an oscillator or mode
v_i	displacement in y_i direction
$\underline{V}$	velocity vector
x_i, y_i, z_i	3-D orthogonal spatial coordinates pertaining to plate i
Y	mechanical mobility
Z	mechanical impedance
w_i	displacement in z_i direction
α_i	propagation angle of bending wave in plate i
β	propagation angle of longitudinal wave
β	Cremer's parameter -- Appendix C

∂	partial derivative
Δ	incremental
η_i	internal loss factor - plate i
η_{ij}	coupling loss factor between subsystems i and j
η_{ij}^F	coupling loss factor between subsystems i and j, when flexural transmission only is assumed
$\eta_{ij}(BB)$	coupling loss factor between two flexural subsystems
$\eta_{ij}(BL)$	bending to longitudinal coupling loss factor
$\eta_{ij}(BT)$	bending to shear coupling loss factor
$\eta_{ij}(LL)$	coupling loss factor between two longitudinal subsystems
$\eta_{ij}(LB)$	longitudinal to bending coupling loss factor
$\eta_{ij}(LT)$	longitudinal to shear coupling loss factor
$\eta_{ij}(TT)$	coupling loss factor between two shear subsystems
$\eta_{ij}(TB)$	shear to bending coupling loss facotr
$\eta_{ij}(TL)$	shear to longitudinal coupling loss factor
$\eta_{ij}(PP)$	in-plane to in-plane coupling loss factor
$\eta_{ij}(PB)$	in-plane to bending coupling loss factor
$\eta_{ij}(BP)$	bending to in-plane coupling loss factor
λ	wave length
π	pi
Π_{ij}	net power flow between subsystems i and j
Π_{inp}^i	power delivered by an external source to subsystem i
Π_{DIS}^i	power truly dissipated by subsystem i
ρ	density of material
ρ_s	surface density
ν	Poisson coefficient

Σ	summation
$\tau_{ij}(\theta)$	transmission coefficient from a subsystem in plate i to a subsystem in plate j, for the angle of incidence θ
$\bar{\tau}_{ij}$	average transmission coefficient from a subsystem in plate i to a subsystem in plate j
τ^{F}_{ij}	average transmission coefficient from a subsystem in plate i to a subsystem in plate j, when flexural transmission only is assumed
$\tau_{ij}(BB)$	bending to bending average transmission coefficient
$\tau_{ij}(BL)$	bending to longitudinal average transmission coefficient
$\tau_{ij}(BT)$	bending to shear average transmission coefficient
$\tau_{ij}(LL)$	longitudinal to longitudinal average transmission coefficient
$\tau_{ij}(LB)$	longitudinal to bending average transmission coefficient
$\tau_{ij}(LT)$	longitudinal to shear average transmission coefficient
$\tau_{ij}(TT)$	shear to shear average transmission coefficient
$\tau_{ij}(TL)$	shear to longitudinal average transmission coefficient
$\tau_{ij}(TB)$	shear to bending average transmission coefficient
$\tau_{ij}(BP)$	bending to in-plane average transmission coefficient
$\tau_{ij}(PB)$	in-plane to bending average transmission coefficient
$\tau_{ij}(PP)$	in-plane to in-plane average transmission coefficient
ϕ_{ij}	coupling coefficient for power flow between two modes -- modal coupling coefficient
X_{ij}	dimensionless parameter -- equation D.74
ψ_{ij}	dimensionless parameter -- equation D.76
θ	incident or propagation angle of a wave of any nature
ω	radian frequency
$\underline{\Omega}$	angular velocity vector

CHAPTER 1

INTRODUCTION

1.1 Noise on Ships

During the last sixteen years noise generation and transmission in merchant vessels have been seriously analyzed. The fundamental motivation for these investigations was the introduction (by the different Maritime Administrations) of more rigorous regulations of maximum allowed sound pressure levels (SPL) inside ship compartments. These maximum SPL requirements (function of frequency and compartment nature) have become clauses in a ship acquisition contract. If they are not fulfilled, delays in the ship's acceptance may result and modifications after the ship is built will be required. This means penalties and extra cost. Therefore, noise analysis has been included as an important activity in the merchant ship design process.

With respect to naval vessels, other requirements besides maximum allowable SPL inside compartments have to be satisfied; these include detection, interference, activation of acoustics weapons, etc. The noise generation and transmission have been a major concern of any Navy for a long time, and a very special attention has always been dedicated to it on ship design (since the earliest phase) and through research programs. This concern has grown significantly during the last two decades as a result of the continuous increase of the ship's sophistication.

1.2 Noise Generation and Transmission

The main propulsion machinery (diesel engines, gas turbines, gear boxes), auxiliary machinery (electrical power generators, air-conditioned units, pumps, etc.) as well as the propellers are the primary noise sources

in a ship. The propellers transmit noise to the structure through the shaft line and through the pressure field generated at the ship's stern. The machinery radiates noise to the surrounding air (air-borne-noise) and transmits noise to the ship structure through its foundation, (structure-borne noise).

The air-borne noise (ABN) can be significant inside a machinery space and mainly affects the neighboring compartments, transmitted to them through the deck and bulkheads. It also contributes to the transmission of noise to the water, through the ship's hull and bottom structure. The structure-borne noise (SBN) is recognized to be the major cause of noise problems in ships; it is able to propagate through the steel structure, contributing predominantly to the noise level inside compartments that are far away from the noise sources. Therefore, SBN has been the object of most attention on ship noise analysis and is the basic concern of this thesis.

1.3 Noise Analysis and Ship Design

Throughout the whole ship design process, the primary tasks of a design office, when undertaking a noise analysis are:

1. To continuously verify the compliance with the requirements, and
2. To implement the necessary reduction actions to have the requirements satisfied, such as:
   - (a) selection of less noisy machinery,
   - (b) vibration isolation of primary noise sources,
   - (c) introduction of dissipative mechanisms at compartment boundaries and/or at the structure between them and the noise sources,
   - (d) modifications of the ship structure in order to improve noise attenuation or alter the noise transmission paths,

(e) a careful arrangement of ship compartments, trying to separate the compartments subject to more stringent requirements from the sources as much as possible,

(f) compartment isolation.

Clearly, item (c) is, in principle, the most attractive alternative to apply to existing ships without creating a drastic impact. Items (b) and (f) are also usually considered for this purpose.

Some of the actions listed above, specifically the machinery isolation, have been used successfully in many ships. However, in addition to the cost penalty, some may not be feasible or efficient enough due to possible conflict with primary ship requirements and specifications.

A quieter diesel engine, for example, means a lower speed engine and consequently a loss in weight and space, as well as, usually, a rigid connection to the foundation. For a large merchant vessel this is the best solution, especially when considering the required power, fuel consumption and maintenance. For a smaller vessel, a medium speed engine (720-1000 rpm) with turbocharging is often a better solution. However, the level of emitted noise is higher when compared with low speed engines. Since the ship is small and the living compartments are much closer to the machinery spaces, it aggravates the noise problem. A resiliently mounted installation could then be considered.

In a war vessel the problem is more critical. Since the primary function of a combat ship is as a weapon system, the goal for propulsion and auxiliary machinery is to have the highest possible ratio between output and weight. Gas turbines (3600/5600 rpm) and high speed diesel engines (1200-1800), both for propulsion and electrical power generation become the adequate

options. Despite the stringent noise and shock requirements imposed on those equipments, their installation on vibration and shock isolators is mandatory. The gas turbines and even diesel engines (in some plants) have their own acoustical enclosures, because of the high level of air-borne noise they radiate. In such sophisticated installations the gear boxes become the object of very special attention and concern, requiring a high level of quality, since they usually turn out to be a stronger source of noise than the main engines, basically because they are normally rigidly mounted to their foundations, receive high power, and have light casing structures (usually made by plates with reinforcement strips) to save weight.

The isolation of the machinery is usually not enough to reduce noise on a naval vessel and to satisfy the requirements. A careful ship insulation design has to be carried out. Acoustic and thermal insulation are treated together, the pursuit of a minimum weight being also a primary objective.

The dimensions of the ship's structural elements are determined by the structural analysis and by fabrication and economical aspects, especially standardization, so that only minor or local changes are usually acceptable, when noise is the concern. An appropriate foundation design, however, is an important point to consider and fight for.

The compartment's arrangement is mainly dictated by the ship's operation and functionality; noise being a secondary aspect.

Some other areas such as deck coverings and ship fluid loads (tanks) are also related to noise transmission and dissipation.

The noise analysis has to be a compromise between all these design aspects, and, of course, others not mentioned here. The difficulties of

fulfilling the noise specifications and requirements are not small and may be costly. Thus, the designers must have available the proper tools to efficiently accomplish their tasks.

It is, therefore, of fundamental importance to:

1. Understand the noise generation, its transmission and the dissipative mechanisms
2. Identify and select the appropriate and reliable approach from which the proper design tools and procedures can be derived.

1.4 Approaches For Structureborne Noise Analysis

When undertaking a SBN analysis, three major aspects have to be considered:

1. The interaction between machinery and the structure;
2. The transmission through the steel structure.
3. The interaction between the structure and the adjacent media (noise radiated to the sea and into the compartments).

Many studies, especially during the 1960's, were devoted to the interaction between acoustical spaces and between vibrating structures (plates, reinforced panels, shells, etc., commonly encountered on ships) and a media or reverberating field. The intended applications were on aircraft and space vehicles noise and vibration problems as well as building acoustics. Most of the principles and many of the results are applicable for ships.

The transmission of noise through a structure is a more difficult problem to undertake, particularly aggravated in a ship, by its structural complexity, as will be discussed in Chapter 4.

From the three aspects mentioned above, the third is the one that appears to offer the least problems. The structure is the link between the sources and the media, placing on it the primary interest of this thesis.

From basic acoustics, it is known that if the motion of a mechanical noise surface source, such as a vibrating plate, can be described as a velocity field, then, in principle, it is possible to determine the pressure field generated by such a source, as well as the power radiated.

A modal analysis approach can be used to determine the velocity response of the structure of interest. The source of excitation is usually expressed as a a moment and force vector. The structural dynamic characteristics are represented as a mobility or transfer matrix. The suitable definition of the mode shapes of interest, of the corresponding resonance frequencies and the associated modal damping loss factor become necessary. The first two can be determined, for a complex structure, by using techniques such as *Finite Element Methods* (FEM).

This approach is time consuming, complex and costly, especially when sensitivity analyses are necessary. It also requires the knowledge of structural details not available at the earlier design phases and is usually limited to low frequencies. As frequency increases and the number of excited modes gets higher, the amount of computation starts to be excessive, accuracy decreases, and the output (vibration description) becomes difficult to interpret and consequently begins to lose its practical value. For those situations, it is more meaningful to consider average responses and their distribution over the structure.

Energy approaches, based on modal analysis and wave propagation

principles are the most used in ship's SBN analysis.

When adopting an energy approach the questions are:

1. How much power (or energy) is delivered by the machinery to its foundation?

2. How much of this power reaches the compartment's boundary or structural section of interest?

The answer for the second question is intimately related to the transmission mechanisms and to the energy paths along the structure and associated attenuating and dissipative effects. Most of the studies have been devoted to this, which is easy to understand since they could lead to the implementation of feasible and economical solutions for problems on existing ships.

The power dissipated by the structure and the power radiated to the media are evaluated in two ways:

1. By determining the energy level of the structure and its loss factor, as in room acoustics, and

2. Through the concept of power or energy decay on its way through the structure. A wave propagation description is adopted and the dissipation factor included in the wave number.

The power input is a function of the machinery, mountings, and foundation characteristics. The source and mounting characterizations are usually obtained from equipment tests data (from the factory). The interaction between machinery and foundation is discussed in more detail in Chapter 4, and in Appendix B.

In a complicated built-up structure there will be many types of

transmission mechanisms and paths, involving different kinds of energy propagation. In such a situation, approximations in a theoretical assessment of the vibrational characteristics have to be made. Two important aspects have to be considered: (1) How to model the structure, and (2) What are its predominant motions.

1.5 Structural Motions

The noise radiated from a structure into an adjacent media is primarily caused by its flexural (bending) motions. This is why most of the works on "SBN" have been concentrated on bending transmission.

Longitudinal motions can, in principle, radiate sound because of the cross sectional alterations associated with them. When the adjacent media is water, the power radiated by longitudinal motions may have some significance. However, when the surrounding fluid is air, the radiated sound is comparatively much smaller than the power radiated by bending unless the longitudinal energy level is very high.

Aside from flexural motions, other kinds of motions may be important in ship SBN analysis because:

1. They can be induced in the structure. As a result of the machinery-foundation interaction, the power can be transmitted as bending, longitudinal, transverse shear and torsional energy (waves) to the ship structure.

2. Motion transformations can occur at the different structural discontinuities of the ship.

The question is: "Are these motions really important in a SBN transmission problem?" Although most of the works have considered only

bending transmission, the recommendations or remarks very often suggest that a more detailed SBN analysis should take into account other forms of motions. Emphasis will be given to this subject in this thesis.

1.6 Structural Modeling

When undertaking an analysis of a complicated structure, it is important to try to reduce it to an ensemble of simpler elements. A ship in a macroscopic and gross sense can be regarded as a plate shell reinforced by transverse (frames) and longitudinal stiffeners, the hull, that it subdivided internally by reinforced panels (decks and bulkheads). Examined in more detail, a ship can be considered as a very large multi-joint structure consisting of a collection of plates and beam elements. This representation is particularly possible as frequency increases and the structural wavelengths of interest are shorter than the characteristic dimensions and spacing between the structural elements. The vibrational characteristics of such elements will be very much like those observed when they are isolated from the rest of the structure.

The choice of an analytical and/or experimental model is very important in a SBN study. Plate-like and grillage (main frames and associated plates) have been used. The longitudinal stiffeners and smaller size frames, except in rare cases, are usually not considered. The choice of a proper model has to be based on the ship's structural characteristics and on the frequency of interest. The dimensions and the thicknesses of the structural members (plates and beams) as well as the frames and stiffener spacings can deeply influence the choice, since the vibrational structural behavior depends on those parameters. The nature and main direction of the induced excitation is also very important, and this will depend on the machinery, the founda-

tion design and the position of the support points with respect to the frames. It is not improper to say that different models (beam, plate and beam, or plates) may have to be used for different frequency ranges.

1.7 Energy Approaches

Basically three energy approaches have been used in SBN analysis of ships. They are: (1) Semi-Empirical, (2) Nilson's Grillage Method, and (3) Statistical Energy Analysis.

The semi-empirical approaches are based on measurements and data taken on board ships. In general, expected energy levels at various ship locations are estimated by using attenuation factors or transmission losses along structural discontinuities. The one most referenced is the TNO calculation method by Janssen and Buiten [1]. In this method the transmission losses were considered to be independent of structural dimensions and of frequency. Further developments were introduced by Buiten [2], Suhara [3], and Kihlman and Plunt [4]. Frequency dependence was considered and more detailed reduction in energy level per structural discontinuities taken into account, although no general formulations have been presented. Plunt [5] also developed empirical formulations to estimate the power delivered by the machinery. A more complete and detailed work was also carried out by Plunt [6] on prediction of noise levels on ships associated with a computer program and statistical energy analysis.

Nilsson [7,8] used a grillage model (frames and associated plates) to analyze transmission along the hull and superstructures. He considered that the main path would be upward in the frame direction. His model showed that the flexural motion of the frames could be dominant for low frequencies. As the frequency increases, the plates flexural motions be-

come more important, the frame acting as wave guides for the noise transmission. A wave propagation description was used and the dissipation included as an energy decay along the structure through the wave number.

Statistical Energy Analysis (SEA) is the energy approach used in a larger number of studies [4,6,9,10,11,12,13,14]. SEA deals with coupled systems and power balance equations are used to estimate the energy level of the different systems. Basically, it is assumed that the power delivered by a system is proportional to its total energy, the coefficients of proportionality being the loss factors. Two types of loss factors can be identified:

1. Loss factor -- associated with the power dissipated by the system
2. Coupling loss factor -- associated with the power lost by a system to another coupled to it (power flow between systems).

The primary variable is energy and the input is the power delivered to the systems by external sources. A fundamental point is the definition of a "SEA" system: "a group of similar resonant modes of a given nature". It is not a structural element, but is directly associated with the motions that can be induced in this element. The fundamentals of SEA are presented in reference [15].

1.8 Choice of Approach

Any method has its limitations and its strenghts, but it is hard to believe that a particular approach could give all the answers needed for a complex problem such as noise transmission on ships. When selecting an approach, several aspects have to be taken into account. Strictly speaking about ships, it is essential that answers and results be given during the early design phases with the necessary accuracy and confidence, compatible

with the available data and the cost constraints. The ability to explain existing problems and give support to recommendations for improvement is also very important. In a ship, the machinery can be considered as broad band random noise sources; the frequency range of interest, particularly in a war vessel, usually goes from 0.2 to 16 kHz. The more general, broad and simple the method, the more attractive it becomes. The ideal choice would then be the one that could comprise all these aspects.

A semi-empirical method is always a very valid tool in the early design phases when the ship is a first concept. The results are even more valuable when the method is derived or incorporates data from measurements of ships in the same class or family. As more detailed data starts to be available, more accurate answers and deeper analyses are required, making an analytical approach necessary.

The practical value of Nilsson's grillage method has been demonstrated in the analysis of ship superstructures. Its contribution to the understanding of the wave propagation mechanisms upwards along the hull is of vital interest to ship noise analysis. However, it is thought to be not general enough when the whole noise analysis and design process are under consideration.

Finite elements and statistical energy analysis are completely general. FEM has been used extensively for ship structural analysis and optimization at more detailed design phases. The power of FEM for modal analysis is undoubted, particularly when considering that the junctions between structural elements and boundary conditions can be efficiently and explicitly represented. Its limitations in cases where only a few excited modes are present have already been mentioned. These disadvantages are increased in

the design phases when the necessary details of the structures for the FEM application are still unknown and when sensitivity analyses need to be carried out.

SEA has been widely used for the last twenty years for the analysis of coupled systems with applications on buildings, aircrafts, and ships. SEA is a frame of study rather than a specific technique.

The definition of SEA subsystems as a group of similar resonant modes of a given nature (flexural, torsional, etc.) makes its modelling principles suitable to include, without a physical restriction, the different kinds of motions that are possible to be induced in the ship's structural elements. The energy transmission mechanisms and energy conversions can then be understood as sharing and flowing between the coupled mode groups. SEA does not eliminate the complexity of a structure modelling task, but rather offers a fundamental option to it. It is also of vital importance to emphasize that in addition to SBN, ABN can also be included in a SEA model, through the interaction between the modes of the ship's acoustical spaces, and between them and the flexural modes of the structural boundaries. Therefore, in principle, the complete noise transmission problem can be modelled and analyzed by using SEA.

Another attractive aspect of SEA is the simplicity of its power balance equations, demanding little computational work, handled by library programs developed for solving systems of linear equations. Being a statistical approach, SEA gives statistical answers and, therefore, offers an inherent degree of uncertainty. This can be regarded either as an advantage or a disadvantage. Combined with the simplicity factor, this is very important to the design phases, when the details of the ship are not yet defined. In

these phases, trade-off, comparative and sensitivity analyses are often carried out and compliance with limiting or upper bound specifications or levels are continuously verified. In this situation, approximate results are often satisfactory and can be utilized as guidance and an indication that a more accurate analysis or more detailed information is essential. As more data becomes available and is used, better results are obtained.

In a statistical approach, average parameters are often used. They are based on an ensemble or population and as this population becomes smaller, less accurate results are obtained. This is usually referred to as a limitation of SEA, especially at low frequencies where few modes are excited in a structure. However, this does not invalidate the SEA approach but only shows that the use of parameters and concepts based on average properties or characteristics of the elements, usually derived when a minimum number of modes are present, are no longer the most appropriate. Even then the results, in principle, can be regarded as reference values, especially if it is known that they are an over or under estimation of the real world situation.

Another aspect that has to be emphasized is that an absolute number is not always the necessary answer. The understanding, identification and interpretation of a problem and the determination of a line of action may be essential to support a decision on a ship design phase or in the analysis of an existing ship problem, and SEA may be suitable for this purpose.

Of course, SEA has its limitations and the major difficulties are related to the proper determination of its parameters and to its sub-systems identification.

This reasoning as well as the positive results obtained on ship applications are considered enough to justify the use of SEA in this work. SEA is an approach that appears to be conceptually able to respond to most of the demands in a ship analysis, as a whole, throughtout the complete design process.

It is essential to make clear that the choice of SEA for this work does not mean that the value of other methods is not recognized. On the contrary, when ship design is the field of application all of them have to be considered and the method able to give the more appropriate results used. From the previously specified aspects that need to be considered when an approach is selected, one can easily infer that the use of different approaches, even simultaneously for different areas of the ship, may naturally occur because methods complement each other. The choice of a method is a matter of judgment by the designer as is made quite obvious from the foregoing discussions. As an example, FEM can be used to analyze a particular structural area in a frequency range where few modes are excited and when such a structure is well enough defined, if the results given by SEA are not considered accurate enough. Also, when the conception of a ship is starting there is no sense to use an approach other than an empirical formulation or data from similar ships. Depending on the frequency, excitation nature and area of interest, a grillage method may have to be considered.

1.9 Thesis Structure

In this introduction the main aspects associated with noise on ships and its analysis were presented, emphasis being placed on the design point of view. The choice of SEA as the approach to be used in this thesis was basically justified and "SBN" was identified as its driving interest.

The movitation and objectives of this work are outlined in Chapter 2.

In Chapter 3 the basic concepts of SEA are summarized to allow a better understanding of this thesis.

Chapter 4 is concerned with the application of SEA, consisting basically of:

(1) Conception of a basic physical model from the bottom structure of an actual vessel and identification of the SEA subsystems. The basic model is built-up and studied in four steps, in order to allow a better understanding of the vibration transmission.

(2) Determination of the applicable SEA parameters: internal loss factors, mode count and coupling loss factors. Two analytical models are investigated:

    (a) assuming only flexural transmission, and

    (b) considering other motions and energy conversions.

Chapter 5 contains the description of the experimental work carried out to evaluate the flexural energy levels of the models elements in each step. A comparison is made between measured values and the predicted values resulting from SEA application.

Chapter 6 presents a summary of the work carried out, its conclusions and suggestions for further works.

CHAPTER 2

MOTIVATION AND OBJECTIVES

The Brazilian Navy is undertaking a long term construction program to take full advantage of local shipbuilding and associated industries. This program's goal is to develop and improve the capability of building and designing ships. Strong emphasis has been placed on design. Existing institutions have been improved and a new organization has been created and expanded by the Navy. Locally designed naval vessels have been built in Brazilian shipyards with national resources.

In order to efficiently perform his job, a designer must have knowledge of design methods and the capability of choosing the right one, considering the specifications to be satisified and the applicable constraints. Fundamental tasks are, therefore, to create, develop and make available the proper tools and procedures for the design work. In this goal lies the main motivation of this thesis.

Noise analysis is a priority area in any naval design organization, being the driving interest of this work. An actual 2,000 ton naval surface vessel is the reference ship. The major aspects associated with noise on ships were discussed in Chapter 1.

The basic objective of this thesis is the understanding of the transmission of structureborne noise (the most critical in a ship) by utilizing "statistical energy analysis", an approach that is conceptually able to respond to most of the demands on a ship noise analysis (as discussed in Chapter 1), and from which design tools and procedures can, in principle, be derived.

Any theoretical study of a practical problem particularly when vibration and noise are the concern involves an experimental tests. In this thesis a scaled physical model (1:2.5) idealized from the reference ship is studied both analytically and experimentally. The predicted results obtained by applying SEA are compared with laboratory measurements.

A SBN transmission analysis on a ship is very complex, requiring extensive work. Therefore, the area of study is restricted to the bottom structure of the ship. The reasoning for this choice can basically be summarized as follows:

1. It is the area of the ship where the machinery (main propulsion and the majority of the auxiliary equipment) and the shaft lines are installed and interact through their foundations.
2. Most of the published works (to the author's knowledge) on SBN transmission have concentrated on other structural areas such as the hull, decks, platforms and bulkheads.
3. It is the area where most of the different forms of structural motions are expected to be induced and relevant energy transformations to take place.
4. The ship's bottom is a short structural path between the machinery and the sea.
5. It is the section of the reference ship where most of the water, fuel oil and lube oil tanks are located.

With respect to item 4, the noise radiation to the sea is a major mechanism of dissipation in the hull. It is also a goal in a naval

vessel design to minimize the transmission of sound to the ocean by the machinery, especially for those ship speeds where the contribution from machinery vibration is greater than that from the propellers, which are major sources of noise radiation to the sea.

As the primary concern of this work is the structure, neither the sea nor the tank fluid load effects will be evaluated. They are considered complex enough to justify specific research efforts.

Even though the structural area of interest is restricted to the ship's bottom, a detailed SBN transmission analysis is so complex that a simple model is used. This model can be considered as a basic model that can be extended:

1. In size, in transverse (toward the hull and/or ship center line) and in fore-and-aft (toward the machinery spaces bulkheads) directions,
2. In complexity: by adding more structural details, including more sources, filling with fluid, etc.

Each representative aspect and detail can be separately analyzed first and gradually incorporated into the model to have their individual and combined effects investigated. The idealized model is then a starting step of a more detailed and complex modelling (analytically and experimentally) of the reference ship's bottom sturcture.

The bottom is also the structural area of the ship that has the highest mass density and stiffness. Its elements have, in general, higher fundamental frequencies than those of other areas of the ship's structure.

This may sound inconsistent with the chosen approach since, in principle, these structural characteristics are usually referred to as restrictions to a SEA application. On the other hand, it appears to be an attractive area for a FEM application. It is, therefore, essential to point out the following:

1. The reference ship has a light structure, the thicknesses of the bottom elements varying from 6.3 mm to 12.7 mm and those of the main foundations from 8 mm to 19 mm.

2. Because noise analysis as a whole and ship design are the ultimate concern, the interest is not restricted to a specific frequency range.

Therefore, the bottom of the reference ship may better offer the possibility of investigating when one method is more appropriate than another, and, more importantly, of investigating their possible interfacing, particularly of FEM and SEA. These possibilities are not the objective of this thesis nor is it to develop any new formulation for SEA. Both aspects are considered subject of a future research. This thesis concentrates on the application of SEA, to the model, using existing formulations and parameters determined from well-established concepts.

The frequency interval of 0.63 to 20 kHz (in the model) is broad enough to include:

1. The range of lower frequencies where beforehand it is expected that the SEA parameters used here will not lead to the most accurate prediction;

2. The range of higher frequencies where it is expected that energy conversions will take place;

3. The range of frequency where it is expected that the flexural motions are predominant.

The specific objective of this thesis is to investigate the applicability of the herein used SEA formulations, especially when energy transformations occur, by comparing predicted and measured flexural energy levels of the different elements of the scaled model, in four steps.

In summary, this work and its analytical and experimental results can be considered as a first step of a more detailed SEA analysis of SBN transmission from machinery to foundation and through the ship's bottom structure. It is part of the overall noise analysis of the reference ship and of the process of creating proper tools for ship design.

CHAPTER 3

STATISTICAL ENERGY ANALYSIS

3.1 A Brief Introduction

"SEA" was originated and developed from analysis of power flow between coupled systems. The fundamentals and theory are presented in Part I of reference [15], while Part II is dedicated to the engineering applications. The major aspects and concepts are summarized in this chapter for the sake of a better understanding of this thesis and are especially addressed to those not familiar with SEA.

From Lyon [15]:

> "The earliest works that can be associated with SEA were carried out independently by Lyon and Smith, 1959. Lyon calculated the power flow between two lightly coupled linear oscillators excited by statistically independent white noise sources. Smith calculated the response of a resonator excited by a diffuse broad band field. Lyon and Maidanik [16] extended Lyon's work by analyzing the interaction between multimode systems. A particular application investigated was the power flow between several structural modes and a reverberant field, the kind of problem studied by Smith [17]."

Several investigations and works followed (as listed from pages 153-169 of reference [15]):

(a) further analyzing the power flow between coupled oscillators and the interaction between vibrating systems and reverberant fields,

(b) dealing with structure-structure interaction,

(c) being dedicated to the determination of SEA parameters,

(d) trying to improve the statistical description of the SEA systems, parameters and results.

3.2 SEA Systems and Subsystems

In a SEA approach each coupled element is denominated as a subsystem and a set of such elements is a SEA system.

As stated by Lyon ([15], pages 10-11 and Chapters 6, 8, 10), the definition of SEA sybsystems is based on classes or groups of resonant modes of a same nature rather than on physical or geometric substructuring of the system. The fundamental element of a SEA model is a group of similar energy storage modes. These modes can be of flexural or in-plane nature that exist in some section of a structural system, such as a plate, or the modes of an acoustical space. One of the criteria for modal similarity is that the modes have nearly the same half power bandwidth in a given frequency band (page 239, reference [15]).

3.3 Interaction Between Coupled Subsystems -- Power Balance Equations

The fundamental equations and expressions of SEA as well as the basic aspects and assumptions concerning the interaction between multimode subsystems are presented in Appendix A.

Energy is the SEA primary variable. Its sharing between coupled subsystems subjected to external independent excitations is estimated, as a solution of a set of linear equations: the power balance equations.

The basic power expression used in SEA is:

$$\Pi/\omega = \eta E \qquad (3.1)$$

where: Π: power

ω: frequency

η: Loss factor

E: energy

Equation (3.1) can be understood as: the energy lost by a subsystem (Π/ω) is proportional to the total energy (E) stored in that system. The coefficient of proportionality is η, the loss factor. Two types of loss factors can be identifed

(a) The internal or dissipative loss factor (η_i) -- associated with the power dissipated (π_i), that represents the energy truly lost by i, basically due to friction (internal damping -- $\eta_{(int)}$) and by radiation (η_{rad}) to the adjacent media. ($\eta_i = \eta_{int} + \eta_{rad}$).

(b) The <u>coupling loss factor</u> (η_{ij}) -- that governs the <u>power</u> transmitted from subsystem i to subsystem j.

As an example of power balance equations, consider the coupling between two independently excited SEA subsystems (Fig. 3.1):

Power dissipated by 1(2):

$$\Pi_{DIS}^{1(2)} = \omega \eta_{1(2)} E_{1(2)} \tag{3.2}$$

Net power flow between 1 and 2:

$$\Pi_{1-2} = -\Pi_{2-1} = \omega \eta_{12} E_1 - \omega \eta_{21} E_2 \tag{3.3}$$

Power input: $\Pi_{INP}^{1(2)}$ (from an external source).

Power balance equations:

$$\begin{aligned} \Pi_{INP}^{1} &= \omega\eta_1 E_1 + \omega\eta_{12} E_1 - \omega\eta_{21} E_2 \\ \Pi_{INP}^{2} &= \omega\eta_2 E_2 + \omega\eta_{21} E_2 - \omega\eta_{12} E_1 \end{aligned} \tag{3.4}$$

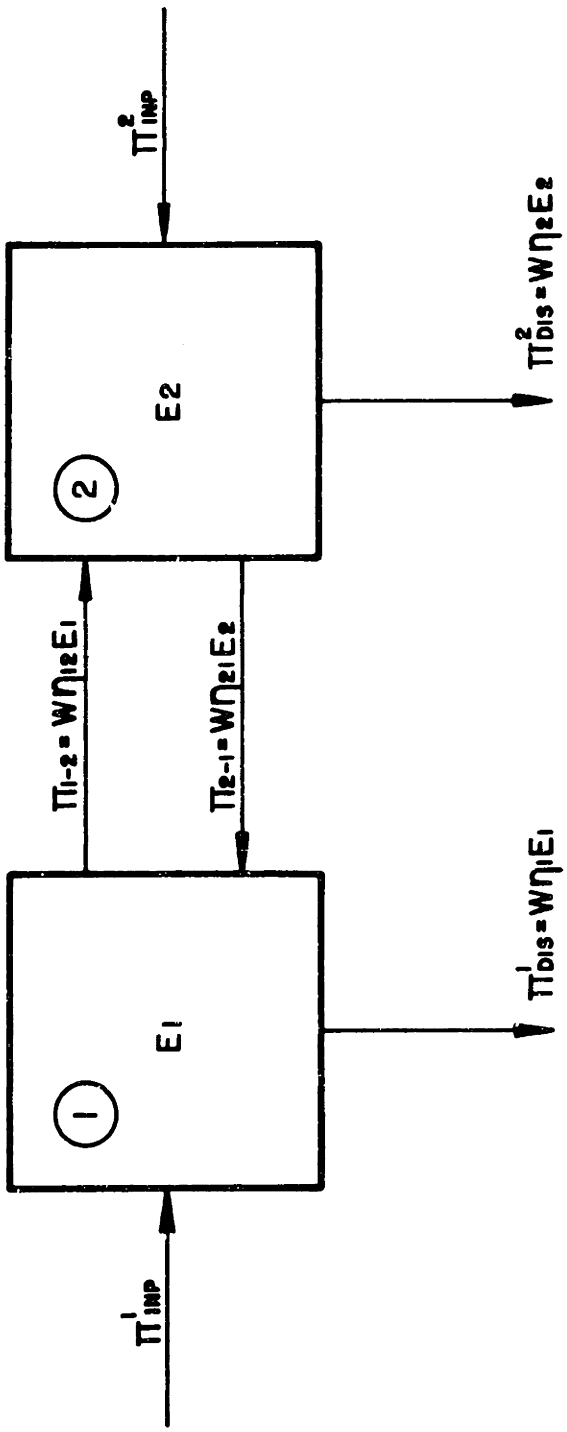

FIGURE 3.1: POWER FLOW FOR TWO COUPLED "SEA" SUBSYSTEMS INDEPENDENTLY EXCITED

Using matrix notation: (3.4) becomes

$$\begin{bmatrix} \eta_1 + \eta_{12} & - & \eta_{21} \\ - \eta_{12} & & \eta_2 + \eta_{21} \end{bmatrix} \begin{bmatrix} E_1 \\ E_2 \end{bmatrix} \quad \begin{bmatrix} \Pi^1_{INP/\omega} \\ \Pi^2_{INP/\omega} \end{bmatrix} \tag{3.5}$$

The power balance equation for a subsystem coupled to any number of other subsystems is a generalization of (3.4) (Chapter 8 of reference ([15]).

$$\Pi^i_{INP} = \omega \eta_i E_i + \omega E_i \sum_{\substack{j=1 \\ j \neq 1}}^{n} \eta_{ij} - \omega \sum_{\substack{j=1 \\ j \neq 1}}^{n} E_j \eta_{ji} \tag{3.6}$$

where:

Π^i_{INP} = power delivered to i by an external source

$\omega \eta_i E_i$ = power dissipated by i.

$\omega E_i \sum_{\substack{j=1 \\ j \neq 1}}^{n} \eta_{ij}$ = power lost from i to the subsystem coupled to it

$\omega \sum_{\substack{j=1 \\ j \neq 1}}^{n} E_i \eta_{ij}$ = power received by i from the subsystems coupled to it

This expression was derived by Eichler [18], 1965, when investigating the power flow from one acoustic field to another inside a box structure (3 SEA subsystems). It was also used by Lyon and Scharton [19], 1965, in the analysis of energy transmission from one flat plate to another via a connected flat beam. Since then equation (3.6) has been used and has had its applicability investigated in several other works, such as [9-14, 20-24], without any modification being introduced.

When considering the general case of coupling between N systems, the

application of equation (3.6) to each subsystem leads to a set of N equations

$$\left[\begin{array}{cc:c:c} \eta_{11} & -\eta_{21} & -\eta_{(N-1)1} & -\eta_{N1} \\ -\eta_{12} & \eta_{22} & -\eta_{(N-1)2} & -\eta_{N2} \\ \hdashline -\eta_{1(N-1)} & -\eta_{2(N-1)} & \eta_{(N-1)(N-1)} & -\eta_{N(N-1)} \\ -\eta_{1N} & -\eta_{2N} & \eta_{(N-1)N} & \eta_{NN} \end{array}\right] \left[\begin{array}{c} E_1 \\ E_2 \\ \hdashline E_{N-1} \\ E_N \end{array}\right] = \left[\begin{array}{c} \Pi^1_{INP/\omega} \\ \Pi^1_{INP/\omega} \\ \hdashline \Pi^{N-1}_{INP/\omega} \\ \Pi^N_{INP/\omega} \end{array}\right] \tag{3.7}$$

where

$$\eta_{ii} = \eta_i + \sum_{\substack{j=1 \\ j\neq 1}}^{N} \eta_{ij} \tag{3.8}$$

If two subsystems don't interact, the coupling loss factor is taken as equal to zero.

Equation (3.7) shows that if the power input and the loss factors are known the energy of the different subsystems can be estimated and, therefore, (from equation 3.1) the power lost by each subsystem.

Even if the power input is not known, equation (3.7) can be useful for a comparative analysis. The energy level of a subsystem is taken as a reference and energy ratios are estimated (E_n/E_r), instead of absolute values.

When the energy level of each different subsystem is measured, equation (3.7) can be used to interpret these measurments, verify the

applicability of the loss factors being utilized and estimate the power input.

In a structureborne sound transmission analysis, the power input is the power delivered by the machinery to its foundation. This is the subject of Appendix B.

Another important equation in SEA (derived in Appendix A) is the consistency or reciprocity relationship:

$$\eta_{ij} N_i = \eta_{ji} N_j \qquad (3.9)$$

where $N_{i(j)}$ = number of modes of subystem i(j). It greatly simplifies the calculation of the coupling loss factors.

From equations (3.1) and (3.9) and from the definition of SEA subsystem, it is not difficult to understand why the loss factors and the number of modes (mode count) are usually referred to as the SEA parameters. Actually, only the coupling loss factor is a concept inherent to SEA. The other two are concepts from acoustics and structural dynamics, that play an important role in a SEA approach.

The fundamental aspects concerning each parameter and its determination are presented in Appendix A and applied in Chapter 4. Relevant aspects related to applications of SEA to SBN transmission on ships are presented and discussed throughout the different chapters of this thesis, especially in Chapter 4, and in Appendices A and C.

CHAPTER 4

APPLICATION OF STATISTICAL ENERGY ANALYSIS TO THE REFERENCE SHIP

4.1 Modelling

4.1.1 Machinery Spaces -- Ship Bottom Structure-Equipment Foundations

The reference ship has two machinery spaces, each one 12 m long (fore-and-aft direction) and approximately 11 m wide. As in any navy vessel, the concentration of equipments in both spaces is very high. It is, therefore, not difficult to infer that a detailed SBN transmission analysis for the bottom structure, considering all the sources, is a very demanding task.

The machinery foundations differ in dimensions, but are, in terms of concept, fundamentally the same. The double bottom is symmetric with respect to the ship center line, and, except for minor local details, is identical along the total length of the machinery spaces. Based on those aspects, the analysis will be restricted to the interaction between a propulsion diesel engine and the structure. Figures 4.1.1(a) to 4.1.1(d) show a top view, a transverse section and longitudinal sections of the ship bottom structure and diesel engine foundation.

4.1.2 Scaling Problem

When analyzing the vibrational response of a structure by using an exact geometrically similar model [25], it is required that the non-dimensional parameters -- $\frac{\rho\omega^2 L^2}{E}$ and ν -- be identical in the model and prototype. When they are built of the same material, ν, ρ and E are assumed to be the same so that only the following expression has to be satisfied:

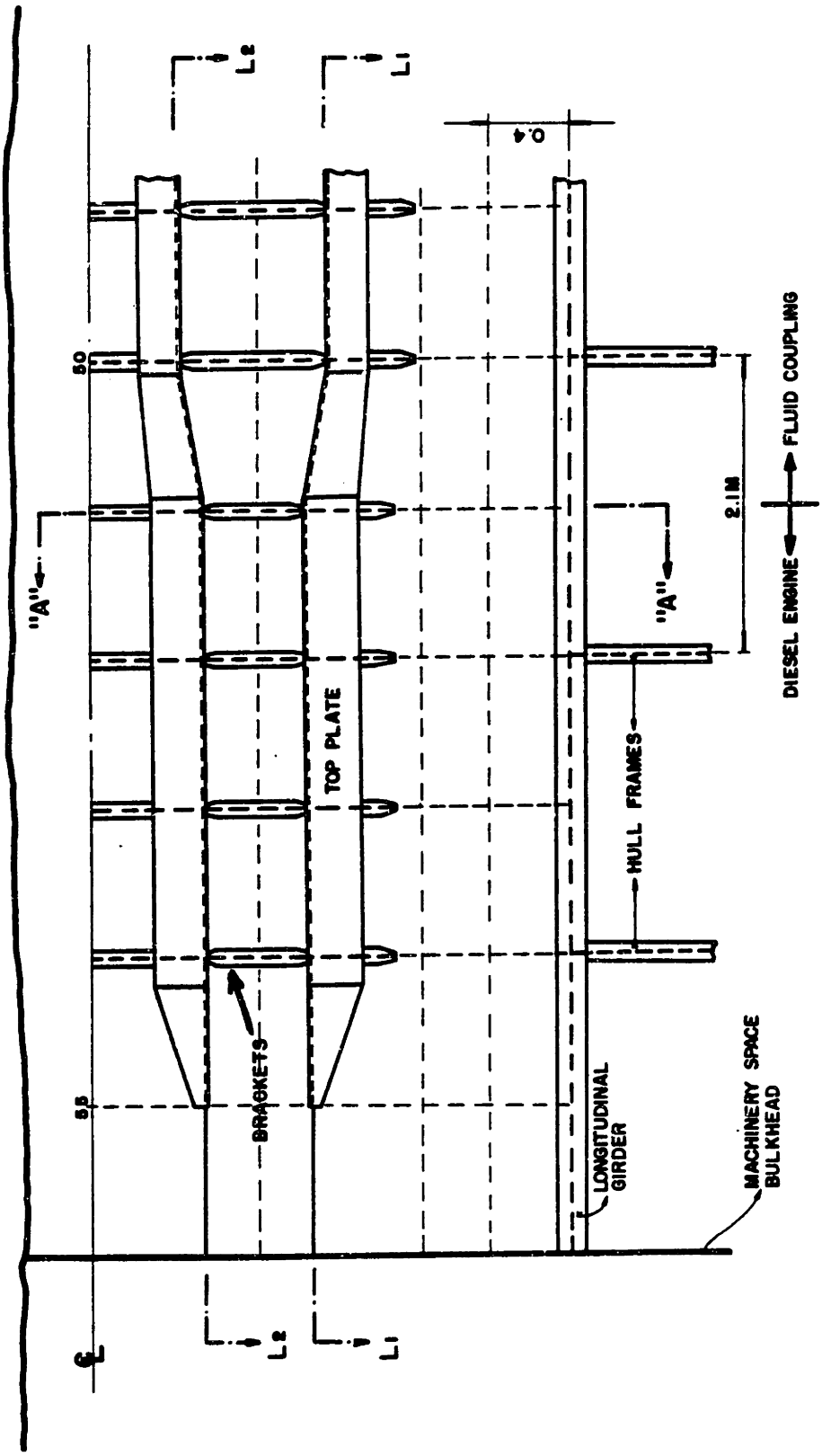

FIGURE 4.1.1a: DIESEL ENGINE FOUNDATION AND DOUBLE BOTTOM STRUCTURE

-- TOP VIEW --

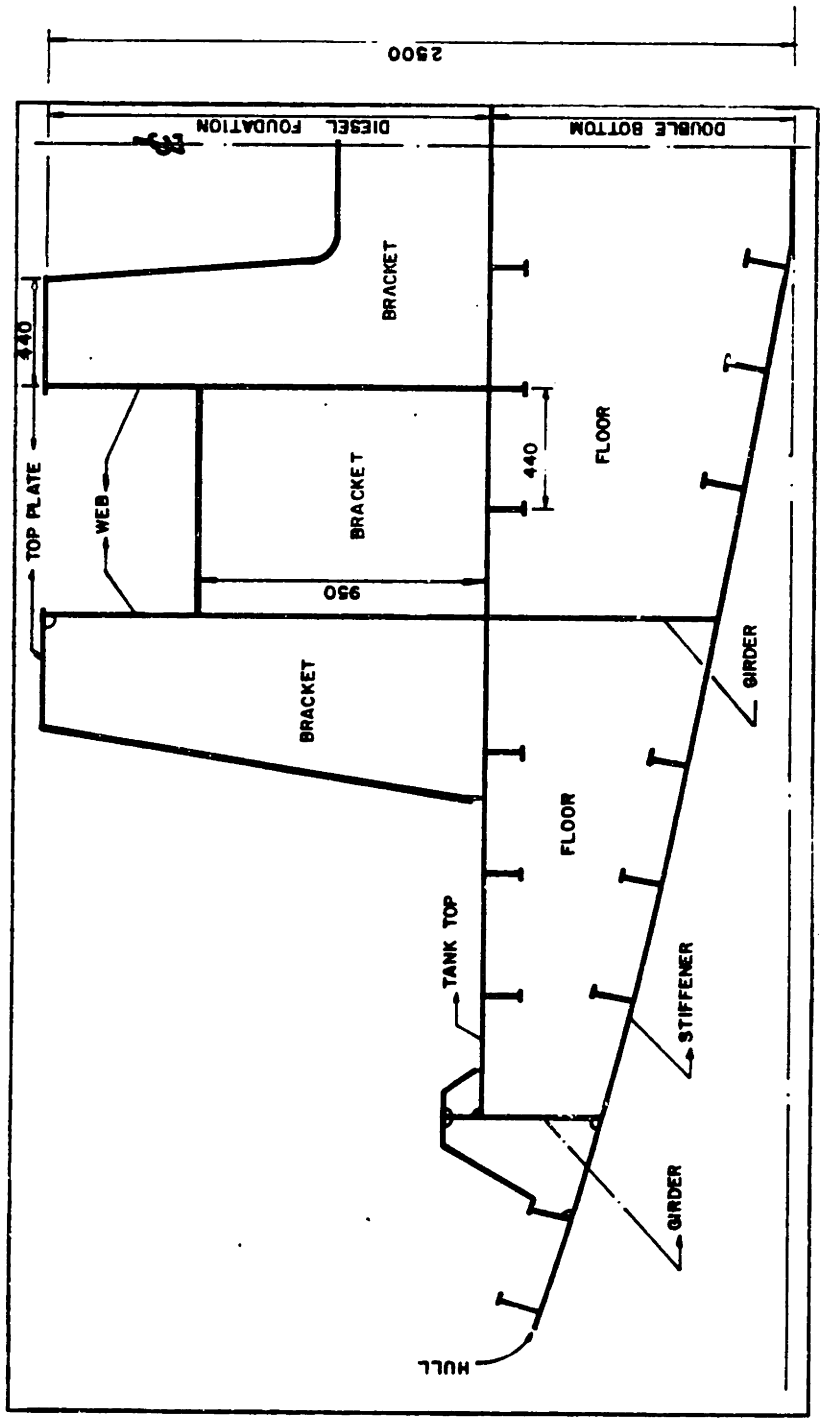

FIGURE 4.1.1b: DIESEL ENGINE FOUNDATION AND SHIP BOTTOM STRUCTURE
-- TRANSVERSE SECTION (A-A) --

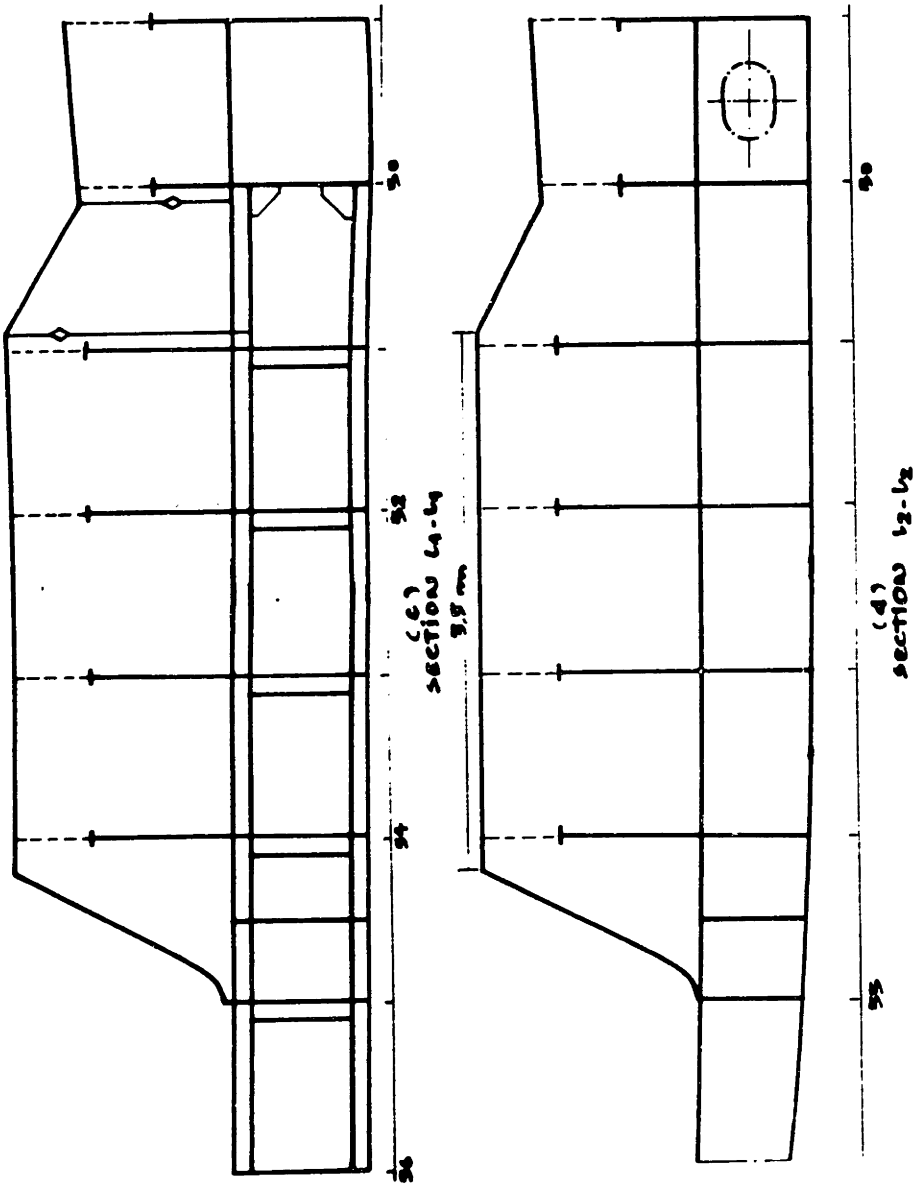

FIGURE 4.1.1c and d: DIESEL ENGINE FOUNDATION AND DOUBLE BOTTOM STRUCTURE
-- LONGITUDINAL SECTIONS --

$$(\omega L)_{model} = (\omega L)_{ship} \qquad (4.1.1)$$

When conceiving a physical model from an actual ship structure, some practical aspects have to be considered:

(a) size and weight

(b) cost

(c) limitation of available laboratory equipment

(d) welding

The smaller the model, the lesser its weight and usually the cost. It is also much easier to handle. However, when the dimensions are scaled down:

1. Frequency has to be multiplied by the same scale factor, and, the higher the frequency, the more special equipment is required.

2. The susceptibility to deformations caused by welding increases since the thicknesses are smaller.

A compromise is, therefore, needed. Despite the weight disadvantage, the use of steel (as in the ship) was found to be more meaningful, by allowing an easier and more direct correlation with the full scale situation.

Even restricting the analysis to the diesel structure interaction, an area about 15 m^2 has to be considered so that any further possible simplification is highly desirable.

When trying any simplification, it is very important to seek a model which represents as closely as possible the real world situation by including the fundamental aspects of the full scale problem. To accomplish this goal and also have a model that allows a clear interpretation of ex-

perimental results, the best approach seems to be the following: Identify a starting point and from there gradually build up the model in a planned sequence, incorporating step-by-step those details or complexities that have more significance in expressing the actual structure and the SBN transmission problem.

4.1.3 Ship Structural Modelling

From a structural point of view there are several ways in which the different areas of a ship can be modelled.

1. As a made-up just by beams (See Figure 4.1.2).
2. As a plate-like structure (see Figure 4.1.3).
3. As an association of beams and plates, such as reinforced panels. (See Figure 4.1.4).

Important aspects of structural models are presented in Appendix C, summarized from some works related to SBN transmission in ships.

From these works, generally, the following can be inferred:

1. In SEA applications, unstiffened plate-like structures have been used as the model.
2. There is a stronger tendency in assuming a transverse (upward in the frame direction) energy path as the most important.
3. For the reference ship the transmission of energy in the fore-and-aft direction may also be relevant. This is basically due to the alignment between the foundation web and longitudinal girder and because some sources are very close to the machinery space bulkheads.

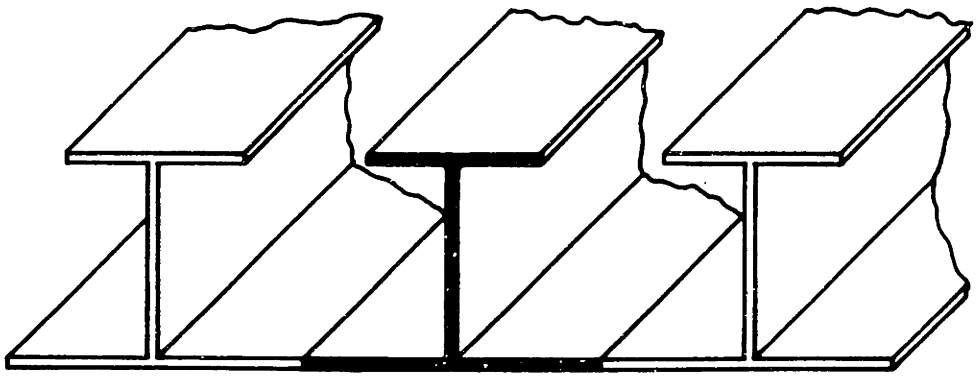

(A)

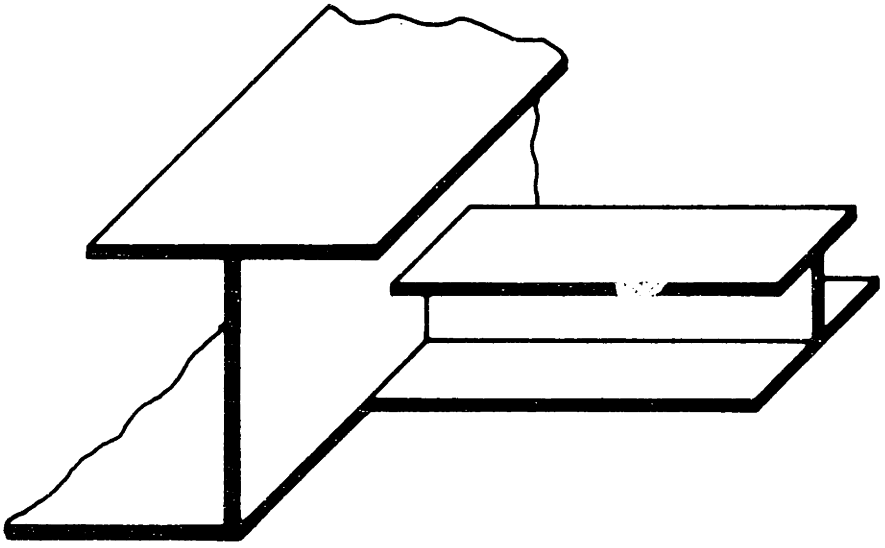

(B)

FIGURE 4.1.2: BEAM-LIKE STRUCTURAL MODELS

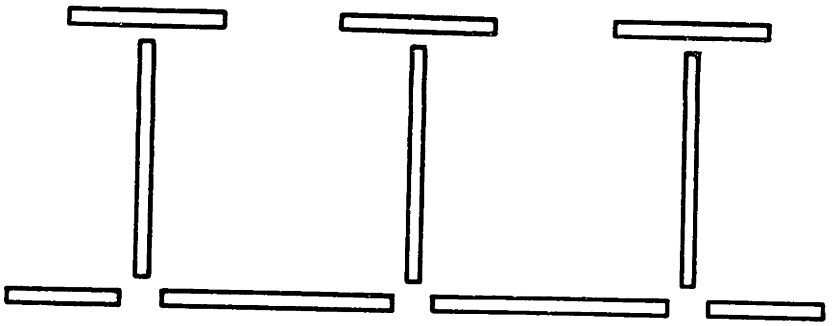

(A)

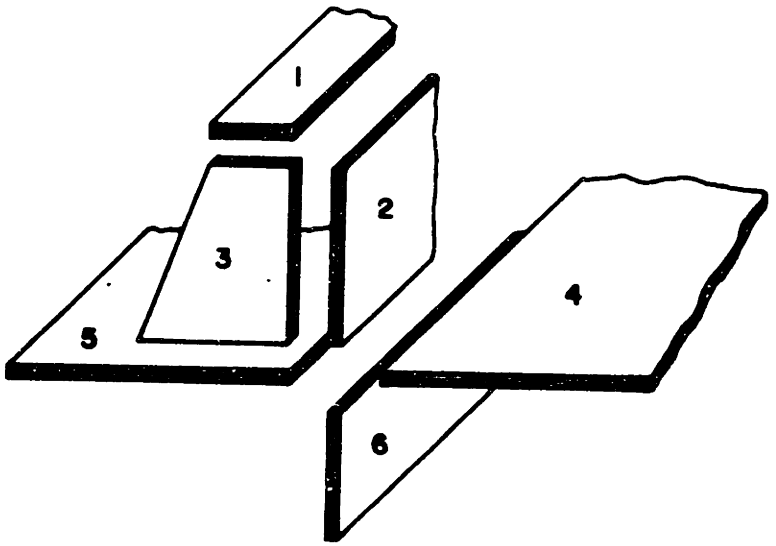

(B)

FIGURE 4.1.3: PLATE-LIKE STRUCTURAL MODELS

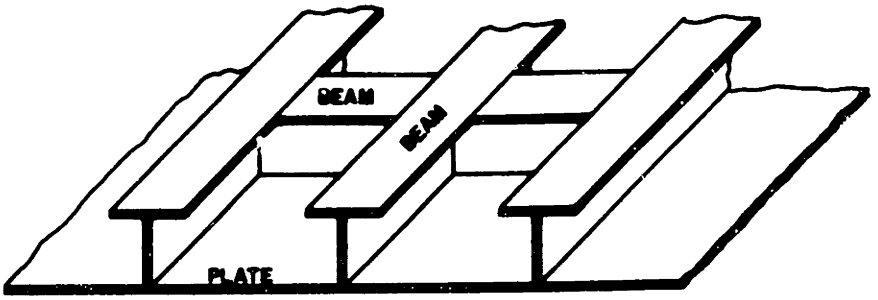

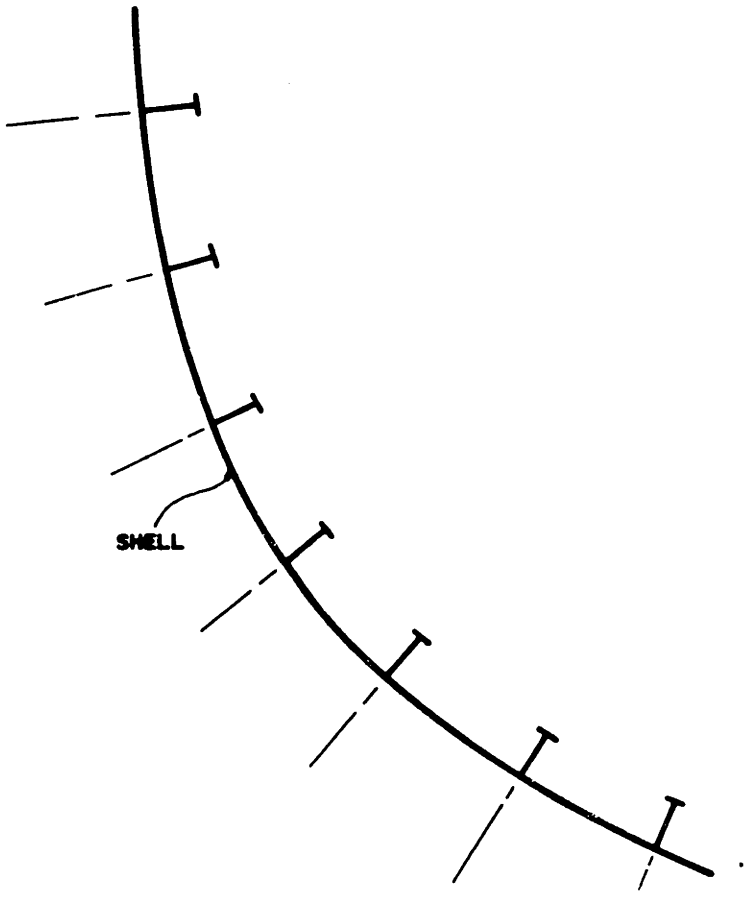

FIGURE 4.1.4: REINFORCED PANELS

4. Each ship has its own characteristics and particularities, requiring individual analysis.

4.1.4 Structural Models -- SEA System

As SEA is the selected approach to be applied, the modelling task is not restricted to a physical model conception, but also related to the definition of the SEA system and subsystem. The basic conceptual criteria (for SEA modelling) can be derived from the system's definition: identification of the nature of the possible induced structural motions and of those motions that are predominant, through the determination of the number of resonant modes available to store energy.

In a complex structure (as mentioned in Chapter 1) as frequency increases, the basic elements (beams and plates) tend to behave very much as they would when separated from the structure.

Concentrating on the diesel engine foundation, two basic behaviors may be expected. (See paragraph 4.1.5, Appendices B and C).

1. As a beam -- Flexural motion in the fore-and-aft direction. Figure 4.1.5 shows three different representations, including or not a possible contribution of the tank top (4.1.5b) or of the double bottom (4.1.5c).

2. As plates welded together -- Figure 4.1.6.

Similarly, some representations that can be associated with the double bottom structure are shown in Figure 4.1.7.

The number of modes available to store energy can be estimated in each case by utilizing the concept and formulations of modal density. As dis-

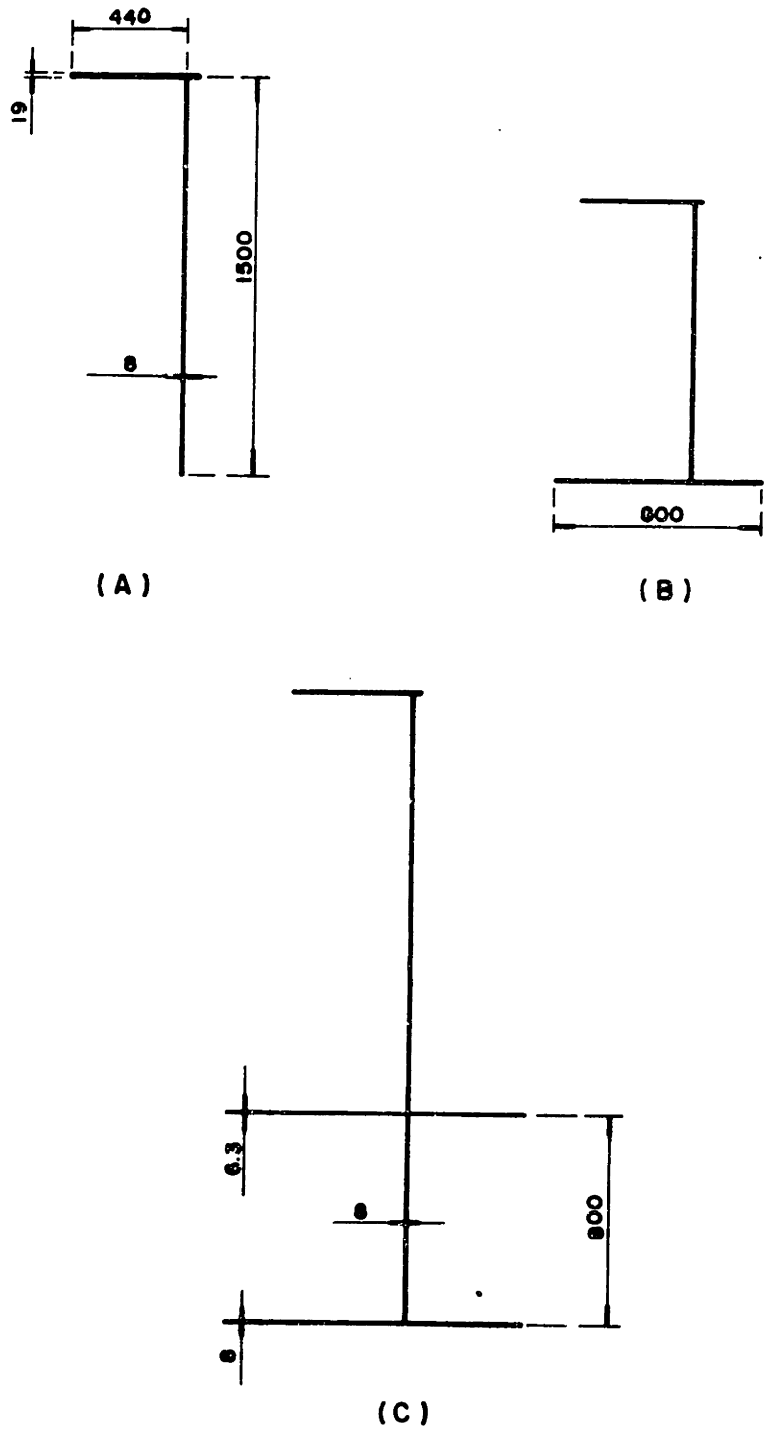

FIGURE 4.1.5: BEAM-LIKE STRUCTURAL MODELS FOR THE DIESEL FOUNDATION

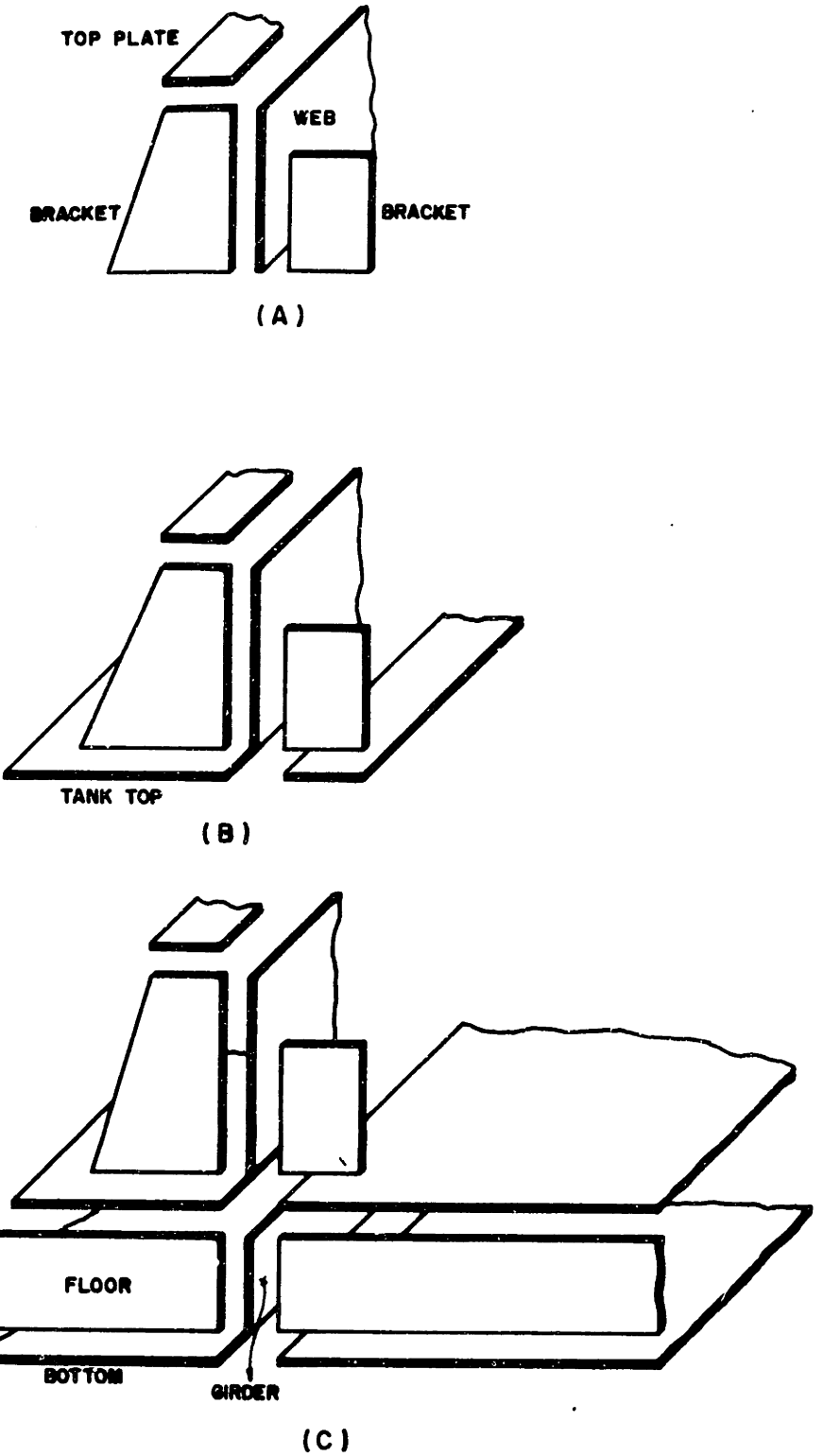

FIGURE 4.1.6: PLATE-LIKE STRUCTURAL MODELS FOR THE DIESEL ENGINE FOUNDATION

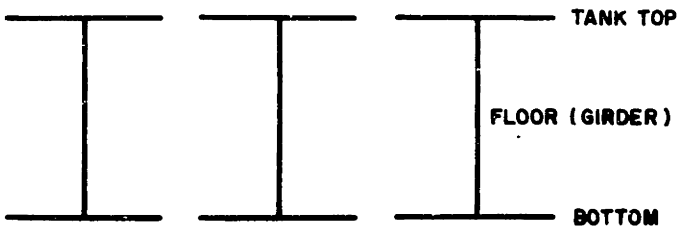

(A) BEAM MODEL

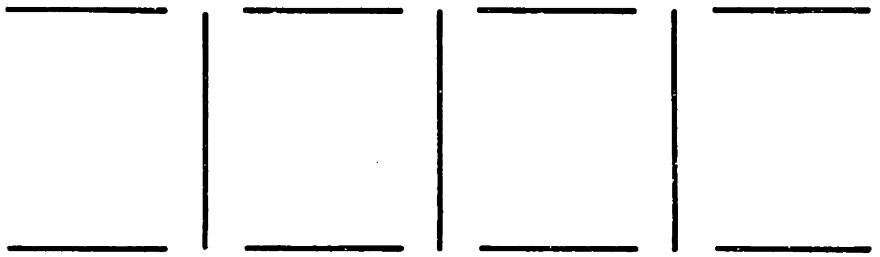

(B) PLATE MODEL

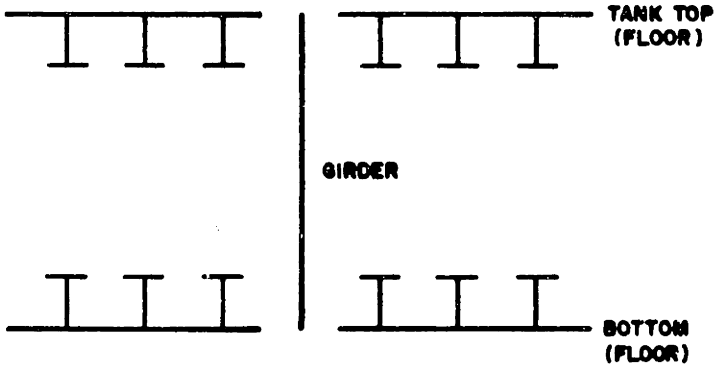

(C) PLATE AND REINFORCED PANELS

FIGURE 4.1.7: STRUCTURAL MODELS FOR THE DOUBLE BOTTOM

cussed in Appendix A, the modal density can be efficiently used (instead of the actual mode count), when the number of modes in the frequency band is of the order of at least ten. The predicted number of modes, when less than ten, can be regarded as reference values. Independent of the number of modes, a comparison between modal densities is always useful, and in many cases, can directly indicate when a motion is predominant. Basic expressions of modal densities for beams and plates are shown in Table 4.1.1 [15, 26].

The number of modes can also be determined theoretically from the applicable equation of motion and proper boundary conditions. For some boundary conditions (such as beam hinged at both ends) the computation is simple. For more complex cases, there are available formulas for evaluation of natural frequencies (usually the first resonances). Formulations for beams and plates (bending) can be found in references [27, 28] and in standard textbooks of structural vibration.

In order to identify the most representative model, first we consider the diesel foundation by comparing the beam representation (4.1.5a) with the corresponding plate representation (4.1.6a).

The calculated modal densities are shown in Table (4.1.2). These numbers strongly indicate a predominancy of the plate motions along the entire frequency interval of interest. With respect to the other two beam representations of the foundation (Figure 4.1.5b) and 4.1.5c), the calculated radius of gyration are higher than that of representation (4.1.5a), which leads to lower values of modal densities. As more plates are present, the plate motions will be even more predominant.

PLATES		BEAMS	
BENDING	IN-PLANE	BENDING	TORSION
$2\pi fA/c_\phi c_g$			
$A\sqrt{3}/hc_L$	LONGITUDINAL: $2\pi fA/c_l^2$ SHEAR: $2\pi fA/c_T^2$	$L/(2\pi K_g c_L f)^{1/2}$	$\frac{2L}{c_T}\left(\frac{K_\phi^2 A}{J}\right)^{1/2} = \frac{2L}{c_T}$

TABLE 4.1.1

Modal Densities

BEAM REPRESENTATION (Fig. 4.1.5a)	$n_B = 4.2 \times 10^{-3} f^{-1/2}$ (including the fluid coupling foundation and disregarding any possible effect of the brackets)				
	f (Hz)	20	1000	2000	16000
	n_B	9.5×10^{-3}	1.3×10^{-3}	0.95×10^{-3}	0.3×10^{-3}

PLATE REPRESENTATION (Fig. 4.1.6a)	PLATE	FLEXURAL MOTIONS	IN-PLANE MOTIONS		
	TOP PLATE	$n = 42 \times 10^{-3}$			
				2000 Hz	16000 Hz
	WEB	$n = 328 \times 10^{-3}$	$n = 7 \times 10^{-6} f$	14×10^{-3}	112×10^{-3}
	BRACKET (EACH)	$n = 30 \times 10^{-3}$	$n = 0.66 \times 10^{-6} f$	1.32×10^{-3}	10.6×10^{-3}

TABLE 4.1.2

Modal Densities Associated with a Beam (Fig. 4.1.5a) and a Plate-like (Fig. 4.1.6.a) Representations of the Diesel Foundation.

Table 4.1.3 shows the expected number of modes associated with Figures (4.1.5a) and (4.1.6a) (and their possible motions), in those third octave bands which are considered more significant for such comparison. Formulas for determination of natural frequencies were also used for the lower bands. To allow a better comparison Table 4.1.3 also includes the expected number of modes associated with the sections of the top plate and web between the brackets.

From those numbers the following basic conclusions can be drawn:

1. The foundation is basically a plate-like structure. The number of modes associated with plate motions, particularly bending, being much higher than those associated with the beam modes, even at the lower frequencies. This is also quite true when just a section between brackets is compared with the entire beam. When the brackets are included, the predominancy of the plate behavior is enhanced.

2. Consistent with the statement made in Appendix A, the modal density formulations may not be appropriate for predictions when the number of modes is small in a frequency band. For example, the first beam mode for the foundation (Figure 4.1.5a) is expected at 125 Hz, as estimated by natural frequency formulation. While applying modal density, the first natural frequency is predicted to occur in the band centered at 10 kHz. Below this frequency the modal density formulas lead to a number of modes that is a fraction of a unit. Thus, it is certain that resonant modes will exist at lower frequencies than those estimated by modal density for the first mode.

CENTER FREQUENCY (Hz)	BEAM REPRESENTATION (BENDING) (Fig. 4.1.5a)		PLATE REPRESENTATION (Fig. 4.1.6a)											
			TOP PLATE (BENDING)		WEB			BRACKETS MODAL DENSITY		SECTION BETWEEN BRACKETS				
					BENDING		IN-PLANE			TOP PLATE		WEB		
	MODAL DENSITY	NAT. FREQ. (HINGED BOTH ENDS)	NAT. FREQ. (SIMP.SUP.)	MODAL DENSITY	NAT. FREQ. (SIMP.SUP.)	MODAL DENSITY	MODAL DENSITY	BENDING	IN-PLANE	BENDING		BENDING		IN-PLANE
										NAT. FREQ. 1EDGE FREE 3 SIMP. SUP.	MODAL DENSITY	NAT. FREQ. (SIMP. SUP.)	MODAL DENSITY	MODAL DENSITY
80		0	0	0/1	5	6	0	0/1		1		1	1	
125		1	0	1	7	9	0			0	0/1	0	1/2	
200		0	0	2	12	15	0	1/2		1		2	3	
400		0	3	3/4		30	0	2/3	0	2		5	5/6	0
500		1	3	4/5		38		3/4		0	1	6	7/8	
630		0	3	5/6		48	0/1	4/5		1	1	9	9	
800	0/1	0	4	7		60		5/7		1	1/2	11	11/12	
1250		1	13	11		94	1/2	8/9	0/1				18	0/1
2000		1	11	17		151	5/6	14	0/1		3/4		29	1/2
4000		0		35		303	25	28	1/2		6/7		58	3/5
5000		1		44		379	40	35	3/4		8/9		73	6/7
6300		1		55		478	64	44	5/7		10/11		92	12
8000		1		70		607	104	56	9/10		13/14		117	19
10000	1	0		88		759	162	70	14		17		146	31
12500	1/2	2		110		949	253	88	23		21		183	49
16000	1/2	1		141		1215	254	113	38		27		234	81

TABLE 4.1.3

Expected Number of Modes for a Beam and a Plate-like Representation of the Diesel Engine Foundation

With respect to plates, a significant difference can also occur at lower frequencies, especially because of the boundaries effect and depending on the aspect ratio.

3. In-plane modes are available at the web, above 1250 Hz (possibly 500 Hz). The number becomes more significant as frequency increases.

4. The modal density of the brackets is about half of the value of the section of the web between brackets. The number of modes available at each bracket is significant, especially above:

   (a) 1 kHz -- for flexural motions

   (b) 4 kHz -- for in-plane motions

Carrying out similar calculations for the bottom representations (not including the stiffeners), Figures 4.1.7a and 4.1.7b, one can infer (based on equivalent reasoning as for the foundations that the bottom may also be considered as a plate-like structure. Table 4.1.4 shows the modal densities associated with the floor, longitudinal girders, tank top and bottom plates. It is clear that the floors and girders influence cannot be disregarded since they have an important contribution in number of modes available to store energy (about the same order as the bottom plates and brackets respectively) along the same frequency interval.

The diesel foundation and double bottom structure can, therefore, be considered basically as a plate-like structure. Nevertheless, two aspects have to be carefully analyzed: the longitudinal stiffeners effect and the in-plane motions. How important are they?

The longitudinal stiffeners may assume, in a large frequency range, different simultaneous behaviors of the same significance (See Appendix C)

	TOP TANK	BOTTOM PLATE	FLOOR (*)	(LONG GIRDER) (*)
BENDING	104×10^{-3}	81.7×10^{-3} (*)	72×10^{-3}	39.7×10^{-3}
IN-PLANE	$10.8 \times 10^{-6} f$	$10.8 \times 10^{-6} f$	$9.6 \times 10^{-6} f$	$5.4 \times 10^{-6} f$

(*) Based on Averaged Areas

TABLE 4.1.4

Modal Densities for the Ship Double Bottom Plates

1. As a rotary inertia and stiffness.

2. As a beam, in torsion and bending.

3. As plates, in bending, especially its web; the flange behaves up to approximately 5 kHz, basically as an inertia and stiffness.

The plate behavior seems to predominate at higher frequencies (above 6300 Hz). It is also important to point out that up to this frequency, the number of each different type of modes is not high.

The stiffeners effect is further discussed in Appendix C, where some aspects from previous works are presented. It may be significant, so that the bottom, tank top and floor would be better modelled as stiffened panels. However, in including the stiffeners, the complexity of the analysis is substantially increased (especially when plate in-plane motions are taken into account) justifying a separate effort to evaluate their effect. Based on this fact and on the principle of conceiving a model step-by-step, gradually increasing complexity, the stiffeners will not be considered. After being separately evaluated they can be (in a future work) added to the model and have their effect better investigated.

With respect to in-plane modes, it was shown that they are available. The question becomes how strong is their influence, or how much energy is going to be stored by them and how much is going to be transformed back to bending. As mentioned in Chapter 1, only flexural transmission is usually considered in a SBN analysis. Some important aspects related to this subject are presented in Appendix C. This appendix also shows, based on SEA principles and on a criterion suggested by Swift [23], that a bending excitation in the top plate can transfer a significant amount of energy to the in-plane

modes in the web, and that energy transformations cannot be neglected beforehand above 2 kHz.

The diesel engine foundation and double bottom structure will be, therefore, modelled as an unstiffened plate-like structure. In terms of SEA modelling, three subsystems (groups of modes) can be, in principle, expected in each plate, associated with bending transverse shear and longitudinal motions.

4.1.5 Machinery-Foundation Interaction

Emphasis has been given to the structure itself. A step forward in the model conception has resulted, but a problem still remains: How small? How long in each direction?

To give substance to the idealization, an important aspect cannot be left aside: the interaction between the diesel engine and the foundation. The engine is placed on the foundation resiliently mounted with vibration isolators, bolted at eight different positions (four on each side) to the sections of the top plates between brackets. In such a multipoint connection installation, the power delivered through each support has a contribution from all others, especially from those located at the same top plate. In an interaction between machinery and foundation, actually six degrees of freedom have also to be considered. These aspects are discussed in Appendix B, where the concepts of point, transfer and overall effective mobility are presented. In this work only the predominant force from the diesel, in the vertical direction, will be considered (a simplification of the real world situation).

M. Ohlrich [29], from measurements on scaled models, and Petersson and Plunt [30], based on onboard measurements, analyzed the interaction between

diesel engines and foundations of a similar nature (also similar to the one under analysis herein). Both reached the conclusion that the point mobility of the foundation seemed to be mainly determined by the local stiffness of the excited plate section between brackets up to its first resonance frequency. For higher frequency the characteristic mobility will determine the mobility together with the superimposed response of the resonances. Petersson and Plunt also concluded that the point mobility might be sufficient for the description of the dynamic properties of the foundation and engine structure when their coupling is analyzed (See Appendix B).

These conclusions reinforce the modelling as a plate-like structure. It also can be inferred that the section of the top plate between brackets plays a major role in the machinery-foundation interaction and also has a high significance for the modelling task.

4.1.6 Physical Models

Based on the discussions in the previous paragraph, the top plate section between brackets may be identified as a starting point for the physical model idealization. The entire top plate can be considered as built-up by sections and each contact point with the diesel engine can be regarded as an individual point source, delivering power. Two adjacent sections are separated by a bracket, which may have a significant number of modes able to store energy. Thus, the power received by a top plate section will have three possible paths to choose: the brackets, the web, and the neighboring sections.

The discussion in paragraph 4.1.3 showed that two main directions of transmission may have to be considered:

1. transverse: toward the hull

2. fore-and-aft: toward the machinery space buldheads.

It was also shown in paragraph 4.1.4 that the influence of the transverse structural elements (brackets and floors) as well as of the longitudinal girders cannot be disregarded.

A scaled physical model of the whole foundation and double bottom, with all eight sources delivering power, would be unnecessarily complex, making the interpretation of the results more difficult. Following the simplification principle (Paragraph 4.1.2), the foundation and double bottom can be regarded as built-up by sections, each one consisting of transverse plates (floors and brackets) welded to the plate structure between floors (bottom, girders, tank top, web and top plate), (See Figure 4.1.8). This can be assumed as a first idea for the physical model.

The longitudinal path and the interaction between the sources at the same top plate can be later investigated by successively adding sections and sources.

When considering the practical aspects listed in paragraph 4.1.2 (size weight, equipment limitation, and welding) simultaneously with the aspects concerning motion transformation, the scale of 1:2.5 was found to be ideal:

1. The minimum plate thickness in the model, 2.6 mm, is acceptable, when considering the resulting plate area and the expected deformation due to welding.

2. The upper frequency bound, 20 kHz (8 kHz in the ship) is not the highest value of interest, but high enough to include a signifi-

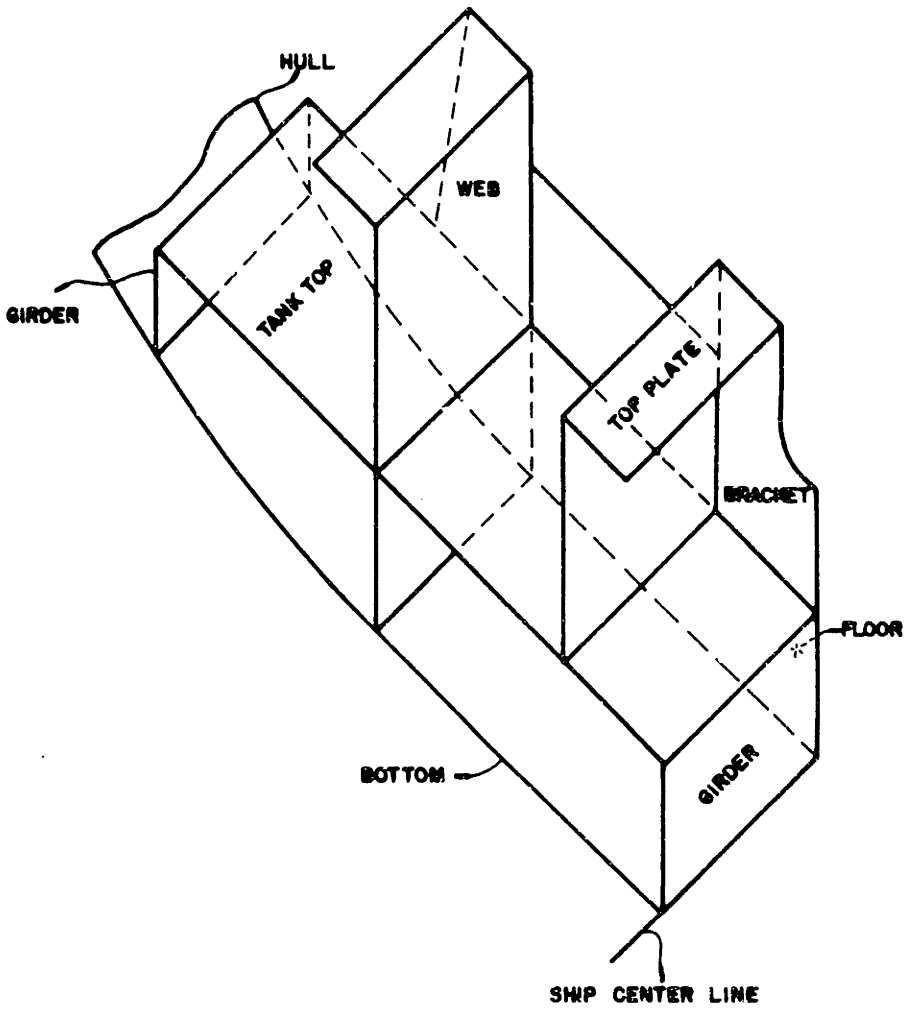

FIGURE 4.1.8: A FIRST CONCEPTION OF A PHYSICAL MODEL

cant frequency range within which energy transformations are expected to occur and to be important.

To save weight and have a smaller model to handle, the width can be restricted to the distance between the center line of the foundation and the junction line between the ship's hull and bottom. No significance is lost and no fundamental aspect is disregarded by doing this. This model is shown in Figure 4.1.9. The inclination of the bottom was eliminated and an average height for the longitudinal girders was adopted making the model's construction and handling easier. Its study can be understood as the first step of an analysis of vibration transmission from the diesel engine through its foundation and the ship's double bottom structure. This basic model can be:

1. Extended in both directions to allow the investigation of alternative transmission paths and of the resulting effect of adding other sources, including the interaction between them and the influence of their positions.

2. Made more complex by gradually adding details or important aspects subject to a separate investigation, such as the stiffeners, structural openings and the tank fluid load, to allow a better understanding of their impact when incorporated to the model.

Table 4.1.5 summarizes the geometrical characteristics of each plate (scale 1:2.5). The values of modal densities are also included in this table.

1 - TOP PLATE

2 - WEB

3 , 4 - TOP TANK

5 , 12 - GIRDERS

6 , 7 - BOTTOM

8 , 9 - BRACKETS

10 , 11 - FLOOR

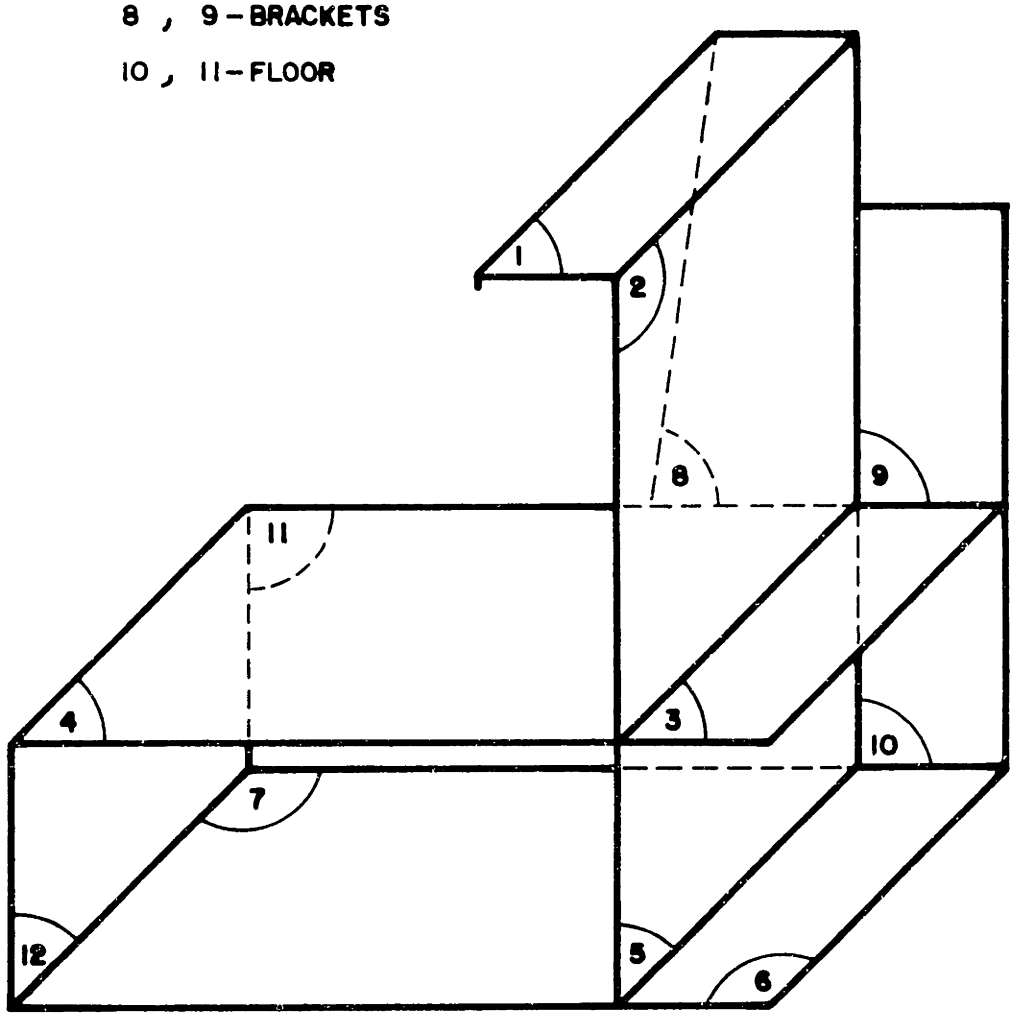

FIGURE 4.1.10: THE BASIC PHYSICAL MODEL

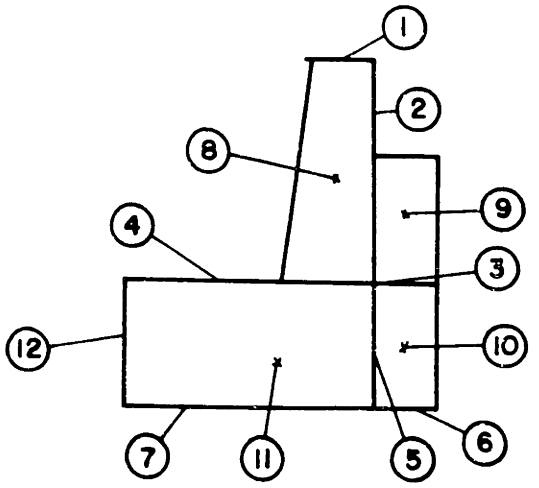

PLATE		THICKNESS (MM)	AREA (M^2)	DIMENSIONS (MM)	WEIGHT (Kg)	MODAL DENSITY ($\times 10^3$)	
						BEND	IN-PLANE
1	TOP	8.2	0.077	178X432	5.335	3.1	—
2	WEB	3.3	0.225	584X432	6.654	22.2	$0.2\times10^{-3}f$
3	TANK TOP	2.6	0.088	203X432	1.698	11.2	$0.8\times10^{-4}f$
4	TANK TOP	2.6	0.329	762X432	6.624	41.8	$0.3\times10^{-3}f$
5	LONG GIRDER	3.3	0.143	330X432	3.717	14.1	$0.12\times10^{-3}f$
6	BOTTOM	3.3	0.088	203X432	2.107	8.6	$0.8\times10^{-4}f$
7	BOTTOM	3.3	0.329	762X432	8.154	32.3	$0.3\times10^{-3}f$
8	BRACKET	3.3	0.126	178X254X584	3.306	12.4	$0.11\times10^{-3}f$
9	BRACKET	3.3	0.077	381X203	2.027	7.6	$0.07\times10^{-3}f$
10	FLOOR	3.3	0.067	203X330	1.778	6.6	$0.06\times10^{-3}f$
11	FLOOR	3.3	0.251	762X330	6.668	24.7	$0.22\times10^{-3}f$
12	LONG GIRDER	3.3	0.143	330X432	3.717	14.1	$0.12\times10^{-3}f$

TABLE 4.1.5: BASIC MODEL-PLATES CHARACTERISTICS

Based on the values of modal density in Table 4.1.5, one can infer that, for some frequency bands, it is expected:

1. Interaction between subsystems with a small number of modes:
2. Interaction between subsystems with a small number of modes and subsystems with a large number of modes.

In both cases, averaged SEA parameters may not lead to the most accurate prediction. This is discussed in Appendix A.

To determine bounds for SEA applications to connected structures was among Swift's objectives [23]. He analyzed the bending energy transmission between welded plates. The suggested lower bound (in terms of minimum number of modes) and upper bounds (related to modal overlapping) are presented in Appendix A. For a multi-joint structure it was suggested that those limits should be determined from the elements in the major transmission paths.

For the physical model, Figure 4.1.9, it is more than probable that the top plate and web fulfill this condition. Applying Swift's criteria, the following limits result:

$$f_{min} = 8375 \text{ Hz}$$

$$f_{max} = 10000 \text{ Hz} \quad \text{, for an internal loss factor of } \eta = 0.004$$

$$f_{max} = 50000 \text{ Hz} \quad \text{, (with adjustment)}$$

The lower bound is a very interesting value since it is much higher than 5 kHz (2 kHz full scale), a frequency above which in-plane motions in the web are expected to be significant (in accordance with the principles discussed in paragraph 4.1.4). Swift's work also suggests that the SEA predictions below 5 kHz (less than four flexural modes at the top plate) will be less accurate than 2 dB. In addition, this model offers different paths for energy

transmission and therefore constitutes a special challenge for SEA, despite being a very basic model.

As mentioned in Chapter 2, this work's objective is not only to verify the applicability of SEA parameters (by comparing analytical predictions and experimentally determined energy levels), but also to understand the vibration transmission (using SEA principles). In considering the model as a whole, the results may be more difficult to interpret. Therefore, following the principle outlined in paragraph 4.1.2, the basic model will be considered as built-up by parts. The top plate is the starting point and the other plates are added in an appropriate sequence. A special attention will be given to the bottom plates, which are in direct contact with the sea in an actual situation. In the basic model, the bottom plates can be considered as the last elements in the transmission paths from the top plate.

This approach leads to intermediate or sub-models. Through their analysis the vibration transmission can be better understood, especially when motion transformation may occur. The sub-models are presented in paragraph 4.5 and their conception is based on the discussion of this paragraph and on the SEA parameters, analyzed in paragraphs 4.2 and 4.3.

The discussion (related to the expected number of modes) associated with experimental convenience (use of only one shaker -- See Chapter 5), supported the choice of 630 Hz as the lower center frequency for this work. The frequency interval (630- 20000 Hz) is therefore large enough to include frequency ranges in which it is expected that:

1. A predominant flexural transmission and not the most accurate SEA predictions will occur (630 - 5000 Hz)
2. Energy transformations will be significant (5000 - 20000 Hz).

4.2 Determination of the Loss Factors and Mode Count

4.2.1 Dissipative Loss Factors

The fundamental aspects of the main dissipative mechanisms associated with a structure as well as those concerning the determination of the loss factors are summarized in Appendix A, based on Lyon [15] and Plunt [6]. As discussed in this appendix, they are usually obtained experimentally.

The decay method is used in this thesis to determine the loss factor of each individual plate of the model. The choice was based on the following aspects:

1. Decay is accepted as a method of standard practice and it appears to be the one utilized in all applications of SEA to SBN transmission on ships;
2. It is simpler than the steady state methods;
3. The required laboratory equipment is available.

Specific aspects related to both decay and steady state methods as well as to the difficulties associated with them are presented in Appendix A.

Each plate was excited by a hammer impact. The time history of the magnitude and log-magnitude of the signal from an accelerometer attached to the plate was recorded after passing through a third octave band filter.

The impact was monitored by a FFT spectral analyzer in order to ensure the clearest time history (force peak) and the most flat force auto-spectrum possible (within 3 dB), inside the entire third octave band. The analyzer was also used to obtain:

1. The time history of the acceleration signal from the third octave band filter output (after passing through its digital filter; double filtering).

2. The transfer functions between force and acceleration for the lower frequency bands and, so,

    (a) Determine the number of modes inside the band (mount count).

    (b) Identify the heavily and weakly damped modes to better interpret the decay responses.

The loss factor for each impact was determined from the initial slope of the time history of the logarithm of the acceleration magnitude. As a verification, loss factors were also determined by using the time interval for magnitude to decay by 50 percent (6 dB). The values obtained were consistent with those resulting from the analyzer records.

At the lower frequencies, some tests were conducted by using a band limited excitation, through a shaker. From the transfer function between the force and acceleration at the driving point, the modal damping was obtained for each individual mode from the analyzer (directly and by using its zoon and Inverse Fourier Transform Technique). This helped to better identify the mode contribution. Despite the resolution not being very high, the resulting loss factors were in reasonable ($\pm$ 20%) agreement with those determined through decay. It appears to be a promising technique to use when the modes are well spaced [15], especially with the increased resolution being provided in some new equipment.

The loss factor for each plate was determined by averaging the results from at least eight impacts at different plate locations. Initially the

accelerometer was moved around, but the best position was found to be at a plate corner.

To minimize the energy losses via the supports, the plates were hung from the ceiling by very thin nylon lines. These lines were used in order to create an impedance mismatch (between plate and support), resulting from the difference in mass and material, and, therefore, to block more efficiently the energy flow to the supports. As noticed by Swift [23], the use of piano wires is not efficient in avoiding such losses.

The loss factors of a naked plate (without added damping) was found to be very low when compared with those reported in different applications of SEA, especially at the lower frequencies. Above the coincidence frequency, the main contribution to the loss factors was clearly from radiation.

As discussed in Appendix A, the loss factor measured with the individual plates decoupled from the structure may not be the most representative of the actual situation, where other dissipative mechanisms are present (such as joint dissipation and edge radiation). The acoustical space where the plates radiate also changes.

One basic objective of this thesis is to verify the applicability of the SEA parameters in predicting energy levels. Therefore, it is important to try to minimize the uncertainties introduced by unmeasured effects.

Constrained layers of damping material were applied to each plate in order to increase the internal damping and reduce the overall variation of the loss factors from the uncoupled to the actual condition, and also reduce the influence of any losses due to the support system. In addition, the constrained layers were used to obtain values of loss factors consistent

with references, such as [4,6,9,10,11]. Figure 4.2.1 shows a curve for welded plates from Lyon [31]. This curve was utilized as the basic reference, scaled to be consistent with the model. In obtaining the loss factors, the goal was to have values above this curve, not only because it is important to minimize the variation from uncoupled to coupled condition, but also because the dissipation in the ship double bottom is supposed to be high (due to the interaction with the sea water and tank fluid loads). However, it was very difficult (with the material used) to have the loss factors at lower frequencies (below 4000 Hz) increased to the level of the reference curve. The opposite effect was verified at higher frequencies (the values of the curve were obtained with very few layers of damping material). These results are consistent with Swift [23]. For most of the plates, the loss factors at lower frequencies seem to be in agreement with the values suggested by Budrin and Nikiforov [9] and Jensen [11]. However, based on reference [31], it may be possible that the meaasured loss factors up to 4 kHz are an underestimation of the actual coupled situation.

These aspects supported the decision to use the MIG (Metal Inert Gas) process in order to minimize losses due to welding.

Eighty percent of the bottom plate area was covered with the damping material and the resulting loss factors were used as reference. Values of the same order or higher were obtained for the longitudinal girders and floors. A lighter damping was applied to the brackets, web and tank top. The measured values (average) for each plate are shown in Table 4.2.1.

It is important to emphasize that all that has been presented is related to loss factors associated with the flexural motions of the plates.

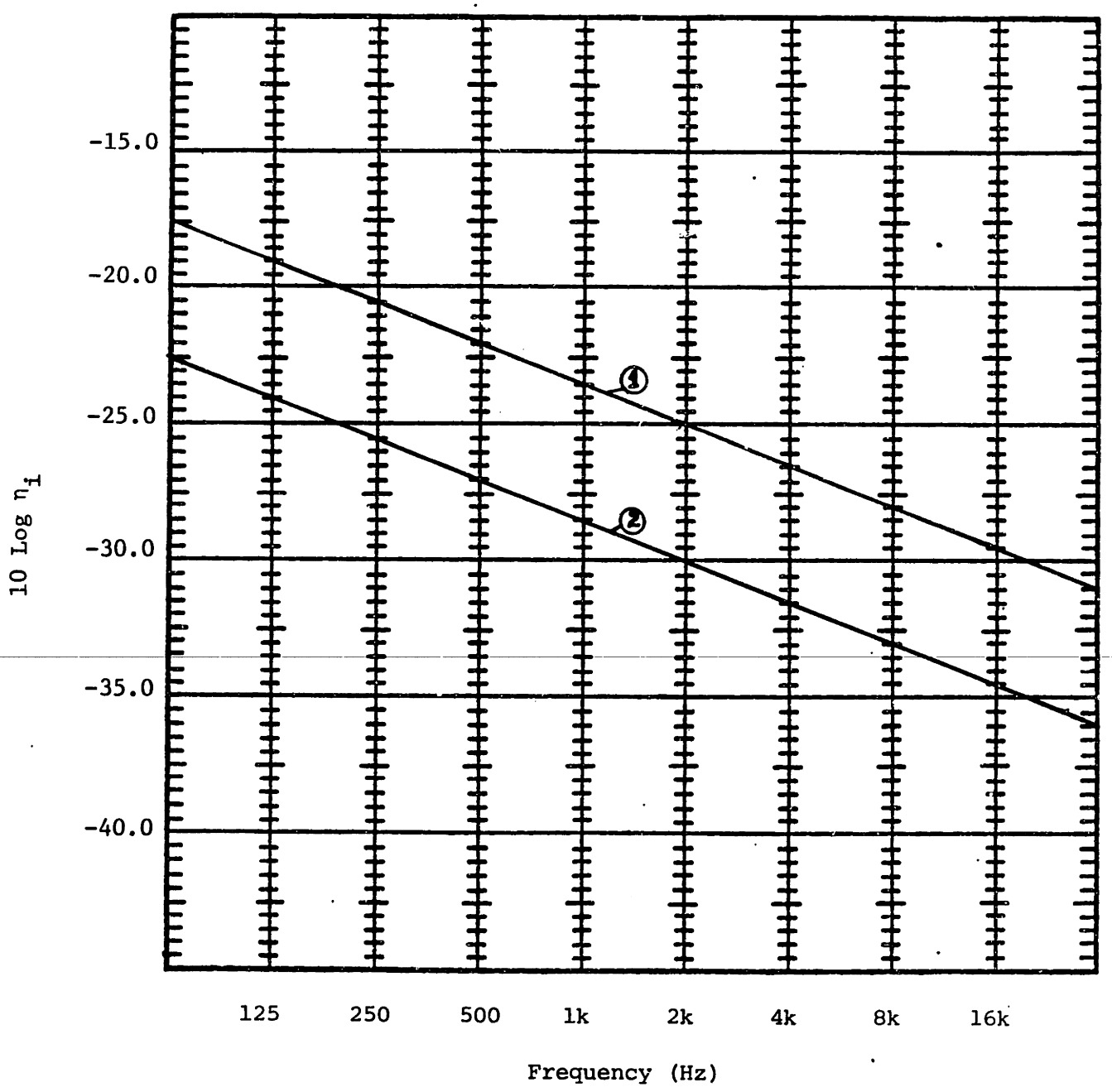

FIGURE 4.2.1: LOSS FACTORS FOR WELDED PLATES WITHOUT ADDED DAMPING, FROM REFERENCE [31]

① : Bending, ② : In-Plane

1/3 OCTAVE BAND (kHz)	TOP PLATE (1)	WEB (2)	TANK TOP (3)	TANK TOP (4)	LONG GIRDER (5,12)	BOTTOM PLATE (6)	BOTTOM PLATE (7)	BRACKET (8)	BRACKET (9)	FLOOR (10)	FLOOR (11)
0.63	1.30	1.60	1.00	1.00	3.20	1.45	1.50	1.00	1.05	3.85	4.05
1.25	1.85	2.45	1.30	1.30	4.40	2.40	2.35	1.65	1.75	3.90	3.95
2.0	2.75	2.20	1.00	1.30	3.70	2.80	2.80	2.00	2.00	3.20	3.30
2.5	2.80	2.70	1.60	1.60	4.20	3.40	3.40	2.25	2.40	3.45	3.60
3.15	2.90	3.60	2.10	2.10	4.50	4.00	3.95	2.70	2.80	4.15	4.35
4.0	2.95	4.60	2.60	2.50	5.60	5.70	5.70	3.15	3.35	5.55	5.60
5.0	2.75	4.20	4.00	4.40	5.40	5.50	5.55	2.60	2.70	5.35	5.40
6.3	2.50	4.00	3.50	3.90	5.50	5.60	5.60	2.80	2.80	5.20	5.30
8.0	2.25	4.20	3.70	3.80	5.00	5.10	5.15	2.30	2.40	4.65	4.80
10.0	1.75	3.90	4.00	4.20	5.60	5.70	5.70	2.20	2.30	4.20	4.25
12.5	1.70	4.30	4.30	4.10	5.90	5.90	5.90	2.00	2.10	4.80	4.70
16.0	1.65	4.60	4.10	4.00	6.00	6.20	6.20	1.90	1.95	4.70	4.80
20.0	1.60	4.30	4.30	4.10	5.70	5.80	6.00	1.70	1.75	4.00	4.00

Fig. 4.2.1
Dissipative Loss Factors (x 10^3)

With respect to in-plane motions, no reference to measurements of loss factors were found. The values used herein were obtained from Lyon [31]. Since the damping layers, in principle, add a constraint to the in-plane motions, a correction factor was used, based on the comparison between the values for naked plates, Figure 4.2.1.

One important aspect to consider is the impact on the SEA predictions of the accuracy of the loss factor. This depends on the comparison between loss factors and the related coupling loss factors. In terms of energy level, when the coupling loss factors are stronger, they will tend to dictate the energy sharing. But an inaccuracy in damping can directly affect the estimation of the power dissipation, and important variable in SBN transmission. Attention will be given to this aspect in Chapter 5 and in paragraph 4.3.5.

4.2.2 Mode Count

The mode count (flexural modes) in each third octave band was determined experimentally only when the number was equal or less than twelve. The count was obtained during the impact tests, as mentioned in the previous paragraph. For some of the smaller plates, it was checked by exciting the plates with a sinusoidal wave signal and by counting the resonances on an oscilloscope screen. Table 4.2.2 shows the results for each individual plate.

Modal density formulations were used to estimate the number of flexural modes, when they were greater than twelve, and also to estimate the number of in-plane modes in each plate, per third octave band.

1/3 Octave Band (kHz)	Top Plate (1)	Web (2)	Tank Top (3)	Tank Top (4)	Long. Girder (5,12)	Bottom Plate (6)	Bottom Plate (7)	Bracket (8)	Bracket (8)	Floor (9)	Floor (10)
0.63	1	2	2	5	2	1	4	2	2	1	4
1.25	3	8	4	12	4	3	10	6	4	3	6
2.0	2	12	4	↑	6	3	↑	5	3	4	9
2.5	2	↑	6	↑	8	5	↑	7	4	4	↑
3.15	3	↑	8	↑	10	6	↑	9	6	5	↑
4.0	3	↑	10	↑	12	8	↑	10	8	7	↑
5.0	3	↑	↑	M.D.	↑	9	↑	↑	9	10	↑
6.3	5	M.D.	↑	↑	↑	12	M.D.	↑	11	↑	↑
8.0	7	↑	↑	↑	↑	↑	↑	↑	↑	↑	M.D.
10.0	8	↑	M.D.	↑	↑	↑	↑	M.D.	↑	↑	↑
12.5	9	↑	↑	↑	M.D.	M.D.	↑	↑	M.D.	M.D.	↑
16.0	12	↑	↑	↑	↑	↑	↑	↑	↑	↑	↑
20.0	M.D.	↓	↓	↓	↓	↓	↓	↓	↓	↓	↓

TABLE 4.2.2: NUMBER OF FLEXURAL MODES IN EACH PLATE, RESULTING FROM MODE COUNT (EQUAL OR LESS THAN 12)

M.D.: Number estimated based on modal density

4.3 Determination of the Coupling Loss Factors

4.3.1 General Expression

As discussed in Appendix A, an approach based on transmission losses is the most widely used to evaluate the coupling loss factors for systems connected along a line. This approach is conceptually simple and also appropriate in describing the coupling when motion (or energy) transformations occur at the joint.

The basic expression used to determine the coupling loss factor is:

$$\eta_{ij} = \frac{c_g L_{ij}}{2\pi^2 f A_i} < \tau_{ij}(\theta) \cos\theta >_{\theta_t} \qquad (4.3.1)$$

where

c_g = group or energy velocity

L_{ij} = common length

A_i = area of subsystem i

$\tau_{ij(\theta)}$ = transmission coefficient from subsystem i to subsystem j.

θ = angle of wave incidence at the junction line

θ_t = total range of incident angles

$<\tau_{ij}(\theta) \cos(\theta)>_{\theta_t} = \bar{\tau}_i$, average transmission coefficient between i and j.

The transmission coefficient is defined as the ratio of transmitted to incident energy at the joint and, in general, depends on the direction (θ).

Expression (4.3.1) was derived by Lyon [15], based on a wave description for the vibrational energy of the systems and on the following primary assumptions [15,32]:

1. The intensity of energy is equal in all directions.

2. Waves travelling in different directions are temporarily incoherent.

When measuring absorption coefficients on plates, Heckl [33] indirectly derived expression (4.3.1) by analogy with room acoustics. He applied Sabine's equation to bending waves on plates and considered the two-dimensional mean free path as derived by Kosten [34].

The derivation of expression (4.3.1) is also presented by Swift [23], based on the energy decay of a two-dimensional field.

When the coupling between two systems has two or more values of $\bar{\tau}$ associated with it, (4.3.1) becomes [23]:

$$\eta_{ij} = \frac{c_g}{2\pi^2 A_i f} \Sigma L_{ij} \bar{\tau}_{ij} \qquad (4.3.2)$$

where L_{ij} is the common length related to each $\bar{\tau}_{ij}$. The coupling between the web and the brackets, in the model (Figure 4.1.9), is a good example of when (4.3.2) is applicable.

Basically, in all derivations, a diffuse or reverberant field is assumed to exist in each coupled system. The implication of such assumption on SEA applications utilizing (4.3.1) has been already mentioned in paragraph 4.1 and is discussed in Appendix A.

4.3.2 The General Problem

The physical model is a welded steel plate-like structure. As discussed in paragraph 4.1, for the higher frequency bands (f>5000 Hz), it is expected that energy transmissions and transformations associated with flexural and in-plane motions are going to occur. Therefore, in each plate, three SEA

subsystems (groups of modes) are identified, associated with bending (B), longitudinal (L) and transverse shear (T) motions. In terms of transmission mechanisms, this is the most general case and the coupling loss factors between any two of these SEA subsystems have to be determined. The simplest case occurs when only bending energy transmission is expected to be present.

The general case is schematically illustrated in Figure 4.3.1 for the interaction between two plates. The plate area, the coupling length, and energy velocities -- variables in expression (4.3.1) -- are readily available. The first two are directly obtained from the model. The energy velocity for in-plane motions is a function of the material properties, and in the case of flexural motions it is also a function of frequency and plate thickness (h).

$$c_g \text{ (bending)} \simeq 2.634 \, (f \, c_L h)^{1/2} \tag{4.3.3}$$

$$c_g \text{ (longitudinal)} = c_L \tag{4.3.4}$$

$$c_g \text{ (transverse shear)} = c_T \tag{4.3.5}$$

where:

c_L = longitudinal wave phase velocity = $(E/(\rho(1-\nu^2)))^{1/2}$ (4.3.6)

c_T = transverse shear wave phase velocity = $(G/\rho)^{1/2}$ (4.3.7)

As

$$G = E/(2(1+\nu)) \tag{4.3.8}$$

$$c_T = ((1-\nu)/2)^{1/2} c_L \tag{4.3.9}$$

By substituting (4.3.3), (4.3.4), (4.3.5) and (4.3.9) in (4.3.1)

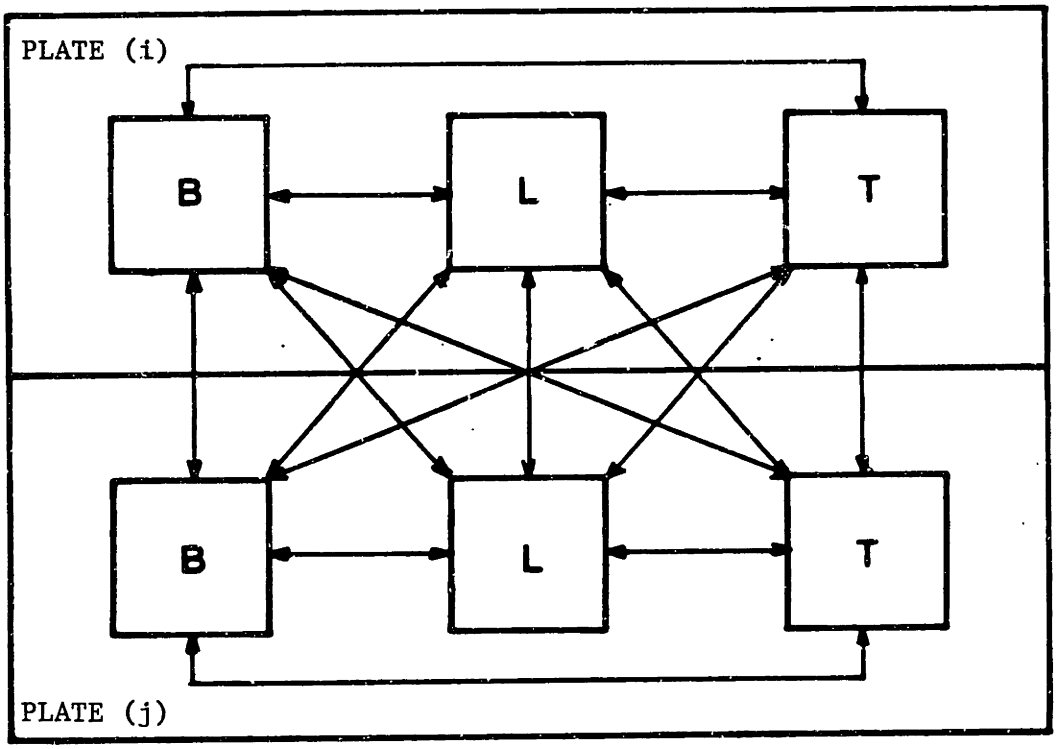

Bending-to-	Bending - $\eta_{ij}(BB)$ Longitudinal - $\eta_{ij}(BL)$ Shear - $\eta_{ij}(BT)$	Shear-to-	Shear - $\eta_{ij}(TT)$ Bending- $\eta_{ij}(TB)$ Longitudinal - $\eta_{ij}(TL)$
Longitudinal	Longitudinal - $\eta_{ij}(LL)$ Bending - $\eta_{ij}(LB)$ Shear - $\eta_{ij}(LT)$		

$i = 1,2 \qquad j = 1,2$

FIGURE 4.3.1: COUPLING BETWEEN SEA SUBSYSTEMS OF TWO PLATES
-- GENERAL CASE --

the coupling loss factor between bending or longitudinal or shear in plate i and any subsystem in plate j can be written as a function of c_L, h_i, L, A_i and $\bar{\tau}_{ij}$.

Bending: $$\eta_{ij}(B) \cong 0.1362 \left(\frac{L_{ij}}{A_i}\right) \left(\frac{c_L h_i}{f}\right)^{1/2} \bar{\tau}_{ij}(B) \qquad (4.3.10)$$

Longitudinal: $$\eta_{ij}(L) = 0.51 \left(\frac{L_{ij}}{A_i}\right) \left(\frac{c_L}{f}\right) \bar{\tau}_{ij}(L) \qquad (4.3.11)$$

Transverse Shear: $$\eta_{ij}(T) \cong 0.51 \left(\frac{1-\nu}{2}\right)^{1/2} \left(\frac{L_{ij}}{A_i}\right) \left(\frac{c_L}{f}\right) \bar{\tau}_{ij}(T) \qquad (4.3.12)$$

To evaluate η_{ij} between any two plates of the model, it is, therefore, necessary to determine the related $\bar{\tau}_{ij}$.

4.3.3 Average Transmission Coefficients

The more general problem occurs when four plates have a common joint and when the three motions or wave fields are considered.

Cremer [35] investigated the wave transmission and attenuation at the junction of two concrete walls at right angles. This study was later reviewed, generalized for any two structures, and included as a section of reference [36]. The problem of oblique bending incidence (diffuse field), then, was fully analyzed. The transmission and reflection coefficients (bending-bending, bending-longitudinal, and bending-shear) were determined as a function of the incident angle.

The four-plate problem was first analyzed by Rudrin and Nikiforov [37], but for normal incidence only. Kihlman [38, 39] investigated the wave transmission through a four-plate structure considering oblique bending wave incidence and the generation of in-plane waves at the joint. As he stated,

the calculations were similar to those carried out by Cremer [35]. Considering Figure 4.3.2, he assumed:

1. Thin-plate theory ($\lambda > 6h$).
2. Incident bending wave in plate 1.
3. The same thickness and material in the opposite plates (1 and 3; 2 and 4).

To simplify the calculations, Kihlman took advantage of the symmetry and of the fact that only bending waves are transmitted to plate 3. The boundary conditions to be satisfied along the joint were basically: continuity of linear and angular displacements, equilibrium of moments about the y axis, and the equilibrium of forces in the z direction. An interesting point is that Kihlman combined the longitudinal and transverse shear waves in plates 2 (and 4) and expressed them in terms of an impedance relating an in-plane force to the displacement in the z-direction. This differs from Cremer's approach to the two-plate problem [36], where the in-plane waves were treated individually, making it necessary to consider another boundary condition: equilibrium of forces along the y axis.

Kihlman's approach was utilized by Craik [24], whose work was mainly dedicated to thick plates (rotary inertia and shear effects were included). In his main calculations, in-plane waves were not taken into account, a decision based on previous results by Gibbs [22].

Swift [23] also investigated the four-plate problem, examining the three wave fields and bending incidence in one of the plates. He assumed that all plates were made of the same material, but could have different thicknesses. The two in-plane waves were treated separately, as by Cremer [35, 36]. The

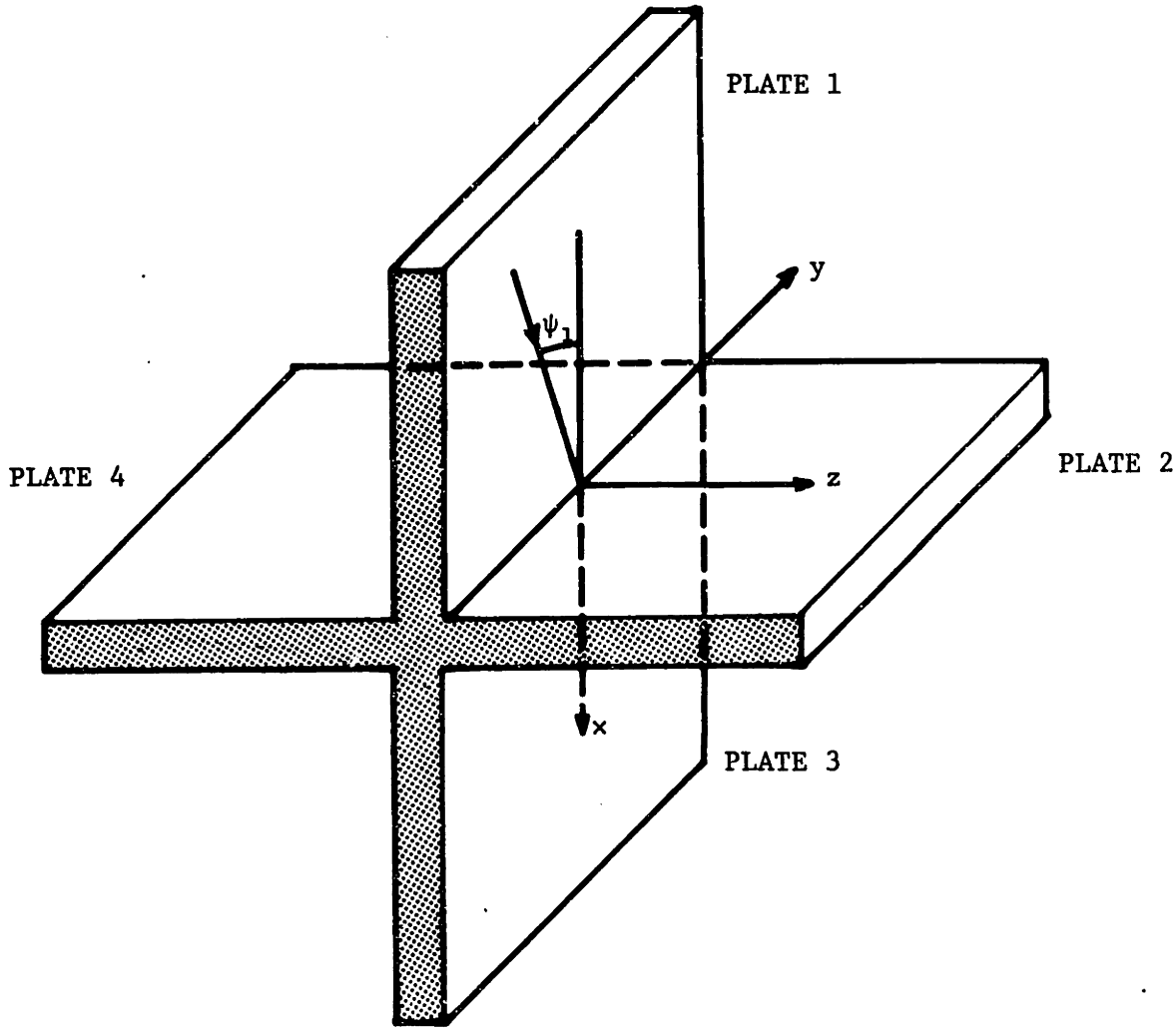

FIGURE 4.3.2: COORDINATE SYSTEM USED BY KIHLMAN TO INVESTIGATE THE FOUR-PLATE PROBLEM, CONSIDERING OBLIQUE INCIDENCE AND THE GENERATION OF IN-PLANE WAVES

basic difference between Swift's approach and those undertaken by Kihlman and Cremer lies in the assumed boundary conditions at the joint. Despite considering oblique incidence (a two-dimensional problem), Swift established the boundary conditions based on beam flexural and longitudinal analysis, referring to a unit width of the plates in the plane normal to the junction line. He also assumed that the displacement along this junction should be equal to zero, differing from Cremer who postulated a continuity of displacement and a force equilibrium along this line.

In this thesis, the transmission coefficients are derived using Cremer's [36] conceptual approach for the two-plate problem without any attempt at simplification. A thin-plate theory is used since the plate wave length is always greater than 6h for all plates in the whole frequency range. As in Swift's work [23], the four plates are considered to be of the same material (steel), but allowed to have different thicknesses, and the three wave fields are treated individually, except that two-dimensional wave expressions are utilized. Swift's reference system, Figure 4.3.3, is also adopted. The boundary conditions along the junction line are those specified by Cremer [36], and two-dimensional expressions are used for bending moments and forces (longitudinal, shear, edges), in terms of displacement as in [36, 40, 41]. Bending, longitudinal and shear wave incidence were analyzed individually. The details of the derivations are shown in Appendix D.

Figure 4.3.4 illustrates schematically the work carried out. A unit amplitude wave coming from plate 1 generates at the joint in each plate:

1. Three propagating waves (bending, longitudinal and shear), transmitted (2,3,4) and reflected (1).

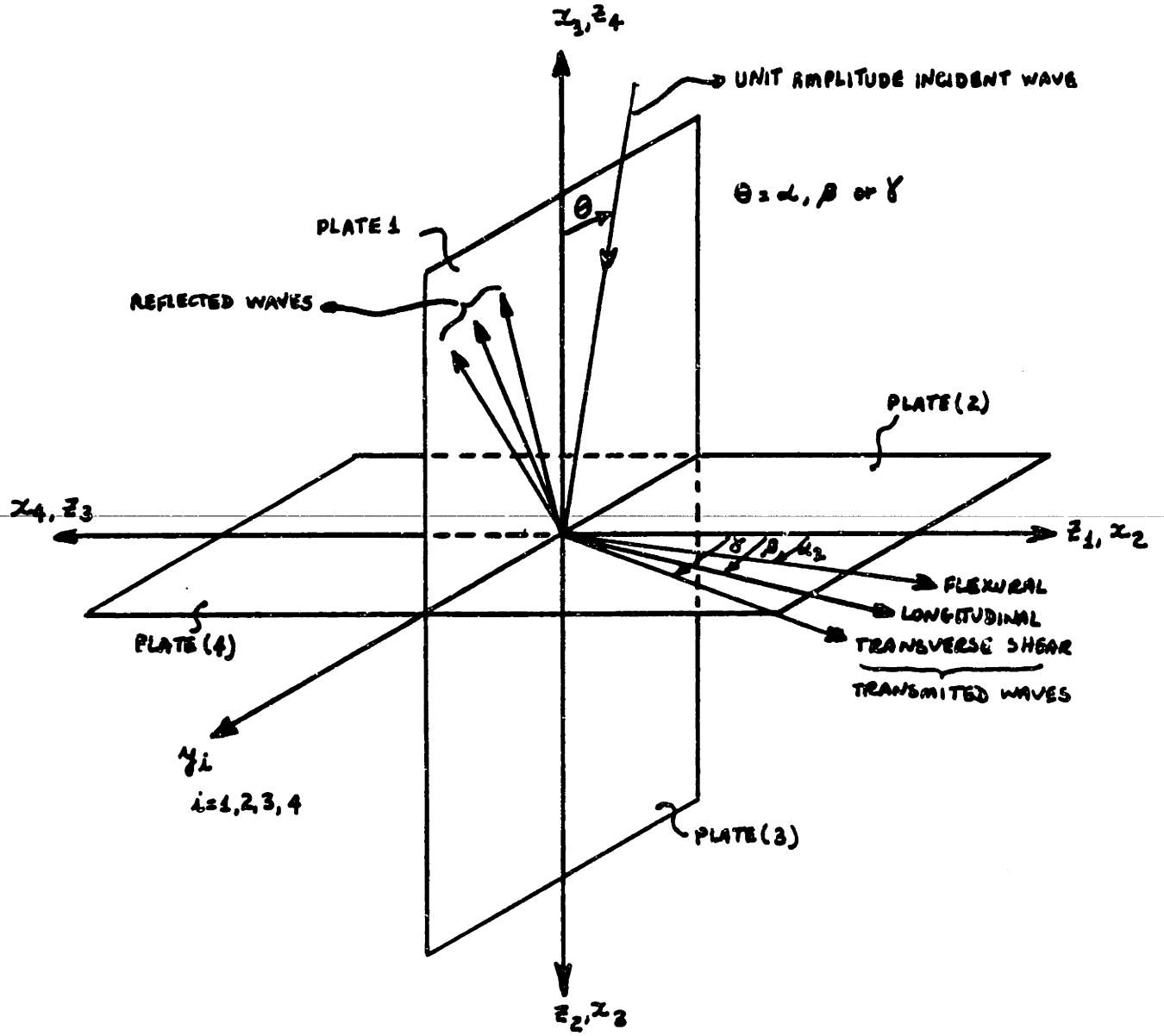

FIGURE 4.3.3: COORDINATE SYSTEM - FOUR PLATES AT A COMMON JOINT - THREE WAVE FIELDS

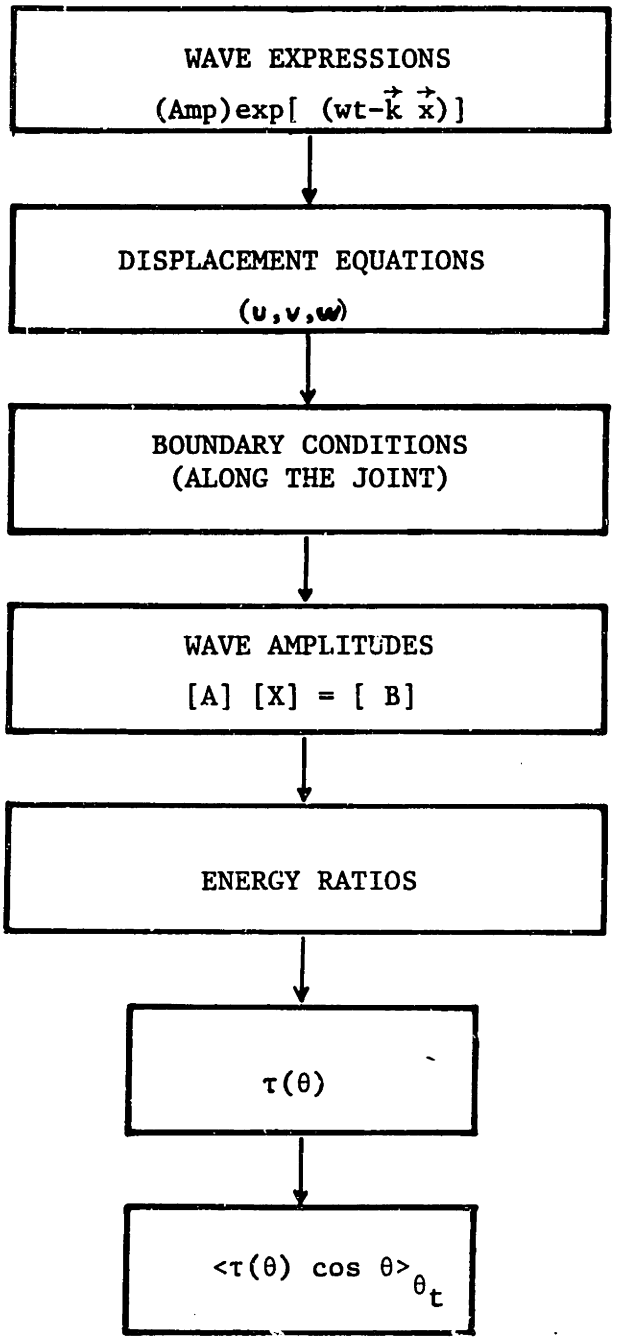

FIGURE 4.3.4: DETERMINATION OF THE AVERAGE TRANSMISSION COEFFICIENTS - BLOCK DIAGRAM

2. Non-propagating bending waves (near fields).

From the wave expressions, the displacement equations are obtained. The application of the boundary conditions results in a system of sixteen equations and sixteen unknowns (the travelling waves and near fields amplitudes). In matrix notation: [A][X] = [B]. Determining the amplitudes, the energy ratios (transmitted or reflected to incident) are an immediate consequence as are the transmission coefficients for each angle of incidence. Similar to the work carried out by Swift, a computer program (as explained in Appendix D) was developed to:

1. Set up matrix [A] and [B].
2. Solve linear equations with complex coefficients.
3. Calculate the transmission coefficients as a function of the incidence angle.

The two- and three-plate solutions are obtained by setting plate thicknesses to zero, as needed, in the four-plate problem.

Since no losses are assumed at the joint, energy conservation requires that:

$$\sum_{n=1}^{4} \tau_{1n}(BB) + \tau_{1n}(BL) + \tau_{1n}(BT) = 1 \qquad (4.3.13)$$

Equation (4.3.13) is used as a check on the computed values, and is always satisfied. Another check carried out was a comparison with Cremer's result for the two plates for bending incidence. Figure 4.3.5 shows the curves from Cremer [36] and those obtained from the computer program, for the same conditions. They are identical.

A separate computer program was developed to determine the transmission coefficient (τ^F) as a function of the angle of incidence for the cases when

Figure V/36[1] illustrates this behavior of the three transmission and three reflection efficiencies for the special case of $\beta^2 = 0.09$; conservation of energy demands that the sum of these efficiencies always is equal to unity:

$$\tau_{BB} + \tau_{BL} + \tau_{BT} + \varrho_{BB} + \varrho_{BL} + \varrho_{BT} = 1. \tag{358}$$

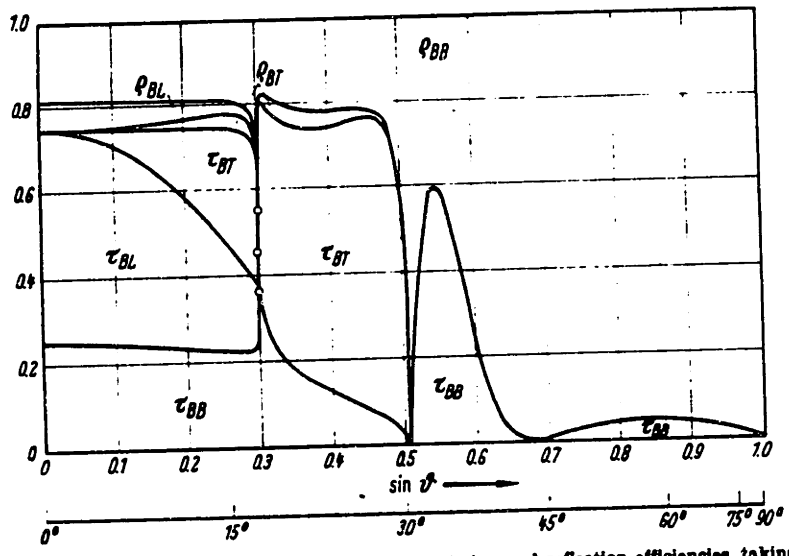

Fig. V/36. Variation with angle of incidence of transmission and reflection efficiencies, taking into account secondary longitudinal and transverse waves.

FIGURE 4.3.5a: FROM CREMER [36], page 406

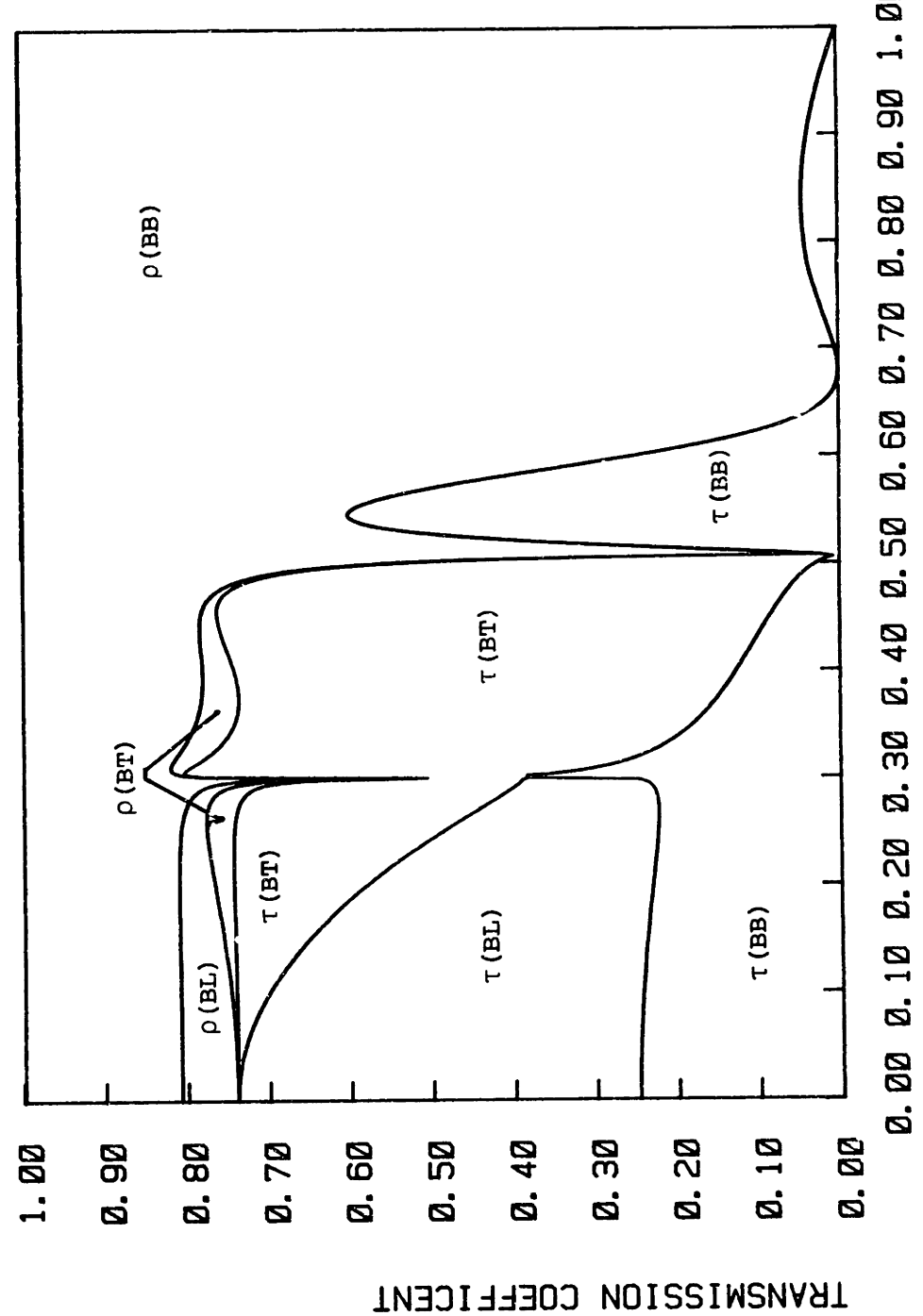

FIGURE 4.3.5(b): VARIATION WITH ANGLE OF INCIDENCE OF TRANSMISSION EFFICIENCIES TAKING INTO ACCOUNT SECONDARY LONGITUDINAL AND TRANSVERSE SHEAR WAVES, FROM COMPUTER PROGRAMS DEVELOPED BASED ON EQUATIONS DERIVED IN APPENDIX D -- TWO-PLATE JOINT, $\beta^2 = 0.09$, AS IN CREMER [36], Page 406

only flexural transmission is assumed. As discussed in Appendix D, the solution for pure flexural transmission can be derived from the more general equations. However, this was not found practical.

Figure 4.3.6 shows two curves of $\tau^F(\theta)$ (only bending) and $\tau(BB)(\theta)$ (three wave fields solution) for a two-plate joint, assuming bending incidence in plate 1.

To determine the integral values of $\tau(\theta)$ and hence the average transmission coefficients, programs based on Simpson's rule are used, having the previous programs as subroutines.

Figure 4.3.7 to 4.3.14 allow a comparison between average transmission coefficients of different types associated with typical joints identified in the physical model (L, Tee and Cross).

The largest differences between τ^F_{ij} and $\tau_{ij}(BB)$ occur at the higher frequencies (above 5 kHz) associated with the two-plate joint (Figure 4.3.7) and with two opposite plates, in a three-or four-plate joint (Figures 4.3.8 and 4.3.14). In these curves $\tau_{ij}(BB)$ may assume a value as low as 60% of τ^F_{ij}. In terms of transmission losses (10 log $1/\tau$), the differences (below 2 dB) are not very significant.

The generation of in-plane waves in the web from a bending incidence at the top plate (discussed in paragraph 4.1 and Appendix C) is illustrated in Figure 4.3.7. It shows the growing importance of the in-plane motions in the web as frequency increases. $\tau_{(BB)}$ is much higher than $\tau_{(BL)}$ and $\tau_{(BT)}$ at low frequencies (about 10 dB difference at 630 Hz). The three values are approximately the same at 12500 Hz. The difference is of about 3 dB at 5000 Hz, the frequency above which (as concluded in paragraph 4.1) the wave

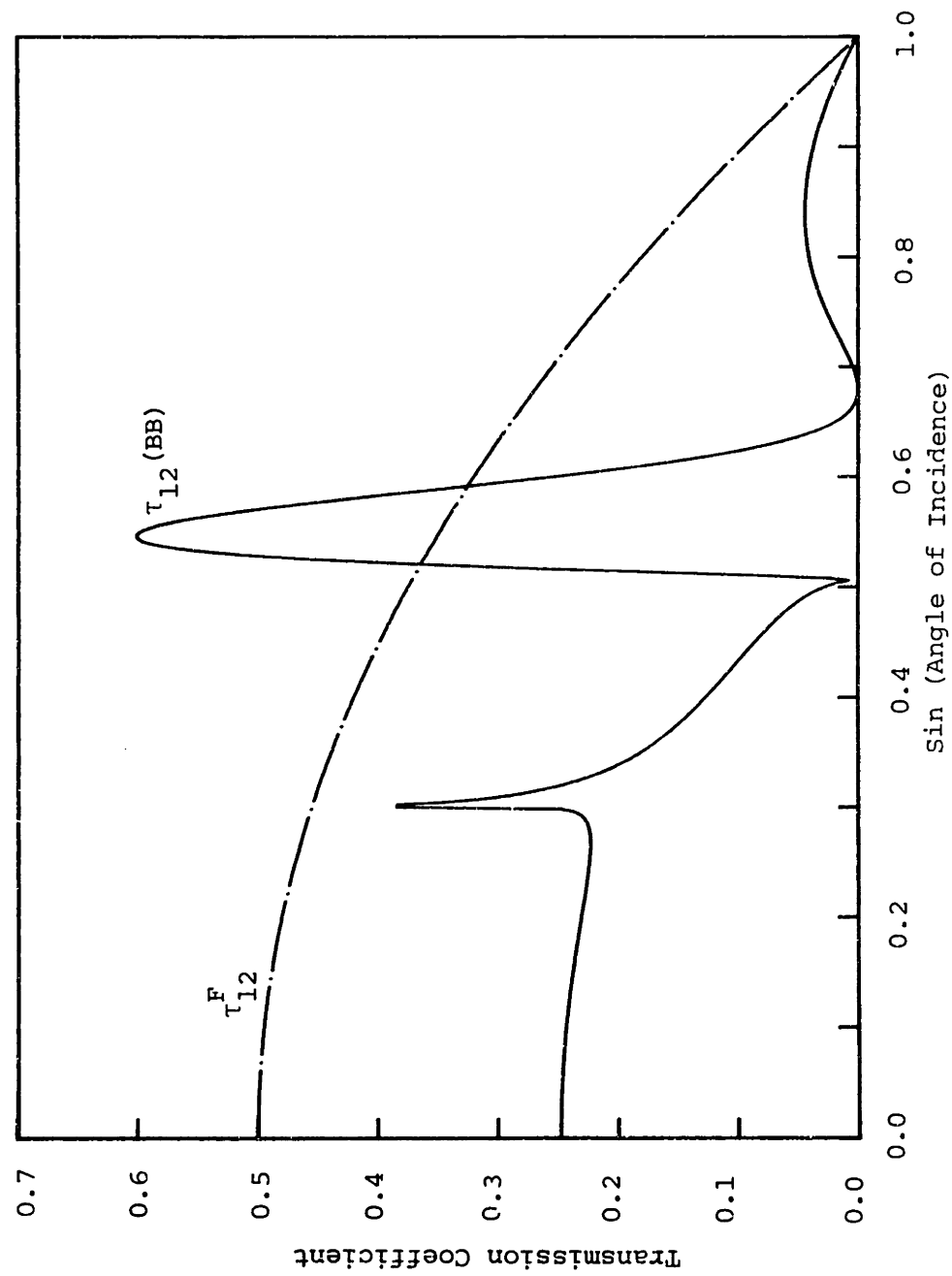

FIGURE 4.3.6(a): VARIATION WITH ANGLE OF INCIDENCE OF THE BENDING TRANSMISSION COEFFICIENTS BETWEEN (1 to 2) TWO PLATES OF SAME THICKNESS (19 mm) FOR f = 13900 Hz

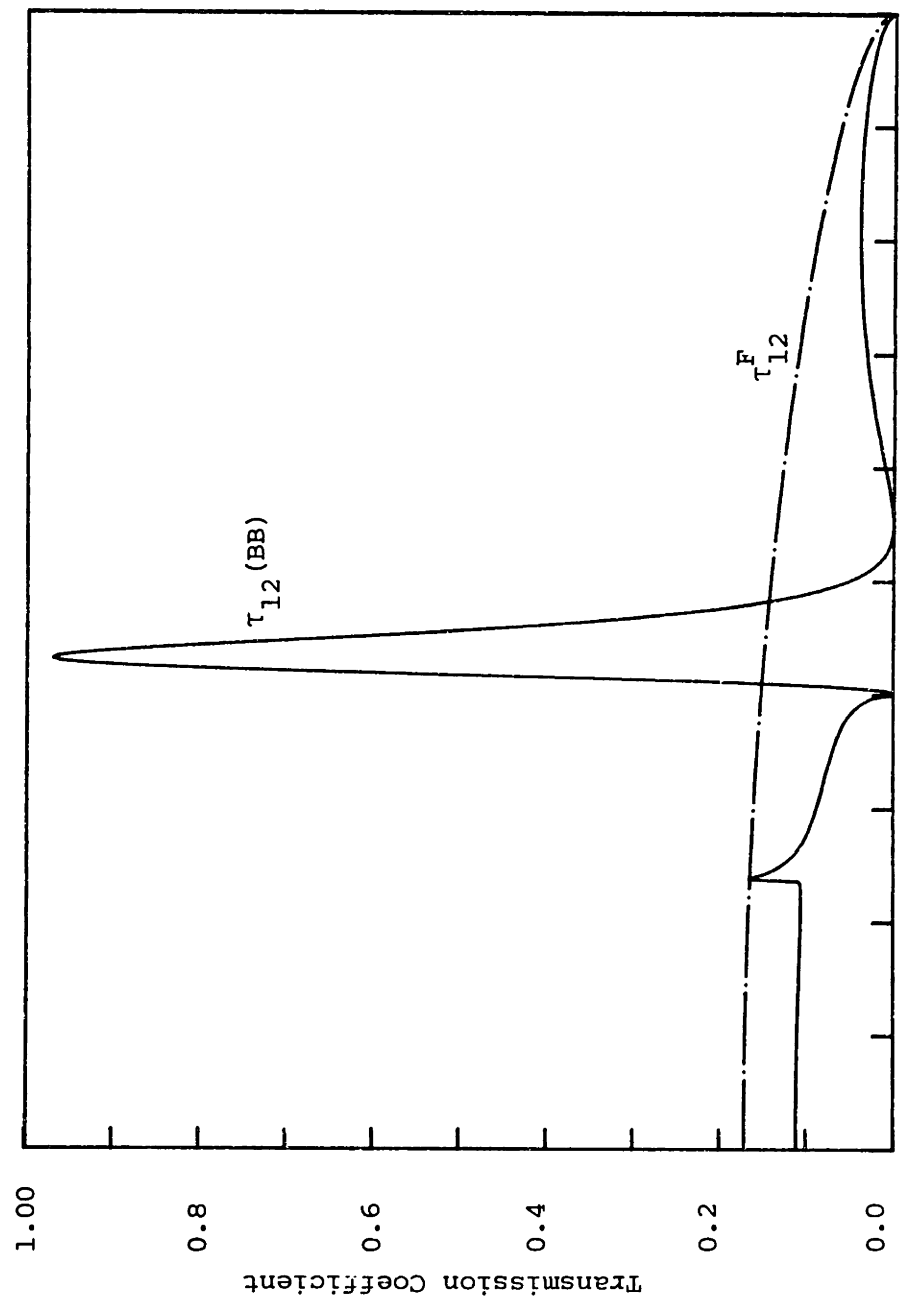

FIGURE 4.3.6(b): VARIATION WITH ANGLE OF INCIDENCE OF THE BENDING-TO-BENDING TRANSMISSION COEFFICIENTS - τ^F_{12} and τ_{12}(BB)-BETWEEN THE TOP PLATE (8.2mm) AND THE WEB (3.3 mm), FOR f = 20 kHz

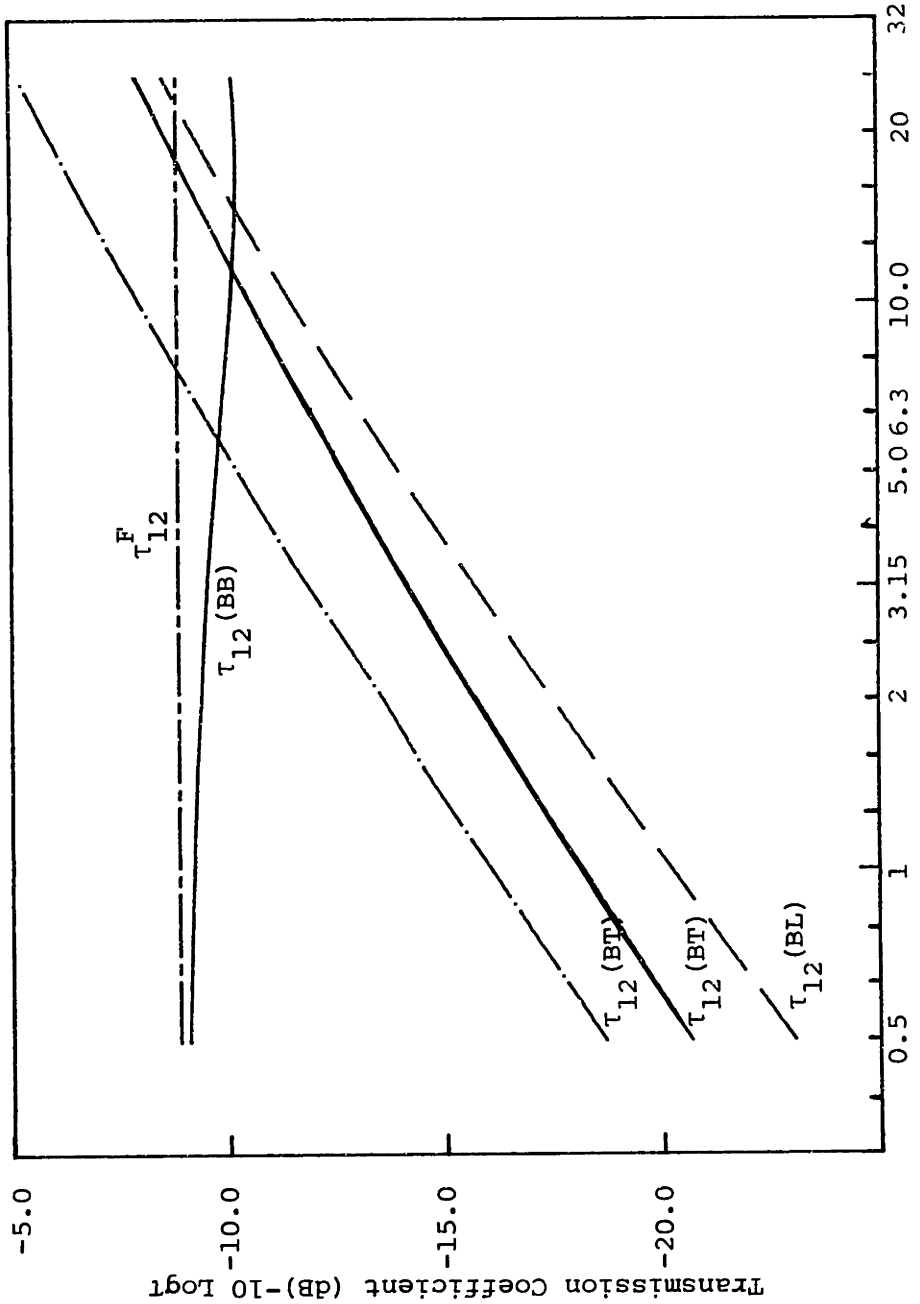

FIGURE 4.3.7: VARIATION WITH FREQUENCY OF THE AVERAGE TRANSMISSION COEFFICIENTS - τ_{12}^F, τ_{12}(BB), τ_{12}(BL), τ_{12}(BT) and τ_{12}(BP) - BETWEEN THE TOP PLATE (1) AND THE WEB (2) -- L JOINT

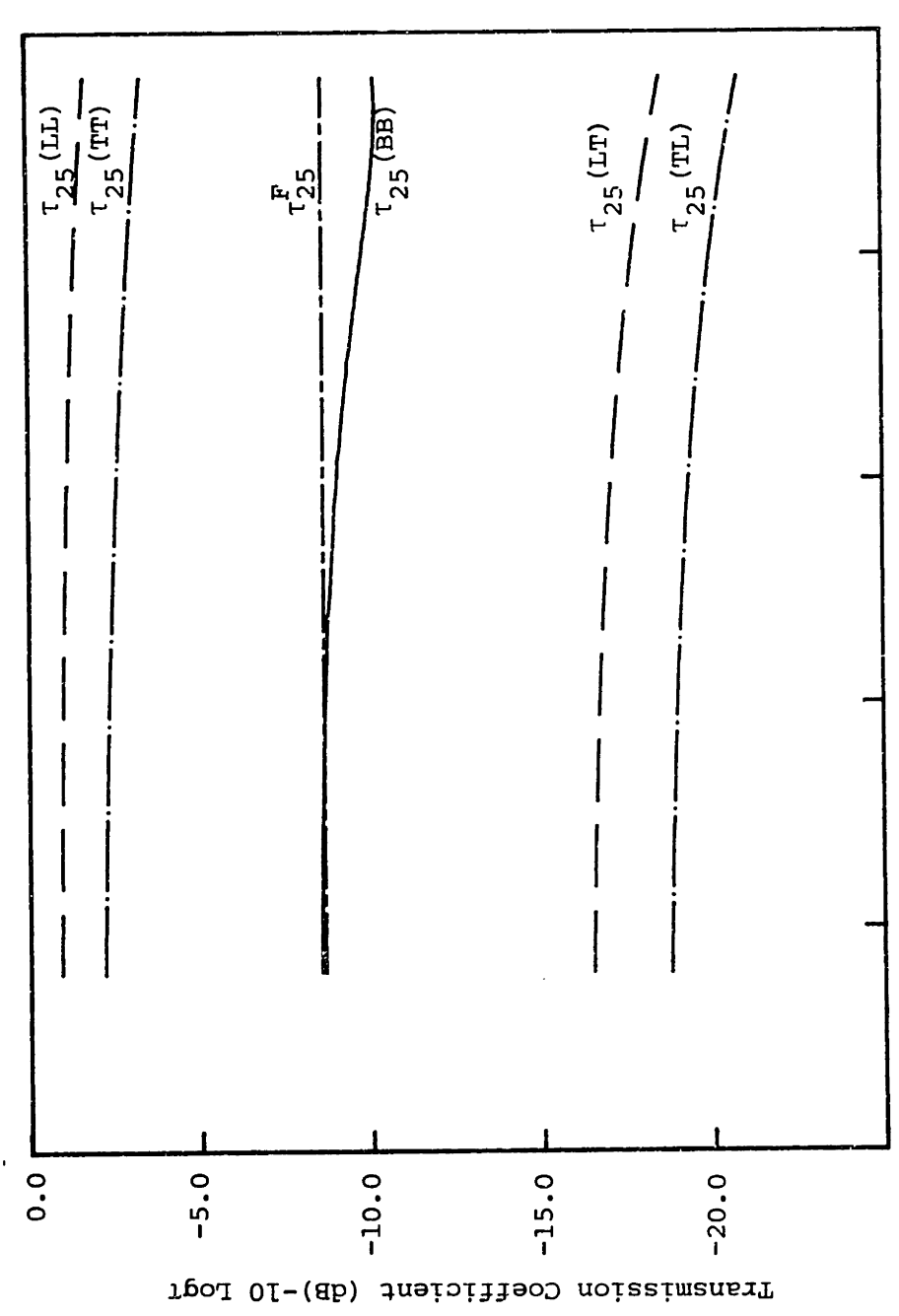

FIGURE 4.3.8: VARIATION WITH FREQUENCY OF AVERAGE TRANSMISSION COEFFICIENTS -- $\tau_{25}(LL)$, $\tau_{25}(LT)$, $\tau_{25}(TT)$, $\tau_{25}(TL)$, τ^F_{25}, $\tau_{25}(BB)$ -- BETWEEN THE WEB (2) AND THE LONGITUDINAL GIRDER (5) -- CROSS JOINT

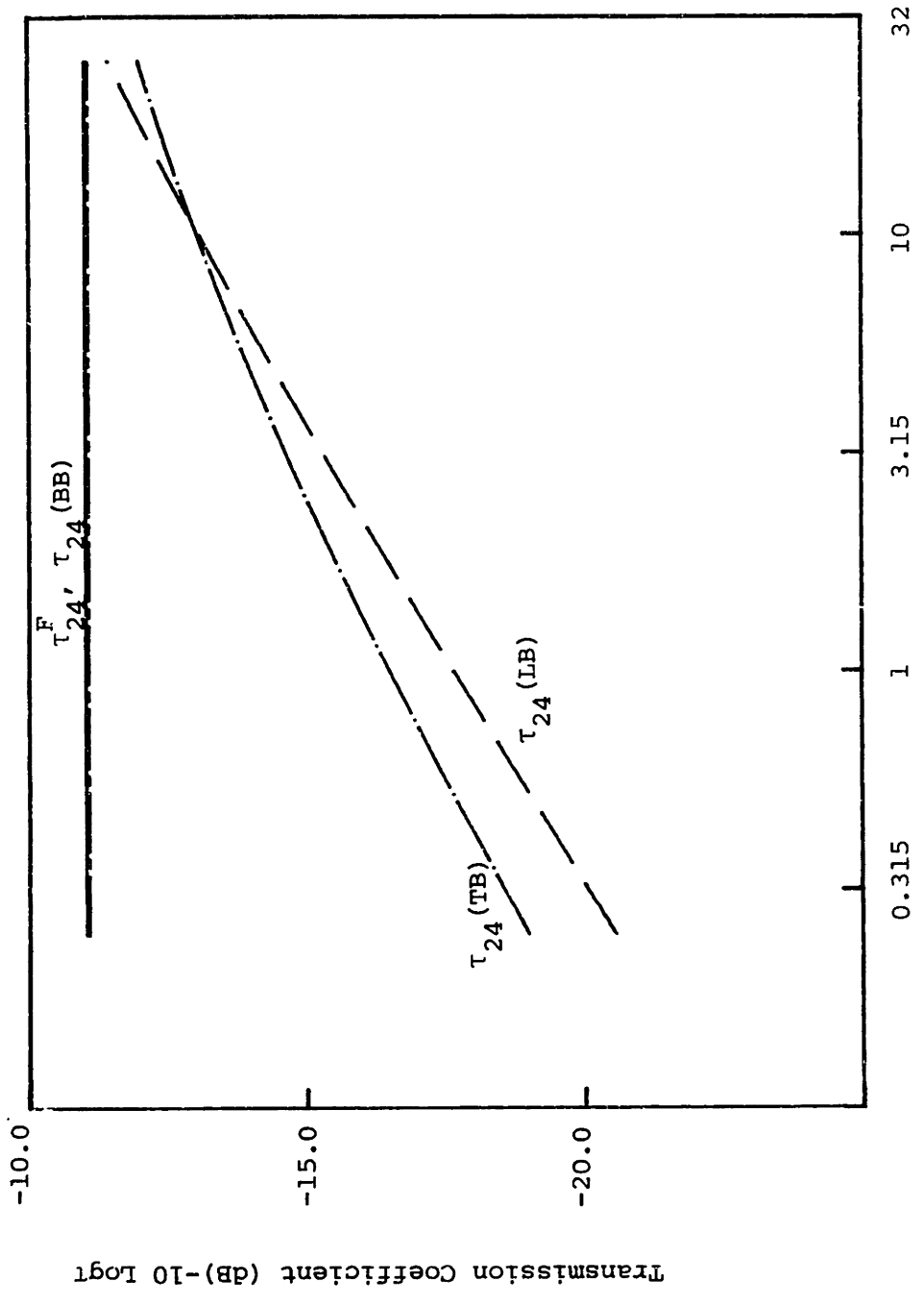

FIGURE 4.3.9: VARIATION WITH FREQUENCY OF AVERAGE TRANSMISSION COEFFICIENTS -- τ_{24}(BB), τ_{24}^{F}, τ_{24}(LB), τ_{24}(TB) -- BETWEEN THE WEB (2) AND THE TANK TOP PLATE (4) - CROSS JOINT

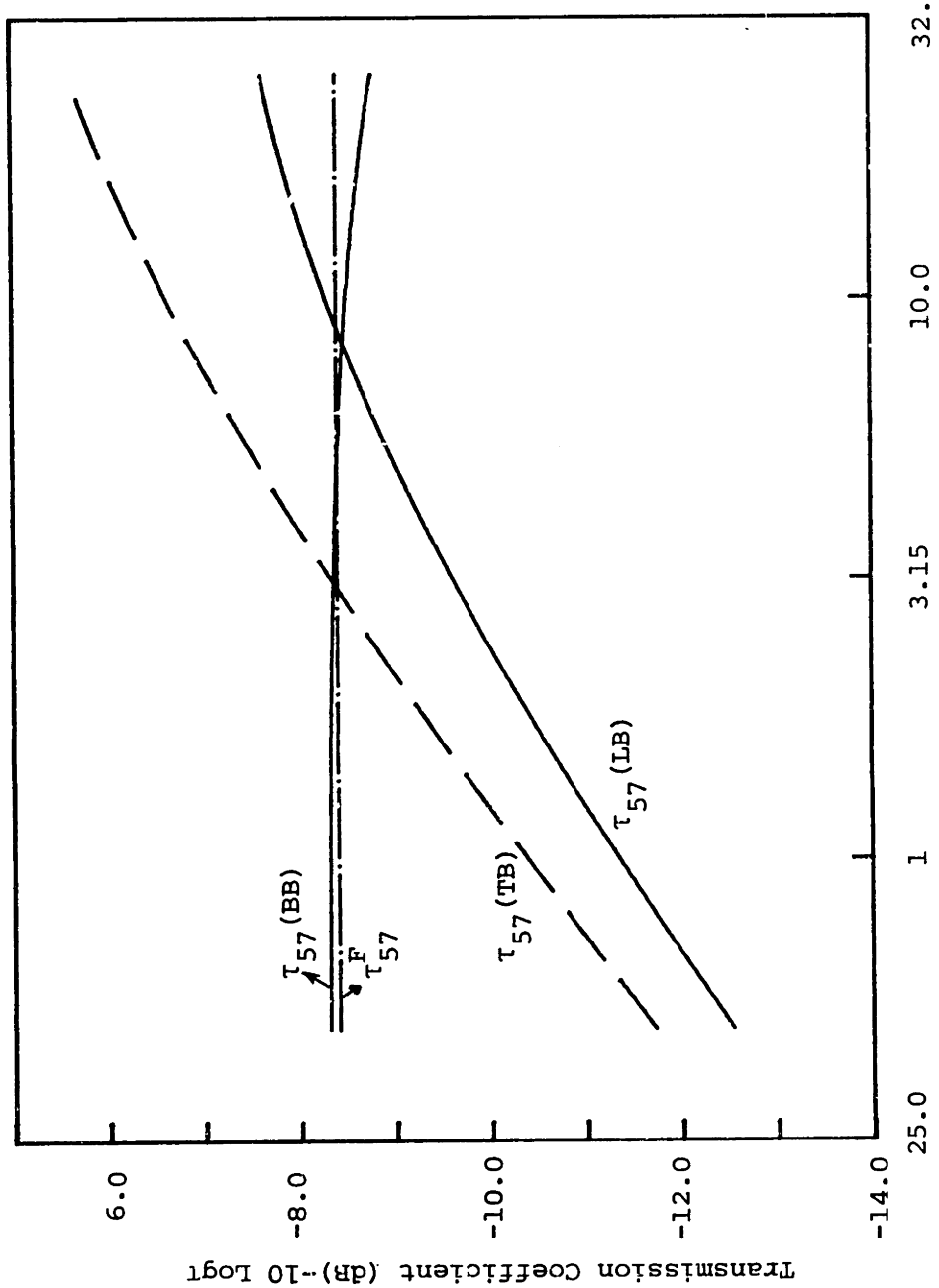

FIGURE 4.3.10: VARIATION WITH FREQUENCY OF AVERAGE TRANSMISSION COEFFICIENTS -- τ_{57}(BB), τ_{57}^F, τ_{57}(LB), τ_{57}(TB) -- BETWEEN THE LONGITUDINAL GIRDER (5) AND BOTTOM PLATE (7) - TEE JOINT

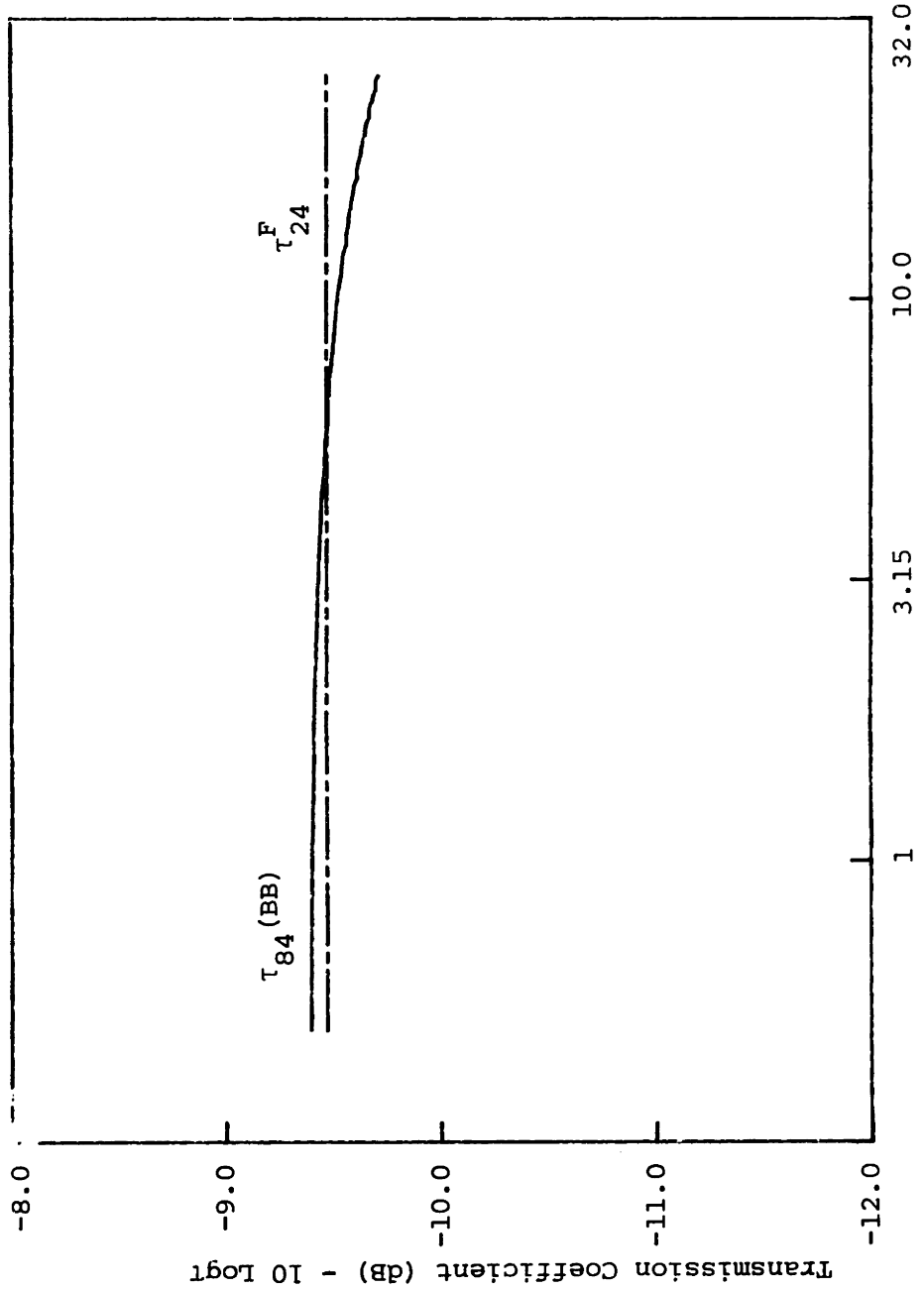

FIGURE 4.3.11: VARIATION WITH FREQUENCY OF BENDING-TO-BENDING AVERAGE TRANSMISSION COEFFICIENTS -- τ_{84}^{F} and τ_{84}(BB) -- BETWEEN THE BRACKET (8) AND THE TANK TOP PLATE (4) -- TEE JOINT

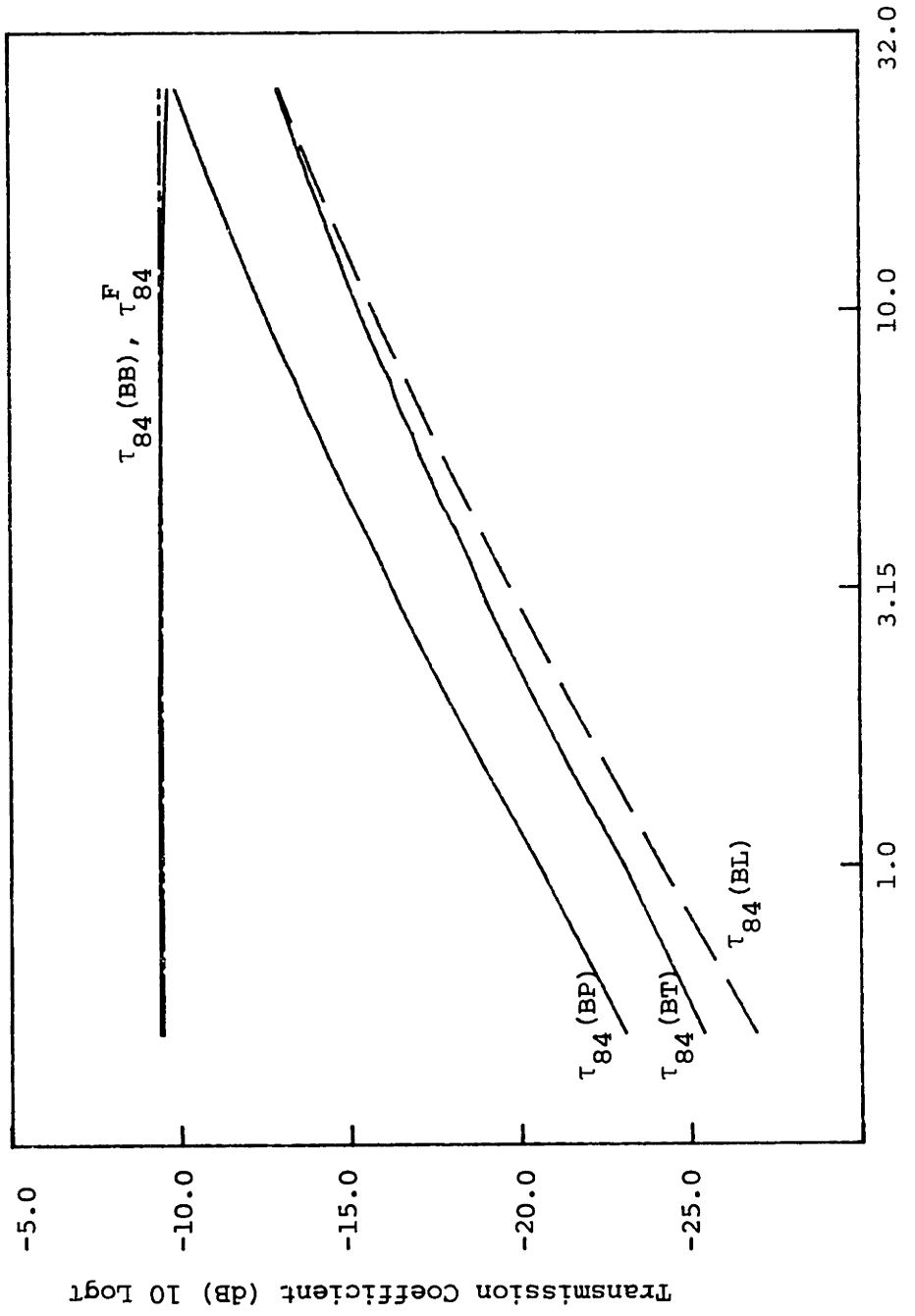

FIGURE 4.3.12: VARIATION WITH FREQUENCY OF AVERAGE TRANSMISSION COEFFICIENTS -- τ_{84}(BB), τ^F_{84}, τ_{84}(BL), τ_{84}(BT), τ_{84}(BP) -- BETWEEN THE BRACKET (8) AND THE TANK TOP PLATE (4) - TEE JOINT

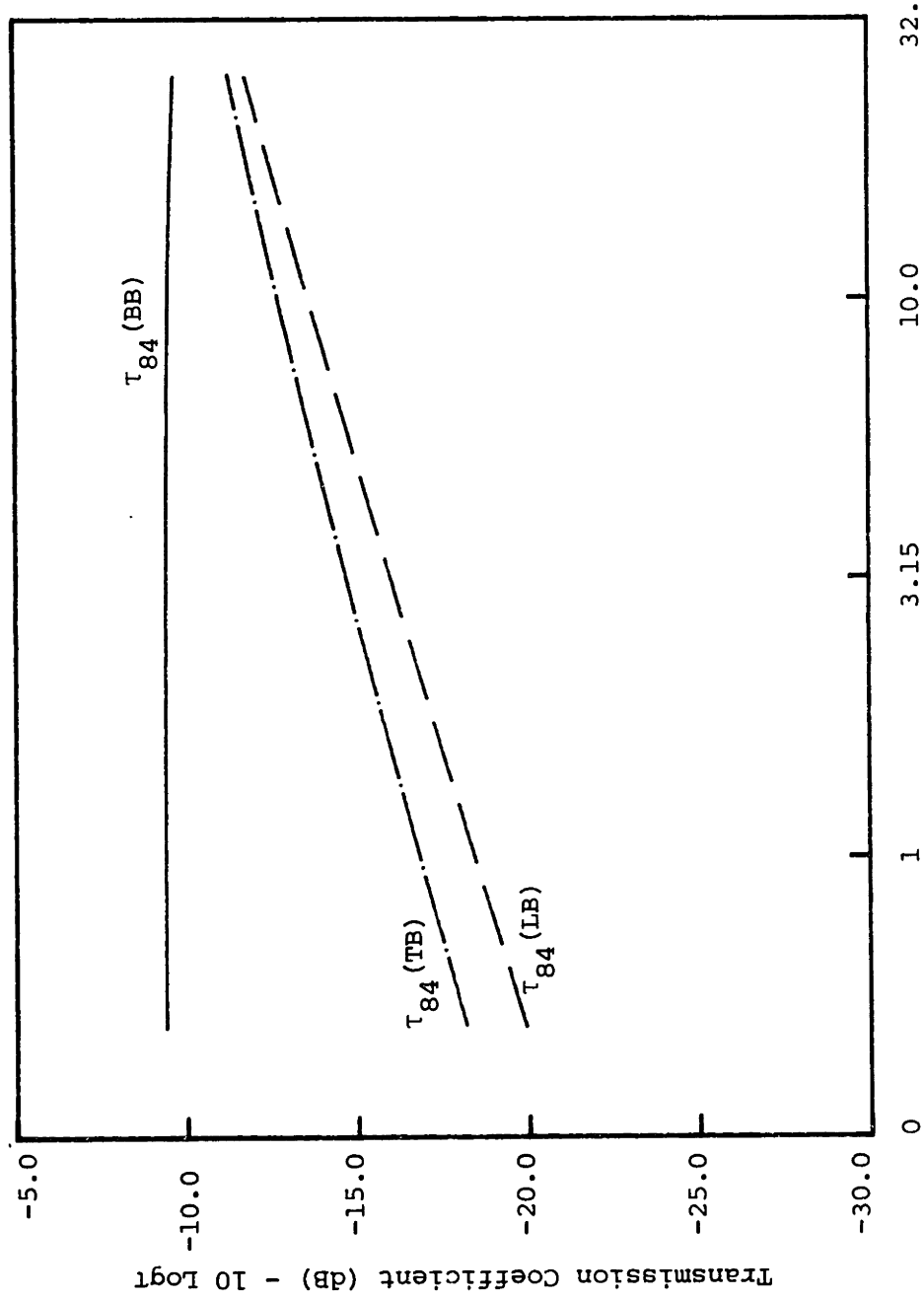

FIGURE 4.3.13: VARIATION WITH FREQUENCY OF AVERAGE TRANSMISSION COEFFICIENTS -- τ_{84}(BB), τ_{84}(LB), τ_{84}(TB) -- BETWEEN THE BRACKET (8) AND THE TANK TOP PLATE (4) -- TEE JOINT

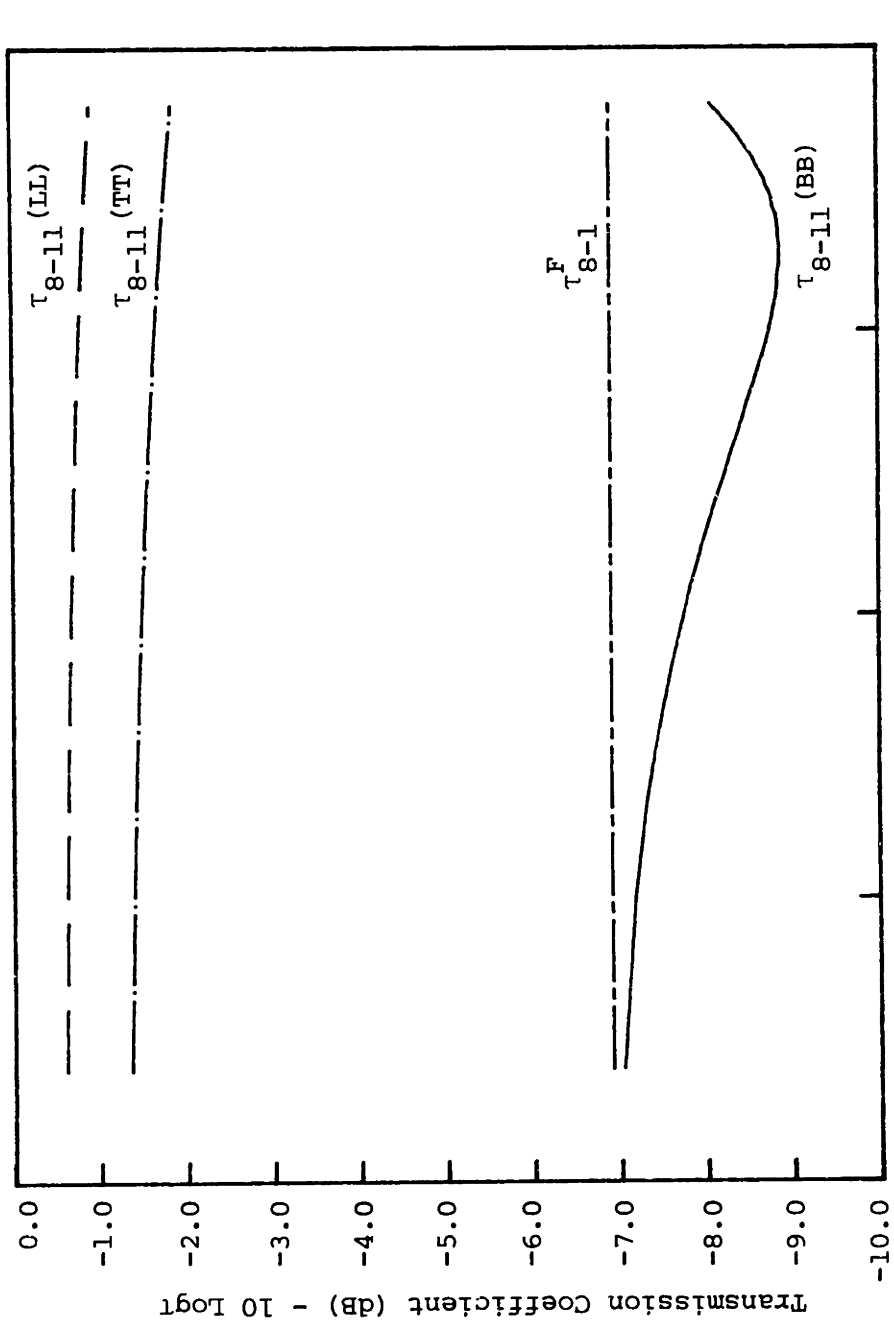

FIGURE 4.3.14: VARIATION WITH FREQUENCY OF AVERAGE TRANSMISSION COEFFICIENTS $\tau_{8-11}(LL)$, $\tau_{8-11}(TT)$, τ_{8-11}^{F}, $\tau_{8-11}(BB)$ -- BETWEEN THE BRACKET (8) AND THE FLOOR (11) -- TEE JOINT

transformations are expected to be significant. It is also important to point out that above 5700 Hz the total in-plane energy (longitudinal plus shear) transmitted to the web is greater than the transmitted bending energy since $\tau_{(BB)} < \tau_{(BP)}$ (Bending to In-Plane Average Transmission Coefficient).

Curves 4.3.8 and 4.3.9 show that when opposite plates are considered the transmission losses of in-plane motions of some nature (LL or TT) are much smaller than the bending-to-bending losses.

Paragraph 4.3.5 discusses other aspects related to the average transmission coefficients associated with the model.

4.3.4 Coupling Loss Factors

The evaluation of η_{ij} is made by a main program, utilizing the expressions (4.3.10) to (4.3.12) and the SEA consistency relation (3.9). This program uses a set of subroutines derived from all the previous referred programs developed to determine $\bar{\tau}_{ij}$.

The consistency relation ($n_i \eta_{ij} = n_j \eta_{ji}$) is also utilized to verify the computed results. If n_i, n_j, and η_{ij} are known, η_{ji} is determined from (3.9). η_{ji} is also obtained from the program by assuming the incidence occurring at plate j. Both values are then compared. They are exactly the same when the coupled subsystems have the same nature (e.g., shear-shear). When the nature is not the same, a difference may result, but always less than 2%.

The program is then used to determine the coupling loss factors between the SEA subsystems of any two plates of the physical model, at each different joint. Figures 4.3.15 to 4.3.18 show some calculated values of η_{ij} as a function of frequency. The difference between $\eta_{ij}(BB)$ and η_{ij}^{F} is not very

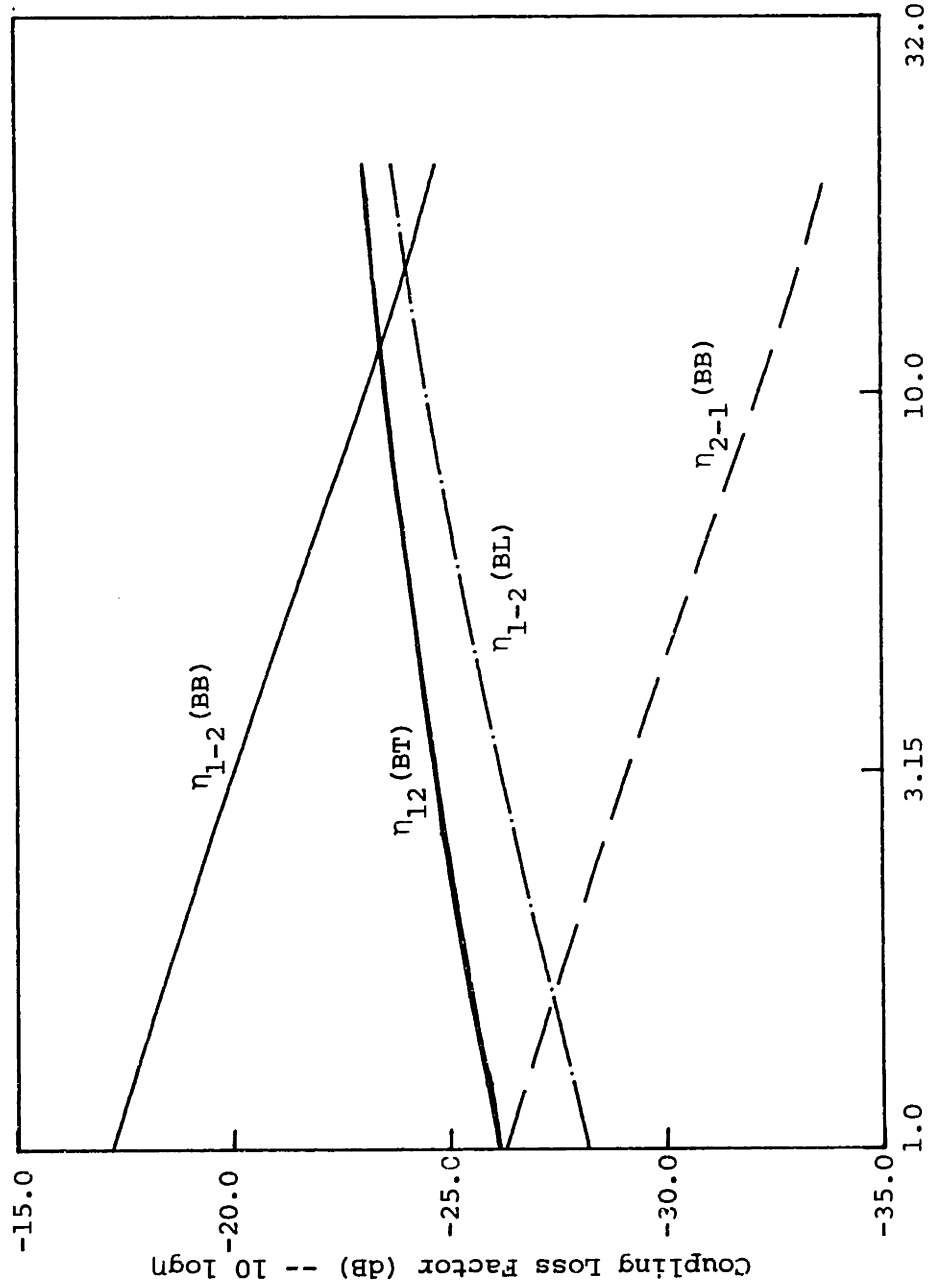

FIGURE 4.3.15: VARIATION WITH FREQUENCY OF COUPLING LOSS FACTORS -- $\eta_{12}(BB)$, $\eta_{22}(BL)$, $\eta_{12}(BT)$, $\eta_{21}(BB)$ -- BETWEEN THE TOP PLATE (1) AND THE WEB (2)

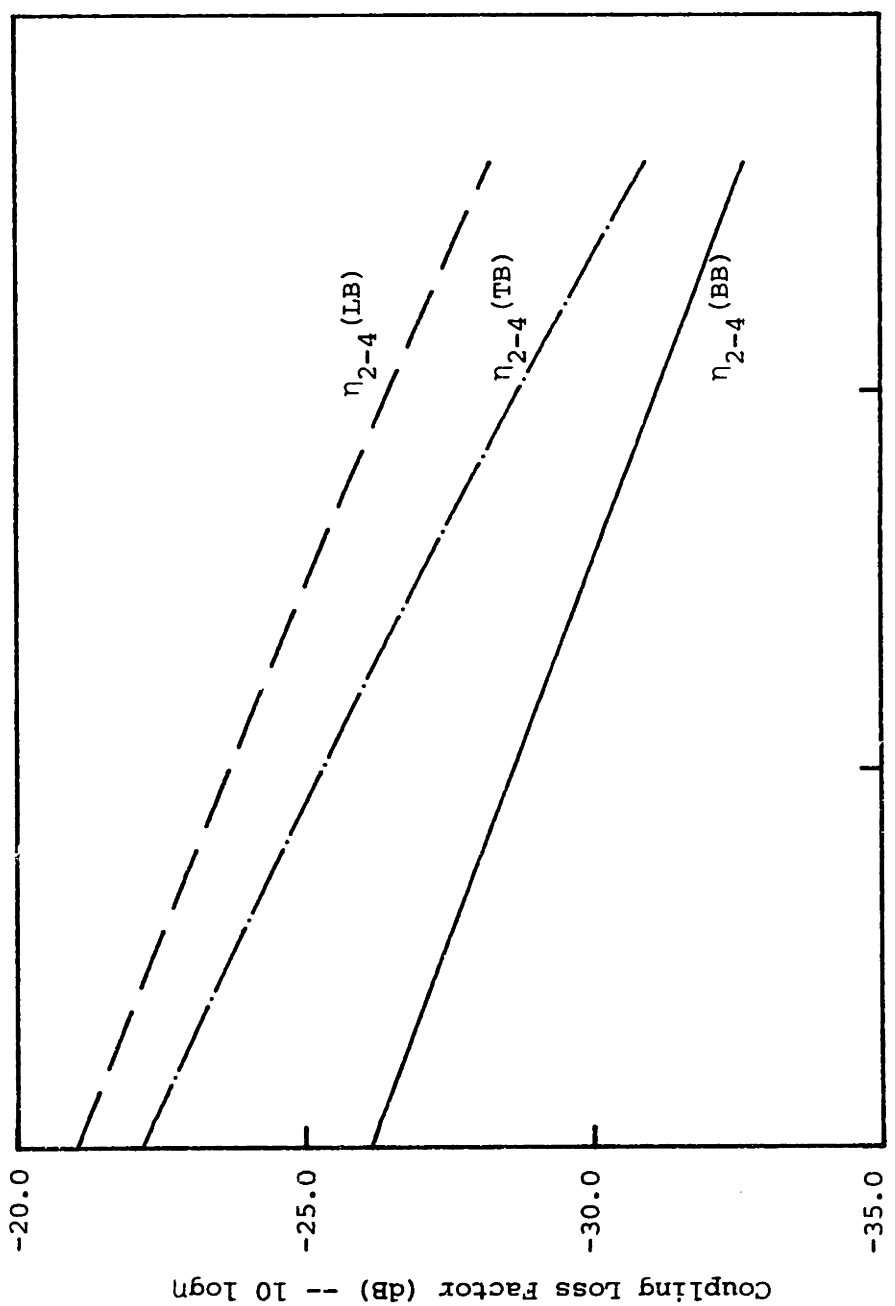

FIGURE 4.3.16: VARIATION WITH FREQUENCY OF THE COUPLING LOSS FACTORS -- η_{2-4}(BB), η_{2-4}(LB), η_{2-4}(TB) -- BETWEEN THE WEB (2) AND THE TANK TOP PLATE (4)

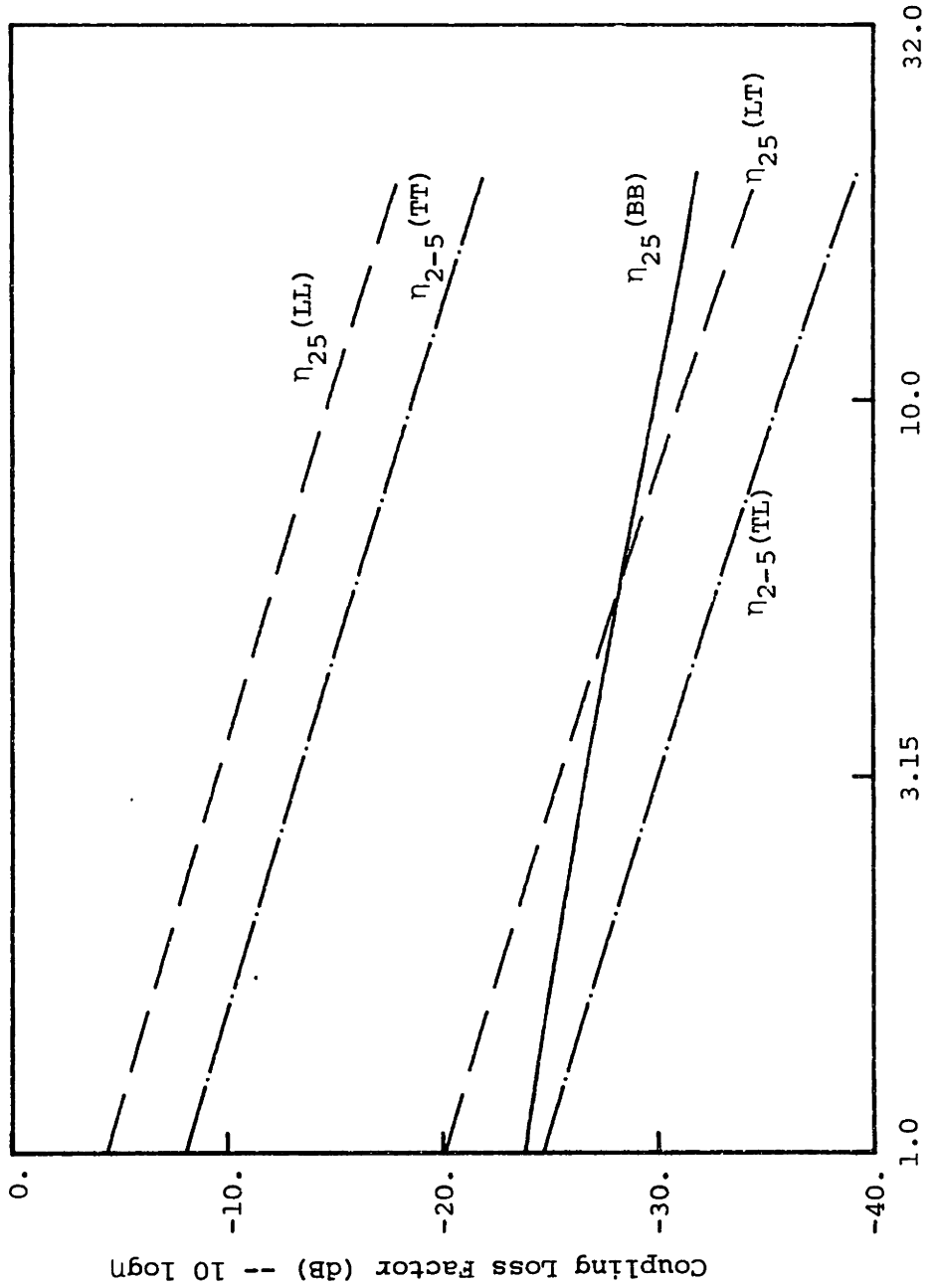

FIGURE 4.3.17: VARIATION WITH FREQUENCY OF THE COUPLING LOSS FACTORS -- $\eta_{25}(LL)$, $\eta_{25}(TT)$, $\eta_{25}(BB)$, $\eta_{25}(LT)$, $\eta_{25}(TL)$ -- BETWEEN THE WEB (2) AND THE LONGITUDINAL GIRDER (5)

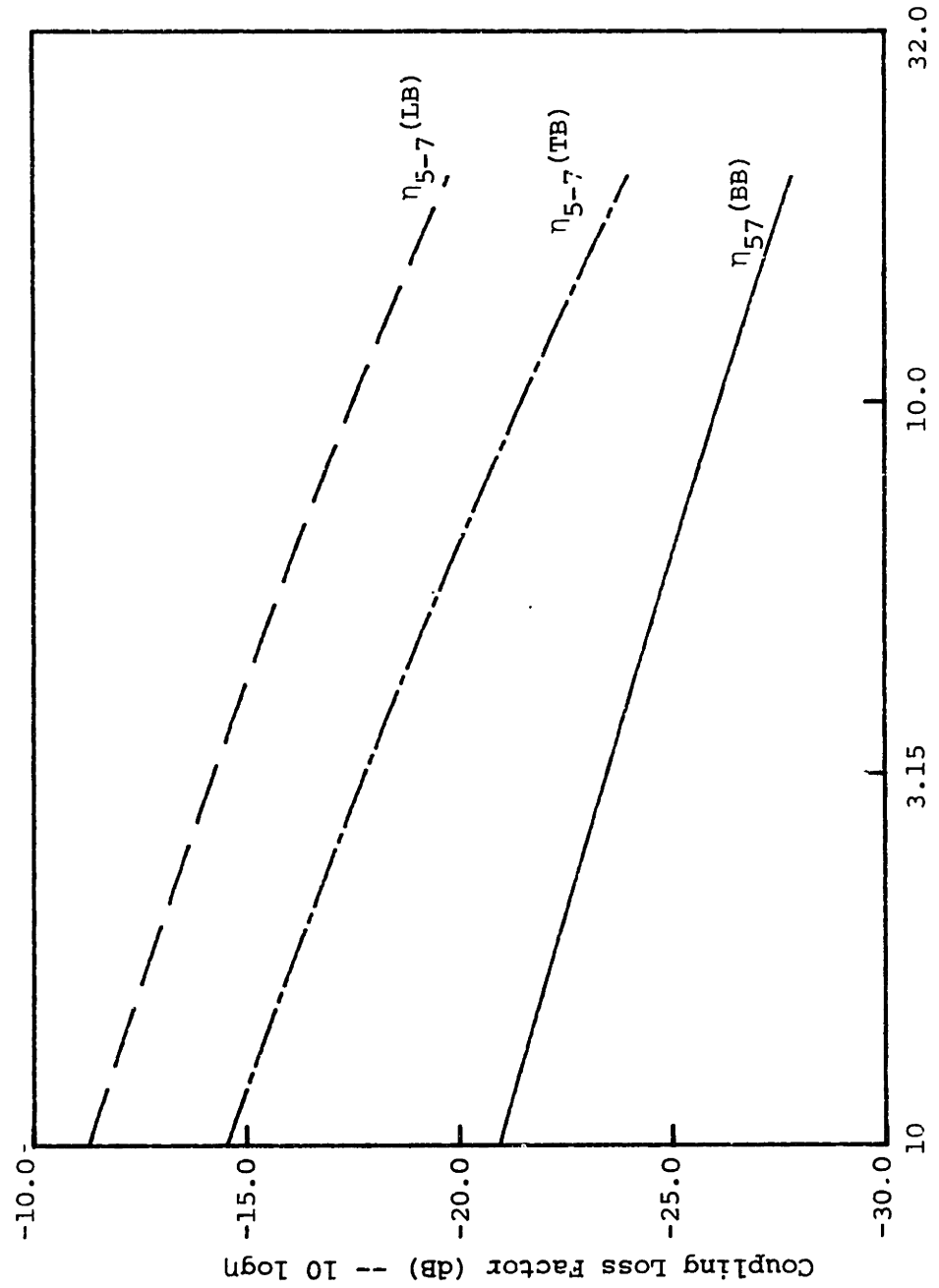

FIGURE 4.3.18: VARIATION WITH FREQUENCY OF THE COUPLING LOSS FACTORS η_{57}(BB), η_{57}(LB), η_{57}(TB) -- BETWEEN THE LONGITUDINAL GIRDER (5) AND THE BOTTOM PLATE (7)

significant, which can be inferred from expression 4.3.1 and from the comparison between $\tau_{ij}(BB)$ and τ^{F}_{ij} (as discussed in section 4.3.3). Thus, for the sake of simplicity, only $\tau_{ij}(BB)$ is plotted.

It is interesting to notice that all curves are straight lines inside a significant frequency interval when plotted in a log-log coordinate system. It this is generally true, precious computational time may be saved. This point justifies further investigation.

4.3.5 Energy Conversions -- SEA Parameters

As discussed in Paragraph 4.1, Swift [23] (based on curve of $\tau(BB)$ and $\bar{\tau}^{F}$ versus P_{ab}) suggested a criterion to verify under which circumstances the energy transformations (in-plane motions) should or should not be considered. Different types of joints (L, Tee, Cross) were analyzed for different plate thickness ratios. As will be discussed, the Swift parameter is considered very useful. However, since the application of SEA is the concern, a possible criterion should be based on the SEA parameters (mode count, coupling loss factors, loss factors), rather than on bending-to-bending average transmission coefficients. A first basic point is that the modes to be excited must be available, as discussed in 4.1. A second point is the strength of the coupling, especially between bending (the primary concern) and the in-plane motions. Finally, how comparable are η_{ij} and η_{i} (loss factor)? No attempt is made here to derive such a criterion. Only the model under analysis is the concern.

Expression 4.3.1 shows that when comparing coupling loss factors between a subsystem of a given nature and other subsystems, such comparison can just be based on the transmission coefficients, as seen in Swift's work [23]. The inverse situation, however, is not true. For example, when $\eta_{ij}(BB)$

η_{ij}(LB) and η_{ij}(TB) are compared, one cannot say that: if τ_{ij}(TB) and τ_{ij}(LB) are smaller than τ_{ij}(BB), the related coupling loss factors (η_{ij}(TB) and η_{ij}(LB) will be smaller than η_{ij}(BB). This is because the energy velocities on plate i (4.3.2, 4.3.3, 4.3.4) are usually higher for in-plane than for flexural waves (equation 4.3.1). This situation is well illustrated by Figure 4.3.9 and 4.3.16. They show that η_{ij}(LB) and η_{ij}(TB) are higher than η_{ij}(BB) when τ_{ij}(LB) and τ_{ij}(TB) are significantly lower than τ_{ij}(BB). It is also interesting to notice in these figures, that as frequency increases and the differences between average transmission coefficients decreases, the corresponding differences between coupling loss factors also decrease. The comparison between the different η_{ij} can be easily made by using expressions 4.3.10 to 4.3.12. For example:

$$\frac{\eta_{ij}(LB)}{\eta_{ij}(BB)} = 3.7445 \left(\frac{c_L}{fh_i}\right)^{1/2} \frac{\tau_{ij}(LB)}{\tau_{ij}(BB)}$$

Another important aspect is that in a multijoint structure the significance of each transformation at a joint cannot be judged individually. A weak coupling can be followed by a stronger coupling or vice versa, etc. The "next" joint will always play an important role in the analysis.

A good illustration is offered by the structure in Figure 4.5.1c, drawn from the physical model. Figure 4.3.15 shows the coupling loss factor between the top plate (excited on bending) and the web. It can be noticed that comparing η_{ij} is the same as comparing $\bar{\tau}_{ij}$ (Figure 4.3.7), which was done in the previous paragraph. η_{21}(BB) is much smaller (10dB) than η_{12}(BB), since more modes are always available at plate 2 (web).

The coupling loss factors at the next joint (between web, tank top, and longitudinal girder) are shown in Figures 4.3.16 and 4.3.17. Figure 4.3.17 shows that η_{25}(LL) and η_{25}(TT) are much greater (10-20dB) than η_{25}(BB), which is of about the same order as η_{25}(LT). This means that the percentage of the total in-plane energy of the web (2) that flows to the in-plane subsystems of the longitudinal girder (5) is comparatively much higher than the percentage of the total bending energy of plate 2 that is transmitted to the flexural modes of plate 5. Therefore, above 5700 Hz (when τ_{12}(BP) > τ_{12}(BB)) the in-plane to in-plane absolute power flow is expected to be more representative than the bending-to-bending flow, from 2 to 5.

On the other hand, η_{24}(LB) and η_{24}(TB) are of the same order as η_{25}(LT) and η_{25}(TL), but much smaller (10dB) than η_{25}(LL) and η_{25}(TT).

Therefore, plate 5 offers a preferable path for the transmission of in-plane energy from plate 2. This is enhanced by the fact that no transformation of motion occurs between plates 2 and 5 (this idea could be intuited) and also by the fact that the coupling loss factors between the in-plane motions of plates 2 and 4 (or 3) are negligible.

The same does not happen with respect to bending. The different paths offered by the flexural subsystems of plates 1, 3, 4, and 5 to the bending energy of plate 2 are almost equally important. Of less importance, but not negligible, is the bending to in-plane power flow from 2 to 4 and 3. Thus the bending-to-bending power transmission is much less efficient than the in-plane to in-plane power, from 2 to 5.

Figure 4.3.16 shows that η_{23}(BB) and η_{24}(BB) are smaller (2-5 dB) than

η_{24}(LB), η_{24}(TB), η_{23}(LB) and η_{23}(TB), so that the in-plane to bending power transmission is more efficient than the bending-to-bending transfer from 2 to 4.

Similar situations occur, more significantly, at the joint between the longitudinal girder and the bottom plates (tee joint) as shown in Figure 4.3.18. η_{57}(LB) and η_{57}(TB) are much higher than η_{57}(BB) by 5-10 dB.

It is also important to point out that:

1. The loss factor associated with the flexural motions of plate 2 is higher than the coupling loss factors between the bending subsystem of this plate and the subsystems of all plates coupled to it (1, 3, 4 and 5). Thus the corresponding power dissipated is more significant when it is compared with the amount of power that flows from the bending subsystem of the web (2) through each individual energy path offered by the top plate (1), tank top (3,4) and longitudinal girder (5) subsystems. This is also valid for plate 5.

2. The loss factor associated with the in-plane motions are much smaller (5 dB) than those related to the flexural motions. Thus, the power dissipated by the flexural motions of each plate is more representative than the power dissipated by their in-plane motions.

The two above aspects indicate a strong flanking path of in-plane power flow through plates 2 and 5.

Based on all the previous points, one can expect (without carrying out the complete analysis, through the power balance equations) that: the in-

plane motions (along the web and longitudinal girder) will have a significant contribution to the flexural energy level of the bottom plates. This contribution is expected to be more significant than the resulting from bending transmission. Such in-plane motions will also transfer an important amount of energy to the bending motions of the tank top plates.

4.4 Energy Levels

The system of equations for the general case of coupling between N SEA subsystems is presented in Chapter 3 and is applied to the model (Figure 4.1.9); expression (3.7).

The directly excited subsystem is the group of flexural modes of the top plate, the power input being zero for all other subsystems. To avoid the necessity of measuring the power input, energy ratios (instead of absolute values), are predicted by taking the energy level of a subsystem as the reference level. Therefore, the power input is assumed as a unit power and the power dissipated by each subsystem evaluated as a percentage of this power.

The internal loss factors are those determined in paragraphs 4.2 and the coupling loss factors are obtained from computer programs (as discussed in paragraph 4.3.4).

The evaluations are carried out in third octave bands as already done in paragraph 4.1. Given the filters available, this choice was made in order to be as consistent as possible with the criterion of modal similarity (Appendix A) and with the velocity spectrum of the source (Appendix B).

To solve (3.7) a computer program is used, based on a library program for linear equations with real coefficients utilizing Gauss elimination with coefficients ordination.

The power balance equations are also utilized to determine:

(a) the power dissipated in each SEA subsystem

(b) the net power flow between subsystems

(c) the sensitivity of the predicted energy levels and dissipated power to variations in the plates internal loss factors

4.5 Steps for the Study of the Physical Model

As discussed in Section 4.1, the model is built-up in steps as illustrated in Figure 4.5.1.

First Step -- Two-Plate Model: L Joint

In the physical model, the power delivered to the flexural modes of the top plate (1) will be transmitted to the 'SEA' subsystems in the web (2) and the bracket (8) (and, of course, to the in-plane subsystems of plate 1, when they are present).

The following reasons strongly indicate that the preferable path will be that offered by the web:

(a) η_{12} is greater than η_{18} - since the web and bracket have the same thickness (and so, $\tau_{12} = \tau_{18}$) and because the common length between 1 and 2 is greater than that between 1 and 8 (Equation (4.3.2).

(b) η_{21} is smaller than η_{81} - which can easily be inferred from the consistency relation (Equation (3.1.9)).

(c) The loss factors in the web are greater than those in the bracket.

Because its area is larger, the web also has higher modal densities than the bracket. Therefore:

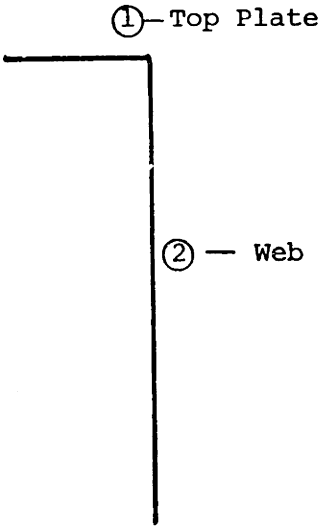

1st Step: Two Plates
(a)

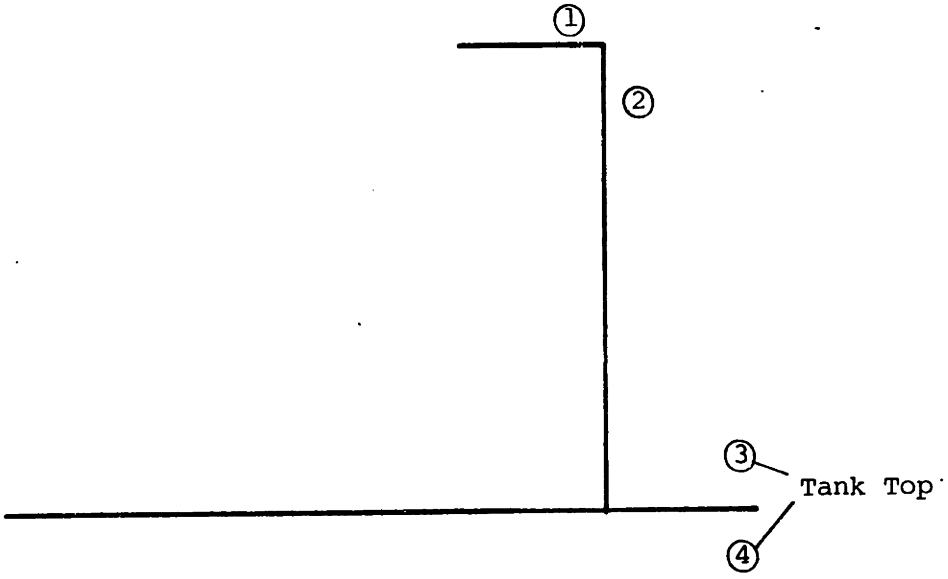

2nd Step: Four Plates
(b)

FIGURE 4.5.1: STEPS FOR THE MODEL'S ANALYSIS

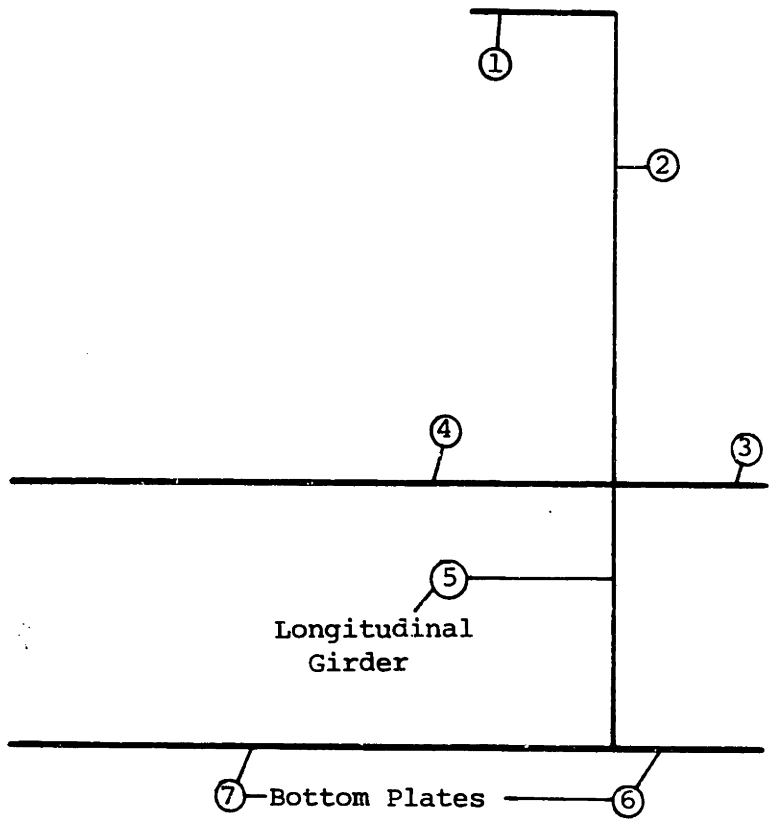

(c) 3rd Step -- Seven Plates

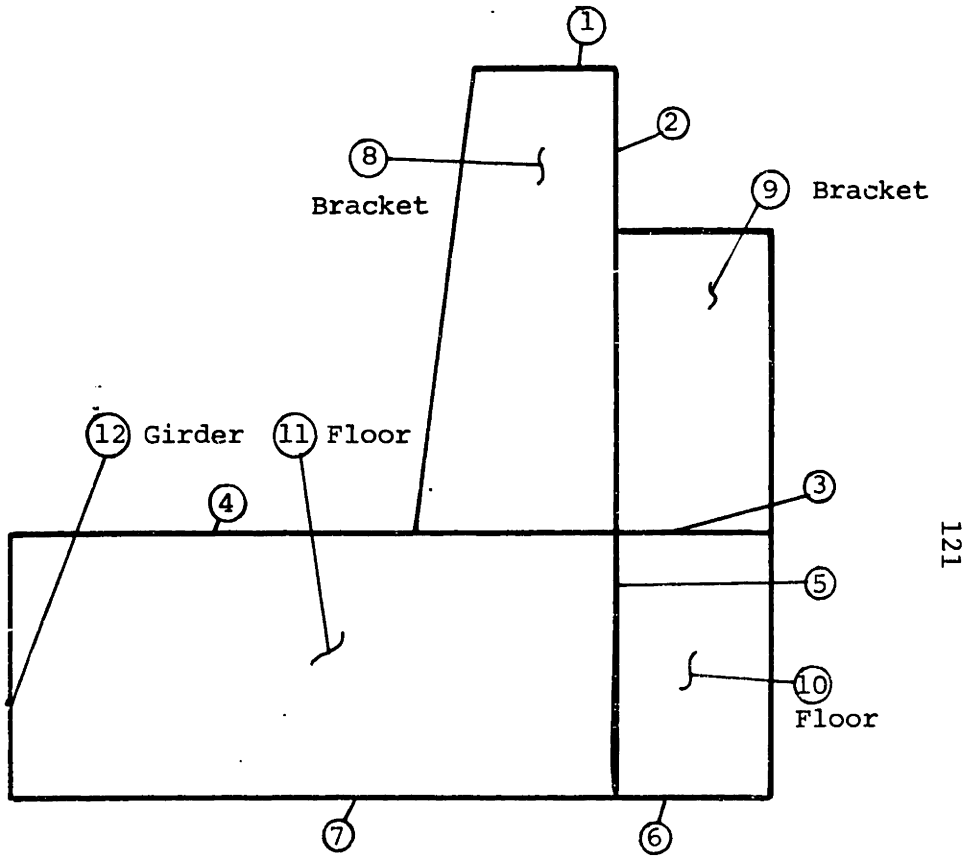

(d) 4th Step -- Twelve Plates

FIGURE 4.5.1: STEPS FOR THE BASIC MODEL ANALYSIS

(a) more modes to store energy are always available at the web.

(b) energy transformation between the top plate and the web is expected to take place first (above 5000 Hz as predicted in Section 4.1).

The above reasoning justifies the first sub-model: two-plate joint, top-plate and web.

In studying this sub-model the following aspects have to be considered:

(1) The top plate has less than six flexural modes in each third octave band up to (and including) the one centered at 6300 Hz. More than 6 are present at the web, starting at the band centered at 1250 Hz. Thus, for those bands few modes interact with a large number (>6) of modes. As discussed in Section 4.1, not the most accurate results may be expected from SEA below 8000 Hz.

(2) In-plane motions are expected to be generated at the web, but without a significant effect on the flexural energy levels of the two plates.

Second Step - Four-Plate Model

The tank top plates are added. An "L" and a "Tee" joint are analyzed. The aspects of the first step are, of course, included in this model. However, as discussed in section 4.3, $\tau_{12}(BB)$ is about the same order as $\eta_{12}(BT)$ and $\eta_{12}(BL)$ above 5 kHz ($\pm$ 3 dB). On the other hand, the coupling loss factors $\eta_{23}(TB)$, $\eta_{23}(LB)$, $\eta_{24}(TB)$ and $\eta_{24}(LB)$) are higher (5 dB) than $\eta_{23}(BB)$ ($\eta_{24}(BB)$), and the in-plane loss factor is smaller by 5 dB than the flexural loss factor at plane 2. Therefore, the influence of the in-plane motions is expected to be noticed through. The contribution of those motions to

the flexural energy levels of plates 3 and 4 (when comparing with the values resulting from the simplified approach considering bending transmission only).

Third Step -- Seven-Plate Model

The longitudinal girder and the bottom plates are added. An "L", a "Cross" and a "Tee" joint are identified. As in the second step, the emphasis is on energy transformation. The influence of the in-plane motions is expected to be accentuated. The main aspects concerning this sub-model were discussed in paragraph 4.3.5.

Fourth Step -- Twelve-Plate Model

Motion Transformations were emphasized in the two previous models. In this last model two new situations are created by the inclusion of the transverse plates (brackets and floors):

a. a multi-path condition for the energy transmission
b. two joints with plates coupled along different lengths (brackets-web and bracket-floor-tank top).

When comparing with the seven-plate model, one can notice that the bracket (8) and the floor (11) offer a new option for the generation and transmission of in-plane energy. On the other hand, the inclusion of the transverse plates means new paths for the bending and in-plane energy of the web (2) and longitudinal girder (5). They are going to drain a percentage of the power that in the previous model flows to the bottom plates. It is not easy to infer without a careful analysis which are the preferable energy transmission paths, and from which of them comes the major contribution to the flexural energy of the bottom plates. This is studied in more detail in Section 5.5.

The predicted energy ratio levels for each step are presented in Chapter 5 together with the experimental results. Two predictions are made: one assuming bending transmission only and the second taking into account the in-plane motions. The flexural energy of only three plates will be experimentally determined at the final step for the following reasons:

(1) Top plate (1) - because it is the driven and the reference plate.

(2) Bottom plate (7) - because it is:

   (a) the major concern, directly associated with a noise requirement;

   (b) the last plate in the transmission paths from the driven plate;

   (c) the plate whose flexural energy level is expected to be more significantly influenced by the in-plane motions generated at the web and at the bracket.

(3) Web - because it is:

   (a) directly coupled to the driven plate;

   (b) coupled to six other plates through the three typical joints (L, Tee and Cross);

   (c) connected to the brackets through different coupling lengths;

   (d) the plate included in all three previous models.

CHAPTER 5

COMPARISON OF PREDICTED AND EXPERIMENTALLY DETERMINED ENERGY-RATIO LEVELS

5.1 Energy Level Measurements

Figure 5.1.1 show the instrumentation utilized to experimentally obtain the flexural energy levels of each plate of the models:

As stated in Chapter 1, machinery can be considered as a broad-band random noise source, usually characterized by its bed plate velocity spectrum and its mobility (Appendix B). As discussed in Chapter 4:

1. The vertical force is assumed to give the major contribution for the power input.
2. Each Diesel support can be understood as a point source (see also Appendix B).
3. The analysis is carried out in third octave bands.

A shaker was used as the source to deliver power to the top plate. The excitation signal came from a random noise generator and was amplified after passing through a filter.

The force signal from the shaker was continuously monitored by using a long time average measuring amplifier. A value was fixed for each frequency band in order to ensure that the same power was being delivered to the structure at every measurement. The force signal shape was also checked by using an oscilloscope.

The mean energy ratio levels were determined from the resulting voltage

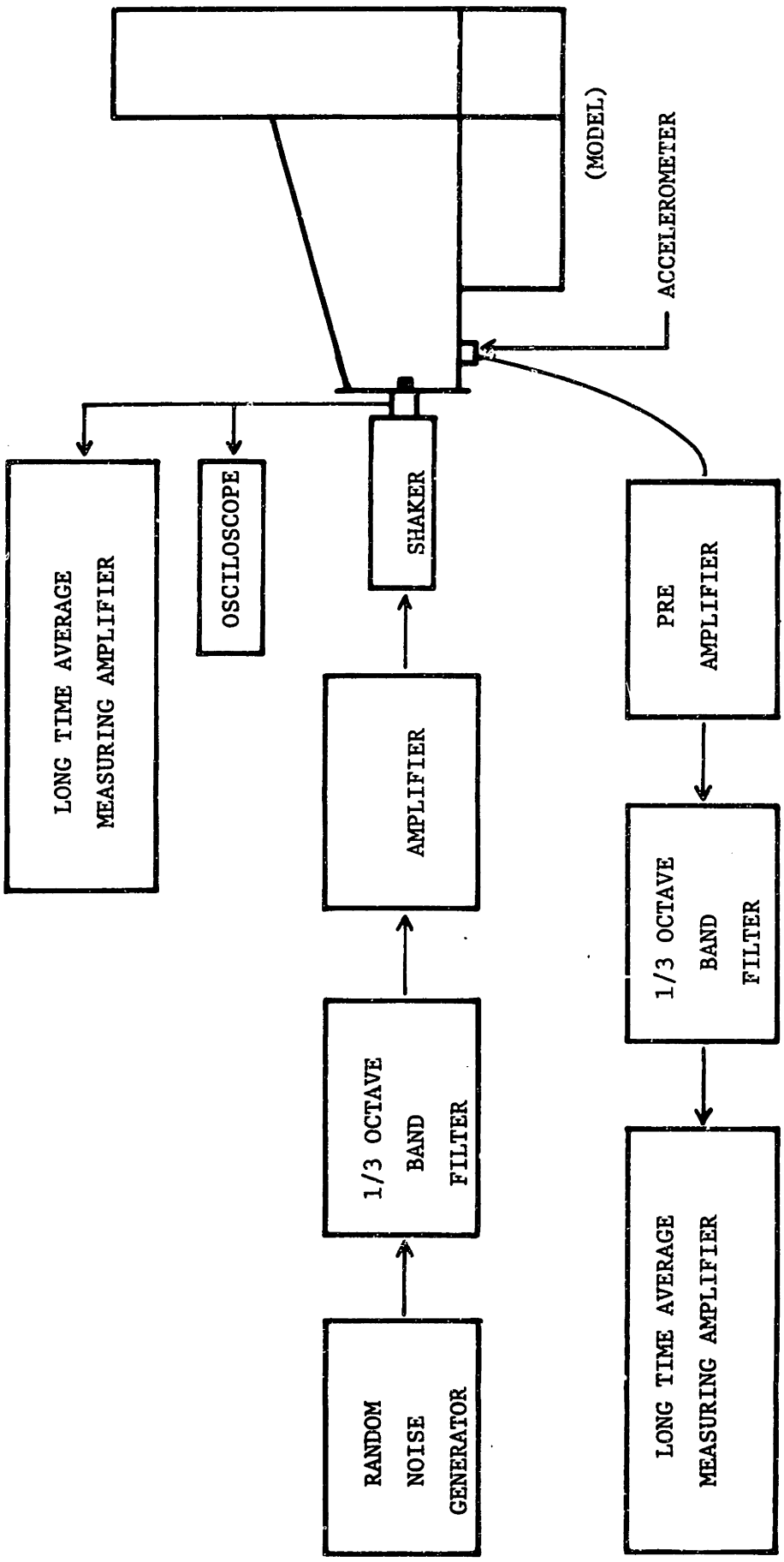

FIGURE 5.1.1: INSTRUMENTATION FOR THE DETERMINATION OF PLATE FLEXURAL ENERGY

acceleration levels of the plates, by applying the following expression:

$$10 \log \frac{\langle E_p \rangle}{\langle E_p \rangle} = 10 \log \frac{M_p}{M_p} + 20 \text{ Log } \frac{\langle \sqrt{a^2}_p \rangle}{\langle \sqrt{a^2}_r \rangle}$$

where:

The subscripts r and p refer to the reference plate and any other plate of the model, respectively.

m - mass of plate

$\langle \sqrt{a^2} \rangle$ - root mean square acceleration

The voltage signal from an accelerometer was obtained from a long time average measuring amplifier, after passing through a third octave band filter. For each frequency band, measurements were made in different locations over the surface of each plate to obtain the mean square acceleration. It is a normal practice to determine the mean energy levels from ten acceleration measurements [23]. In this thesis a minimum of sixteen were taken at each plate. The basic criterion was to place the accelerometer in as many different points as necessary until the average value showed a convergence. The larger the plate, the higher the frequency -- fewer measurements were required, since a more uniform acceleration distribution was verified. In these cases, ten measurements would actually be more than enough. For the smaller size plates at the lower bands, usually 16 to 24 measurements were taken.

Special attention was given to the driven plate, particularly below 8000 Hz, where fewer than six modes were present in each frequency band. The average was based on twenty-four to forty measurements.

A spectral analyzer was used to measure the auto-spectrum of the random noise generator output, of the input force (at the shaker), and of the acceleration signal. This was done to verify the effect of both filters on the acceleration and the force signals and the effect of the structure on the input force, and, therefore to ensure that the major contribution was coming from the frequency band of interest. The filter in the acceleration circuit was used to reinforce this aspect, especially at lower frequencies, in which strong resonances from the neighboring bands could become important.

The structure was hung from the ceiling, by nylon lines, in order to minimize the loss through the support. The same procedure was used when determining the plate loss factors.

5.2 First Step - Two-Plate Joint

The SEA parameters associated with the top plate (reference plate) and the web are shown in Table 5.2.1, Figures 5.2.1 and 5.2.2 reproduced from Chapter 4 for convenience and to illustrate some important aspects applicable to the next steps.

The predicted flexural energy ratio levels which result when only bending transmission is assumed, $(E_2/E_1)F$, are practically the same as those obtained when the three wave fields are considered, $(E_2/E_1)G$. This was expected, since the differences between η_{12}^F and $\eta_{12}(BB)$ are not significant and the in-plane motions generated at the web (above 5 kHz) have little effect in the flexural energy level of plate 1 (Chapter 4).

Below 5 kHz, measurements were carried out in six third octave bands,

1/3 Octave Band (kHz)	0.63	1.25	2.0	2.5	3.15	4.0	5.0	6.3	8.0	10.0	12.5	16.0	20.0
Top Plate	1	3	2	2	3	3	3	5	7	8	9	12	M.D.
Web	2	8	12	←				M.D.	→				

TABLE 5.2.1: MODE COUNT -- FLEXURAL MODES -- TWO PLATE-MODEL

M.D.: Number estimated based on modal density

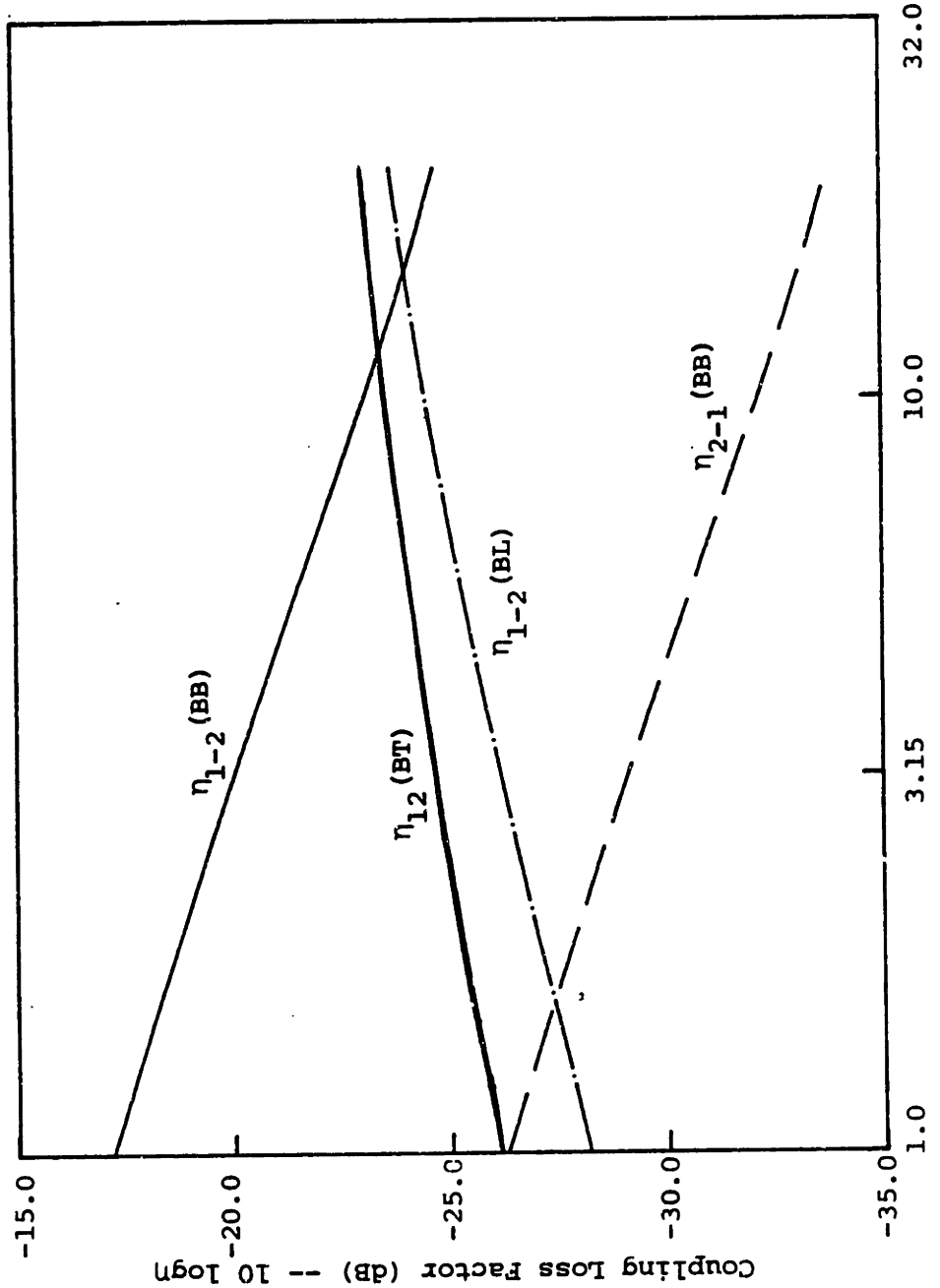

FIGURE 5.2.1: VARIATION WITH FREQUENCY OF COUPLING LOSS FACTORS -- $\eta_{12}(BB)$, $\eta_{22}(BL)$, $\eta_{12}(BT)$, $\eta_{21}(BB)$ -- BETWEEN THE TOP PLATE (1) AND THE WEB (2)

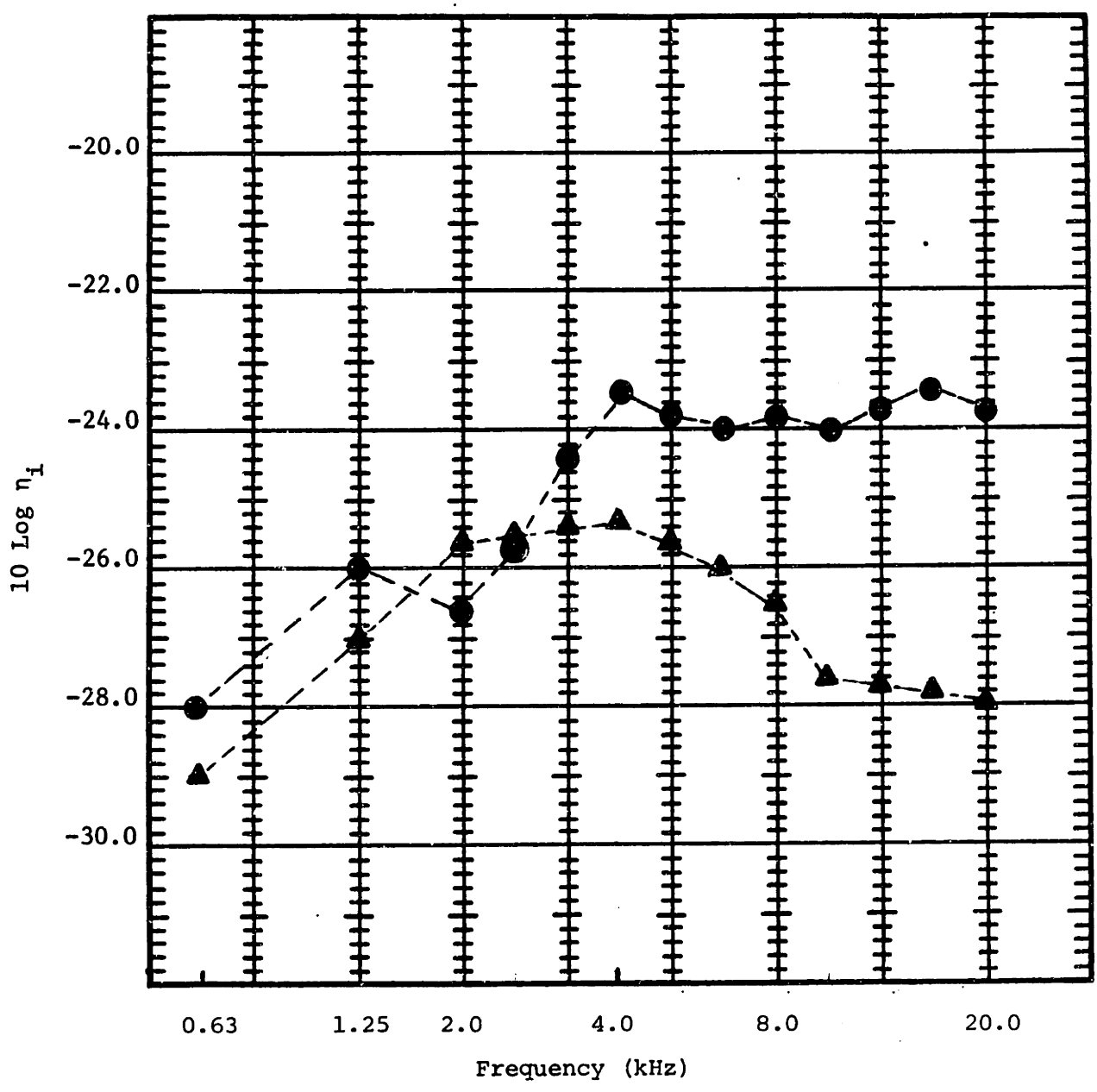

FIGURE 5.2.2: VARIATION WITH FREQUENCY OF THE DISSIPATIVE LOSS FACTORS OF THE TOP PLATE AND OF THE WEB

●: web - ▲: top plate

considered representative enough to verify the SEA predictions when fewer than six modes were excited in the top plate.

Figure 5.2.3 shows the predicted and experimentally determined flexural energy ratios. Three predictions are shown below 4 kHz;

(a) $(E_2/E_1)_{md.}$ - based on the coupling loss factors determined from the computer programs when a diffuse field is assumed in each plate. These coupling loss factors satisfy the consistency relation when the modal density is used instead of the mode count.

(b) $(E_2/E_1)_{mc}$ - obtained when the actual mode count (see paragraph 4.2.2) is used.

(c) $(E_2/E_1)_L$ - calculated when the internal loss factors obtained from reference [31] are used instead of those resulting from the experimental work (section 4.2.1).

The difference between 10 log $(E_2/E_1)_{md}$ and 10 log $(E_2/E_1)_{mc}$ are significant at the bands centered at 630 Hz and 1250 Hz. It is clear that the application of modal density formulations may lead to a poor estimation (about 6 dB above the experimental results, 10 log $(E_2/E_1)E$, in both bands). At 1250 Hz, three modes are present at the top plate and eight at the web (ratio of .375); while the application of modal density indicates 0.9 and 7.2 respectively (a ratio of 0.125). At 2.5 kHz and for higher bands the difference between 10 log $(E_2/E_1)_{md}$ and 10 log $(E_2/E)_{mc}$ is negligible, showing that (in this case) the modal density formulations can be properly used. For all these bands (2.5 kHz and above) the ratio between the modal densities of the two plates is very close to the ratio between their actual mode count (obtained experimentally).

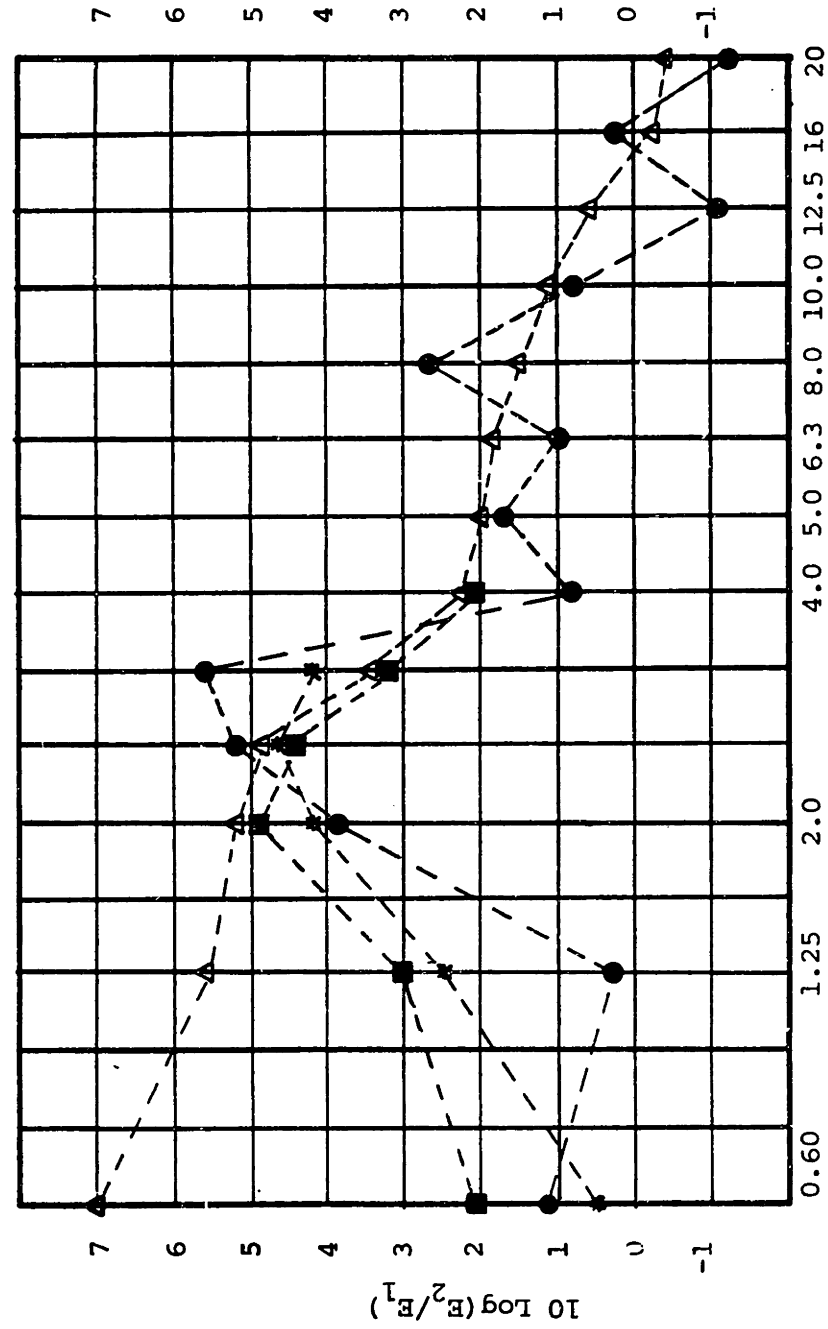

FIGURE 5.2.3: ENERGY RATIO -- WEB-TOP-PLATE -- TWO-PLATE MODEL

●:Experimental Result -- Δ:SEA Prediction - Bending Only (Modal Density)

■:SEA Prediction - Bending Only (mode count) -- ✱ : SEA Prediction (Internal Loss Factors from Reference [31] and Mode Count)

Figure 5.2.3 also shows that the predicted values of 10 log $(E_2/E_1)_{mc}$, are better than expected, when Swift's lower limit is considered (as discussed in Chapter 4). Except for the bands centered at 1.25 and 3.15 kHz, the differences between 10 log $(E_2/E_1)_{mc}$ and 10 log $(E_2/E_1)_E$ are less than $\pm$ 2dB, including those bands (0.63 to 6.3 kHz) where $N_1 < 6$ and also including bands (10 to 20 kHz) above Swift's upper limit.

In Chapter 4 and in Appendix A, an important aspect associated with the internal loss factors was discussed: their impact on the SEA predictions. This impact is directly related to:

(a) The possible variation of the dissipation from the uncoupled to the coupled condition. To have such variation minimized, damping layers and MIG welding were used. However, the comparison of η_i (determined experimentally for each isolated plate) with the values obtained from Lyon [31], indicated a possible underestimation of the actual dissipation for frequencies below 4 kHz.

(b) Accuracy of the determined loss factors.

(c) The relative values of the loss factors with respect to the associated coupling loss factors.

For a two plate joint when only bending transmission is considered, the influence of η_i on the predicted energy ratio values can be directly inferred from the expression:

$$\frac{E_2}{E_1} = \frac{\eta_{12}}{\eta_{21} + \eta_2}$$

For this sub-model the values of η_2 determined experimentally are:

(a) Much smaller than η_{21} at 1250 Hz and below

(b) Of the same order as η_{21} at 2.0 and 2.5 kHz.

(c) Higher than η_{21}, at 3.15 kHz and above (The difference increasing with frequency.)

Therefore, at the lower frequencies the energy sharing tends to be dictated by the coupling loss factors; the internal factor has little influence. As frequency increases E_2/E_1 becomes more and more sensitive to the η_2 variations.

If below 2.5 kHz, the values of η_2 obtained from reference [31] (for welded plates) were used, the corresponding predicted energy ratio levels 10 log $(E_2/E_1)_L$ would be lower than 10 log $(E_2/E_1)_{mc}$, 2 dB closer to 10 log $(E_2/E_1)_E$ (See Figure 5.2.3). This could explain an apparent overestimation of E_2/E_1 at 0.63 and 2 kHz, but not at 1.25 kHz.

The impact of the internal loss factors on the predicted energy ratio levels is better illustrated by Figure 5.2.4. It shows 10 log $(E_2/E_1)_{mc}$ as a function of η_2, for five different frequencies. It can be noticed that:

(a) for the lower frequencies it is necessary to have a variation of 100% in η_2 to result in a variation of about 1 dB in 10 log $(E_2/E_1)_{mc}$. This is because $\eta_2 \simeq 0.3\ \eta_{21}$.

(b) 10 log $(E_2/E_1)_{mc}$ is more sensitive to a variation in η_2 around 4 kHz, where η_2 is greater than η_{21}.

(c) in general, above 4 kHz a variation of 1 dB in 10 log η_2 (maximum acceptable variation that may be associated with the experimentally determined loss factors) will result in a variation of 1 dB or less in 10 log $(E_2/E_1)_{mc}$.

Another interesting aspect is illustrated by Figure 5.2.5: above the value of $\eta_2 = 0.003$, it is shown that it is not worthwhile to increase the loss factor, η_2, to try to improve the power dissipation in Plate 2. As a

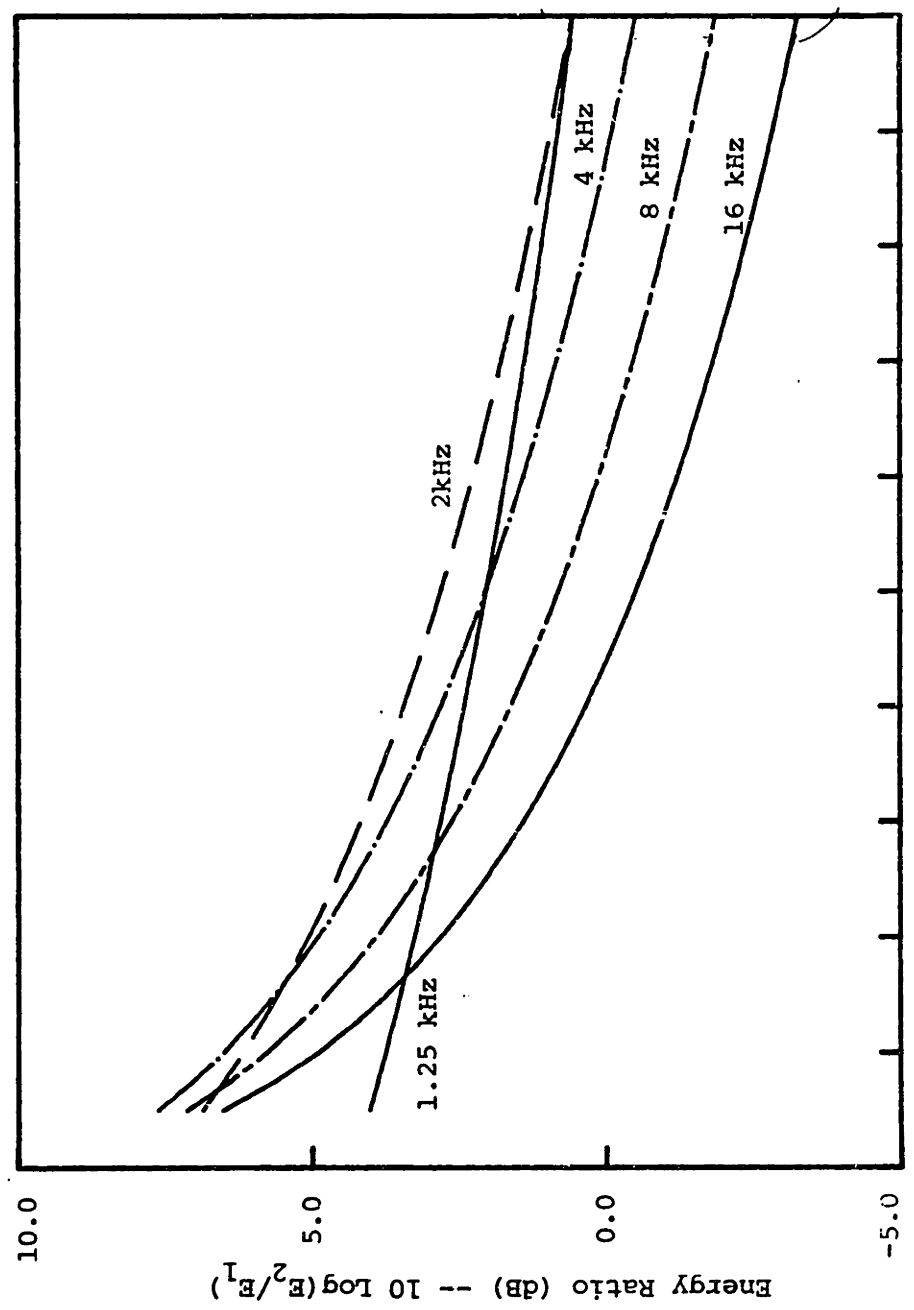

FIGURE 5.2.4: VARIATION OF THE ENERGY RATIO LEVEL FOR THE TWO-PLATE MODEL WITH THE INTERNAL LOSS FACTOR OF THE WEB (2)

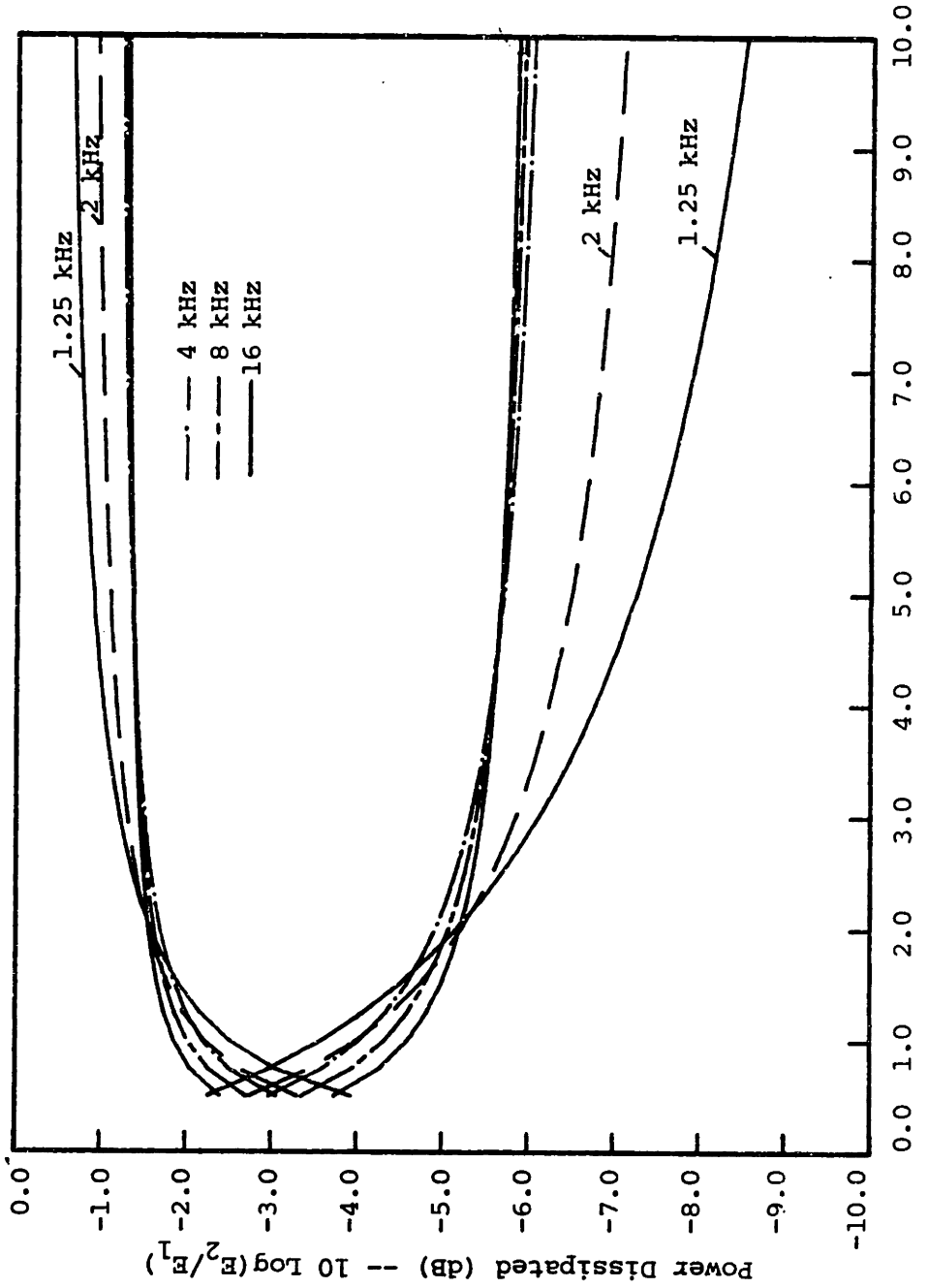

FIGURE 5.2.5: VARIATION OF THE POWER DISSIPATION IN THE WEB (2) WITH ITS INTERNAL LOSS FACTOR

kind of compensation the energies (E_2 and E_1) will decrease, keeping the dissipation at the same level in each plate.

In summary:

(a) A good agreement (within $\pm$ 3 dB), between predicted and experimentally determined energy ratio levels is verified, even for the frequency bands where fewer than six modes are exicted in the top plate.

(b) The application of the modal density formulations instead of the actual mode count could have led to a significant overestimation of 10 log (E_2/E_1), at 630 and 1250 Hz (about 6 dB).

(c) The impact of the internal loss factors on the predicted energy levels is not very significant along the whole frequency interval. The variation at lower frequencies (from uncoupled to coupled conditions) and/or an inaccuracy at higher frequencies have to be high to result in a significant variation of 10 log (E_2/E_1) (See Figure 5.2.4).

5.3 Second Step - Four-Plate Sub-Model

Figures 5.3.1 to 5.3.3 show the energy ratio levels (with respect to the top-plate), resulting from the experimental work, $(E_p/E_1)_E$, and from the application of SEA, $(E_p/E_1)_F$ (only bending) and $(E_p/E_L)_G$ (considering energy transformations). Since in this model more emphasis is placed on energy transformations, measurements were not taken below 1.25 kHz. The values of 10 log $(E_2/E_1)_G$ were determined only above 2.0 kHz, since the first in-plane modes in the web are expected at the band centered at 5 kHz.

Figures 5.3.2 and 5.3.3 illustrate the contribution of the in-plane motions of the web (2) to the flexural energy of the tank top plates

kind of compensation the energies (E and E_1) will decrease, keeping the dissipation at the same level in each plate.

In summary:

(a) A good agreement (within $\pm$ 3 dB), between predicted and experimentally determined energy ratio levels is verified, even for the frequency bands where fewer than six modes are excited in the top plate.

(b) The application of the modal density formulations instead of the actual mode count could have led to a significant overestimation of 10 log E_2/E_1, at 630 and 1250 Hz. (about 6 dB)

(c) The impact of the internal loss factors on the predicted energy levels is not very significant along the whole frequency interval. The variation at lower frequencies (from uncoupled to coupled conditions) and or an inaccuracy at higher frequencies have to be high to result in a significant variation of 10 log E_2/E_1. (See Figure 5.2.4).

5.3 Second Step - Four-Plate Sub-Model

Figures 5.3.1 to 5.3.3 show the energy ratio levels (with respect to the top-plate), resulting from the experimental work, $(E_p/E_1)_E$, and from the application of SEA, $(E_p/E_1)_F$ (only bending) and $(E_p/E_L)_G$ (considering energy transformations). Since in this model more emphasis is placed on energy transformations, measurements were not taken below 1.25 kHz. The values of 10 log $(E_2/E_1)_G$ were determined only above 2.0 kHz, since the first in plane modes in the web are expected at the band centered at 5 kHz.

Figures 5.3.2 and 5.3.3 illustrate the contribution of the in-plane motions of the web (2) to the flexural energy of the tank top plates

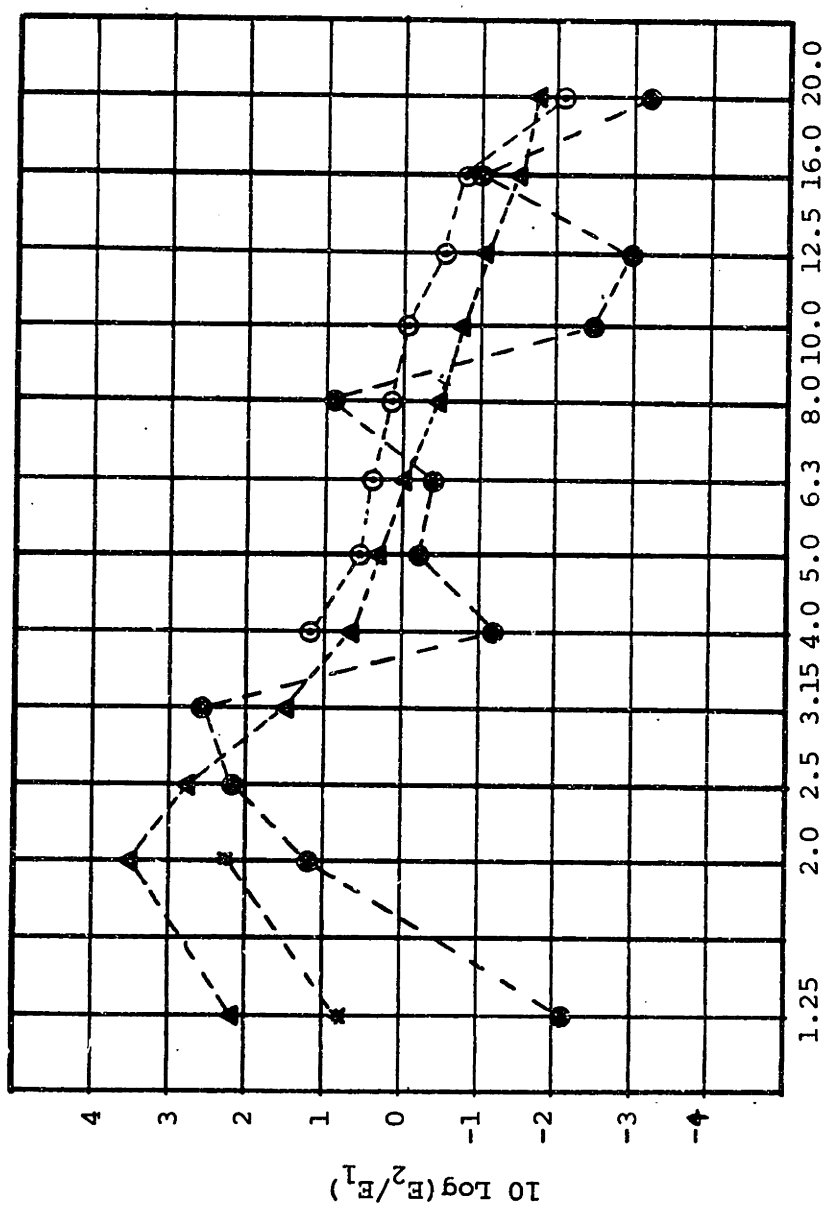

FIGURE 5.3.1: ENERGY RATIO -- WEB - TOP PLATE -- FOUR-PLATE MODEL

●: Experimental Results -- ▲: SEA Predictions - Bending Only --
⊙: SEA Predictions-Energy Transformation

✱: SEA Predictions-Bending Only (Internal Loss Factor from Reference [31])

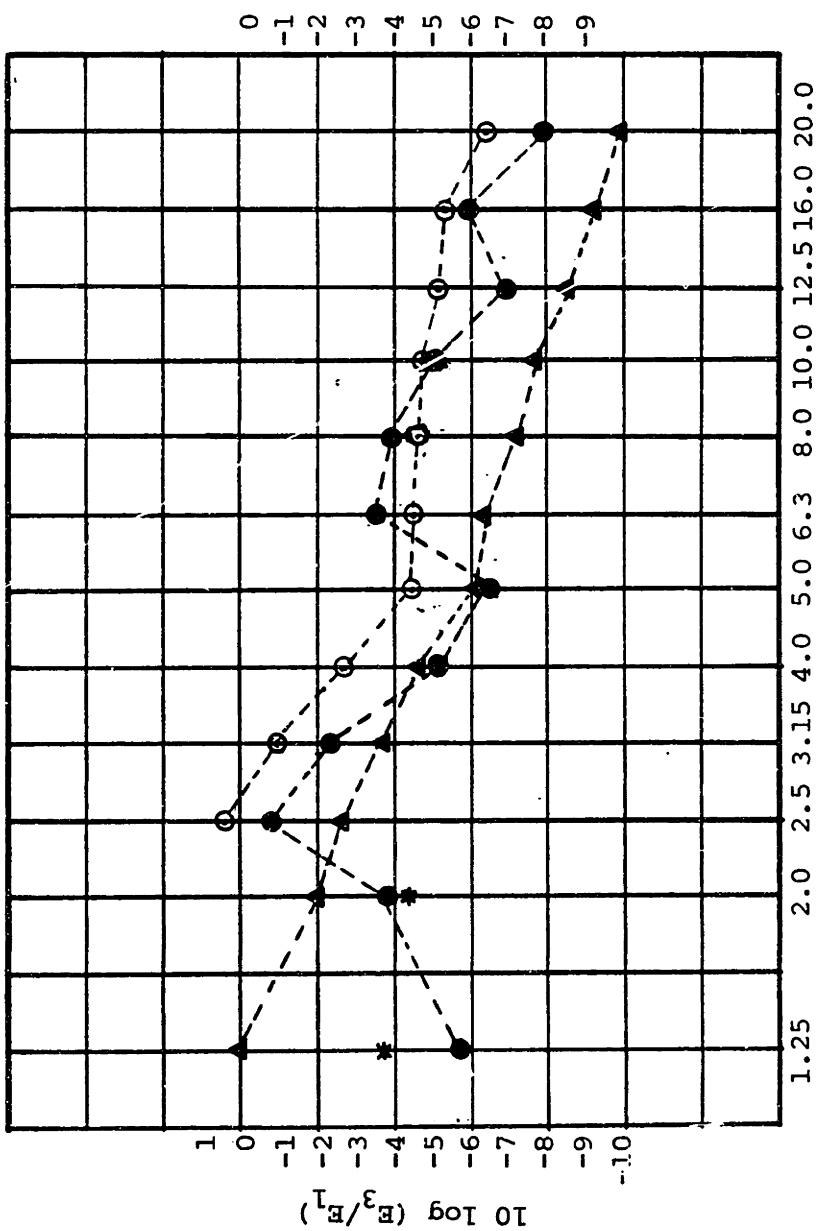

FIGURE 5.3.2: ENERGY RATIO -- TANK TOP PLATE (3) - TOP PLATE (1) -- FOUR-PLATE MODEL

●: Experimental Results, ▲: SEA Predictions-Bending Only,
⊙: SEA Predictions-Energy Transformation

✱: SEA Predictions-Bending Only (internal loss factors from reference [31])

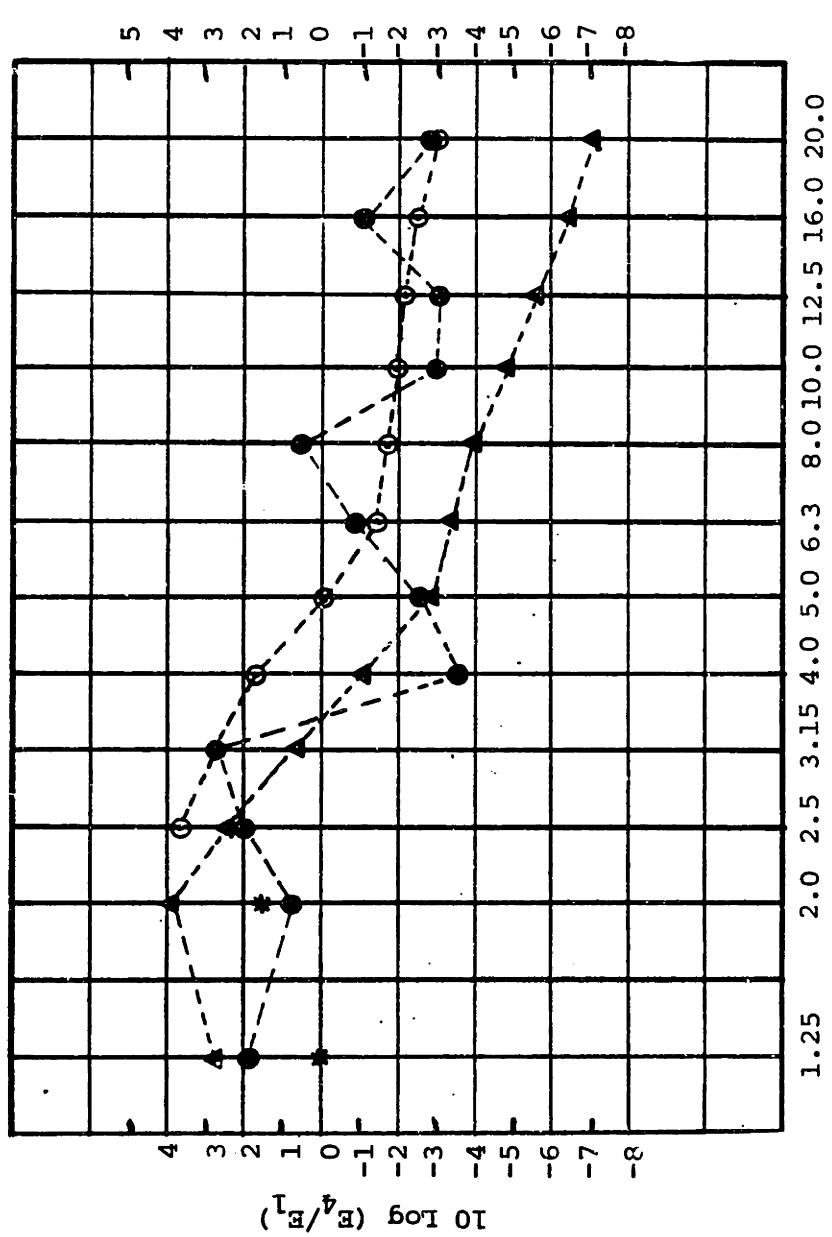

FIGURE 5.3.3: ENERGY RATIO - TANK TOP PLATE (4) - TOP PLATE (1) -- FOUR-PLATE MODEL

●: Experimental Results, ▲: SEA Predictions - Bending Only, ⊙: SEA Predictions - Energy Transformation

✱: SEA Predictions - Bending Only (internal loss factors from reference [31])

(3 and 4). For those last two plates the values 10 log $(E_{3(4)}/E_1)_E$ seem to follow the predicted values of 10 log $(E_{3(4}/E_1)_F$ up to 5 kHz. Above this frequency a change occurs and the experimental results become closer to the 10 log $(E_{3(4)}/E_L)_G$ predictions, up to 20 kHz. As anticipated in Chapter 4, the differences between 10 log $(E_{3(4)}/E_L)_F$ and 10 log $(E_{3(4)}/E_L)_G$ are not high, but significant enough to show the effect of the energy transformations especially from plate 2 to 4. In plate 3 the characterization is not so evident.

With respect to plate 2, as already stated, the differences between 10 log $(E_2/E_1)_F$ and 10 log $(E_2/E_1)_G$ are small (< 1 dB).

For all three plates the predicted values of 10 log $(E_p/E_1)_F$ at 1.25 and 2 kHz seem to be an overestimation of the experimental result. If the values of loss factors from the curve of reference [31] are utilized, then:

(1) The differences narrow to:

(a) 1250 Hz - 3 dB for plate 2 and 2 dB for plate 3.

(b) 2 kHz - less than 1 dB for all plates.

(2) The difference increases to 2 dB for plate 4, at 1.25 kHz.

It was also verified that if consistent errors of 20% were made in the determination of the loss factors, a variation of about 1 dB or less in the predicted energy ratios would result.

The prediction that energy transformations could be important above 5 kHz seems to be confirmed for this model. The agreement between SEA results and measured results is also fairly good:

(a) Plates 2 and 3 - within $\pm$ 2 dB, except at 1.25 kHz (4 dB)

(b) Plate 4-within $\pm$ 2 dB, except at 4 kHz and 3 kHz (within $\pm$ 2.5 dB) and at 2 kHz (less than 3 dB).

This good agreement is particularly important above 4 kHz, since the values of 10 log $(E_p/E_1)_F$ and 10 log(E_p/E_L) were obtained by using average parameters (coupling loss factors and modal density were determined assuming the existence of a diffuse field) even when any number fewer than six in-plane modes were expected.

In plates 1 and 3, the first in-plane modes are expected only above 8 kHz. As a verification, two calculations were performed:

(1) considering 3 SEA subsystems in each plate (12^{th} order problem)

(2) not including between 4 kHz and 8 kHz the in-plane subsystems of plates 1 and 3 (8^{th} order problem).

The results were the same. Even above 8 kHz, the influence of these subsystems was verified to be practically negligible. This simplifies the calculations.

5.4 Third Step - Seven Plate Model

Figures 5.4.1 to 5.4.6 show the energy ratio levels of each plate with respect to the top plate, resulting from the experimental work and from the application of SEA.

As pointed out in Section 4.5, the emphasis in this submodel is on energy transformations. Therefore, except for the web (2) and bottom plates (6 and 7), measurements were taken in only two third-octave bands below

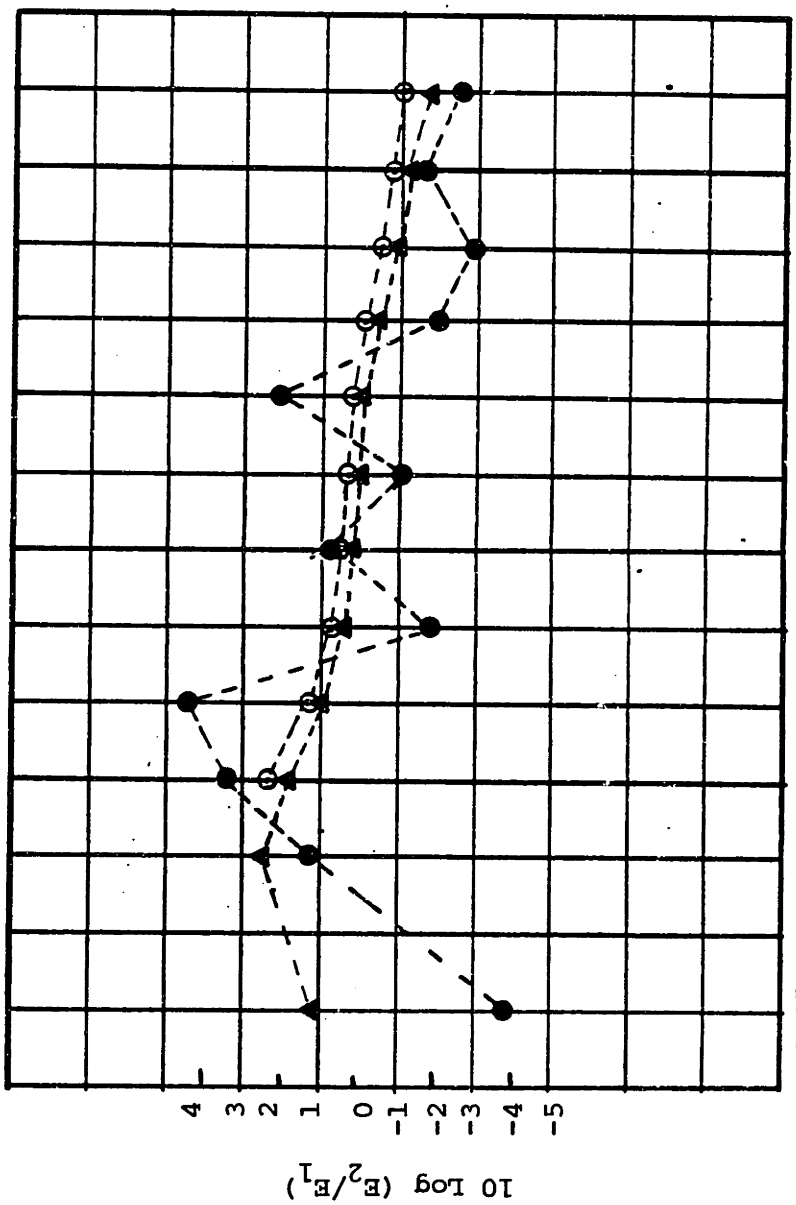

FIGURE 5.4.1: ENERGY RATIO -- WEB-TOP PLATE -- SEVEN-PLATE MODEL

●: Experimental Results, ▲: SEA Predictions - Bending Only

⊙: SEA Predictions - Energy Transformations

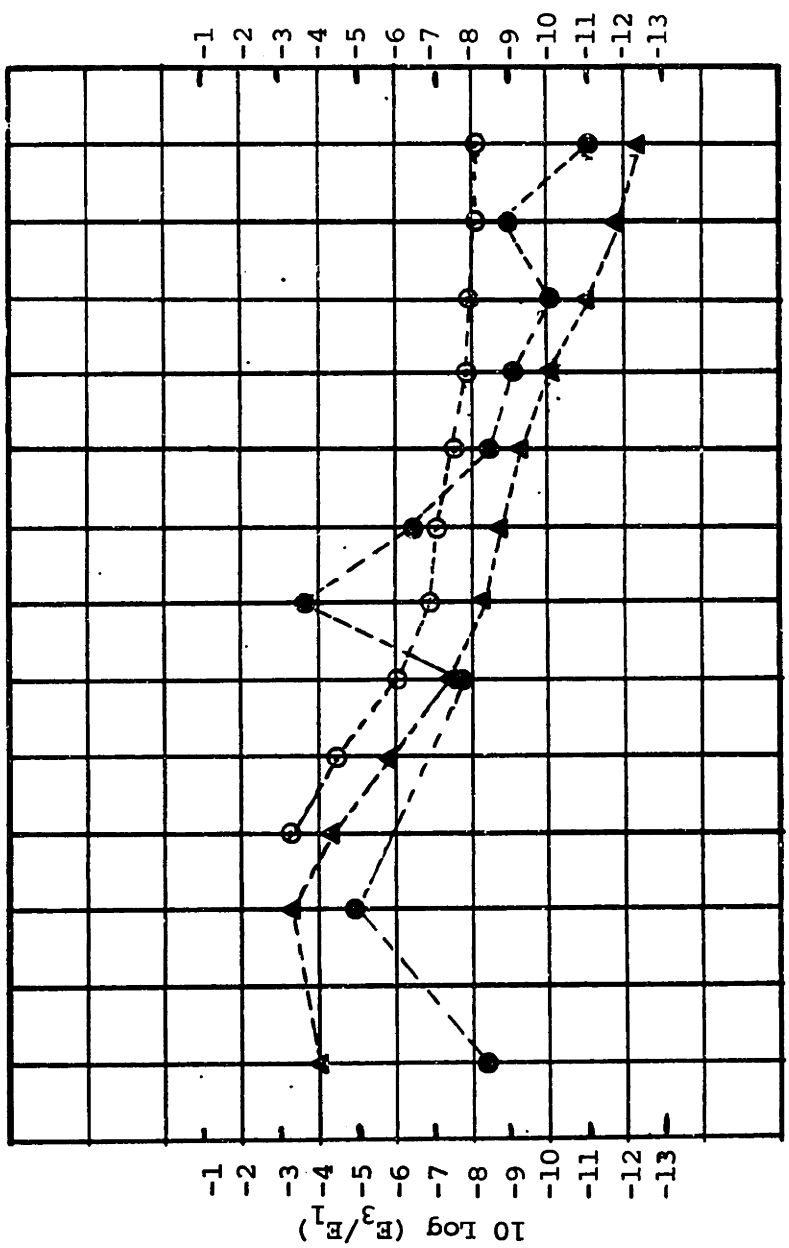

FIGURE 5.4.2: ENERGY-RATIO -- TANK TOP (3) - TOP PLATE (1) -- SEVEN-PLATE MODEL

●: Experimental Results, ▲:SEA Predictions - Bending Only,

⊙:SEA Predictions - Energy Transformation

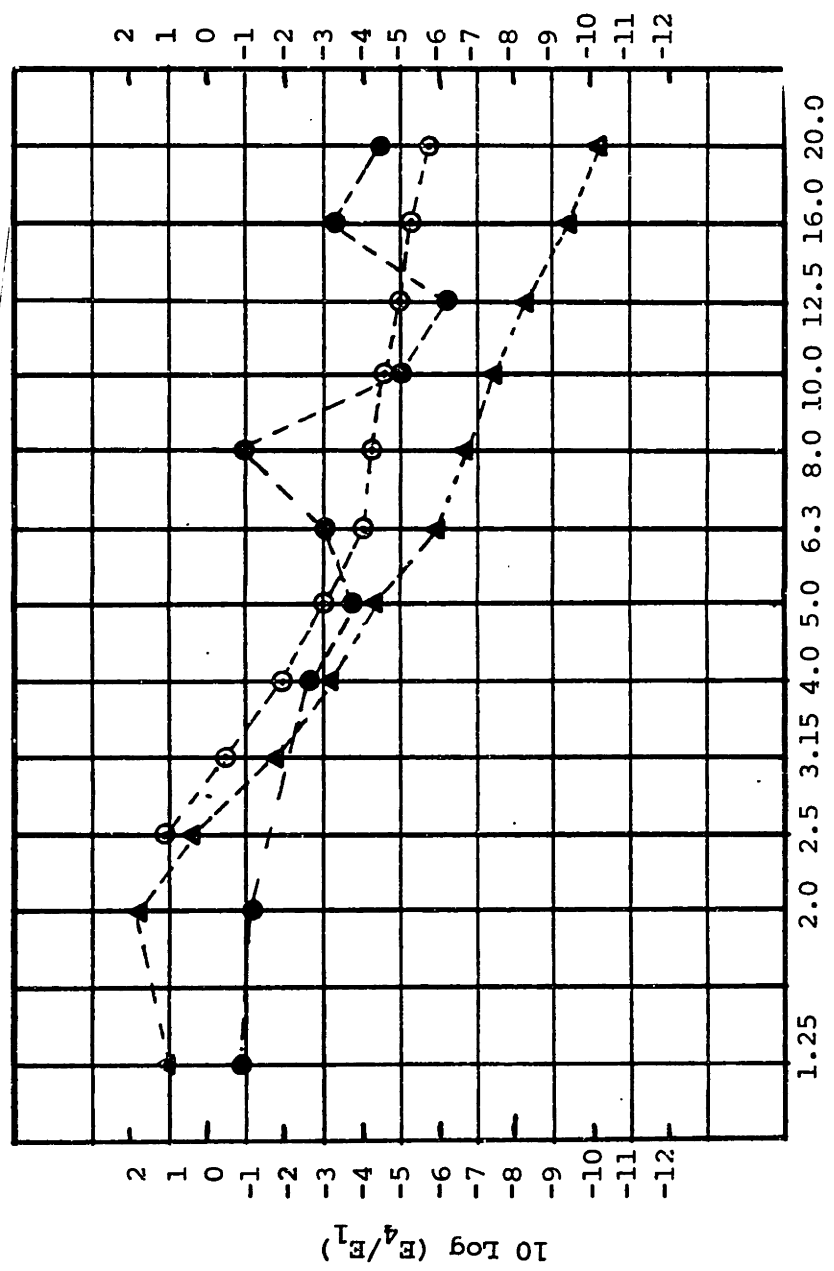

FIGURE 5.4.3: ENERGY RATIO -- TANK TOP PLATE-TOP PLATE -- SEVEN-PLATE MODEL

●: Experimental Results, ▲: SEA Predictions (Bending Only),

⊙: SEA Predictions - Energy Transformation

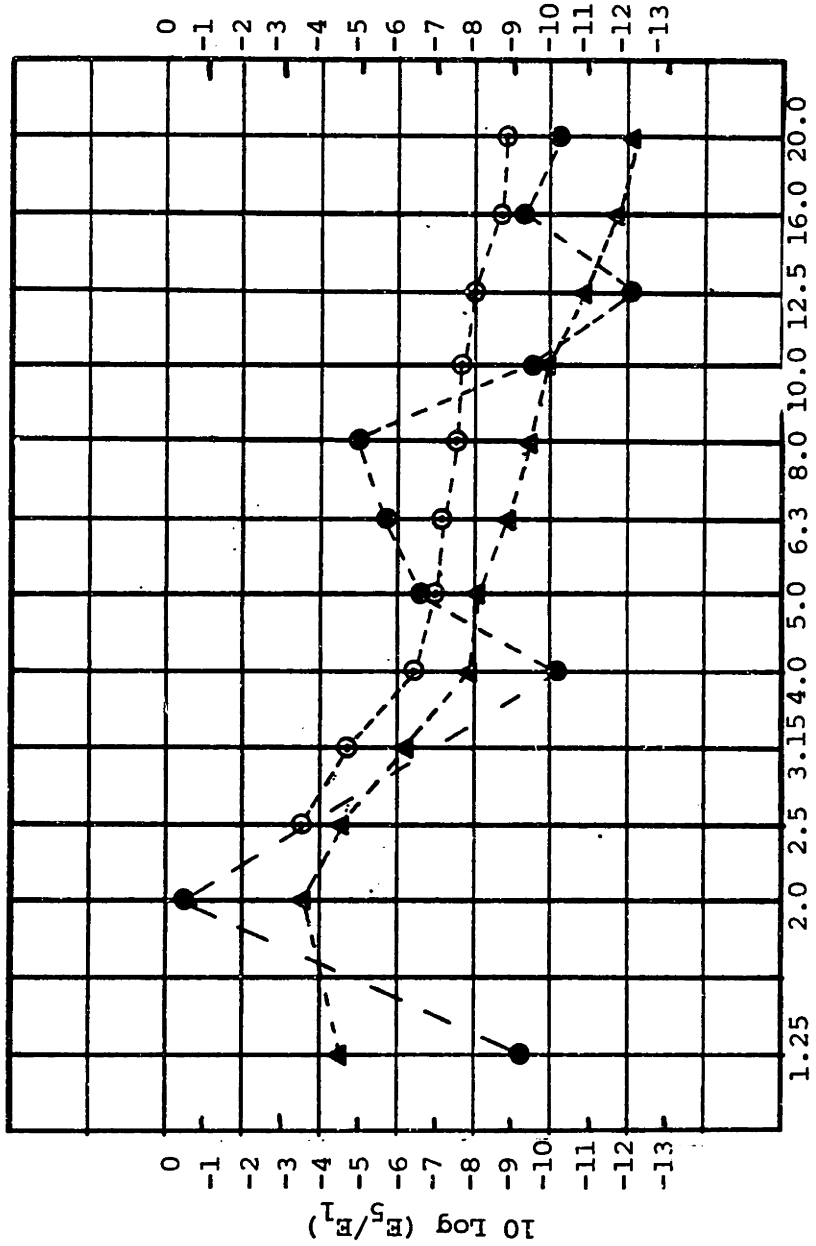

FIGURE 5.4.4: ENERGY RATIO -- LONGITUDINAL GIRDER(5) - TOP-PLATE (1) -- SEVEN-PLATE MODEL

●: Experimental Results, ▲: SEA Predictions - Bending Only,

⊙: SEA Predictions - Energy Transformation

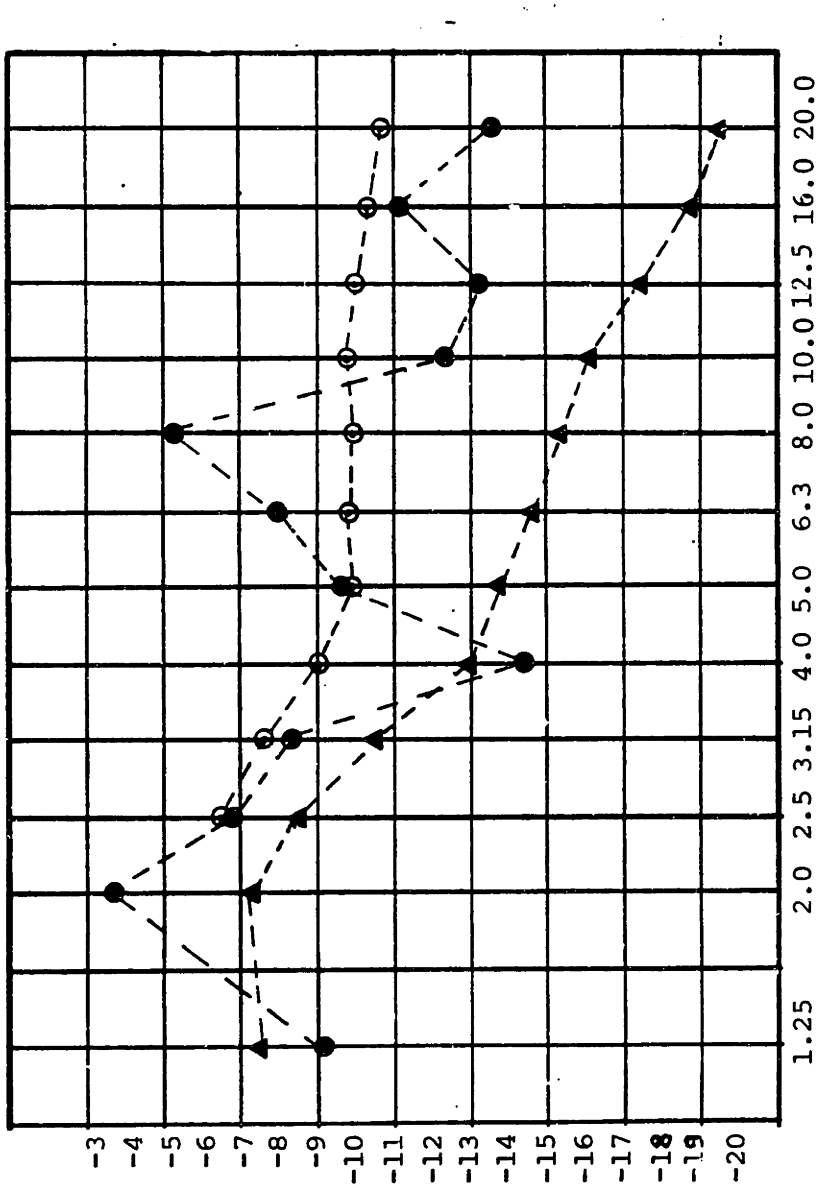

FIGURE 5.4.5: ENERGY RATIO -- BOTTOM PLATE (6) - TOP PLATE (1) -- SEVEN-PLATE MODEL

●: Experimental Results, ▲: SEA Predictions - Bending Only,

⊙: SEA Predictions - Energy Transformation

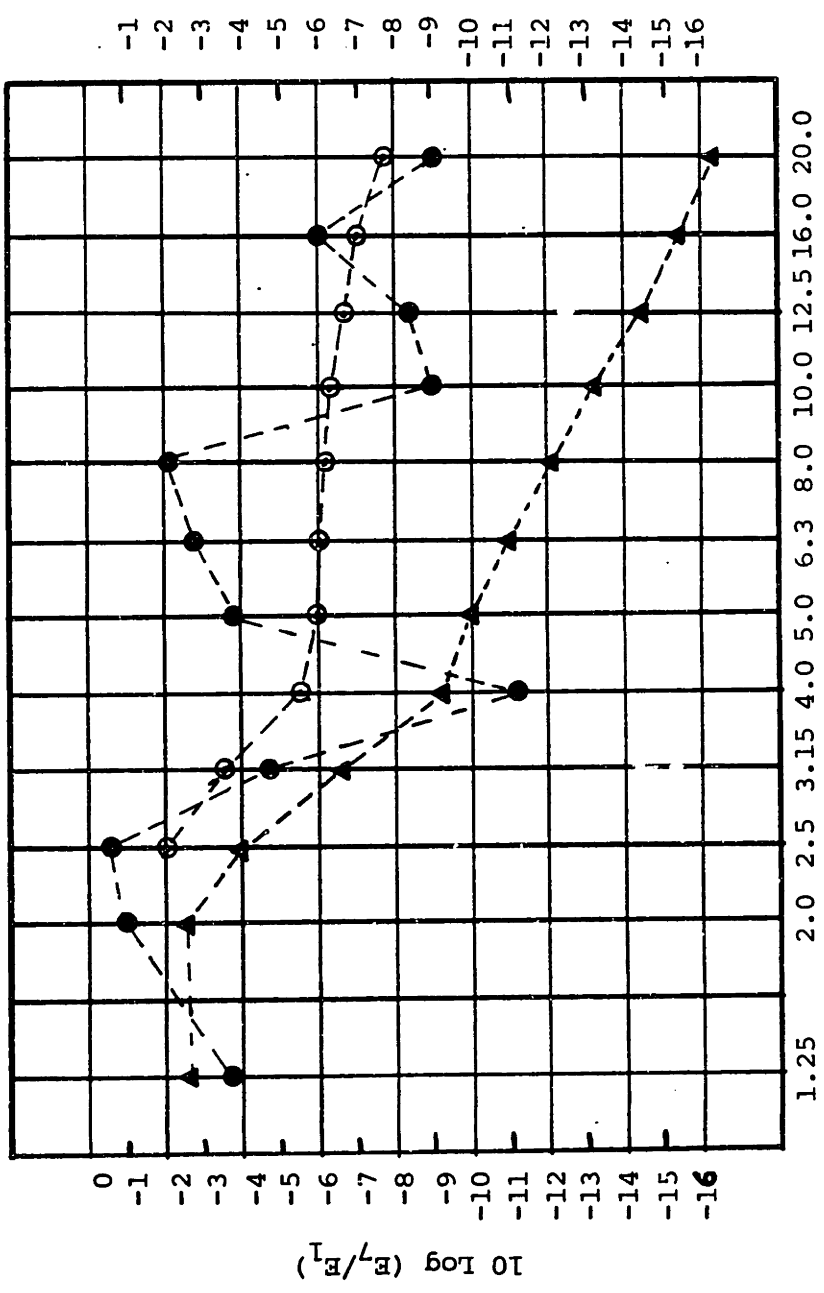

FIGURE 5.4.6: ENERGY RATIO -- BOTTOM PLATE (7) -- SEVEN-PLATE MODEL

●: Experimental Results, ▲: SEA Predictions - Bending Only

⊙: SEA Predictions - Energy Transformation

4 kHz (1.25 kHz and 2 kHz) in order to speed up the process. This decision was based on the following reasons:

(1) The bands centered at 1.25 and 2 kHz are, together with the one centered at 630 kHz, the most unfavorable to the SEA predictions (less than four modes in the top plate).

(2) For the previous two models the agreement between the predicted values and the experimental results was fairly good below 4 kHz, better than expected.

(3) For the lower frequencies the interaction between the web and the top plate (directly coupled) is considered more representative.

(4) In the final step, attention will be given to the web and bottom plate.

(5) In the previous model the contribution of the in-plane motions for the flexural energy of plates 3 and 4 was noticed only above 4 kHz.

(6) Based on SEA parameters (as discussed in section 4.3), a strong flanking path of in-plane energy through the web and longitudinal girder could be expected in this model. It was also anticipated that the in-plane motions on those two plates would contribute significantly to the flexural energy level of the bottom plates.

Figures 5.4.5 and 5.4.6 confirm the importance of the in-plane motions and of the energy conversions in this model. Those figures show that, above 4 kHz:

(1) The experimental results, 10 log $(E_{6,7}/E_1)_E$ are closer to 10 log $((E_{6.7}/E_1)_G$ than to 10 log $(E_{6,7}/E_1)_F$. The differences between

10 log $(E_{6,7}/E_1)_G$ (three SEA subsystems) and 10 log $(E_{6,7}/E_1)_F$ (only bending) are significant and increase with frequency (4 dB at 5 kHz to 8 dB at 20 kHz. Therefore, the assumption that the only mechanism of transmission is bending may lead to significant underestimation of the flexural energy level of the bottom plates. The net power flow between the in-plane subsystems of plates 2 and 5 is a good indication of the importance of the flanking path of in-plane energy through these plates: For example, at 12.5 kHz, it is about six times higher than the net power flow from the flexural subsystems of plates 2, 3 and 4 to the flexural subsystems of plate 5.

(2) The agreement between the experimental results and those predicted by SEA (when in-plane motions are considered) is fairly good at 10 kHz and above, within 3 dB. At the bands centered at 6.3 and 8 kHz a significant difference is verified for plate 7, about 3 and 4 dB respectively. A difference of the same order is also verified for plate 6 at 8 kHz, about 5 dB. These differences (for both plates) may be understood as a possible consequence of a change in behavior that results from the excitation of the in-plane modes when they become available. A similar situation is noticed for plates 3 (Figure 5.4.2) and plate 4 (Figure 4.5.3) at 5 kHz and 8 kHz, respectively. However, it is important to point out that smaller differences (between 10 log $(E_{3,4}/E_1)_E$ and 10 log $(E_{3,4}/E_1)_G$) were observed in the previous model, from 5 kHz to 8 kHz. A possible explanation for the different behavior in the two models may be the creation of a preferable path of in-plane energy towards the bottom (high net power flow), when plate 5 is associated with plate 2. This

may result in a less smooth transition in the seven-plate model.

Figures 5.4.5 and 5.4.6 also show that:

(1) At 4 kHz, 10 log $(E_{6,7}/E_1)_F$ is closer to 10 log $(E_{6,7}/E_1)_E$ than it is to 10 log $(E_{6,7}/E_L)_G$ (difference of about 5 dB).

(2) The predicted values of 10 log $(E_{6,7}/E_1)_G$ at 2, 2.5 and 3.15 kHz are closer to the experimental results than are the predicted values of 10 log $(E_{6,7}/E_1)_F$.

These two last observations lead to the following possible interpretations:

(1) If we concentrate our attention below 5 kHz, it can be inferred from Figures 4.5.4 and 5.4.6 that the experimental results follow the predicted values of 10 log $(E_{6,7}/E_1)_F$. Therefore, despite the good agreement between 10 log $(E_{6,7}/E_1)_G$ and 10 log $(E_{6,7}/E_1)_E$ from 2.0 to 3.15 kHz, one can say that the flexural motions dominate the transmission below 5 kHz.

(2) If we consider the frequency interval from 2 to 20 kHz, Figures 5.4.5 and 5.4.6 show that the predicted values of 10 log $(E_{6,7}/E_1)_G$ constitute a kind of average line for the experimental results, which is a very strong indication that energy transformation occur below 5 kHz. This is very realistic because:

   (a) the limit of 5 kHz is the center frequency of the band in which the first in-plane resonant mode is expected, when the formulation of modal density is applied. This frequency has to be regarded as a reference value, since the modal density concept is

not appropriate to predict the first resonance and may also lead to an improper number of modes in a frequency band, when this number is very small (especially below 5, see Chapter 4). Therefore, it is highly probable that in-plane modes are available at the web and longitudinal girder below 5 kHz.

(b) the limit of 5 kHz was also established based on a criterion suggested by Swift [23], derived from the comparison between bending-to-bending transmission coefficients (see Section 4.1 and Appendix C). In Section 4.3 it was shown that at 5700 Hz the coupling loss factor between the flexural modes of the top plate and the in-plane modes of the web is of the same order as the coupling loss factor between the flexural modes of these two plates. This frequency may be understood as a reference value above which the in-plane motions can't be disregarded and below which their influence may be significant and may have to be considered (see Figure 4.3.15).

(c) the higher impedance of the in-plane motions when compared to the flexural motions. This means that they can carry a great deal of vibratory power (as already shown) even though their amplitudes are small. This higher impedance also means that the internal loss factors associated with the in-plane motions are also less than for flexural motions. Therefore, it is possible that the influence of the in-plane motions starts to be noticeable even before the band in which their first resonances actually occur. They may also be important in the bands (above the first resonance) in which no resonances occur.

Thus, the influence of the in-plane motion of plates 2 and 5 are not

only significant for the flexural energy of the bottom plates above 4 kHz, but such influence may also start to be noticeable at frequencies lower than the expected limit of 5 kHz. This could be the conclusion, if the experimental result at 4 kHz were higher than 10 log $(E_{6,7}/E_1)_F$ (and, therefore, closer to 10 log $(E_{6,7}/E_1)_G$). However, the differences between 10 log $(E_{6.7}/E_1)_G$ and 10 log $(E_{6,7}/E_1)_E$ at 4 kHz (5 dB) are about the same as the difference verified at 8 kHz. Therefore, as already discussed, such differences may be justified as a consequence of a changing behavior that results from the excitation of the in-plane modes, when they become available (possibly below 2.5 kHz).

In Figure 5.4.3, the contribution of the in-plane motions at the web and longitudinal girder to the flexural energy levels of the tank top plate (4) is well characterized above 5 kHz. It is not as significant as in the bottom plates. This was anticipated in Section 4.3.5. As in the previous model, the contribution of the in-plane motions to the flexural energy level of plate 3 is not evident. Above 6.3 kHz the experimental results seem to follow more closely the predicted values, when bending transmission only is assumed, rather than the values predicted for the case when in-plane motions are taken into account. No measurements were taken at the 2.5 and 3.15 kHz bands, but it is important to notice that (as for the previous model) the differences between 10 log $(E_{3,4}/E_1)_G$ and 10 log $(E_{3,4}/E_1)_F$ are small (about 1 dB) from 2 to 4 kHz. Based on this fact, one can infer that if the in-plane motions at plates 2 and 5 are available below 5 kHz (as previously discussed), their influence on plates 3 and 4 is not significant.

Other interesting aspects are shown in Figures 5.4.1 and 5.4.4. As for the previous model the differences between 10 log $(E_2/E_1)_G$ and

10 log $(E_2/E_1)_F$ are negligible. However, this is not quite true for plate 5. For this plate, the differences between the two predicted values increase with frequency, going from 1dB to 3dB from 2 to 20 kHz. Figure 5.4.4 also shows that above 5 kHz the values predicted when energy transformation is assumed seem to constitute an average line for the experimental results. The differences between 10 log $(E_5/E_1)_G$ and 10 log $(E_5/E_1)_F$ may be justified by a possible contribution on the in-plane motions of the coupled plates (especially from Plate 7). The differences between η^F_{25} and η_{25}(BB) are not large enough to justify the differences between the two predicted energy ratio levels, especially because $\eta^F_{25} > \eta_{25}$(BB).

It is also interesting to notice the similarity between Figure 5.4.3 and Figure 5.3.3 (corresponding to the four-plate model) and between Figures 5.4.1, 5.3.1 and 5.2.3. It seems that the addition of plates influences their energy levels but the vibrational behavior remains about the same.

The agreement between experimental results and predicted energy ratios is fairly good, within 3dB, except for some few bands, as already discussed and shown in Figure 5.4.1 to 5.4.6.

The influence of the loss factors in the predictions was also verified. As in the previous model, an increase or decrease of 20% in the loss factors associated with the flexural motions results in a variation not higher than $\pm$ 1 dB in the predicted energy ratio when only bending is considered, and in an almost negligible variation when in-plane motions are present. With respect to the loss factors associated with the in-plane motions, it was verified that a variation in their values of about 60% is necessary to have

a variation in the energy level of about 1 dB. This may be explained by the fact that the coupling between the in-plane motions is much higher than the corresponding loss factors. For this model, the coupling between the in-plane subsystems of Plates 2 and 5 and the flexural subsystems of Plates 3, 4, 6 and 7 are also higher than the in-plane loss factors of those plates.

This model offers a good opportunity to illustrate the usefulness of SEA for design purposes. To minimize the power dissipated in the bottom plates is important since it is directly associated with a noise requirement. Two actions could be intuitively suggested:

(1) Reduce the power delivered by the source.

(2) Increase the power dissipated in other plates by adding damping to them, especially to those in the main transmission path (2 and 5).

As discussed in Appendix B, the power input is a function of the foundation mobility that, for the higher frequencies, can be expressed by the characteristic mobility of the top plate [36]:

$$\mathrm{Re}\{Y\} = 1/2.3\ \rho C_L h^2$$

From this expression and those on Appendix B (related to soft mounting) one can infer that if the thickness of the top plate is increased by 10% a reduction of about 20% in power input may be expected. However, the ratio of thickness h_1/h_2 will increase, which means that $\eta_{12}(BL)$ and $\eta_{12}(BT)$ increases while $\eta_{12}(BB)$ decreases. Therefore, the contribution of the in-plane motions of the web and longitudinal girder to the flexural energy of the bottom plates will be stronger than before. As an overall result, the power dissipated in the bottom plate decreases by 15% instead of 20%.

With respect to the second action, Figure 5.4.7 shows the variation of the power dissipated in plate 7 at 12500 Hz (as an example), as a function of the loss factor of Plate 2, for two cases:

(1) When only bending transmission is assumed.

(2) When the in-plane motions are considered.

The curve corresponding to the first case indicates that it would be worthwhile to try to increase the loss factor of Plate 2 up to .015 in order to have a reduction of 5 dB in the power dissipated in Plate 7. However, the other curve, considering in-plane motions, shows clearly that almost no improvement results by doing that. Both curves help to further characterize the flanking path of in-plane motions along Plates 2 and 5 as mainly responsible for the power dissipated in the bottom. They also show that, in this case, by neglecting the energy transformation the designer can be induced to an inappropriate action (to add damping to Plate (2) to reduce the power dissipated in the ship bottom. For frequencies above 5 kHz a reduction action has to consider the in-plane motions in Plates 2 and 5. This is discussed in the next section.

5.5 Fourth Step -- Twelve-Plate Model

As discussed in section 4.5, the flexural energy levels of only three plates of this model are determined experimentally: top Plate (1), web (2) and the larger bottom plate (7).

Figures 5.5.1 and 5.5.2 show the energy-ratio levels resulting from the experimental work, $(E_p/E_l)_E$ and from the application of SEA, $(E_p/E_L)_F$ and $(E_p/E_L)_G$.

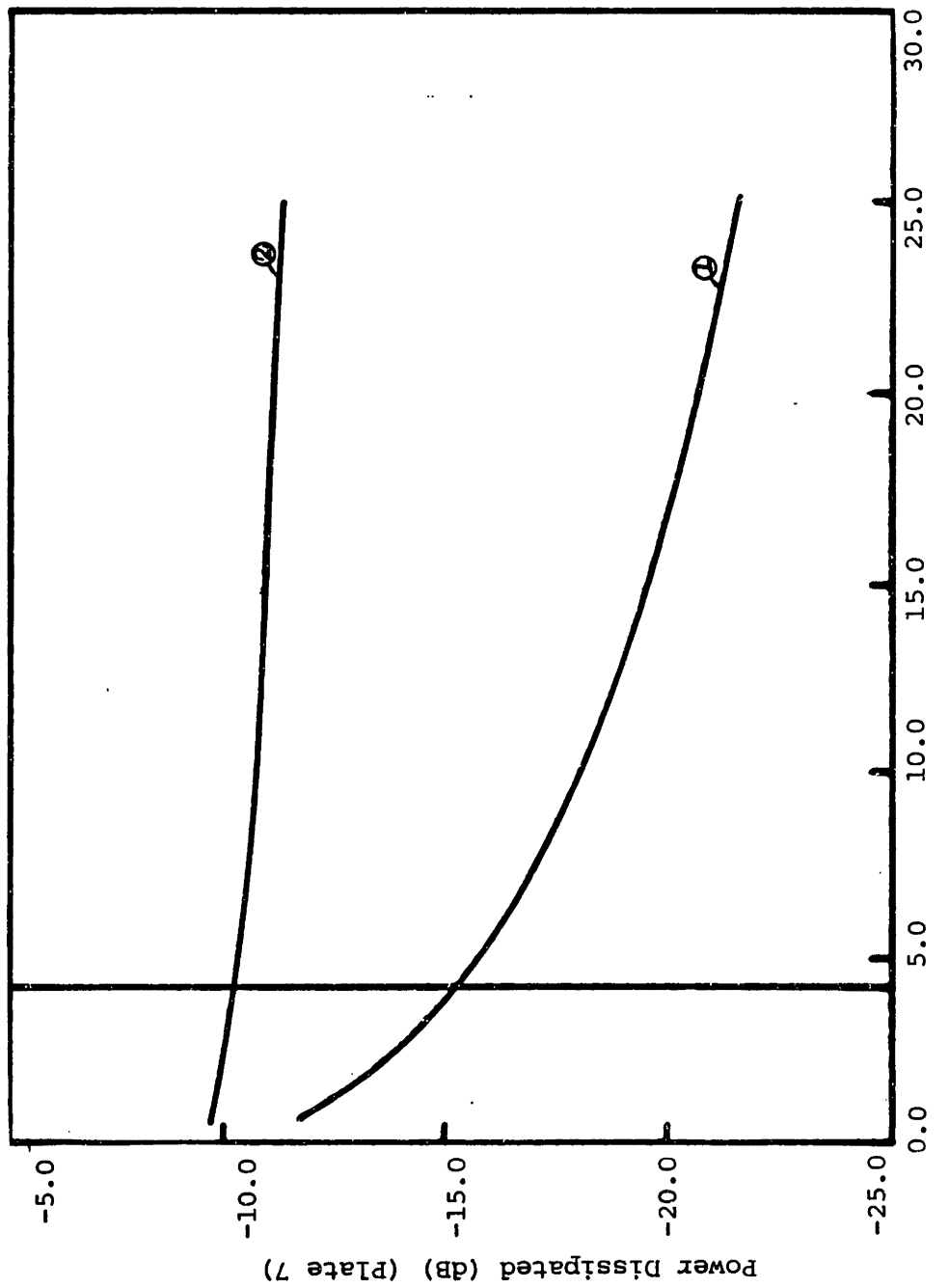

FIGURE 5.4.7: VARIATION OF THE POWER DISSIPATED IN THE LARGER BOTTOM PLATE (7) WITH THE INTERNAL LOSS FACTOR OF THE WEB (2), FOR f = 12.5 KHZ

①: Considering bending only,

②: Considering in-plane motions

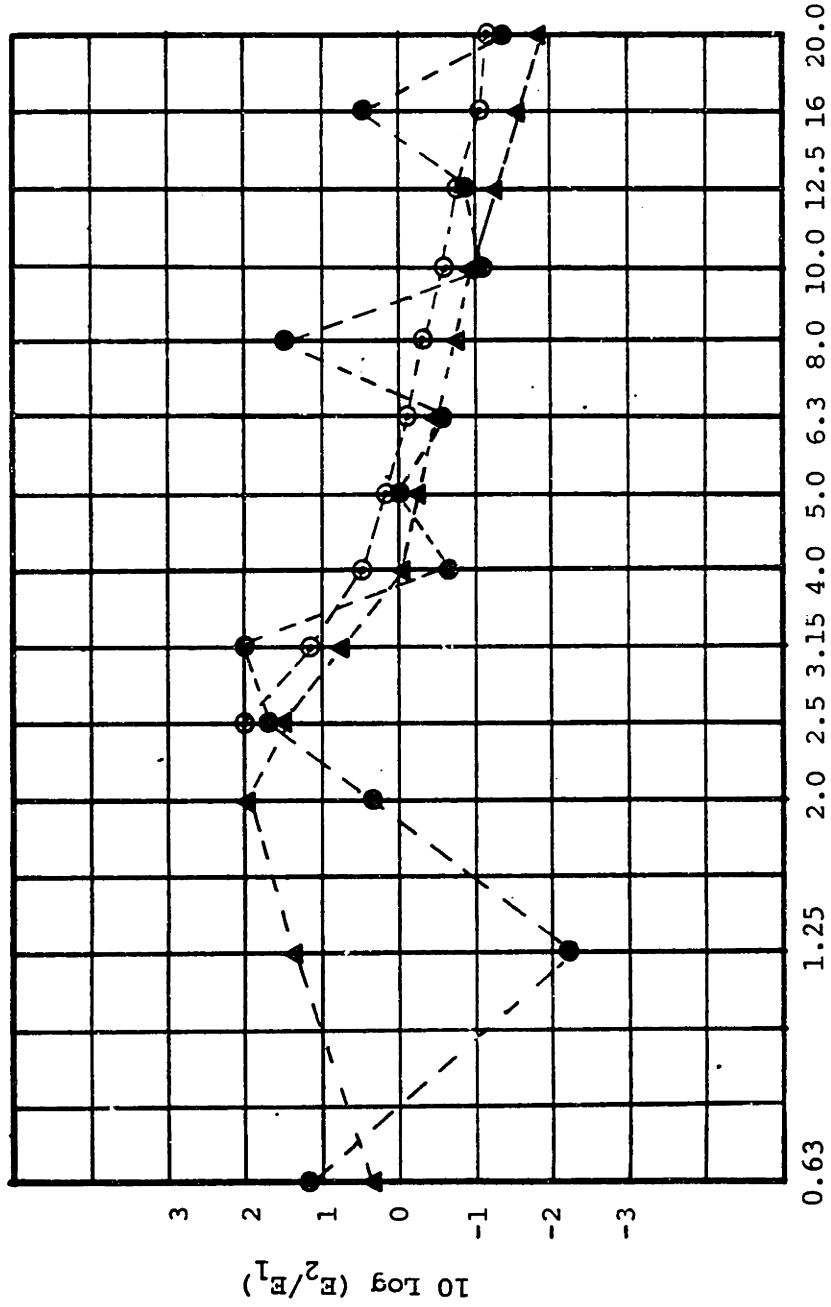

FIGURE 5.5.1: ENERGY RATIO -- WEB (2) - TOP-PLATE (1) -- TWELVE-PLATE MODEL

●: Experimental Results, ▲:SEA Predictions - Bending Only,

⊙: SEA Predictions - Energy Transformations

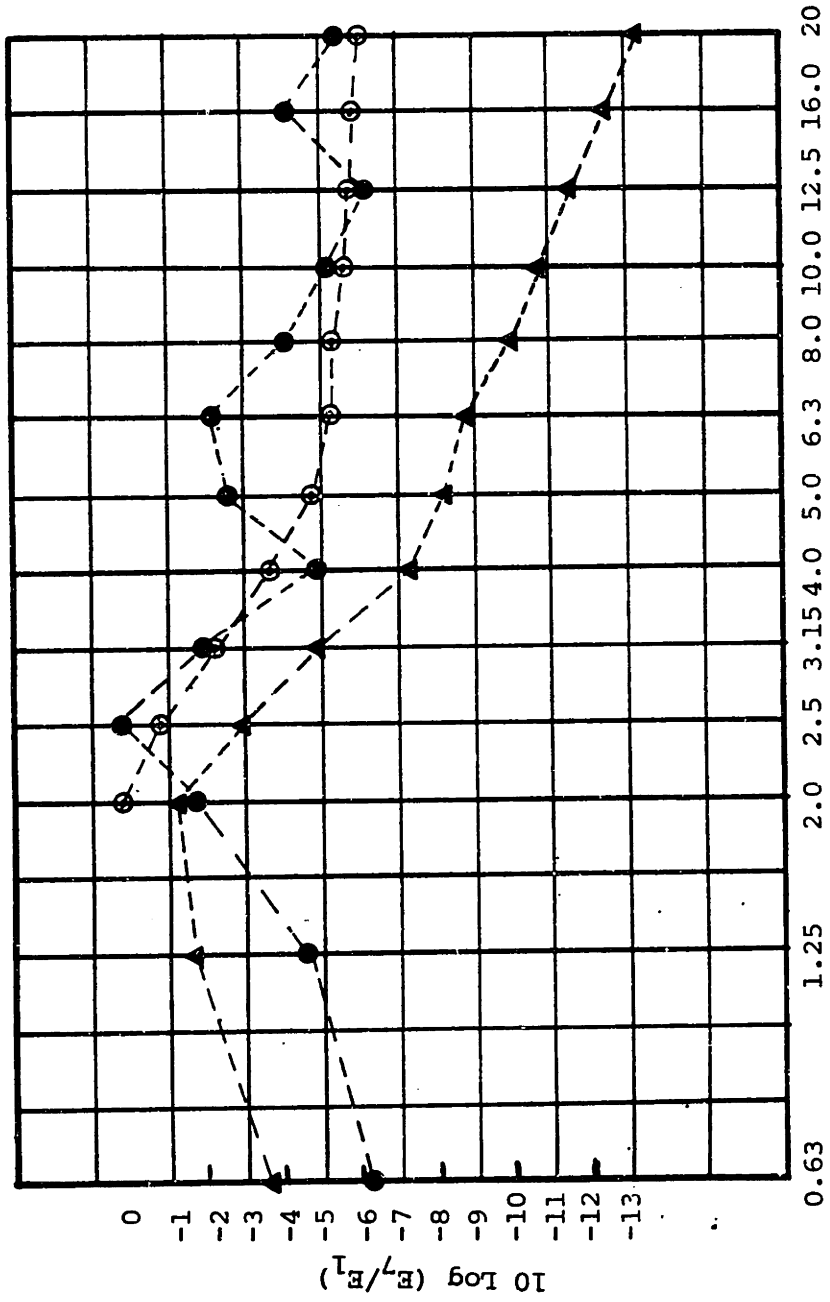

FIGURE 5.5.2: ENERGY RATIO -- BOTTOM PLATE (7) - TOP-PLATE (1) -- TWELVE-PLATE MODEL

●: Experimental Results, ▲: SEA Predictions - Bending Only,

⊙: SEA Predictions - Energy Transformations

As for the previous models, the differences between 10 log $(E_2/E_1)_F$ and 10 log $(E_2/E_1)_G$ are not significant (about 1 dB or less). The agreement between analytical and experimental results, above 2 kHz can be considered good, especially considering that (Figure 5.5.1):

(a) twenty transmission paths are offered to each subsystem of the web, since six plates are coupled to it.

(b) the web is connected to the two brackets by two different coupling lengths.

When comparing the results with those obtained in the previous models the values of 10 log $(E_2/E_1)_F$ seem to be a slight underestimation of 10 log $(E_2/E_1)_E$. On the other hand, the values of 10 log $(E_2/E_1)_G$ seems to to constitute a line that (above 2.5 kHz) is closer to an average line for the experimental results than is the line that results when the values of 10 log $(E_2/E_1)_F$ are connected. This indicates that, despite being very small, a contribution of the in-plane motions to the flexural energy level of the web is noticeable in this model.

For both plates (2 and 7) the differences between analytical and experimental results at 0.63 and 1.25 kHz are consistent with results obtained for the previous models. The most representatives difference are verified at 1.25 kHz (3-5 dB).

Figure 5.5.2 is a confirmation that the in-plane motions and the energy transformations play an important role in the vibration transmission through the physical model. This figure shows that:

(1) the agreement between 10 log $(E_7/E_1)_E$ and 10 log $(E_7/E_1)_G$ is fairly good from 2.0 to 20 kHz within $\pm$ 2 dB except at 6.3 kHz (2.5 dB). As for the seven-plate model, in this frequency interval the predicted values of 10 log $(E_7/E_1)_G$ constitute a kind of average line for the experimental results.

(2) the difference between the predicted values, 10 log $(E_7/E_1)_G$ and 10 log $(E_7/E_1)_F$, starts to be significant at 3.15 kHz (3 dB) and increases with frequency, up to 8 dB at 20 kHz.

Therefore, it is clear that in-plane modes are available below 5 kHz and have a noticeable contribution to the flexural energy level of the bottom plate. This is one more strong indication that the same happens for the seven-plate model (section 5.4).

It is important to call attention to the similarity between Figures 5.5.2 and 5.4.6. Their basic differences are:

(1) The agreement between 10 log $(E_7/E_1)_E$ and 10 log $(E_7/E_1)_G$ is much better for the twelve-plate model, especially at the bands centered at 4, 6.3 and 8 kHz. For these bands, differences of the order of 4 dB were verified for the seven-plate model. Such significant differences may result from a transient vibrational behavior due to the sudden availability of the in-plane modes. However, if this is correct, such transition occurs smoothly in the twelve-plate model, almost as smooth as that verified in the four-plate model. In section 5.4, a possibility was raised: that the more accentuated differences verified in the seven-plate model could be associated with the high net in-plane power

flow between the web and the longitudinal girder toward the bottom. However, for the twelve-plate model, this net power flow (through plates 2 and 5) has a smaller magnitude, since more transmission paths are available for the in-plane energy of these two plates.

(2) For the seven-plate model, as in the twelve-plate model, the values of 10 log $(E_7/E_1)_E$ at 2.5 and 3.15 kHz were closer to 10 log $(E_7/E_1)_G$ than to 10 log $(E_7/E_L)_F$. On the other hand, the agreement between 10 log$(E_7/E_1)_E$ and 10 log $(E_7/E_1)_F$ at 4 kHz was very good. Therefore, a reasonable doubt was created with respect to the actual availability and significance of the in-plane motions below 5 kHz. This kind of doubt does not exist for the twelve-plate model, especially because 10 log $(E_7/E_1)_E$ is in very good agreement with 10 log $(E_7/E_L)_G$ at 4 kHz.

When comparing Figures 5.5.2 and 5.4.6 one also can infer that: from 4 kHz to 20 kHz the differences between 10 log $(E_7/E_1)_G$ and 10 log $(E_7/E_1)_F$ are about the same for both models. For the seven-plate model the main energy transmission path, from the top plate to the bottom plate, was very well defined. A strong flanking path of in-plane energy through plates 2 and 5 was also identified. In the twelve-plate model a multi-path situation exists, created by the inclusion of the transverse plates (brackets and floor). With respect to in-plane motions a new path is offered by the bracket (8) -- coupled to the top plate -- and the floor (11). Therefore, it is not easy to directly infer from which path comes the major contribution to the flexural energy of the bottom plate. A good exercise in trying to understand the

vibration transmission can be carried out based on the SEA parameters and on the net power flow between SEA subsystems, resulting from the power balance equations.

The following aspects are important to be considered (all the numbers relating to net power flow are referred to 12.5 kHz, taken as example):

(1) The coupling length between the top plate (1) and the bracket (8) is about 40% of the coupling length between the top plate and the web, so that η_{12} is greater than η_{18} by 4 dB. The area of the bracket is about 50% of the area of the web, which means that η_{81} is greater than η_{21} by 3 dB. This results in a higher net power flow from 1 to 2. From the power balance equations

   (a) the net power flow from 1 to 8 is about 40% of the net power flow from 1 to 2.

   (b) the net power flow from the flexural subsystem of 1 to the in-plane subsystems of 2, $\Pi_{1-2}(BP)$, is about 60% higher than $\Pi_{12}(BB)$.

   (c) $\Pi_{1-8}(BP)$ is about 80% higher than $\Pi_{1-8}(BB)$.

(2) The internal loss factor of plate 2, η_2 is twice as high as η_8. Therefore, more power is dissipated in plate 2.

(3) Plate (2) has six other plates coupled to it so that, in principle, twenty paths are available for the power transmitted by each subsystem of 2. With respect to bending, the paths offered by the flexural subsystems of plates 3,4,5,8 and 9 have about the same order or importance, the higher net power flow being $\Pi_{24}(BB)$.

With respect to the in-plane motions, the preferable path is still offered by the in-plane motions of plate 5. However, a significant net power is transmitted to the bending subsystems of the brackets (8 and 9) about 60% of $\Pi_{25}(PP)$. This means the less power is transmitted by the in-plane motions to the bottom plates, through plate 2. As the internal loss factors of the brackets are much smaller than the coupling loss factors between them and the attached plates, most of the power that they receive is transmitted to the floors (10 and 11). This is because (despite the fact that $\Pi_{2-8}(PB)$ and $\Pi_{2-9}(P-B)$ are significant) the difference between 10 log $(E_{8,9}/E_1)_F$ and 10 log $(E_{8,9}/E_1)_G$ is less than 1 dB.

(4) The flexural subsystems of the floors offer important paths for the in-plane energy of the longitudinal girder. This is because the coupling between them is about the same order as the coupling between the in-plane subsystems of plate 5 and the flexural subsystems of the bottom plates.

$\Pi_{5-11}(PB)$ is about 80% of $\Pi_{5-7}(PB)$. This means that less in-plane power from 2 and 5 is reconverted to flexural energy at the discontinuity between the longitudinal girders and the bottom plates.

The contribution of the in-plane motions of plates 5 (directly) and 2 (indirectly through the bracket (8)) to the flexural energy level of the larger floor (11) is illustrated by Figure 5.5.3. It is also important to notice that some contribution

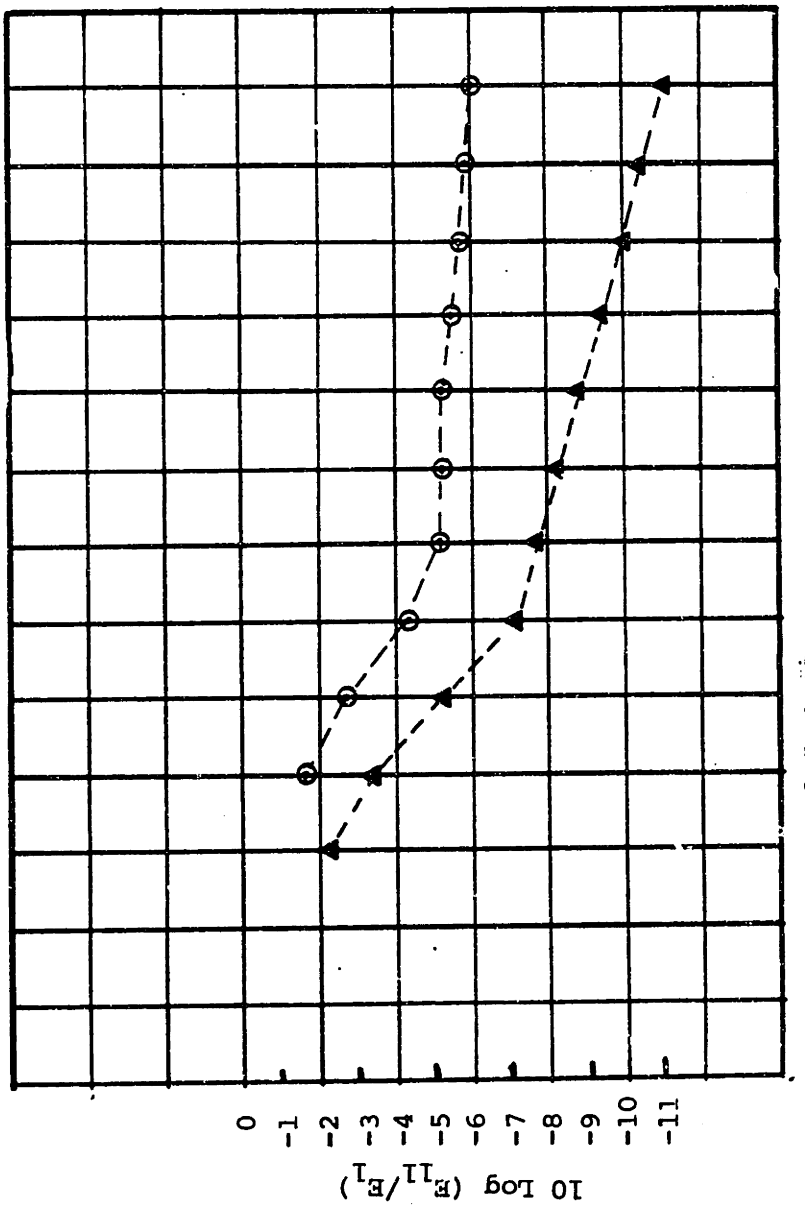

FIGURE 5.5.3: ENERGY RATIO -- FLOOR (11) - TOP PLATE (1) -- TWELVE-PLATE MODEL

▲: SEA Predictions - Bending Only,

⊙: SEA Predictions - Energy Transformations

comes from the in-plane motion of the tank top, plate (4).

(5) Two important paths are offered to the in-plane energy of the bracket (8) by the floor (11) and by the other bracket (9). The coupling length between 8 and 11 is smaller (70%) than the common length between 8 and 9. However, since the area of the floor (11) is almost four times larger than the area of 9, $\eta_{11-8}(PP)$ is much smaller than $\eta_{9-8}(PP)$. As a result $\Pi_{8-9}(PP)$ is about 50% of $\Pi_{8-11}(PP)$. The floor is then the preferable path for the in-plane energy of the bracket. It is important to point out that $\Pi_{8-11}(PP)$ is about 70% of the $\Pi_{2-5}(PP)$.

(6) The in-plane energy of the floor has to choose between four main alternative paths: the flexural modes of the tank top (4), of the longitudinal girder (12), and of the bottom plate (7); and also the in-plane modes (almost none) of the smaller floor (11) which has a very small area when compared to the others. The most important path is between 11 and 7. $\Pi_{11-7}(PB)$ is about the double of $\Pi_{11-12}(PB)$ and $\Pi_{11-4}(PB)$. It is also important to notice that $\Pi_{11-7}(PB)$ is about the same as $\Pi_{5-7}(PB)$. This shows that the two flanking paths of in-plane energy (bracket-floor and web-longitudinal girder) have about the same importance and about the same contribution to the flexural energy of the bottom plate (7).

(7) In this model, the flexural energy level of the larger tank top plate (4), receives the contribution of the in-plane motions of

three plates: web (2), bracket (8) and floor (11). Therefore, the differences between 10 log $(E_4/E_1)_G$ and 10 log $(E_4/E_1)_F$ are more representative than in the previous model. This is shown by Figure 5.5.4.

(8) It is interesting to notice that the in-plane motions in this model also contribute significantly for the flexural energy of the longitudinal girder (12) as illustrated by Figure 5.5.5. It is also important to point out that the major contribution comes from the in-plane modes of the tank top (4) followed by the contribution from the floor (11) and the bottom plate (7).

Emphasis has been given to the in-plane motions and energy conversions. Other important aspects can be inferred by proceeding with such analysis and by considering the interaction between the flexural subsystems of the plates, and also by giving emphasis to the internal loss factors that govern the power truly dissipated by each subsystem (an important variable in SBN transmission).

The above discussion shows that:

(1) A good understanding of the vibration transmission through the basic model can result from the application of the SEA principles, SEA parameters and power balance equations (that gives not only an estimation of the energy level of each subsystem, but also an estimation of the power dissipated by each one and of the net power flow between them).

(2) The in-plane motions and energy transformations really play an important role in the vibration transmission through this model

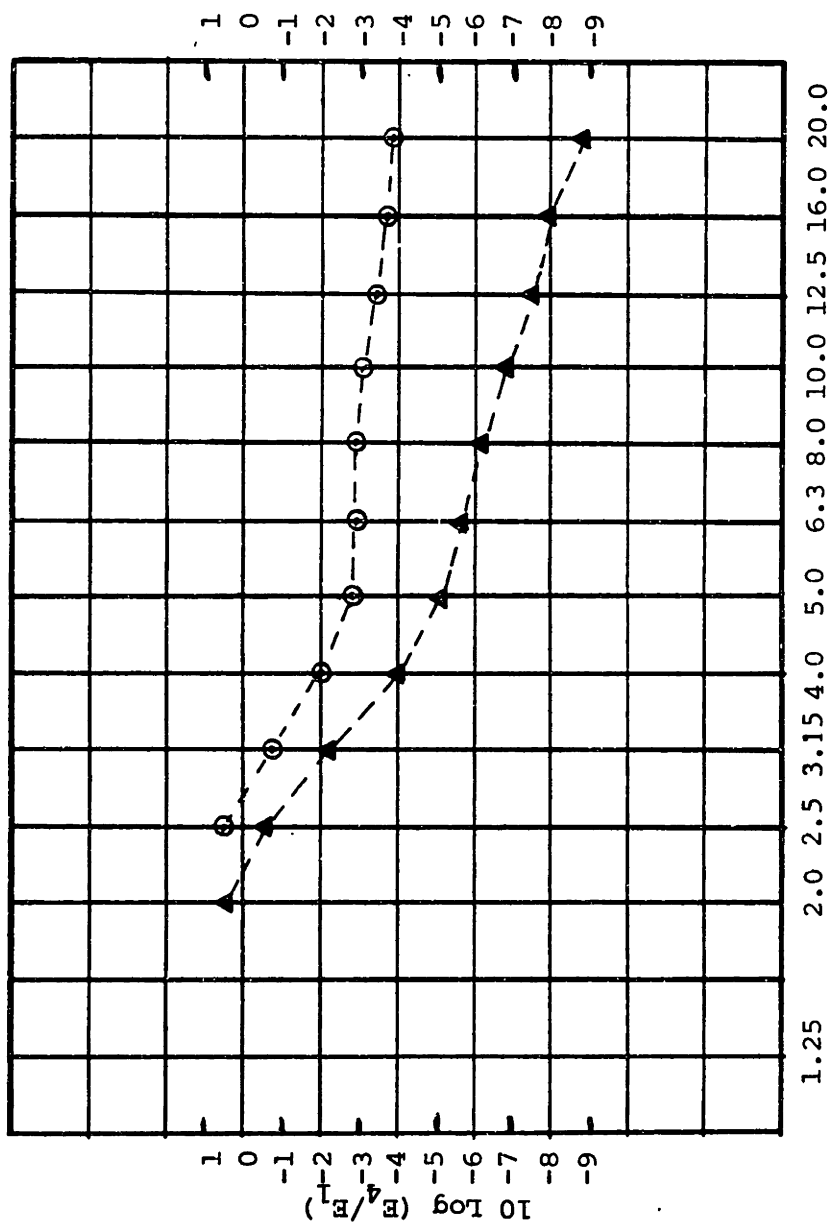

FIGURE 5.5.4: ENERGY RATIO -- TANK TOP PLATE (4) - TOP PLATE (1)
-- TWELVE-PLATE MODEL

▲ : SEA Predictions - Bending Only,

⊙ : SEA Predictions - Energy Transformations

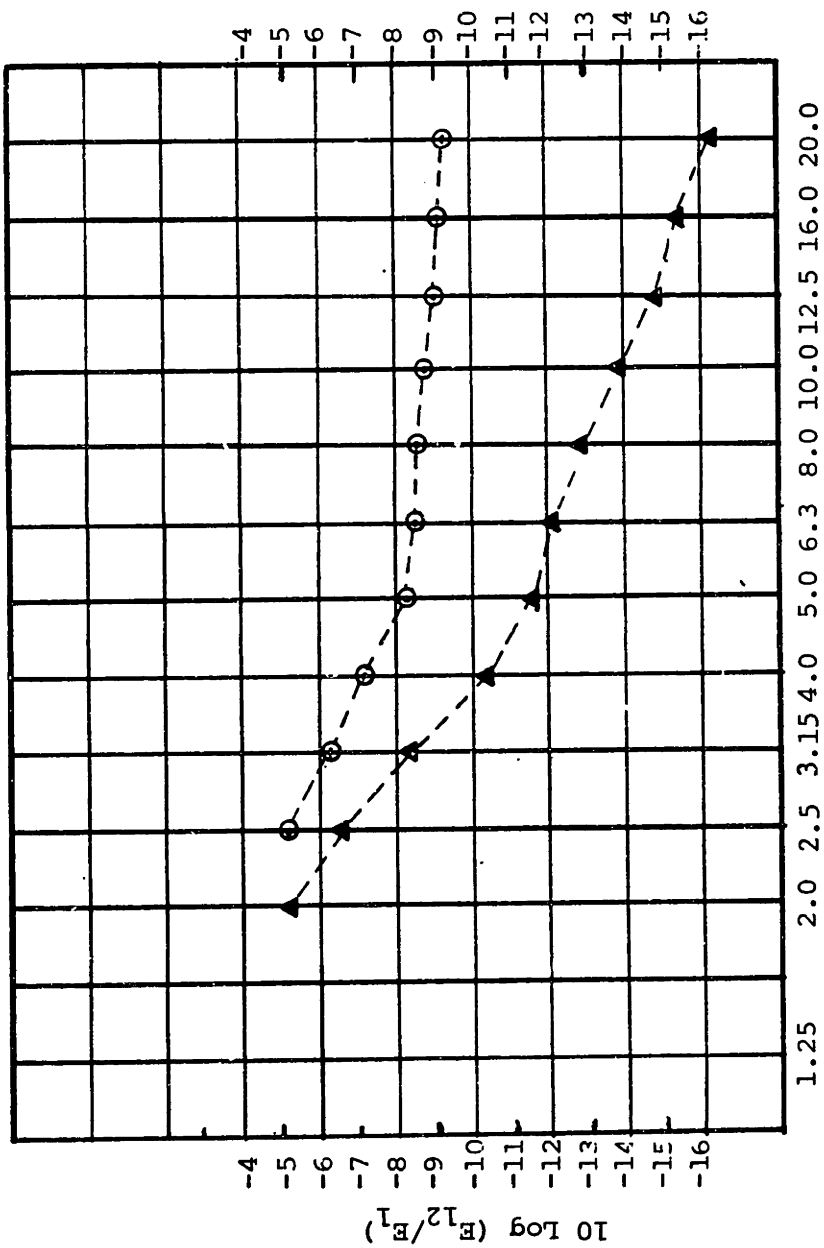

FIGURE 5.5.5: ENERGY RATIO -- LONGITUDINAL GIRDER (12) - TOP PLATE (1)
-- TWELVE-PLATE MODEL

▲: SEA Predictions - Bending Only,

⊙: SEA Predictions - Energy Transformations

above 4 kHz. If they were disregarded in this study poor estimations of the flexural energy levels of important plates would result.

(3) The transverse plates (brackets and floors) play an important role in the vibration transmission through the machinery foundation and ship bottom structure, and can not be disregarded in an accurate analysis of SBN transmission. They offer important paths for the power delivered by the machinery and a representative amount of this power can be dissipated by them. They also can deeply influence the energy distribution of the ship bottom.

(4) In order to minimize the power dissipated in the ship bottom above 4 kHz, any action has to take into account the in-plane motions. A very simple reduction action could, in principle be suggested, based only on the concept of availability of modes to store energy: introduce openings (a very common practice) in the plates along the main in-plane energy paths (web, longitudinal girder, floor). As a result the modal density will decrease and in-plane modes will be available at frequencies higher than before. On the other hand, less energy will be stored by the flexural motions of such plates and less power will be dissipated by them. The strength of their coupling with the plates welded to them will increase. A higher percentage of the power delivered by the machinery will be transmitted through flexural modes of the structure to the bottom plates. Therefore, a compromise has to be reached. Another

possible suggestion would be to avoid structural alignments such as those offered by the web - longitudinal girder and by the bracket-floor. A good idea would be to create discontinuities in order to try to have, at the most extension possible, the in-plane to bending energy conversions occurring at the tank top rather than at the bottom.

To carry out sensitivity analysis is not an objective of this thesis nor is it to identify the most efficient actions that can be adopted to minimize the power dissipated in the bottom plates. The important point is that this kind of analysis can be undertaken by using SEA and its power balance equations. As discussed in Chapter 1 and shown in this chapter, the SEA variables and parameters are directly associated with noise requirements and actions to reduce its transmission through the ship structure.

CHAPTER 6

SUMMARY, CONCLUSIONS AND RECOMMENDATIONS

6.1 Summary of the Work Carried Out

As discussed in Chapters 1 and 2, noise analysis is the driving interest of this thesis and ship design the intended field of application. The main concern of this work lies in the transmission of structure-borne sound generated by machinery. Statistical Energy Analysis (SEA) is the approach selected. SEA, as justified in Chapter 1, is conceptually able to respond to most of the demands of a ship noise analysis and from which design tools and procedures can, in principle, be derived. SEA is also identified as the approach used in a larger number of works related to ship noise analysis.

As each ship has its own peculiarities, the best way to evaluate an approach is to apply it. A 2,000 ton naval vessel is used as the reference ship. A diesel engine foundation and the ship bottom are chosen as the structural area of interest, based on the reasons outlined in Chapter 2.

Since a complete structure-borne sound transmission analysis would be a very demanding and complex task (even if attention were restricted to a specific ship area), it is decided to undertake this task in an appropriate sequence, gradually adding difficulties for the SEA application. This thesis can be understood as the beginning of a detailed 'SEA' analysis of SBN transmission through the equipment foundations and bottom structure of the reference ship.

As a starting point of this overall analysis, an unstiffened plate-like scaled (1:2.5) structural model is conceived. It is based on SEA

principles (Chapter 3) and on other works related to SBN transmission in ships, and it also takes into consideration the machinery-foundation interaction (Chapter 4). Despite being a basic model, it offers special challenges for SEA, in the frequency range of interest (0.63 to 20 kHz):

(a) Energy (motion) transformations are expected to take place and to be important above 5 kHz. The excitation of the flexural modes of the driven plate generates in-plane motions in the plates coupled to it. Such in-plane motions are transformed back to bending in the next joints. Below 5 kHz, the flexural motions are expected to be predominant.

(b) Interaction between SEA sub-systems with a small number of resonant modes (less than six) and SEA sub-systems with a large number of modes. For these cases the most accurate predictions of energy levels are not expected from SEA.

In order to have a better understanding of the vibration transmission, the basic physical model is built-up in four steps.

Two analytical models are investigated. One model assumes that the vibration transmission is associated with the flexural motions only. In the other the in-plane motions (longitudinal and shear) are included and the transfer of energy between the three different motions is taken into account.

To be able to apply SEA, its parameters must be determined either experimentally or analytically. The internal loss factor of each plate is evaluated using a decay method. The mode count is obtained experimentally when the number of modes is less than twelve in each frequency band, and by

using the formulations of modal density when the number is greater than twelve. The coupling loss factors are determined using a wave description of the vibrational field and the concept of transmission losses. Analytical expressions are derived to determine the average transmission coefficients between up to four plates at a common joint, for the general case where the three wave fields (and energy conversions) are considered. Bending, longitudinal and transverse shear wave incidences are treated individually. From the derived equations, computer programs are developed to calculate such average transmission coefficients and the related coupling loss factors. A separate computer program is developed for the case when only bending transmission is assumed.

Based on the determined SEA parameters, an attempt is made to interpret and identify the possible main transmission paths and mechanisms, and also to anticipate above which frequency a contribution of the in-plane motions to the flexural energy levels of the plates of the third model would be significant (especially of the bottom plates, that are directly related to a noise requirement).

Finally, the SEA power balance equations are utilized to predict, in each step, the energy-ratio levels of the SEA sub-systems (groups of modes) in each plate. The predicted ratios of flexural energy are then compared with those resulting from laboratory measurements. The power balance equations are also utilized:

(a) to investigate briefly the influence of the loss factors in the predicted energy levels and power dissipated in some plates.

(b) to determine the net power flow between the subsystems and the power dissipated by each subsystem. This information is utilized in association with the SEA parameters to analyze the vibration transmission through the models, in particular through the twelve-plate model (in which a multi-path situation exists).

6.2 Conclusions

Two basic conclusions can be drawn from the comparison between the plates flexural energy-ratio levels determined experimentally and the corresponding values resulting from the application of SEA to the four models studied (Chapter 5):

(1) The in-plane motions and the energy transformations at structural discontinuities play an important role in the vibration transmission through the basic model.

(2) The agreement is fairly good (generally within $\pm$ 3 dB), especially considering that in several frequency bands a small number (less than 6) of in-plane and/or flexural modes are present in some of the plates.

The importance of the in-plane motions and energy transformations is characterized in the study of the four, seven, and twelve-plate models (Figures 4.5.1a to 4.5.1d). This characterization results from:

(1) The good agreement between the experimentally determined flexural energy levels of the tank top and bottom plates and their predicted energy ratio resulting from the application of SEA when the three motions are considered.

(2) The differences between the two predicted flexural energy levels, resulting from the SEA application:

(a) when only bending transmission is assumed;

(b) when the in-plane motions are taken into account.

At the higher frequencies the assumption that the only mechanism of vibration is bending would lead to signficantly low estimates of the flexural energy levels of those plates which receive the major contributions from the in-plane motions, through energy conversions. The most significant differences between the two predicted values are associated with the bottom plates and increase with frequency:

(a) seven-plate model - from 3 dB at 5 kHz up to 8 dB at 20 kHz

(b) twelve-plate model - from 3 dB at 3.15 kHz up to 8 dB at 20 kHz.

The conclusion associated with the significance of the in-plane motions and energy transformations for this model is very important. Just as important is the fact that a good indication of when they have to be considered can be inferred by utilizing SEA principles and parameters. No attempt was made to derive or suggest specific limits. The predictions were only based on fundamental concepts such as:

(1) Availability of the In-Plane Modes to Store Energy.

The formulations of modal density can be applied to estimate the frequency band in which the first in-plane resonance is expected (5 kHz in this thesis). This frequency band has to be regarded as a reference, since the modal density concept is not the most appropriate for such

prediction. It is highly probable that the first in-plane mode is actually available at a frequency band significantly lower than that estimated by applying modal density. This last statement can be used as a general guidance which was confirmed in the study of the twelve-plate model. For this model the influence of the in-plane modes started to be noticed at the band centered at 2.5 kHz.

The modal density formulations may lead to an inaccurate estimation of the number of modes in a frequency band when such number is very small (especially below 5). However, it clearly shows that for the in-plane motions of a plate (of a given material) the number of modes available to store energy depends on the plate area and on the frequency of interest: the larger the area and/or the higher the frequency, the higher is the number of modes available.

(2) Significance of the in-plane motions for the vibration transmission. This means that:

(a) they have to be excited: a representative amount of power has to be delivered to them, directly by a source or through other motions (energy conversions - as for the models studied).

(b) they have to be able to carry a representative amount of power which can be converted in flexural motions by structural discontinuities.

The significance of the influence of in-plane motions is directly related to:

(a) Their higher impedance, when compared to the flexural motions.

This means that they can carry a great deal of vibrating power even though their amplitudes are small. This higher impedance also means that the internal loss factor associated with the in-plane motions is also less than for flexural motions, and that the influence of the in-plane motions may start to be noticeable even before the band in which their first resonances actually occur.

(b) the strength of the coupling between the in-plane motions and between them and flexural motions.

A good idea of the ability of the in-plane motions to receive power from other motions and reconvert it to flexural energy can be inferred from the comparison between:

(a) coupling loss factors at different joints (power transfer)

(b) the internal loss factors of the different subsystems (power dissipated).

(c) internal loss factors and coupling loss factors - (relative magnitude of power dissipated and power transferred)

An important condition to consider occurs when the coupling loss factors between the in-plane and flexural modes are of the same order as the coupling loss factors between flexural subsystems. The frequency bands in which this happens have to be regarded as preliminary reference bands above which the in-plane motions need to be considered and below which they can't be neglected without analysis. For the models studied the in-plane modes were excited through the flexural modes of the driven plate. At 5700 Hz, the coupling between the flexural modes of the driven plate and the in-plane modes of the larger coupled plate is of the same order as the coupling between their flexural subsystems. This means that above this frequency the

in-plane modes can not be disregarded without a careful analysis. Below such frequency their influence may also be significant and has to be investigated. The significance of the reconversion depends on the amount of power dissipated in each plate and of the coupling at the next joints. Special attention has to be given to the tee and cross joints: their opposite plates constitute a preferable path for in-plane motions, offering almost no transmission losses when they have the same thickness, while the losses related to bending transmission are significant.

The application of such principles to the models studied indicated that the in-plane modes and energy transformations should be considered above 4 kHz. The experimental and analytical results showed that the contribution of the in-plane motions:

(1) To the flexural energy levels of the bottom plates started to be noticed and to be significant, respectively, at:

   (a) twelve-plate model - 2 kHz and 3.15 kHz;

   (b) seven-plate model - 2 kHz and 5 kHz.

(2) To the flexural energy level of the tank-top plates started to be noticed and to be significant above 4 kHz.

With respect to the good agreement between experimental and analytical results it is important to point out that they were not expected to be so good, since:

(1) A small number of flexural modes (less than 6) are present in some plates (especially at the top plate), up and including 8 kHz. In addition to that, the in-plane modes at the web

start to be present possibly at 2.5 kHz, their number being less than six up to 10 kHz.

(2) Except at the frequency bands centered at 630 Hz and 1250 Hz (for both of which the mode count was applied) the formulations of modal density were used associated with coupling loss factors that were determined assuming the existence of a diffuse field in each plate. With respect to the flexural modes, this was shown to be appropriate from 2 kHz since the ratio between modal densities between two coupled plates was close to the ratio between their actual number of modes obtained experimentally. However, the same may not be necessarily valid for the in-plane modes, since it was clearly shown for the two-plate model that the use of modal density instead of mode count could have led to a significant overestimation of the plate energy levels (6 dB).

Thus, the results must be considered very encouraging. They also demonstrate the ability of SEA to deal with in-plane motions and energy conversions, not only for predictions but also to give an indication when they are important and have to be included in the model.

The analysis of the twelve-plate model using SEA principles confirmed that the transverse plates of the diesel engine foundation (brackets) and of the double bottom structure (floors) as well as the longitudinal girders play an important role in the transmission of the vibration induced by the machinery and cannot be disregarded in an accurate study. They are not only able to store a significant amount of energy, but also to substantially influence the energy sharing and to offer important paths for the vibration

transmission (for bending and in-plane energy), of the same significance as the paths offered by the plates between floors.

As stated several times, not always an absolute number or a very accurate result is required. In some situations, such as in the earlier phases of ship design, when details of the structure are not known, comparative and sensitivity analyses have to be carried out. Therefore, it is important to have available a reliable approach able to offer a good interpretation of the problem and well supported guidelines for its solution. As pointed out the SEA variables and parameters are directly related to the ship noise requirements and to actions that can be adopted to ensure that they are satisfied.

Considering these aspects and the ultimate objective of this thesis its overall conclusion is that: The results obtained are good enough to justify the continuation of this work and further researches that are necessary to allow a complete analysis of the vibration transmission through the machinery foundations and bottom structure of the reference ship, applying the "Statistical Energy Analysis Approach."

6.3 Next Steps - Suggestions for Further Works

The next steps in this analysis as well as further investigations that are considered necessary have been explicitly and also indirectly suggested throughout the chapters of this work. As already mentioned, this thesis is considered as the first step in the application of SEA to study the vibration transmission through the equipment foundations and bottom structure of the reference. As a natural consequence the next steps suggested for its continuation are:

(1) To experimentally determine the flexural energy levels of the remaining plates of the twelve-plate model in order to have it further analyzed.

(2) To investigate in detail the applicability of the SEA parameters for frequencies below 2 kHz and starting at the band centered at 100 Hz, in which no flexural modes are expected at the driven plate.

(3) To apply finite element techniques associated with modal analysis to predict the energy levels of the plates at the lower frequencies and to compare the results with those derived from the SEA application and from experimental work.

(4) To optimize the computer programs to deal with larger systems (especially when the three wave fields are considered) and to perform sensitivity analysis in a faster and more efficient way.

(5) To investigate the possibility of introducing simplifications in the analytical models in order to reduce the amount of calculations.

(6) To analytically investigate the effect in the in-plane power transmission resulting from:

   (a) the elimination of alignment between plates in the main transmission paths (especially when they have the same thicknesses) and the introduction of discontinuities to force the energy conversions to occur and to have the associated power dissipated in plates that are not directly related to noise requirements.

(b) the introduction of openings in the plates along the main transmission paths, to decrease the availability of in-plane modes.

(7) To increase the model in both transverse directions (toward the ship center line and including hull plates) and also in the longitudinal direction, by adding at least one more section. A similar investigation (as in this thesis) would be carried out, but considering items (2) and (3) above, and also using up to four sources to deliver power. Special attention would be dedicated to the following aspects:

(a) the effect of the relative position between the sources and of their position with respect to the brackets.

(b) determination of the input power with each source delivering power and with all of them working simultaneously. This would allow the investigation of their interaction and the determination of the foundation mobilities.

(c) the effect of mountings (soft or hard) with finite area, between the source and the structure.

This larger model would also be important to evaluate:

(a) the influence of the in-plane motions in the energy level of the hull plates (far away from the sources).

(b) the vibration transmission in the longitudinal direction (one source in each top plate).

(c) the effect and usefulness of adding damping to the structure.

With respect to plate-like structures the following can be suggested:

(1) a long term investigation can be carried out, similar to the work done by Swift [23], not only applying SEA to typical plate joints but also to several structural multi-joint models (drawn from actual ships), having plates of different areas and thicknesses. The basic objective would be to have a large enough population of models in order to:

   (a) better verify the accuracy of the SEA predictions, especially at low frequencies and when in-plane motions are important.

   (b) develop specific criteria about SEA application (when in-plane motions are present and when low number of modes are excited).

(2) the development of charts, guidances and procedures for design applications.

To undertake a complete analysis of the vibration transmission through the equipment foundations and bottom structure of the reference ship, the following research efforts are considered necessary:

(1) evaluation of the effect introduced, in the vibration transmission, by the tank fluid loads (water, fuel and lub oil) and by the stiffeners (as well as smaller size frames).

(2) analysis of the interaction between the ship structure and the sea water.

An expected result from these researches would be the generation of practical formulations for the determination of the associated coupling loss factors.

Two other research efforts are also considered very important, to be dedicated to:

(1) the application of finite element techniques to evaluate coupling loss factors in direct analogy with 'SEA' for comparison with the averaged SEA coupling loss factors. This effort could result in an improvement of accuracy from SEA for frequency bands in which a small number of modes are excited.

(2) the determination of reliable loss factors for ships in order to allow better accuracy from SEA. Emphasis should be given to built-up structures and to the correlation between uncoupled and coupled conditions.

REFERENCES

1. Jansen-Buiten, "On Acoustical Designing in Naval Architecture," *Inter-Noise 73 Proceedings, 1973.*

2. Buiten, J., "Experiments with Structure-Borne Sound Transmission in Ships, *Proc. of Int. Symp. on Shipboard Acoustics, 1976* (Ed. J. H. Jansen), Elsevier, 1977.

3. Suhara, J., "Analysis and Prediction of Shipboard Noise," *Proc. of Int. Symp. on Pract. Design in Shipbuilding,* Tokyo, 1977.

4. Kihlman, T. and Plunt, J., "Prediction of Noise Levels in Ships," *Proc. Int. Symp. on Ship Acoustics 1976,* (Ed. J.H. Jansen), Elsevier, 1977.

5. Plunt, J., "Empirical Formulas for Structure-Borne Sound Levels on Ship Machinery, *Internoise,* San Francisco, 1978.

6. Plunt, J., "Methods for Predicting Noise Levels in Ships," Department of Building Acoustics, Chalmers University of Technology, Sweden, Report 80-06, 1980.

7. Nilsson, A. C., "Attenuation of Structure-borne Sound in Superstructures on Ships," *J. of Sound and Vibration, 55(1),* pp. 71-91, 1977.

8. Nilsson, A. C., "Reduction of Structure-Borne Sound in Simple Ship Structures: Results on Model Tests," *J. of Sound and Vibration, 61(1),* pp. 45-60, 1978.

9. Budrin, S. V., and Nikoforov, A. S., "Propagation and Damping of Sound Vibrations in Ship Joints," *Publication Res. Service Translation JPRS 47,* 803, 1969.

10. Sawley, R., "The Evaluation of Shipboard Noise and Vibration Problem Using Statistical Energy Analysis," *Contribution to Stochastic Processes in Dynamical Problems, ASME,* New York, 1969.

11. Odegaard-Jensen, J., "Calculation of Structure-Borne Transmission in Ships, Using the 'Statistical Energy Analysis' Approach," *Proc. of Int. Symp. on Ship Acoustics, 1976,* (Ed. J. H. Jansen), Elsevier, 1977.

12. Irie, Y. and Takagi, S., "Structure-Borne Noise Tranmission in Steel Structures Like a Ship," *Proc. Inter-Noise,* San Francisco, 1978.

13. Odegaard-Jensen, J., "Calculation of Structure-Borne Sound in Plate Structures by the Application of 'Statistical Energy Analysis', *Proc. NAM78*, p 165, Odense, 1978.

14. Fukuzawa, K., and Yasuda, S., "Studies on Structure-Borne Sound in Ships," *Proc. Inter-Noise 79*, p. 623, Warszawa, 1979.

15. Lyon, R. H., *Statistical Energy Analysis of Dynamical Systems*, MIT Press, 1975.

16. Lyon, R. H. and Maidanik, G., "Power Flow Between Linearly Coupled Oscillators", *J. Acoust. Soc. Am., 34* (5), May, 1962.

17. Smith, P.W., "Response and Radiation of Structural Modes Excited By Sound", *J. Acoust. Soc. Am., 34*, (5), May, 1962.

18. Eichler, E., "Thermal Circuit Approach to Vibration of Coupled Systems and the Noise Reduction of a Rectangular Box", *J. Acoust. Soc. Am., 37* (6), 1965.

19. Lyon, R. H. and Scharton, T. D., "Vibrational Energy Transmission in a Three-Element Structure", *J. Acoust. Soc. Am., 38* (2), 1965.

20. Crocker, M. J. and Price, A. J., "Sound Transmission Using Statistical Energy Analysis", *J. Sound and Vib., 9* (13), 1969.

21. Crocker, M. J.; Battacharya, M. C.; and Price, A. J., "Sound and Vibration Transmission through Panels and Tie-Beams Using Statistical Energy Analysis", *J. of Eng. Ind., Trans. ASME, V. 93*, Series B No. 3, August, 1971.

22. Gibbs, B. M. and Gilford, C. L. S., "The Use of Power Flow Methods for the Assessment of Sound Transmission in Building Structures", *J. Sound and Vibration, 49* (2), (1976), pp. 267-286.

23. Swift, P. B., "The Vibrational Energy Transmission Through Connected Structures", Ph.D. Thesis, University of Adelaide, 1977.

24. Craik, R. J. M., "A Study of Sound Transmission Through Buildings Using Statistical Energy Analysis", Ph.D. Thesis, Heriot-Watt University, Department of Buildings, 1980.

25. Abramson, H. N. and Neville, G. E., "Some Modern Development in the Application of Scale Models in Dynamic Testing", *Colloquium on the Use of Models and Scaling in Shock and Vibration, ASME*, New York, 1963.

26. Hart, F. D. and Shab, K. C., "Compendium of Modal Densities for Structures", NASA, CR1773, 1971.

27. Blevins, R. D., *Formulas for Natural Frequency and Mode Shape*, Van Nostrand Reinhold Company, 1979.

28. Leissa, A. W., "Vibration of Plates", NASA, SP-160, 1969.

29. Ohlrich, M., "On the Transmission of Audio Frequency Vibration from Multi-Point Mounted Engines to Ship Bottom Structure", The Acoustic Laboratory, Technical University, Lyngby, Denmark, 1979.

30. Petersson, B. and Plunt, J., "Structure-Borne Sound Transmission from Machinery to Foundations -- Final Report, Department of Building Acoustics, Chalmers University of Technology, Goteborg, Sweden, 1980.

31. Lyon, R. H., *Machinery Noise and Diagnostics*, 1984.

32. Lyon, R. H., and Eichler, E., "Random Vibration of Connected Structures", *J. Acoust. Soc. Am., 36*, No 7, pp. 1344-1354, 1964.

33. Heckl, M., "Measurement of Absorption Coefficients on Plates", *J. Acoust. Soc. Am., 34*, No. 6, 1962.

34. Kosten, C. W., "The Mean Free Path in Room Acoustics", *Acoustica, 10*, 1960.

35. Cremer, L., "The Propagation of Structure-Borne Sound", Dept. Ind. Res., England, Report, No. 1, 1948.

36. Cremer, L.; Heckl, M. and Ungar, E. E., *Structure-Borne Sound*, Springer-Verlag, 1973.

37. Budrin, S. V., and Nikiforov, A. S., "Wave Transmission Through Assorted Plate Joints", *Soviet Physics, Acoustics 9*, 1964.

38. Kihlman, T., "Transmission of Structure-Borne Sound in Buildings, A Theoretical and Experimental Investigation", National Swedish Institute for Building Research, Stockholm, Report 9: 1967.

39. Kihlman, T., "Sound Transmission in Building Structures of Concrete", *J. Sound and Vibration, 11*, (4), 1970.

40. Timoshenko, S., and Woinowski-Krieger, S., *Theory of Plates and Shells*, McGraw-Hill, 1959.

41. Graff, R. F., *Wave Motion in Elastic Solids*, Ohio State University Press, 1975.

42. Newland, D.D., "Calculation of Power Flow Between Coupled Oscillators", *Journal of Sound and Vibration 3*, (3), 1966.

43. Newland, D.E., "Power Flow Between a Class of Coupled Oscillators, *J. Acoustical Soc. Am., 43*, No. 3, 1962.

44. Scharton, T.D. and Lyon, R.H., Power Flow and Energy Sharing in Random Vibration, *J. Acoustical Soc. Am., 43* (6), 1968.

45. Crandall, S.H. and Lotz, R., "On the Coupling Loss Factor in Statistical Energy Analysis". *J. Acoustical Soc. Am., 49* (1), 1971.

46. Lotz, R. and Crandall, S.H., "Prediction and Measurement of the Proportionality Constant in Statistical Energy Analysis of Structures", *J. Acoustical Soc. Am., 54* (2), 1973.

47. Ungar, E.E., "The Status of Engineering Knowledge Concerning the Damping of Built-up Structures", *J. Sound and Vibration 26*, 1973.

48. Smith, P.W. and Lyon, R.H., "Sound and Structural Vibration", NASA Contractor Report CR-160, March 1962.

49. Maidanik, G., "Response of Ribbed Panels to Reverberant Acoustic Field", *J. Acoustical Soc. Am., 34* (6), 1962.

50. Fahy, F.T., "Statistical Energy Analysis - A Critical Review", *The Shock and Vibration Digest 6* (7), 1974.

51. Heckl, M., Compendium of Impedance Formulas, BBN Report, No. 774, 1961.

52. Lyon, R. H., Vibration Transmission in Machine Structures", *Noise Control Engineering Journal, 20* (3), May-June 1983.

53. Lu, L.K.H., Hawkins, W.J., Downard, D.F. and Dejong, R.G., "Comparison of Statistical Energy Analysis and Finite Element Analysis Vibration Prediction with Experimental Results, Shock and Vibration Bulletin, 53, Part 4, page 145, May 1983.

54. O'Hara, G.J., "Mechanical Impedance and Mobility Concepts", *J. Acoustical Soc. of Am.*, Vol. 41, 1967.

55. Popkov, V.I., Vibro Acoustic Diagnosis and Reduction of Vibration of Shipboard Machinery", JPRS, Arlington Translation 64931, 1975.

56. Goyder, H.G.D. and White, R.G., "Vibrational Power Flow from Machines into Built-in Structures", Parts I, II and III", *Journal of Sound and Vibration*, Vol. 68 (1), 1980, pages 59-117.

57. Ungar, E.E., "Transmission of Plate Flexural Waves through Reinforcing Beams; Dynamic Stress Concentrations", *J. Acoust. Soc. Am., 33*(5), 1961.

58. Heckl, M., "Wave Propagation on Beam-Plate Systems", *J. Acoust. Soc. Am., 33* (5), 1961.

59. Fahy, F.J. and Lindquist, E., "Wave Propagation in Damped Stiffened Structures Characteristic of Ship Construction", *J. of Sound and Vibration, 45,* pp. 115-138, 1976.

60. Fahy, F.T., "A Theoretical Evaluation of the Effectiveness of Reducing Vibration Transmission in Hull-Frame of a Ship by Damping", *Proc. of Int. Symp. on Shipboard Acoustics, 1976* (Ed. J.H. Jansen), Elsevier, 1977.

61. Roark, R.J. and Young, W.C., "Formulas for Stress and Strain", McGraw-Hill, 1975.

APPENDIX A

SEA FUNDAMENTAL EQUATIONS AND PARAMETERS

A.1 Fundamental Equations

The fundamental power equation [15] for two lightly coupled oscillators (by inertia, elastic and gyroscopic elements) excited by statistically independent white noise sources can be written as:

$$\Pi_{ij} = \omega \eta_{ij} \, (U_i - U_j) \tag{A.1}$$

where

Π_{ij} = average net power flow between oscillators i and j

ω = frequency

$U_{i(j)}$ = average energy of oscillator i(j).

Π_{ij} is then proportional to the difference in the oscillator energy. The coefficient of proportionality, η_{ij}, is a function of the oscillator and coupling parameters, but not of the energy. If a parallel with heat transfer is made, U can be associated with temperature, and η_{ij} understood as a power flow coefficient. The power dissipated by a single oscillator undergoing stationary random vibration excited by a wide-band source can be expressed by: $\Pi_{diss} = \eta_2 \, \omega \, U_i$, where η_i is the loss factor. By association η_{ij} was denominated as coupling loss factor since it is related to the power lost from one oscillator to the other. Lyon and Maidanik [16] analyzing lightly coupled oscillators, demonstrated that the power flow is from the high to the low energy oscillator and is proportional to the difference in the average energy that the oscillators would have if they were uncoupled, but subjected to the same excitation. Further work

on coupling between oscillators was carried out by Newland [42,43]. Scharton and Lyon [44] showed that the time-average power flow between the oscillators is proportional to the difference in the actual time-average energies of the oscillators even when they are strongly coupled. Important aspects related to these works and coupling loss factors are analyzed by Crandall and Lotz [45,46].

When two multimode structures are coupled, their modes are coupled and each mode can be understood as an oscillator. Therefore, the power flow equation and coupled oscillators calculations combined with a modal or wave description of distributed systems were applied [15] to describe the energy exchange between interacting multimode elements.

The power flow between mode i of subsystem A and j of subsystem B can be written as:

$$\Pi_{ij} = \phi_{ij} \, (U_i^A - U_j^B) \tag{A.2}$$

where ϕ_{ij} is the modal coupling coefficient between i and j.

In considering the interaction between the N_A modes of subsystem A and the N_B modes of subsystem B (Figure A-1), existing in a given frequency band, $\Delta\omega$, the following basic assumptions are made:

1. The energy of each subsystem is equally distributed among the resonant modes;

2. The modes have incoherent motions and have natural frequencies that are uniformly probable over the band.

The first statistical concepts are then introduced. These assumptions are made in association with the kinetic theory version of statistical

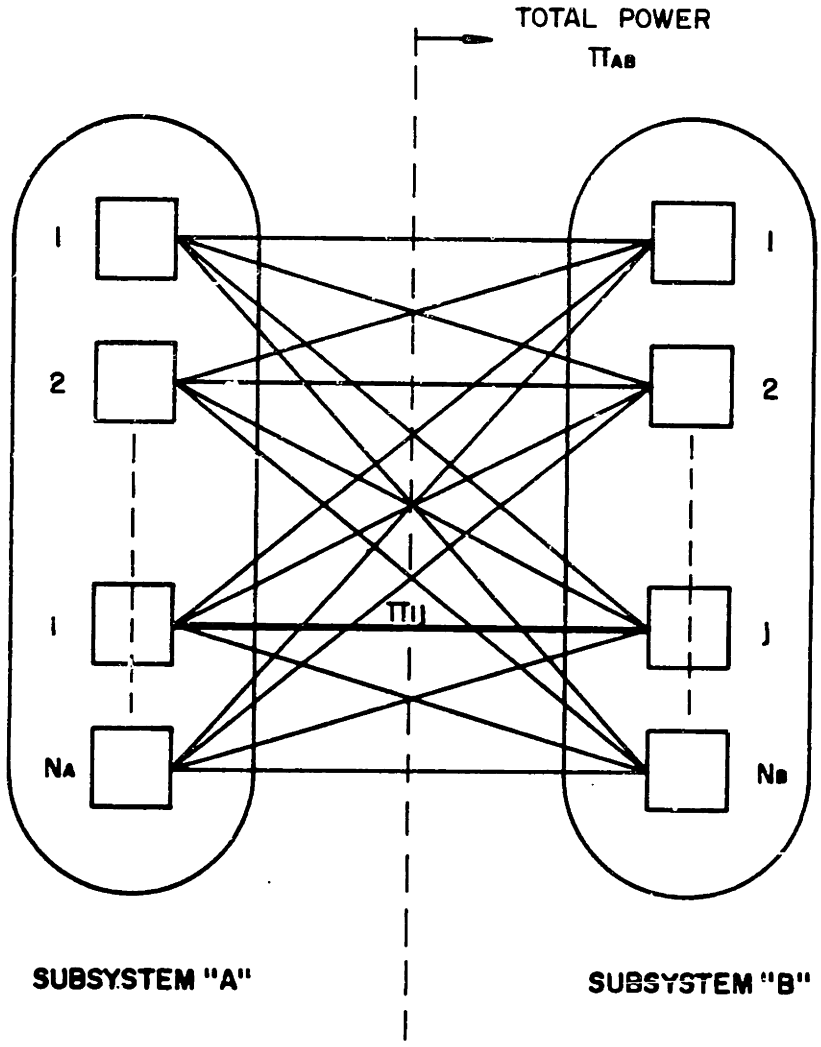

FIGURE A-1: COUPLING BETWEEN MULTIMODE SUBSYSTEMS

mechanics and non-equilibrium thermodynamics, where the possibility for different temperatures in different parts of the system is allowed. In SEA, the modes in different frequency bands are allowed to have different energies. The modes that resonate in different frequency bands may be considered to be uncoupled from each other.

As stated by Lyon [ref. 15, pg. 16]: "the inability to deal with modal coherence is the most glaring deficiency of SEA". The modal coherence may lead to such phenomena as "direct waves" discussed in Chapter 2 of reference [15].

Another assumption is that the excitations are drawn from random populations of functions that have certain similarity, but are individually incoherent.

One of the criteria for modal similarity is that the modes have nearly the same damping (half power bandwidth) in a given frequency band. This tends to be true for complex systems and greatly simplifies the formalism.

Based on these assumptions, the total net power flow between two subsystems (A and B) can be obtained by summing the contributions of the individual pair of interacting modes. Therefore:

$$\Pi_{AB} = N_A N_B \, \phi(U_A - U_B) \tag{A.3}$$

Defining: $\eta_{AB} = \frac{\phi N_B}{\omega}$, as the coupling loss factor between A and B, equation (A-3) becomes:

$$\Pi_{AB} = \omega N_A \, \eta_{AB} \, (U_A - U_B) \tag{A.4}$$

By symmetry:

$$\Pi_{BA} = -\Pi_{AB} = \omega N_B \eta_{BA} (U_B - U_A) \tag{A.5}$$

From (A.4) and (A.5):

$$N_A \eta_{AB} = N_B \eta_{BA} \tag{A.6}$$

Equation (A.6) is denoted by Lyon [15] as the consistency relation that allows the determination of η_{BA} once η_{AB}, N_A and N_B are known. This greatly simplifies the calculation and can be used to verify the proper determination of the coupling loss factors.

As the modes are assumed to be equally energetic:

$$\Pi_{AB} = \omega N_A \eta_{AB} \left[\frac{E_A}{N_A} - \frac{E_B}{N_B}\right] \tag{A.7}$$

where

$E_{A(B)}$ is the total energy of A(B).

Applying (A.6), (A.7) can be written as

$$\Pi_{AB} = \omega\eta_{AB} E_A - \omega\eta_{BA} E_B \tag{A.8}$$

where $\omega\eta_{AB(BA)}E_{A(B)}$ is the power delivered by subsystem A(B) to subsystem B(A), coupled to it. This is the basic power expression used in SEA.

A.2 SEA Parameters

A.2.1 Mode Count

The number of resonant modes available to store energy is used when modelling the system as a SEA system and may also enter in the power balance

equations, directly or through the consistency relation (A.6).

When the number of modes in a frequency interval is high, it is difficult to be exactly determined, analytically or experimentally. It becomes, therefore, reasonable to work with an expected number of modes, calculated theoretically by using the concept of density of modes in the frequency band of interest:

$$[N_i] = bn_i, \text{ where}$$

b = bandwidth

n_i = modal density, defined as the average number of natural frequencies per unit frequency in the excitation band of width b.

It is important to emphasize that the mode count is the fundamental concept for SEA in all cases, the modal density being a derived quantity.

In accordance with [15], the modal density can be efficiently used when the density of modes is great enough or the bandwidth is large enough so that the estimated number of modes is of the order of at least ten. When a subsystem has a small mode count, it may still be modelled as a SEA subsystem, even when the concept of modal density is inappropriate.

The mode count can be determined either experimentally or theoretically. Its evaluation is discussed in detail in Chapter 13 of reference [15]. When few modes are present a simple measurement can be made. As the number increases the estimation by modal density increases in reliability. Modal density is very simple to calculate, using formulations available in the literature [15, 26]. It is also important to mention that the total mode count may be estimated by adding the number of expected modes for each subsystem [15, 26].

A.2.2 Internal Loss Factors (η_i)

All the major aspects concerning loss factors and its determination are presented in Chapter 12 of reference [15] and (more specifically, related to ships) in paragraphs 7.23 and 8.2.2 of reference [6]. Basic points are herein presented.

The most commonly used method of determining the loss factor is to measure it. This is mainly due to the lacking of reliable theoretical formulations for estimation. During preliminary analysis, reference values derived from experimental works are normally used.

When considering a structure, two basic mechanisms of dissipation can be identified: material damping and radiation. The mechanisms of damping in metals are very complex [15], "including thermal conduction, grain boundary motions, molecular site transitions, dislocations, oscillations, and at larger amplitudes nonlinear effects such as plastic flow". Formulations for radiation loss factors are available in the literature for interaction between structure and air. When the adjacent media is water or oil, reliable information is still missing.

When considering a built-up structure, the dissipation introduced by the joints has also to be taken into account [6,15]:

1. For riveted joints due to the surface slip and plastic deformation of the overlapping surfaces, or due to viscous flow in the region between the metal surfaces.

2. For welded structures due to stress concentration.

With respect to welding it is also important to mention the dissipative losses added to the material damping due to residual weld materials.

Therefore, it is not difficult to infer that it is more reliable to measure η_i unless a particular mechanism is predominant and reliable information to the prediction are available.

In a SEA approach, η_i is usually determined for each individual subsystem in the uncoupled condition from the structure, but coupled to a surrounding fluid, usually air. However, the dissipation can differ significantly from the uncoupled to the coupled condition. This may not be only due to the joint's effect, but also because the change of the acoustical space into which the structural elements radiate and because the edge conditions are altered. These aspects have to be carefully considered when applying SEA.

Not much progress has been made in the determination of loss factors for built-up structures since Ungar [47]. Useful references are the curves of loss factors as a function of frequency presented by Lyon [31] for welded plates.

Two basic experimental strategies can be utilized for loss factors measurements: steady state and decay methods.

Decay is the method normally used in SEA applications to ships. The structure is excited by a transient (hammer blow or impact) or by a steady state band-limited noise. After the excitation is removed, the decay of the structure response is recorded and evaluated. The loss factor is determined through the reverberation time or the decay rate. Some difficulties are associated with this method. The response curves often show different slopes and sometimes continuously varying slopes. It is generally agreed that the initial slope is the one which should be used. This is related to the presence in the frequency band of dissimilar modes (with different modal damping). As

point out by Plunt [6], the measured response (mean square short time average of a signal) may be dominated by the response of the modes with relatively low modal damping, since these modes have a tendency to get larger initial amplitudes. When the modes are more alike, the decay method leads to better results. Also, when few modes are excited their contribution may also be more clearly identified. Another aspect to consider, as emphasized by Lyon [15], is the interruption of the source. If the modes are closely spaced, the abrupt termination of the excitation will cause additional modes to be excited. When a large number of modes is present, it is important to ensure that as many as possible are excited and decay together.

Among the steady state methods the measurement of the input power is the one considered as most closely related to the SEA concepts. The element is excited by a band limited noise source. The input power is obtained by measuring the force and velocity at the driving point and then comparing with the energy of the test element, expressed in terms of spatial mean square velocity responses ($\eta = \Pi_{inp}/M < v^2 > \omega$).

This seems to be a more suitable method to be used when a large number of modes is excited and high modal overlap exists. Despite that, it has not been accepted as a standard practice. It requires more sophisticated and accurate equipment and technique. Since no standard equipment is readily available, it is usually home built. Force and velocity have to be measured, multiplied and integrated in time domain, requiring a very special attention with phases shifts and compensation. This method was investigated in detail by Swift [23]. As pointed out by Plunt [6] it appears to give higher values of loss factors, that, in principle, are a kind of weighted average modal loss factors, weakly and highly damped modes giving their contribution.

Another possibility of measuring damping is offered by the FFT analyzers associated with either decay or steady state methods. When the resonance are reasonably spaced (Δf > power bandwidth) the modal damping of each mode can be obtained through the transfer function between force (driving or impact) and the velocity (at the driving point) or acceleration of the test object, and its inverse Fourier transform. However, accuracy limitations may be associated with this procedure, related to the number of points or resolution used to perform the calculations. This is being improved in the newer equipments. In principle the power input can also be obtained through the force and velocity signals and their cross spectrum.

It is clear that no method is easy to be used, all having associated difficulties and limitations, making the determination of η_i a very demanding task.

A.2.3 Coupling Loss Factors (η_{ij})

The derivation of the basic expressions for the determination of coupling loss factors between oscillators and multimode systems are presented in detail in Chapter 3 of reference [15]. Chapter 14 of the same reference discusses the evaluation of coupling loss factors between different types of subsystems.

Coupling loss factors has been measured for some systems, but it is often calculated. Expressions are available for the evaluation of η_i, between elements commonly identified in a built-up structure such as:

1. Beam to beam -- Scharton and Lyon [44] and Crandall and Lotz [45].
2. Cantilevered beam and a plate -- Lyon and Eichler [32].
3. Beam and plate edges -- Lyon and Scharton [19].

4. Acoustical spaces and plates -- Smith and Lyon [48], Crocker and Price [20].

5. Acoustical spaces and reinforced panels -- Maidanik [49].

6. Plate-to-plate -- Lyon and Eichler [32], Heckl [33], Lyon [15].

One important aspect of the evaluation of the coupling loss factors is the coupling strength. This is analyzed by Lotz and Crandall [46] and discussed by Fahy [50], in a critical review of SEA. In the earlier evaluations of the η_{ij} a light coupling was usually assumed. It is, however, difficult to consider two structural elements as being weakly coupled. Commenting on this subject, Lyon (page 8 of reference [15]) stated: "Two independent studies, by Ungar and Scharton showed that the light coupling assumption was unnecessary if the uncoupled system were defined as the blocked system, meaning that the other system was held fixed while the system being considered was allowed to vibrate. Also the energy flow relations were valid whether one was using the blocked energies of the system as the driving force or the actual energy of each system with the coupling intact." SEA has been applied with good results to SBN transmission regardless of the coupling strength.

Two basic strategies can be used for the evaluation of the coupling loss factors:

1. To apply the blocking concept and express the coupling loss factors in terms of subsystems and junction impedances or mobilities.

2. To utilize the concept of transmission losses, based on wave propagation principles, and the basic SEA power expression (3.1)

$$(\eta_{12} = \Pi_{12}/\omega E_1).$$

The first strategy is particularly effective when the coupling is mainly through forces between the subsystems, such as: when the connection is at a point (pages 97-101 of reference [15]) or when the interaction between a pressure field and a velocity field of a surface is considered [48]. Different expressions for impedances are available in the literature, such as in references [36], [51], usually calculated or measured for other reasons. For example, the coupling loss factor for two structures at a point can be evaluated by the expression [52]:

$$\eta_{12} = \frac{1}{\omega M_1 G_1} \frac{G_1 G_2}{|Y_1+Y_2|^2} \qquad (A.9)$$

where

Y_1, Y_2 = junction input mobility of the two structures

G_1, G_2 = real part of Y

$\bar{G}$ = driving point average conductance of the structure at the connection point.

When the structures are joined by tack welding, or rows of rivets or bolts and the joining points are well separated (half wave length or greater) one can treat the junctions as N incoherent transmitters [52].

Similar expressions to (A.9) may be obtained for coupled structures along a junction line, Y becoming moment mobility, when bending is present [52]. For such coupling (e.g. continuous welding), however, the second strategy is the most widely used, being employed in SEA applications to SBN transmission in ships. Both strategies shall, in principle, lead to the same results, but the wave propagation approach is considered simpler, and also

efficient in describing the coupling when motions or wave transformations occur at the joint. This is the approach used in this thesis. The general expression for the coupling loss factor is presented and discussed in Section 4.3 of Chapter 4.

In both strategies, when continuous systems are considered, averaged values, either of mobilities or transmission losses, are normally utilized. A basic assumption is that a diffuse or reverberant field is present in each coupled element. This implies, in principle, that a minimum number of resonant modes should be present in a frequency band of interest. As the number of modes decreases, we may not have enough to allow predictions with an acceptable degree of accuracy. This is usually regarded as a limitation of SEA.

One of the objectives of Swift's thesis [23] was to determine a lower bound in terms of minimum number of modes, for the application of SEA to analyze bending energy transmission between welded plates. He also had as an objective the determination of an upper bound associated with modal overlapping, based on Crandall and Lotz [45], a possible restriction for SEA application at higher frequencies.

Based on his experiments, Swift suggested as lower bound $N_{min} = 6$ and as upper bound $R_{max} = 1$, within which SEA would be applied to predict the vibrational energy distribution in single joint structures up to four, with arbitrary coupling strength, with an accuracy of 2 dB and at least 90 percent confidence. N is the number of resonant modes in the excitation frequency bandwidths (the tests were carried out using third octave broad-band noise). The upper bound, defined as modal overlap factor is $R = n\eta_{max}$ where η is the

damping loss factor and n is modal density. Rewriting the limits in terms of frequency, they become:

$$f_{min} = \frac{25.92}{n_{min}} \tag{A.10}$$

$$f_{max} = \frac{1}{\eta\, n_{max}} \tag{A.11}$$

where

n_{min} = lowest modal density at the joint

n_{max} = highest modal density at the joint.

It was also stated that the upper frequency limit can be extended to $5/\eta\, n_{max}$ with an adjustment to the predicted energy ratio levels.

Swift also carried out experiments with multi-joint structures. He concluded that it was more difficult to state which elements should be used to determine the frequency bounds. It was suggested that probably the N and R values of these elements in the major vibration energy transmission paths would be those which determine the upper and lower frequency bounds for the structure, but it was recognized that further experimental work was required.

Those limits and criteria are applied to the model and discussed in Section 4.1 of Chapter 4.

The expressions of coupling loss factors based on average values has been generally used even when only a couple of resonant modes are present. In some applications acceptable agreement with measurements have been reported, such as by Craik [24]. The primary aspect to be considered in applying these formulations is the desired accuracy. In some cases, such as in the earlier ship design phases, not enough structural details are available.

Thus, the goal is to have a first estimation or a guidance, making the application very valid.

If more accuracy is required, the interaction of structures when small number of modes are present may better be described by a deterministic approach such as modal analysis utilizing finite element techniques. A comparison of modal analysis and SEA predictions (based on average parameters) with experimental results may be a more clear way to evaluate the applicability of SEA averaged parameters, when the number of modes is small. This is the subject of the study carried out by Lu, Hawkins, Downward and DeJong [53], and is a potential area of research.

Another aspect to consider as pointed out by Lyon [52], is the utilization of finite element to evaluate coupling loss factors in direct analogy with SEA for comparison with the averaged SEA coupling loss factors. This also appears to be a potential area of research.

APPENDIX B

MACHINERY-FOUNDATION INTERACTION

This appendix is included only for the sake of completeness, since the power delivered by the machinery to the foundation was assumed to be known. It is especially addressed to those not familiar with the subject. Fundamental aspects regarding the interaction between machinery and foundation, which supported the model idealization (Chapter 4), are summarized herein from works concerned with this subject, especially references [30,52].

A reasonable estimation of the power input requires an appropriate characterization of the vibration source and its foundation.

An excited structure will oppose motion and its response is usually represented by its velocity or acceleration. Excitation and response are related by a mobility ([Y]) matrix, completely determined by the dynamic characteristics (mass, inertia, stiffness and internal losses) of the structure.

The mechanical force mobility of a structure is defined [54] as the complex ratio between the velocity, at a given location, and the excitation force

$$Y^F = \underline{V}/\underline{F} \qquad \text{(B.1)}$$

When moment is the excitation, a moment mobility is analogously defined, $\underline{F}$ being replaced by $\underline{M}$ and $\underline{V}$ by the angular velocity $\underline{\Omega}$:

$$Y^M = \underline{\Omega}/\underline{M} \qquad (B.2)$$

For writing convenience only the force mobility will be referred to, the superindex being omitted.

When the concern is the response of the structure at the position where the force and/or moment are applied, expressions (B-1) and (B-2) constitute the so-called input mobilities. When the positions are different, the denomination of transfer mobilities applies.

As stated by Petersson and Plunt [30], the definition of force mobility is not unambiguous since the area on which the force is acting is not defined. When the dimensions of this area are small compared with the wave length, Y^F is called point mobility, $\overline{V}$ being the average velocity of that area (when the input mobility is considered).

The complex power transmitted by a force to a structure through a single contact point and in one direction (i) can be written as:

$$\Pi_i = \frac{1}{2} \underline{F}_i^* \underline{V}_i = \Pi_A + i\Pi_R \qquad (B.3)$$

where:

$\underline{F}_i$ and $\underline{V}_i$ are the complex force and velocity at the point of contact (at the structure)

(*) denotes the complex conjugate of $\underline{F}_i$.

Π_A and Π_R are the active and reactive power, respectively.

The average transmitted (active) power is given by:

$$\langle \Pi_i \rangle = \frac{1}{2} \text{ Re } \{\underline{F}_i \ \underline{V}_i^*\} = \frac{1}{2} \text{ Re } \{\underline{V}_i \ \underline{F}_i^*\} \qquad \text{(B.4)}$$

Substituting (B-1) in (B-4), $\langle \Pi_i \rangle$ can be rewritten as:

$$\langle \Pi_i \rangle = \langle V_i^2 \rangle \ \text{Re}\left\{\frac{1}{Y^F}\right\} \qquad \text{(B.5)}$$

or

$$\langle \Pi_i \rangle = \langle F_i^2 \rangle \ \text{Re}\{Y^F\} \qquad \text{(B.6)}$$

Expression (B-5) is normally used in association with on board or factory measurements since the velocities and acceleration are much easier to obtain than forces and moments measurements.

A source of vibrational energy [52] can be characterized by its free velocity $\underline{V}_S$ (which expresses the motion that it would generate if vibrating free in space) along with its internal mobility, Y_S (a function of its dynamic characteristics), at the mounting points. $\underline{V}_S$ and Y_S define the ability of machinery to generate vibration in the foundation. The source can be schematically represented (as in Fig. B-1) by analogy with an electrical source. When machinery is installed, the supporting structure will react to the vibration and the engine will transmit energy through the supports by both forces and moments. Thus, the actual velocity of the source will be equal to its free velocity diminished by the velocity induced in the source structure by the forces and moments, through the corresponding source mobilities:

$\underline{V} = \underline{V}_S - Y_S\underline{F}$ (when a force interaction is considered).

The resulting velocity induced by the force in the supporting structure, through its mobility is: $\underline{V}_F = Y_F\underline{F}$.

Figure B-2 illustrates schematically the interaction between a vibrational source, resiliently mounted, and a structure. If we make a parallel with an electric circuit, $\underline{V}$ can be understood as voltage and $\underline{F}$ as current.

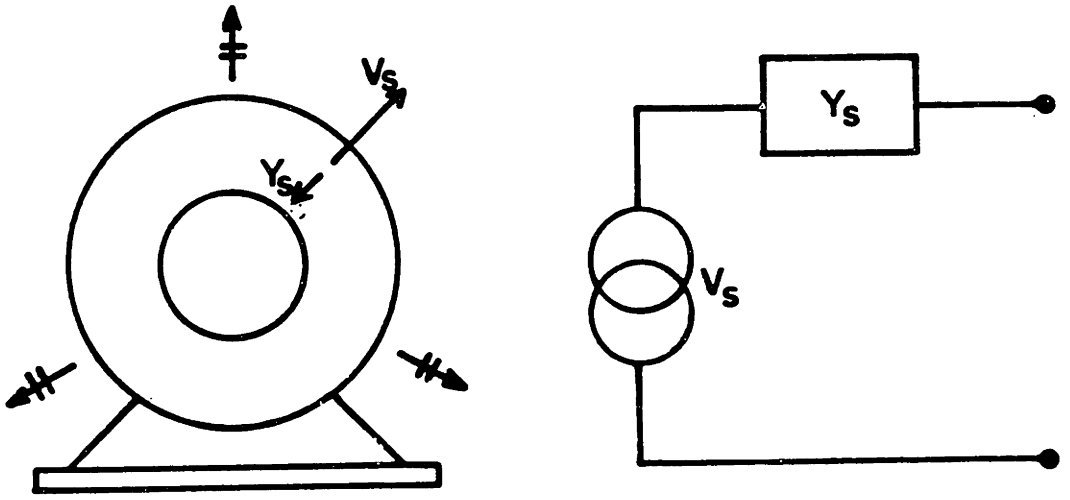

FIGURE B.1: CHARACTERIZATION OF A VIBRATIONAL SOURCE

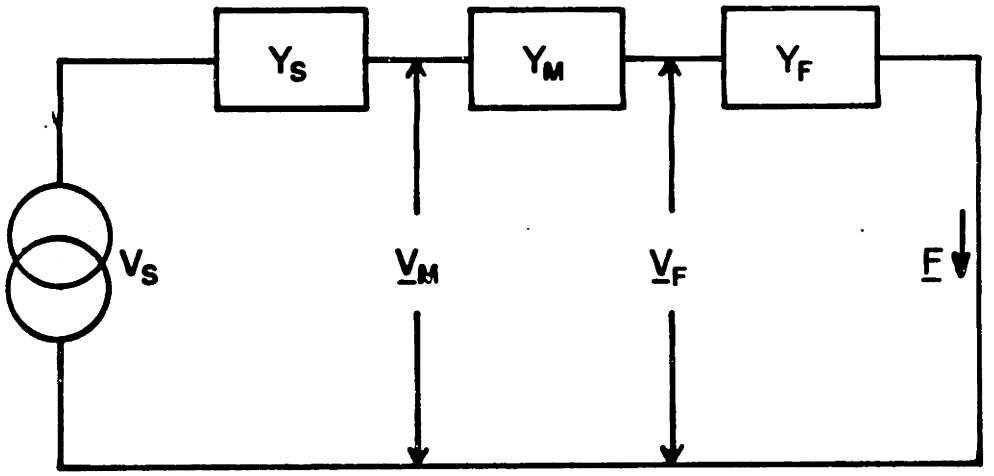

FIGURE B.2: INTERACTION BETWEEN A VIBRATIONAL SOURCE AND A STRUCTURE. SCHEME FOR CALCULATING THE POWER TRANSMISSION

Based on Fig. B-2 and on equation (B-5), the average power delivered by the source to the structure can be written as:

$$\langle \Pi_F \rangle = \frac{\langle V_F^2 \rangle \ \mathrm{Re}\{Y_F\}}{|Y_F|^2} = \frac{\langle V_M^2 \rangle \mathrm{Re}\{Y_F\}}{|Y_F+Y_M|^2} = \frac{\langle V_S^2 \rangle \mathrm{Re}\{Y_F\}}{|Y_S+Y_F+Y_M|^2} \qquad (B.7)$$

In an actual installation the machinery is connected to the foundation through several (N) supports. In general, there are three components of forces and moments to consider at each support: a six degree of freedom problem. They are associated with the six independent components of motion, three translations and three rotations. Therefore, each component of motion (and associated power input) at a given position will incorporate, in principle, a contribution from:

(a) The other five components at the same contact point.

(b) The six components of each other support.

In such situations a total mobility matrix has to be considered. From Petersson and Plunt [30]: each element of this matrix can be written as:

$$\underline{Y}_{ij}^{m\kappa} = \frac{\underline{V}_j^{\kappa}}{\underline{F}_i^{m}} \quad \begin{matrix} (m,\kappa = 1,2,\ldots,N \\ i,j = 1,2,\ldots,6) \end{matrix} \qquad (B.8)$$

where $\underline{F}^m_i$ is the force in point m in the direction i and $\underline{V}^k_j$ is the velocity of point k in the direction j, due to this force.

When i = j and m = k, we have the input mobility.

The total velocity at k in the j direction can be obtained by adding the contribution of each force $\underline{F}^m_j$, by assuming all others as zero (superposition principle) and by using the mobilities expressions:

$$\underline{V}^K_j = Y^{KK}_{jj} \cdot F^K_j + \sum_{\substack{i=i \\ i\neq j}}^{6} Y^{KK}_{ij}\underline{F}^K_i + \sum_{i=1}^{6}\sum_{\substack{m=1 \\ m\neq K}}^{N} Y^{mK}_{ij}\,\underline{F}^m_i \qquad \text{(B.9)}$$

Accordingly, the complex power transimitted can be calculated from:

$$\Pi^K_j = \frac{1}{2}\,\underline{F}^{K*}_j\,\underline{V}^K_j \qquad \text{(B.10)}$$

The total average power from machinery to foundation can, therefore, be determined by:

$$\Pi_A^{TOT} = Re\left[\sum_{j=1}^{6} \sum_{K=1}^{N} \Pi_j^K\right] \qquad (B.11)$$

This equation illustrates the complexity associated with a multipoint installation. A considerable amount of computation and of experimental difficulties may, therefore, be anticipated.

In an actual situation, however, not all components of motions are important, the contribution to power associated with some of them being predominant (for example: the vertical force of a diesel engine resiliently mounted). Some of the transfer mobility may also be unimportant. The proper simplifications of the problem is a matter of judgement and will depend on the particular installation and on previous experiences.

Popkov [55] proposed a method to reduce the calculations and measurements that may be associated with a multipoint installation (Equation B-11). It consists basically of the determination of:

(a) <u>An effective mobility</u> for each individual point, taking into account the interaction with the other points, and considering the different directions.

From Petersson and Plunt [30]:

$$Y_{ii_{\Sigma,F}}^{nn_{\Sigma}} = \frac{\sum_{\kappa=1}^{N} \sum_{j=1}^{6} \underline{Y}_{ji,F}^{\kappa n} \cdot \underline{F}_{j,F}^{\kappa}}{\underline{F}_{i,F}^{n}} = \frac{\underline{V}_{i,F}^{n}}{\underline{F}_{i,F}^{n}} \qquad \text{(B.12)}$$

where:

$\underline{F}_{j,F}^{\kappa}$ is the complex force acting in point κ and in the direction j.

$\underline{Y}_{ji,F}^{\kappa n}$ is the general mobility from point κ and direction j to point n and direction i.

Σ indicates that all points (superindex) and all directions (subindex) are taken into account.

$\underline{V}_{i,F}^{n}$ is the total velocity at point n and direction i due to all forces.

$\underline{F}_{i,F}^{n}$ is the force applied at point n in the direction i.

(b) <u>An overall effective mobility</u> which is a space averaged mobility over all excitation points. Analogously to the case where only one contact point is considered it is defined as: (from Petersson and Plunt):

$$Y_i^{EFF} = \frac{\sqrt{\langle v_i \rangle^2}}{\underline{F}_i^{EFF}} \qquad \text{(B.13)}$$

where:

i represents the actual direction of motion

$\langle V_i^2 \rangle$ is the mean square average velocity in the i direction (over all points)

$$\underline{F}_i^{EFF} = \frac{\underline{\Pi}_i}{\sqrt{\langle V_i^2 \rangle}} \qquad \text{(B.14)}$$

where

Π_i is the total transmitted complex power in the i direction.

The derivations are shown in detail in reference [55] and the concepts of effective and overall effective mobilities are very well analyzed and also investigated in the laboratory by Petersson and Plunt [30], whose work was concentrated on and applied to ship machinery.

The major aspects concerning the interaction between machinery and foundation have been presented. The question becomes: "How can the designer calculate the mobilities and obtain the source free velocity in order to estimate the power input?"

The mobilities associated with continuous systems where the number of degrees of freedom is infinity can be deduced from the wave equation. They are usually called the characteristic mobilities. Formulas for common mechanical impedances (Z = 1/Y) for infinite systems are presented in references, such as [36,51].

When finite structures are considered, the expressions of mobilities ought to be quite complicated since they are mainly determined by the resonances. As already noted, the response of a structure to a given excitation can always be obtained by using modal analysis. In many cases, however, the resulting expressions are not practical, unless the mode shapes are determined by special methods, such as finite elements.

It is also important to refer to the work by Goyder and White [56]. They analyzed the power flow from machines into built-up structures. Beam, plate-like and beam-stiffened-plate foundations under different excitations were investigated; input mobilities were calculated. Infinite and finite structure (beams and plates) were also compared.

Another way of obtaining the mobilities is, of course, through measurements. Petersson and Plunt [30] carried out measurements of point and transfer mobilities on a diesel-generator base-plate and double bottom structure. They also presented prediction procedures for the mobilities of combustion diesel engines base-plates and stiffened-plate foundation structures.

The interaction between diesel engine and foundation was also the subject of the work carried out by M. Ohlrich [29], who used scaled models of ship sections in his experiments. His main objective was to reveal the characteristics and factors which would influence the power transmission between the engine and the foundation.

Petersson and Plunt [30] and Ohlrich [29] found (for the particular problems investigated) that the point mobility of the foundation seemed to be mainly determined by the local stiffness of the excited plate section, between brackets, up to its first resonance frequency. For higher frequencies the characteristic mobility will determine the mobility together with the superimposed response of the resonances. Petersson and Plunt [30] also concluded that the point mobility might be sufficient for the description of the dynamic properties of the foundation and engine structure when their coupling is analyzed.

Another aspect considered by Petersson and Plunt [30] was the contact area between the mount (hard and soft) and the foundation. In many cases their dimensions are significant when compared to the wavelength so that a correction was suggested for the proper prediction of the mobility.

From all the previous aspects, it is easy to infer that the determination of the mobilities depends on the particular installation being analyzed and is intimately related to the foundation

structural idealization.

With respect to the source characterization, the necessary information is usually obtained from measurements taken during factory tests, as pointed out by Ohlrich [29]. This is a normal contractual clause in an acquisition of naval equipment. For example, consider the test of a resiliently mounted diesel engine. The usual measurement is the vertical velocity taken at the engine support point above the mountings; a velocity spectrum curve being furnished.

$$\langle V_{MT}^2 \rangle = \int_{-\infty}^{\infty} S_{V_T}(\omega)\, d\omega \qquad \text{(B.15)}$$

Considering Fig. B-2 and assuming that the test bed has zero mobility (infinite impedance) we have:

$$V_S = \frac{V_{MT}(Y_S + Y_M)}{Y_M} \quad \text{(free velocity)} \qquad \text{(B.16)}$$

$$\langle V_S^2 \rangle = \langle V_{MT}^2 \rangle \left| \frac{Y_S + Y_M}{Y_M} \right|^2 \qquad \text{(B.17)}$$

Y_M and Y_S can be written as

$$Y_M = \frac{i\omega}{K_M} \tag{B.18}$$

where

K_M is the mounting stiffness, furnished by its manufacturer,

$$Y_S = G_S + i\, S_S$$

Therefore,

$$\frac{Y_S + Y_M}{Y_M} = \frac{iG_S - (S_S + \frac{\omega}{K})}{(\frac{\omega}{K})} \tag{B.19}$$

$$\left|\frac{Y_S + Y_M}{Y_M}\right|^2 = \frac{G_S^2 + (S_S + \omega/K)^2}{(\omega/K)^2} \tag{B.20}$$

usually

$$\omega/K >> G_S, \qquad \omega/K >> S_S$$

Therefore, $\langle V^2_s \rangle = \langle V^2_{MT} \rangle$ and the power flow delivered by the engine to the foundation can be estimated by:

$$\Pi_F \simeq \frac{\langle V^2_{MT} \rangle \, \mathrm{Re}\{Y_F\}}{|Y_M|^2} \qquad \text{(B.21)}$$

A similar approach can be undertaken to obtain the power input in a rigid installation, in terms of the test data.

Before closing the Appendix, it is important, once more, to refer to Petersson and Plunt [30]. They suggested practical possibilities to reduce structure-borne sound power input, from the machinery to the foundation. As they emphasized, the suggestions were based on measurements of the mobilities on the vertical direction only, but they clearly show how important a proper design of the foundation can be.

APPENDIX C

STRUCTURAL MODELLING -- ENERGY TRANSFORMATIONS

C.1 Ship Structural Modelling -- Energy Transmission Paths

Nilsson [7,8] did not apply SEA nor consider the bottom structure in his SBN transmission studies. However, in terms of transmission mechanisms, he stated: "It has been frequently observed that the SBN mainly propagates from the source up through the ship's structure in the direction of the frames." He used a grillage (beam-plate) model. For lower frequencies he concluded that the frame flexural motions were dominant. As frequency increases, the plate flexural motions become more important, and the frames act as wave guides.

A transverse path has also been assumed in some SEA applications [4,6, 11]. They analyzed scaled unstiffened plate-like models of actual ship sections between frames; the plates represented the hull, decks, platforms, bulkheads and the bottom. Jensen [11] explained the reasoning for this structural model choice: "For frequencies at which the flexural wave lengths in the plate is considerably smaller than the frame spacing, it might be permissible to consider the ship section to be composed of a variety of unstiffened plates." No number was associated with the word "considerably."

It appears that this criterion may be appropriate for hulls and decks, but not for the ship bottom, where the transverse members may play an important role in a SBN transmission.

Analyzing the transmission on a small motor boat, Sawley [10] concluded that the main structural energy path was in the fore-and-aft direction, from the bottom girders to the machinery space bulkheads. This may happen

when the machinery foundation is continuous along the entire engine room length, especially when aligned with the bottom longitudinal girders, as is normal in small ships. These situations can be identified in the reference ship (Chapter 4) in which some of the primary sources are installed very closely to the machinery space bulkheads.

Irie and Takagi [12] utilized a three-dimensional plate-like model, without assuming a particular preferable transmission path. Their main purpose was to investigate the applicability of SEA to a structure with many coupled components and, therefore, with different possible energy paths.

Apparently, none of the works on SBN transmission has actually considered the details of the equipment foundations and of the bottom structure. Nilsson [7,8] assumed that the power input was primarily associated with the fore-and-aft moment transmitted from the engine to the foundation and the related angular velocity; the bottom introduces an attenuation, not analyzed, between the source and the hull (Nilsson's major concern).

Jensen, Kihlman, and Plunt (whose models have a well defined transverse transmission path) represented the bottom as plates, where a vertical force (the assumed excitation) was applied (to the tank top). Irie and Takagi also considered the bottom as a plate where a force was applied. Because Sawley's major concern was to interpret on-board measurements and the transmission of vibration energy from the hull and machinery space bulkheads to the deck above, he didn't explore in depth the energy transmission through the ship bottom.

It is also important to mention that in SEA applications an unstiffened plate-like structure has usually been assumed, Plunt [6] and Sawley [10],

however, gave some attention to the stiffener's effect. With respect to the transmission mechanisms, apparently only Kihlman and Plunt [4] have considered other motions than bending (this is discussed in Paragraph C-3).

C.2 Effect of Stiffeners

The effects of the longitudinal stiffeners and smaller size frames are usually not considered in the works related with SBN transmission on ships, without presenting a supporting reasoning.

The stiffeners may substantially increase the complexity of a SBN transmission analysis. A good indication of that can be given by utilizing the formulations of modal density and natural frequencies to estimate the number of modes available to store energy in a frequency band (SEA subsystem) associated with different motions that can be assumed by the stiffeners; similar to what was done in Chapter 4, section 4.1. The stiffeners can be represented as a beam or as a plate-like structure. The number of modes associated with the torsional motions were calculated based on approximate expressions for torsional rigidity from references [27,61], assuming that the center of mass of the beam section coincides with the center of rotation. If the center of mass does not lie in the axis of rotation, which is expected in the actual situation, then the torsional and flexural modes of the beam will be coupled [27].

Therefore, different simultaneous behaviors of the same significance can be expected in a large frequency range:

1. As a rotary inertia and stiffness
2. As a beam, in bending and torsion

3. As a plate

   a. its web in bending;

   b. its flange also in bending at high frequencies

   c. its flange mainly of a rotary inertia and stiffness for low frequencies

It is also important to point out that the number of modes is not high below 6300 Hz, an important frequency interval, in which a significant number of plate flexural modes are excited in the bottom, tank top, and floor sections between stiffeners. From the SEA point of view, the aspects to be considered are: How much energy they can store and how they affect the transmission through the plate to which they are welded. This is related to the coupling strength and loss factors as discussed in Paragraph 4.3.5.

The problem is clearly complex. Ungar [57] studied the transmission of plate flexural waves through reinforcing beams. The intended application was analysis of dynamic stress concentration on flight vehicle structures. An infinite plate with a narrow straight beam continuously attached to a plate was considered. The analysis was restricted to the case where the centroids of the beam cross sections were coincident with the center of twist and lay in the plane of the plate mid-surface.

In a ship we actually have a finite system, with almost periodically spaced beams welded to plates.

Heckl [58] extended Ungar's work to finite systems. An isolated reinforcing rectangular beam and a periodic array of beams were studied. Depending upon the relation between the bending wavelength for the plate

($\lambda_B^{(P)}$) and the distance between the beams (L_s), two different treatments were suggested:

1. $\lambda_B(P) > 4L_s$ -- the system can be treated like an orthotropic plate. This means f < 30 Hz for the reference ship bottom:
2. $\lambda^{(P)} < 2L_s$ -- if the plate is stiffened periodically, it should be treated like a periodic structure; (f > 120 Hz for the reference ship.

Formulations for attenuation of bending waves were derived and compared with measurements. A simplified formula was suggested relating the mean square plate average velocities at each side of a reinforcing beam. The transmissibility from one plate section to another through the beam was, as reproduced by Lyon [15]:

$$\tau = 2 \frac{(\kappa_g c_L m)_p}{(c_\phi m)_b} \left(1+64 \frac{(mc_\phi)_p}{\omega m_b}\right) \qquad \text{(C.2.1)}$$

where

p = plate

b = beam

κ_g = radius of gyration

m_b = mass per unit length of the beam

m_p = mass per unit area of the plate

As Heckl pointed out, the basic simplified formulations which were derived hold for fairly heavy beams. The expression (C.2.1) includes a correction factor to improve the approximation for light beams. The concepts of light and heavy beams are related to the expression:

$$H = \frac{2}{\pi} \frac{m_p h_p}{m_b h_b} \frac{\lambda_p}{b_b} \qquad \text{(C.2.2)}$$

In accordance with two graphs from Heckl's work, a beam may be considered heavy when H = 0.01 and light when H = 0.1.

The works by Sawley [10] and Plunt [6] considered the effect introduced by the stiffeners. Both used Heckl's formulation (C.2.1). As already suggested, Sawley's major concern was the interpretation of on-board measurements, without a strong emphasis on accuracy. Plunt, on the other hand, studied stiffened panels both analytically and experimentally. He concluded that the application of (C.2.1) to junctions made up from relatively weak stiffeners leads to erroneous values of τ, much larger than 1 in the low frequency range. Calculated values, restricted to $\tau < 1$, were compared with measurements, significant differences being observed. Plunt's experimental results also showed that the attenuation introduced by the stiffeners should be considered.

Applying expression (C.2.2) to the top tank and bottom stiffeners of the reference ship, they can only be considered as a light beams for very high frequencies, far beyond the upper limit of practical interest.

Thus, it seems that directly applicable formulations to quantify the stiffener effect are lacking. Further experimental and analytical efforts are necessary, independent of the particular approach being used.

From the above discussions and from the results obtained in paragraph 4.1.4, it is recognized that the stiffeners have to be considered in an accurate analysis. However, they are not included in this thesis model, as justified in Section 4.1 of Chapter 4.

C.3 In-Plane Motions - Energy Transformations

SBN analysis related to ships has tended to focus on bending transmission and has not considered motion transformations. Apparently only two works have considered other types of motions than flexural. One done by Nilsson [8], who did not apply SEA, and the other carried out by Kihlman and Plunt [4], using SEA.

Nilsson's grillage model was referred to in Chapter 1 and in Paragraph C.1 of this appendix. In his model the beams were allowed to bend in a plane normal to the plate and to twist about their junction lines with the plate. Flexural and in-plane motions were allowed in the plates. This model was first analyzed by Fahy [59,60], but without including the in-plane motions.

Kihlman and Plunt applied SEA to interpret results obtained from tri-axial SBN measurements on board of ships. Based on those measurements, they stated that the magnitude of the in-plane wave components were much higher than expected. It was also mentioned that further measurements in ships, where the SBN from the propeller is dominant, supported the assumption that the in-plane waves are mainly directly excited by the main machinery rather than as a result of wave conversion at joints. Commenting on this work, Nilsson argued that the magnitude of the velocity levels in the in-plane direction could be caused by the transverse waves induced by he relative motions of the frames.

The subject is, therefore, controversial, but as mentioned in Chapter 1, works related to SBN, although considering only flexural transmission, frequently suggest in their recommendations that a more accurate analysis should

take into account other kinds of motions. [4,6,11,12]

With respect to this thesis, it was shown in Section 4.1, by using SEA concepts, that a significant number of modes associated with in-plane motions of the model's plates are available to store energy. Therefore, they are expected and the question become: "How can they be excited?"

The junction between the top plate and the web is a right angle structural discontinuity, so that a bending excitation at the top plate can, in principle, induce in-plane motions of the web. The question now is: "Is the amount of energy transmitted from bending to in-plane significant enough? In terms of SEA, this question is directly related with the strength of the coupling between the groups of modes (This is discussed in Chapter 4).

Cremer [36] in his analysis for two plates, identified a parameter which could be used to characterize the generation of longitudinal waves at the joint, from an incident bending wave:

$$\beta_2 = \frac{c_{B_1} \rho_{s_1}}{c_{L_2} \rho_{s_2}} \qquad \text{(C.3.1)}$$

where subscript 1 is the transmitting component and 2 the receiving component.

For plates, (C.3.1) can be rewritten as

$$\beta_2^2 = \frac{1.814}{c_L} \left(\frac{h_1}{h_2}\right)^2 h_1 f \qquad \text{(C.3.2)}$$

No specific values were proposed. Cremer only stated that $\beta = 0.09$ was a rather high value, very near the limit of applicability of the simple bending wave equation.

From (C.3.2) it is obvious that longitudinal and shear (using C_{T2} instead of C_{L2}) may become important as h_1/λ_1 and h_1/h_2 increase.

Swift [23] suggested limits to determine when the effect of longitudinal and transverse shear motions generated at plate joint from a bending incidence should be considered important or not. They were established based on a comparison between bending to bending transmission coefficients from one plate to the other determined for two cases:

1. Assuming only flexural transmission

2. Considering the in-plane motions.

For steel plates the suggested limits are:

$P_{ab} < 50\ ms^{-1}$ -- the in-plane motions need not to be considered, incurring in errors of less than 2 dB in the predicted coupling loss factors.

$P_{ab} > 100\ ms^{-1}$ -- the motion transformations have to be considered.

$50\ ms^{-1} < P_{ab} < 100\ ms^{-1}$ -- only bending transmission can be assumed unless the structure contains two consecutive joints where the plate thickness ratio is greater than two to one.

where

$P_{ab} = h_a^2 f/h_b$, and,

h_a = the thickest plate at the joint

h_b = thickness of a second plate at the joint.

Applying to the junction between the top plate and the web (or brackets) of the diesel foundation.

h_a = 19 mm

h_b = 8 mm

P_{ab} = 100 : f = 2200 Hz.

The results of Paragraph 4.1, reinforced by the application of Swift's criterion, lead to the conclusion that in-plane motions and energy transformation may be significant above 5000 Hz, in the model, and have to be considered in this application.

It is imporrant to mention that Swift's limits are primarily related to the relative magnitude of the transmitted energies from a plate to another, assuming that enough numbers of modes are available to be excited. The criterion was also derived from the comparison between bending to bending transmission coefficients, not between loss factors (the SEA parameters). This is discussed in further detail in Section 4.3.

Before closing this section, a quick analysis of a two plate joint under bending excitation will be carried out. As discussed in paragraph 4.3.5, the comparison of the coupling coefficients may be made, in this case, by comparing the related average transmission coefficients as done by Swift [23]. For plates having the same material, the values of $\bar{\tau}_{ij}$ are a function of the frequency and of the plates thicknesses. Each of the figures from C.3.1 to C.3.3 show curves of average transmission coefficients versus frequency for different values of thicknesses, but for a fixed thickness ratio. The bending to bending transmission coefficient, considering only bending (τ^F_{12}), is also plotted. From those curves, one can infer that:

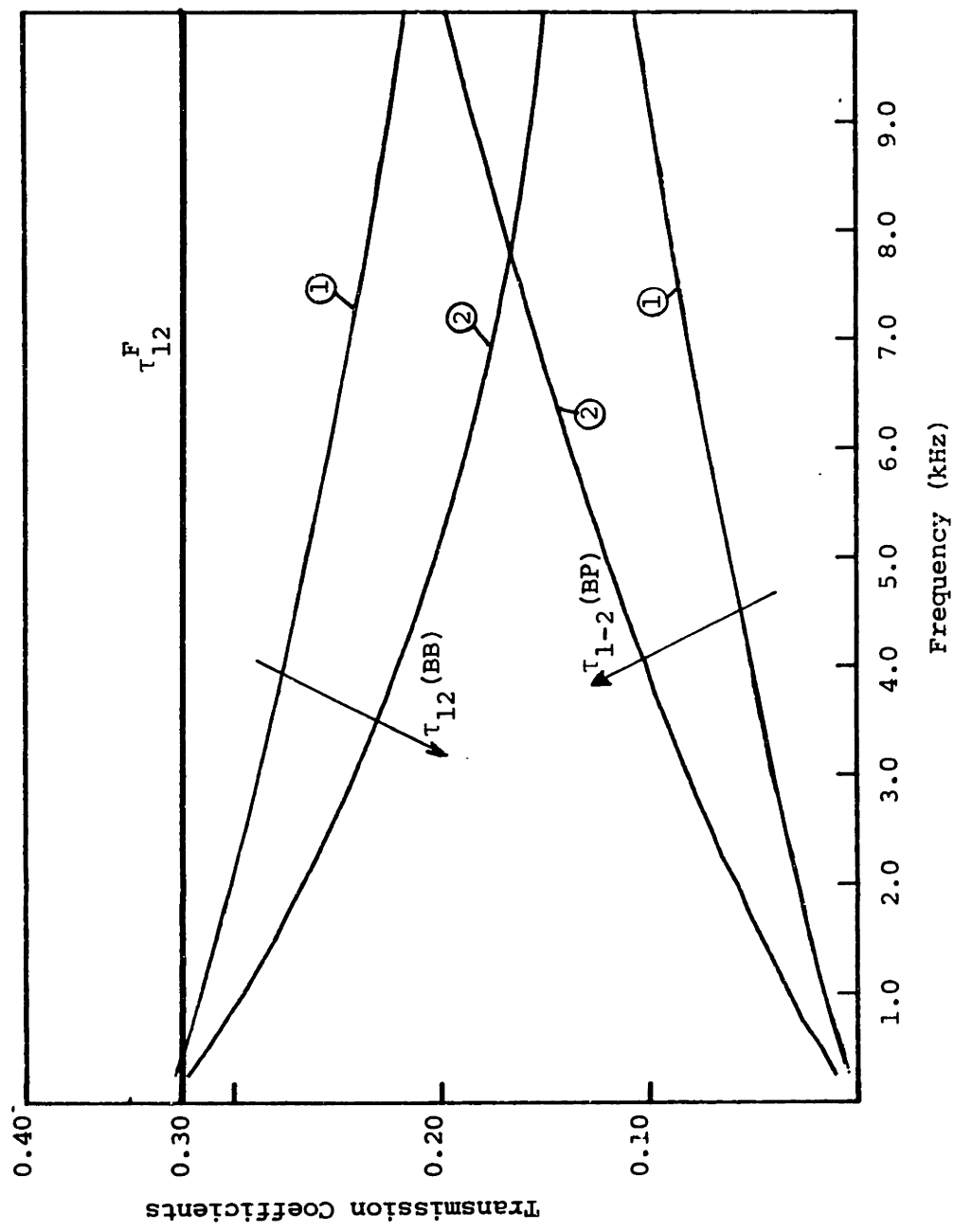

FIGURE C.3.1: VARIATION WITH FREQUENCY OF AVERAGE TRANSMISSION COEFFICIENTS -- TWO-PLATE JOINT -- THICKNESS RATIO = 1:1

① : h = 8 mm, ② : h = 19 mm.

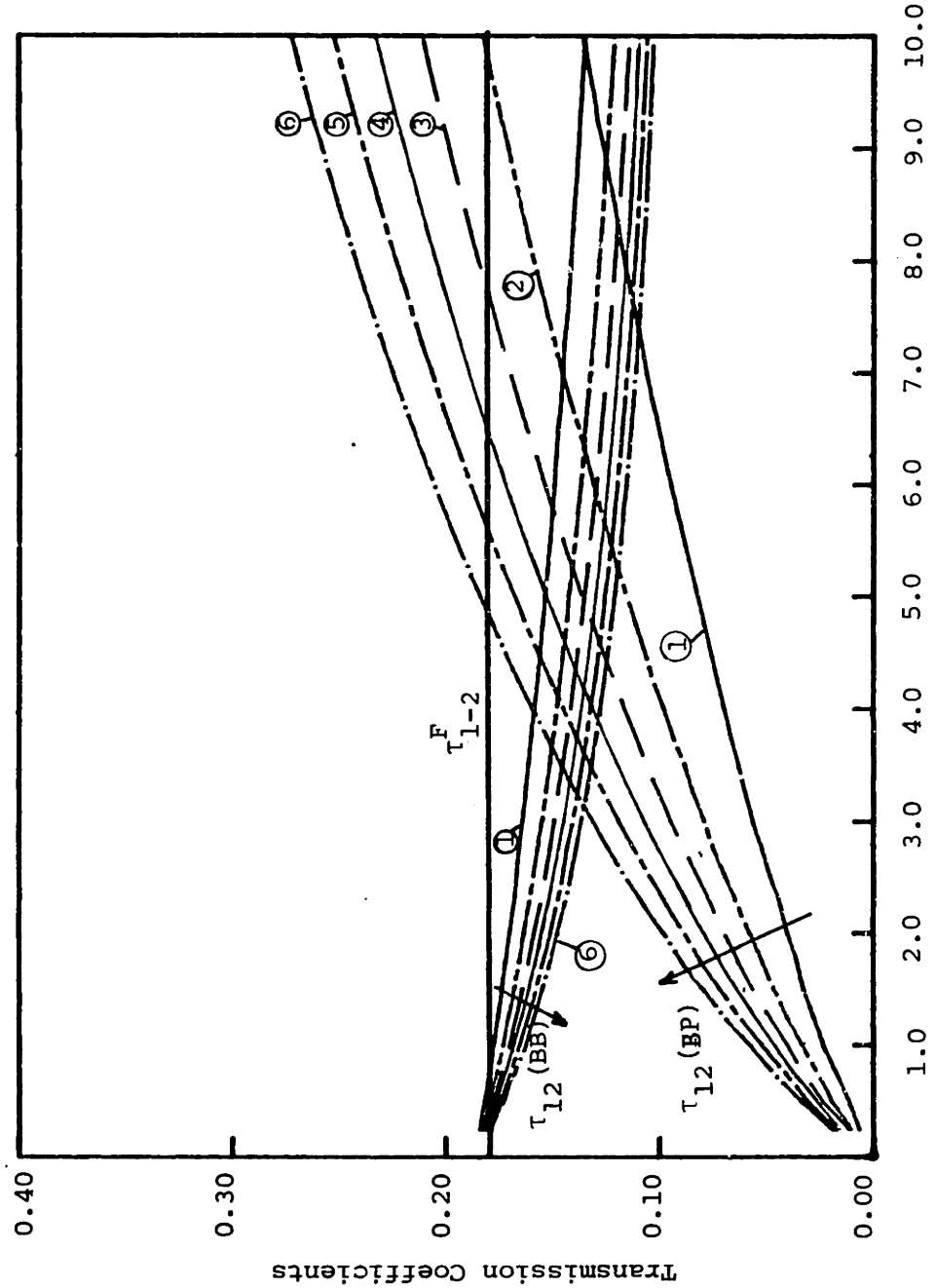

FIGURE C.3.2: VARIATION WITH FREQUENCY OF AVERAGE TRANSMISSION COEFFICIENTS -- TWO-PLATE JOINT -- THICKNESS RATIO: $h_1/h_2 = 2$

①: h_1 = 8 mm, ②: h_1 = 12.7 mm, ③: h_1 = 16 mm,
④: h_1 = 19 mm, ⑤: h_1 = 22 mm, ⑥: h_1 = 25.4 mm

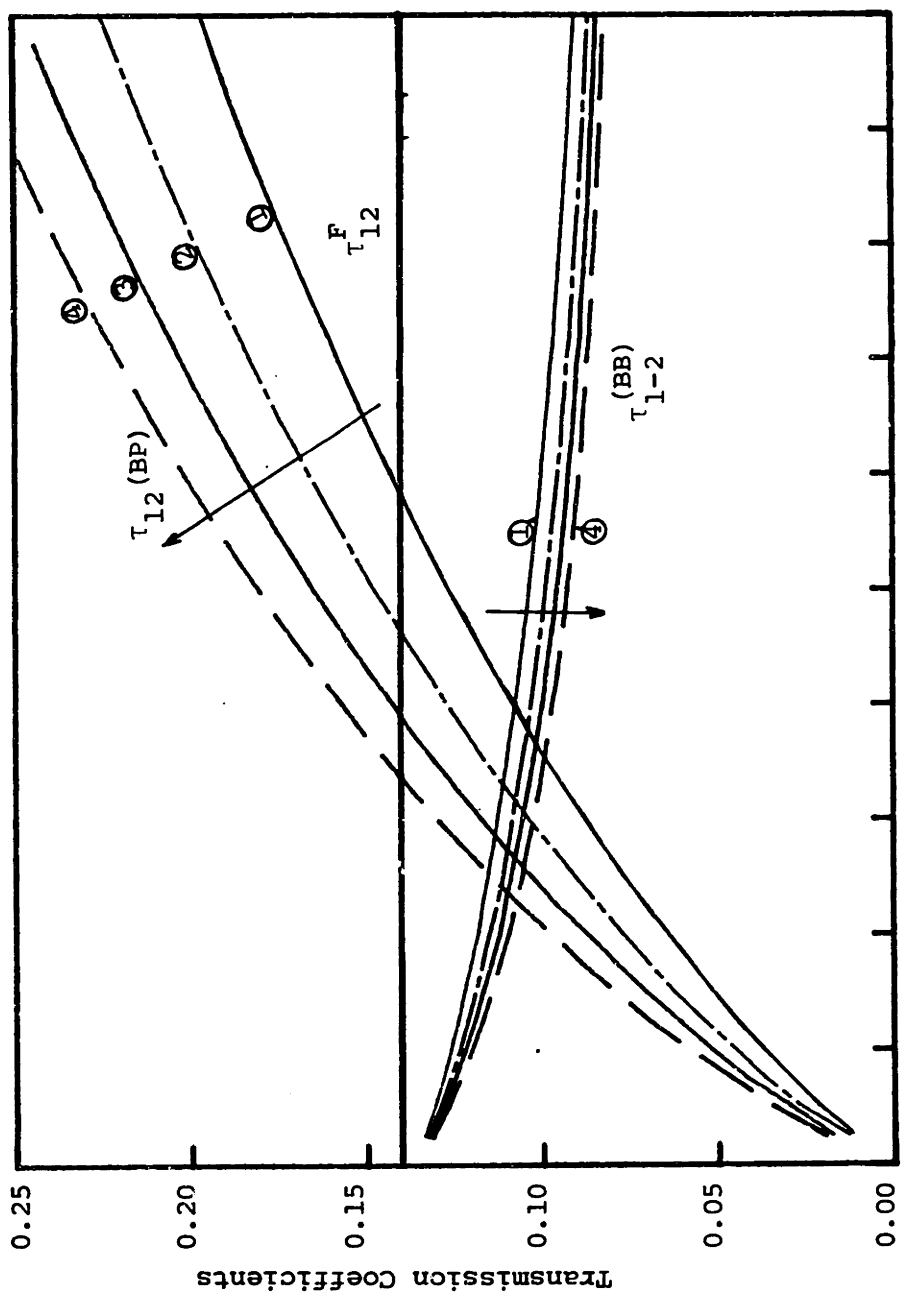

FIGURE C.3.3: VARIATION WITH FREQUENCY OF AVERAGE TRANSMISSION COEFFICIENTS -- TWO-PLATE JOINT -- THICKNESS RATIO: $h_1/h_2 = 2.375$

①: h_1 = 12.7 mm, ②: h_1 = 16 mm, ③: h_1 = 19 mm, ④: h_1 = 22 mm

1. For a given thickness ratio, as the thicknesses of the plates increase $\tau_{12}(BB)$ decreases (increasing the difference with respect to τ_{12}^{F}, and, the bending to in-plane transmission coefficients $\tau(BP)$ increases along the whole frequency interval.

2. As the thickness ratio increases, τ_{12}^{F} and $\tau_{12}(BB)$ decrease and $\tau_{12}(BP)$ increases significantly, especially at higher frequencies.

The variation of the ratio $\tau_{12}(BP)/\tau_{12}(BB)$ with the thickness ratio (h_1/h_2) for a given frequency is better illustrated by the curves in Figure C.3.4.

All those curves show what was stated by Cremer [36]; namely that the generation of in-plane waves at the second plate becomes more important as the thicknesses, thickness ratio and frequency increase, as shown by his parameter (β^2). The parameter used by Swift [23], P_{ab}, is different but conceptually gives the same indication.

The best way to characterize the importance of the wave transformation (for this case) seems to be through the ratio of $\tau_{12}(BP)/\tau_{12}(BB)$, like in curves C.3.4.

It was then decided to plot $\tau_{12}(BP)/\tau_{12}(BB)$ versus Swift's parameter, fixing the thickness ratio, but varying the plate thicknesses. As the result it was found that: the curves are a coincident for the different values of thickness (depending only on the thickness ratio). The same is valid for Cremer's parameter. This demonstrates their usefulness in characterizing the in-plane wave generation in the two plate joints for bending incidence. Figure C.3.5 shows curves of $\tau_{12}(BP)/\tau_{2}(BB)$ versus P_{ab} for two different thickness ratios (h_1/h_2). These aspects justify further

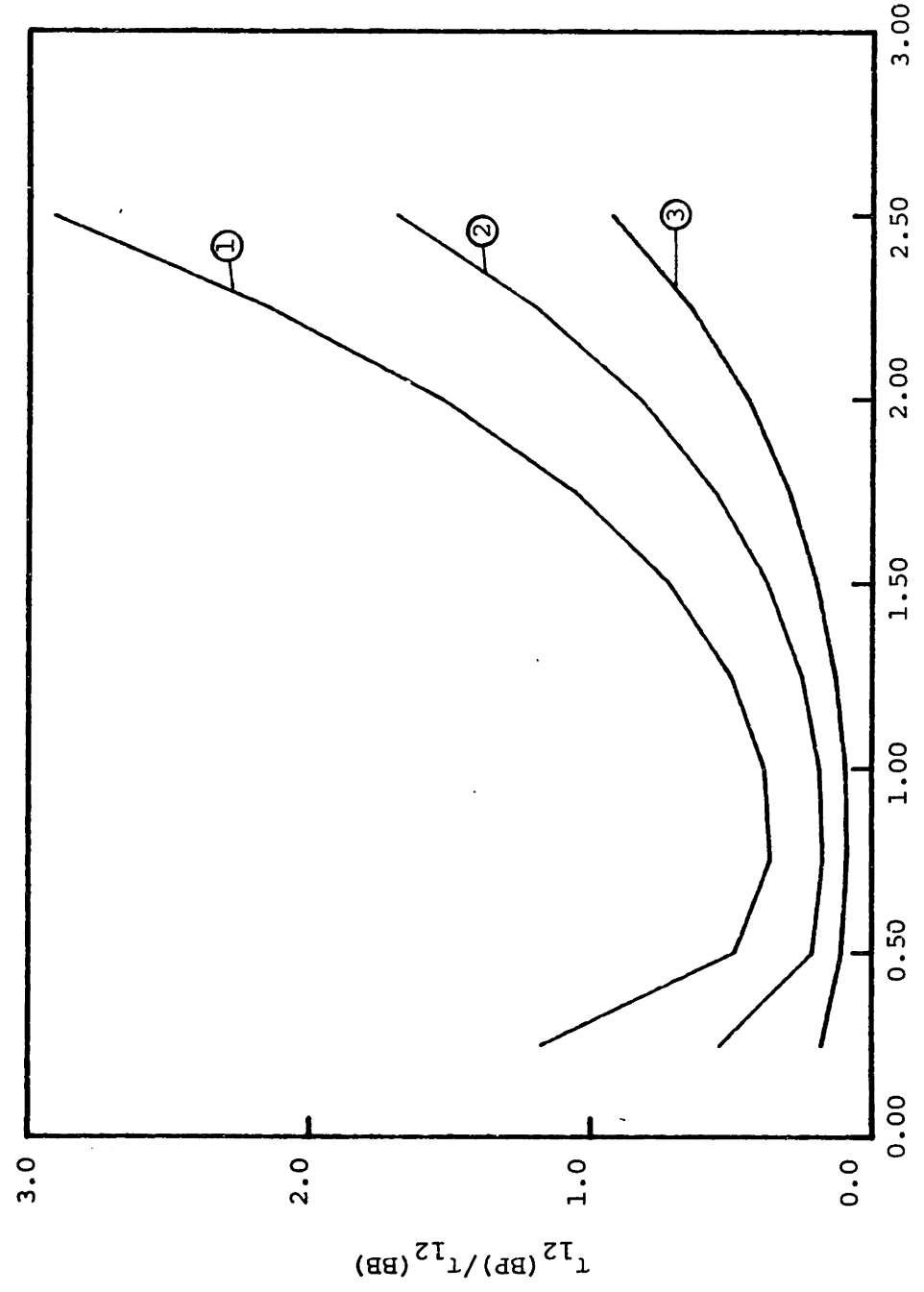

FIGURE C.3.4: VARIATION WITH THICKNESS RATIO (h_1/h_2) OF THE RATIO BETWEEN BENDING-TO-IN-PLANE (τ(BP) AND BENDING-TO-BENDING (τ(BB)) AVERAGE TRANSMISSION COEFFICIENTS -- TWO-PLATE JOINT, h_2 = 8 mm.

①: 8 kHz, ②: 4 kHz, ③: 2 kHz

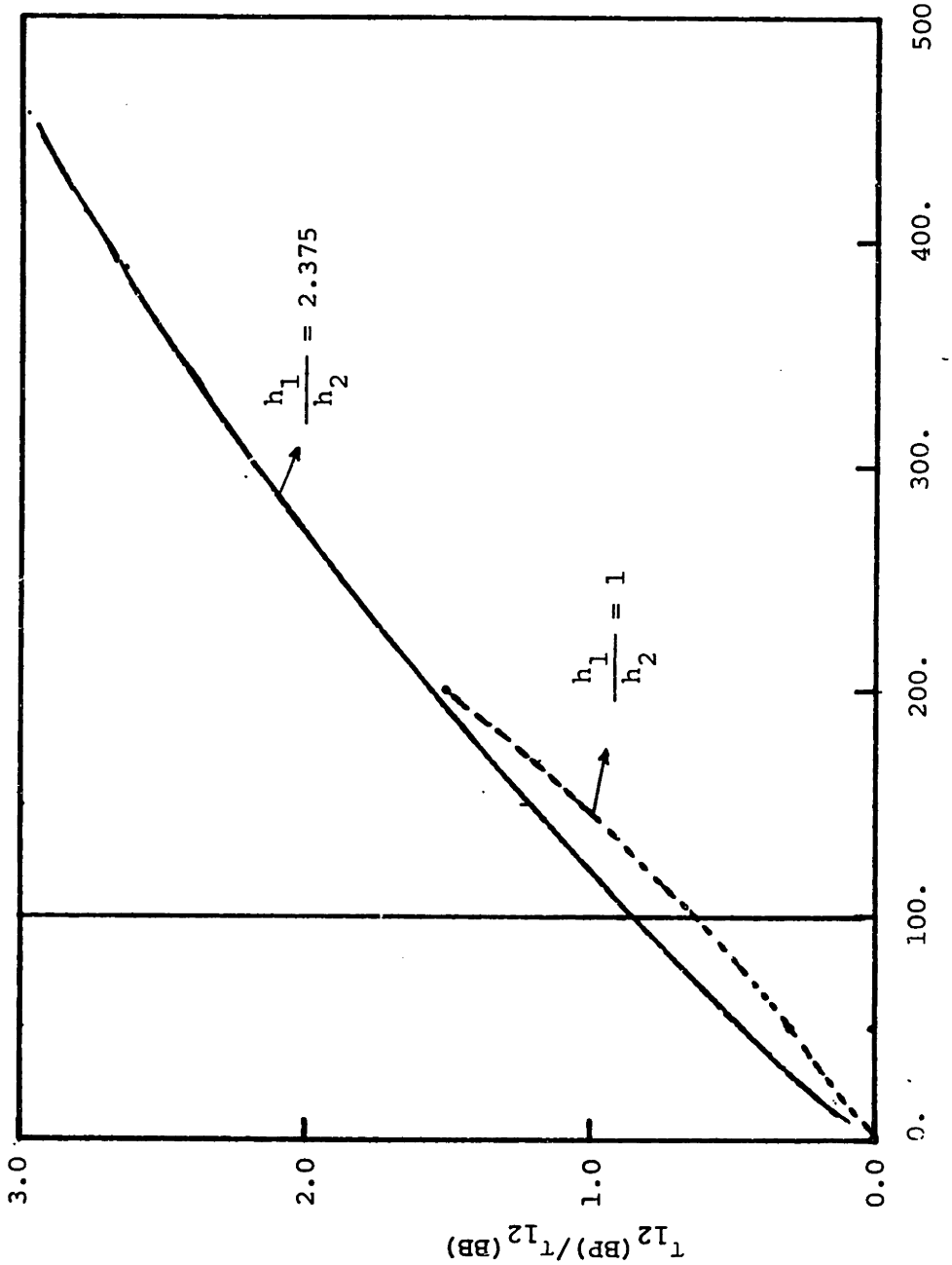

FIGURE C.3.5: VARIATION WITH SWIFT'S [23] PARAMETER (P_{ab}) OF THE RATIO BETWEEN BENDING-TO-IN-PLANE ($\tau_{12(BP)}$) AND BENDING-TO-BENDING ($\tau_{12(BB)}$) AVERAGE TRANSMISSION COEFFICIENTS

investigations comparing coupling loss factors for three and four plate joints and other types of incidence.

All the above discussions were based on a bending excitation at the top plate. However, it is important to mention that the in-lane modes of the brackets and web may be directly excited by the source, depending on how close to these structural elements the contact point between the engine and foundation is located.

Another important aspect related to the possible significance of the in-plane motions is the value of the internal loss factors associated with them. This is discussed in Sections 4.2 and 4.3.

APPENDIX D

TRANSMISSION COEFFICIENTS

D.1 Three Wave Fields

D.1.1 Bending Incidence

As discussed in Chapter 4, four plates at a common joint, when three wave fields are considered, are the general case for the model under study. Since the minimum flexural wave length (λ_{min}) --- for each plate -- is greater than six times the thickness, rotary inertia and shear deformation effects are not included. A thin plate theory (Bernoulli-Euler) is, therefore, applicable.

The adopted coordinate system is shown in Fig. D-1 (same as 4.3.3). The axes are positive in the direction of the arrows. The joint is the y axis.

The incident wave of unit amplitude is assumed to come from plate 1. First we consider a bending incidence that generates (at the joint) in each plate:

1. Propagating waves ---- bending, longitudinal and transverse shear waves;
2. Non-propagating bending waves ---- near fields.

The displacements in the x_n y_n and z_n directions are u_n,v_n and w_n respectively. All plates are allowed to have different thicknesses, but are of the same material (steel), and assumed to

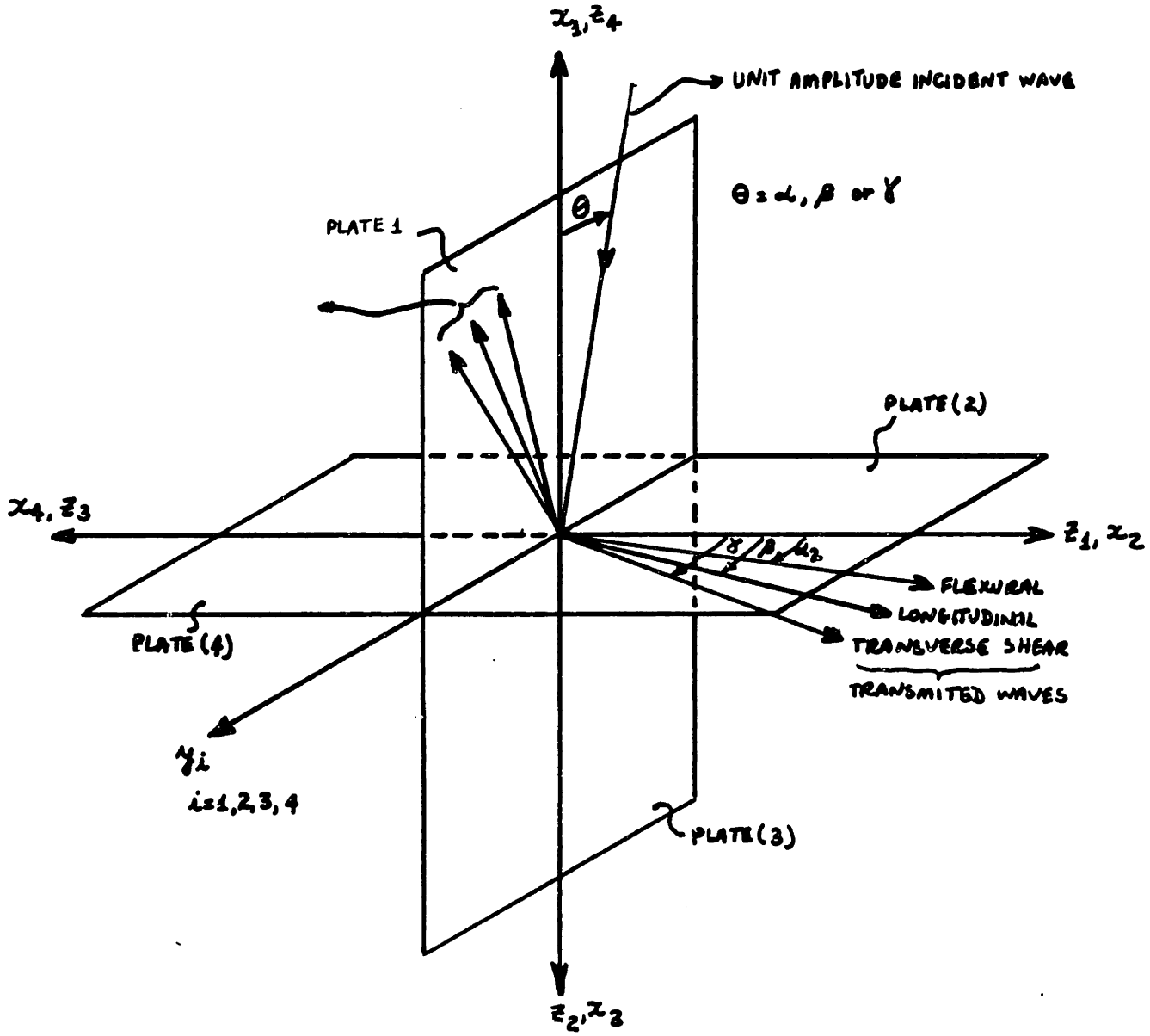

FIGURE D.1: COORDINATE SYSTEM -- FOUR PLATES AT A COMMON JOINT -- THREE WAVE FIELDS

have the same properties. Therefore, the bending wave number may be different for all plates, while the longitudinal and transverse wave numbers are all the same.

$$\ell = \omega c_L = 2\pi f \left(E/\rho(1-\nu^2)\right)^{1/2} \qquad (D.1)$$

$$t = \omega c_T = 2\pi f \left(G/\rho\right)^{1/2} \qquad (D.2)$$

$$\kappa = \left(4\pi f\sqrt{3}/hc_L\right)^{1/2} \qquad (D.3)$$

The trace wavelengths along the y axis are equal for each plate (Snell's law):

$$\ell_1 \sin\beta_1 = \ell_n \sin\beta_n = t_1 \sin\gamma_1 = t_n \sin\gamma_n = \kappa_i \sin\alpha_1 = \kappa_n \sin\alpha_n$$

Therefore, the angles β and γ are the same for all plates and the y, β, γ, ℓ and t subscripts will be omitted. The common

time dependent term, exp [$i\omega t$], is also omitted in the wave expressions that follows:

(1) incident bending wave

$$\exp[i\kappa_1 x_1 \cos\alpha_1 - i\kappa_1 y \sin\alpha_1] \qquad (D.4)$$

(2) reflected bending wave (plate 1)

$$a_1 \exp[-i\kappa_1 x_1 \cos\alpha_1 - i\kappa_1 y \sin\alpha_1] \qquad (D.5)$$

(3) transmitted travelling bending waves:

$$a_n \exp[-i\kappa_n x_n \cos\alpha_n - i\kappa_n y \sin\alpha_n],\ n = 2,3,4 \qquad (D.6)$$

(4) non-propagating bending waves [36]

$$a_n' \exp[-\kappa_n x_n (1 + \sin^2\alpha_n)^{1/2} - i\kappa_n y \sin\alpha_n],$$

$$n = 1,4 \qquad (D.7)$$

(5) reflected (plate 1) and transmitted longitudinal waves:

$$b_n \exp[-i\ell x_n \cos\beta - i\ell y \sin\beta],\ n = 1,4 \qquad (D.8)$$

(6) reflected (plate 1) and transmitted transverse waves:

$$c_n \exp[-it\, x_n \cos\gamma - it\, y \sin\gamma],\ n = 1,4 \qquad (D.9)$$

The transmission coefficients are defined as the ratio of transmitted to incident energy flow at the joint. They depend on the direction that the incident waves are travelling with respect to the joint direction.

The energy associated with each wave type, [23,36] is:

bending:

$$|a_n|^2\ \omega\ D_n\ \kappa_n^3 \cos\alpha_n \qquad (D.10)$$

longitudinal:

$$0.5\ \rho h_n \omega^2 c_L |b_n|^2 \cos\beta \qquad (D.11)$$

transverse:

$$0.5\ \rho h_n \omega^2 c_T |c_n|^2 \cos\gamma \qquad (D.12)$$

where

$$D_n = \frac{E\, h_n^3}{12(1-\nu^2)} = \frac{\rho h_n c_L^3}{12} \quad \text{(Bending Stiffness)} \quad \text{(D.13)}$$

There types of wave transmission coefficients have to be considered:

$\tau_{1n}(BB)$ = bending to bending

$\tau_{1n}(BL)$ = bending to longitudinal

$\tau_{1n}(BT)$ = bending to shear

When n = 1 we have the reflection coefficients (at plate 1). From the definition of τ:

$$\tau_{1n}(BB)(\alpha_1) = (|a_n|^2 D_n \kappa_n^3 \cos\alpha_n)/(D_1 \kappa_1^3 \cos\alpha_1) \quad \text{(D.14)}$$

$$\tau_{1n}(BL)(\alpha_1) = (\rho h_n \omega c_L |b_n|^2 \cos\beta)/(2 D_1 \kappa_1^3 \cos\alpha_1) \quad \text{(D.15)}$$

$$\tau_{1n}(BT)(\alpha_1) = (\rho h_n \omega c_T |c_n|^2 \cos\gamma)/(2D_1\kappa_1^3\cos\alpha_1) \qquad (D.16)$$

The average transmission coefficients (from plate 1 to plate n) are defined as the ratio between the total transmitted to total incident energy considering the whole range of incidence angles. Therefore, they can be expressed as[23]:

$$\langle\tau_{1n}(BB)\rangle_{\alpha_1} = \left(\int_{-\pi/2}^{\pi/2} |a_n|^2 D_n \kappa_n^3 \cos\alpha_n d\alpha_1\right) \Big/ \left(\int_{-\pi/2}^{\pi/2} D_1\kappa_1^3\cos\alpha_1 d\alpha_1\right)$$

$$\langle\tau_{1n}(BB)\rangle_{\alpha_1} = \int_0^{\pi/2} \frac{|a_n|^2 D_n \kappa_n^3}{D_1\kappa_1^3} d\alpha_1 \qquad (D.17)$$

Using $s = \sin\alpha_1$ as the variable of integration, (D-14) becomes:

$$\langle\tau_{1n}(BB)\rangle_{\alpha_1} = \int_0^1 |a_n|^2 \frac{D_n\kappa_n^3}{D_1\kappa_1^3}\frac{\cos\alpha_n}{\cos\alpha_1} ds$$

$$\langle\tau_{1n}(BB)\rangle\alpha_1 = \int_0^1 \tau_{1n}(BB)(s)ds \qquad (D.18)$$

Similarly:

$$\langle \tau_{1n(BL)} \rangle_{\alpha_1} = \int_0^1 \tau_{1n(BL)}(s)ds \qquad (D.19)$$

$$\langle \tau_{1n(BT)} \rangle_{\alpha_1} = \int_0^1 \tau_{1n(BT)}(s)ds \qquad (D.20)$$

In order to determine the different $\tau(\alpha_1)$ it is necessary to know the amplitude of each propagating wave generated at the joint, obtained by applying the boundary conditions along the common length.

Boundary Conditions [36]:

(1) Continuity of Linear Displacements

$$\omega_1 = - u_2 \qquad (D.21)$$

$$w_2 = - u_1 \qquad (D.22)$$

$$u_3 = - u_1 \qquad (D.23)$$

$$w_1 = - u_4 \qquad (D.24)$$

$$u_1 = w_4 \qquad (D.25)$$

$$w_1 = - w_3 \qquad (D.26)$$

$$v_1 = v_n (n = 2,3,4) \qquad (D.27),(D.28),(D.29)$$

(2) Continuity of Angular Displacements

$$\frac{\partial w_1}{\partial x_1} = \frac{\partial w_n}{\partial x_n} \quad (n = 2,3,4) \qquad (D.30),(D.31),(D.32)$$

(3) Equilibrium of Bending Moments

The bending moment at the edge of a plate is given, in standard texts [36, 40, 41], by:

$$M = - D\left(\frac{\partial^2 w}{\partial x^2} + \nu \frac{\partial^2 w}{\partial y^2}\right) \qquad (D.33)$$

therefore:

$$\sum_{n=1}^{4} D_n \left[\frac{\partial^2 w_n}{\partial x_n^2} + \nu \frac{\partial^2 w_n}{\partial y^2} \right] = 0 \quad (n=1,4) \qquad (D.34)$$

(4) Equilibrium of Forces

(a) Along the x_n and z_n directions (perpendicular to y):

The shear forces at the edge of the plate are made up of two components.

1. A two-dimensional equivalent of the bending moment, resulting from shear stresses that act normal to the plane of the plate.

2. A force that counteracts the twisting moment at the boundary.

These combine to give the total force as in Cremer [36], Timoshenko [40] and Graff [41]:

$$Q = D \left[\frac{\partial^3 w}{\partial x^3} + (2 - \nu) \frac{\partial^3 w}{\partial x \partial y^2} \right]$$

Considering these forces and the in-plane forces, we can write:

$$- D_1 \left[\frac{\partial^3 w_1}{\partial x_1^3} + (2-\nu) \frac{\partial^3 w_1}{\partial x_1 \partial y^2} \right] + D_3 \left[\frac{\partial^3 w_3}{\partial x_3^3} + (2-\nu) \frac{\partial^3 w_3}{\partial x_3 \partial y^2} \right] +$$

$$+ E_p h_2 \left[\frac{\partial u_2}{\partial x_2} + \nu \frac{\partial v_2}{\partial y} \right] - E_p h_4 \left[\frac{\partial u_4}{\partial x_4} + \frac{\partial v_4}{\partial y} \right] = 0 \qquad (D.35)$$

$$D_2 \left[\frac{\partial^3 w_2}{\partial x_2^3} + (2-\nu) \frac{\partial^3 w_2}{\partial x_2 \partial y^2} \right] - D_4 \left[\frac{\partial^3 w_4}{\partial x_4^3} + (2-\nu) \frac{\partial^3 w_4}{\partial x_4 \partial y^2} \right] +$$

$$+ E_p h_1 \left[\frac{\partial u_1}{\partial x_1} + \nu \frac{\partial v_1}{\partial y} \right] - E_p h_3 \left[\frac{\partial u_3}{\partial x_3} + \nu \frac{\partial v_3}{\partial y} \right] = 0 \qquad \text{(D.36)}$$

(b) Along the y-axis:

$$\sum_{n=1}^{4} h_n \left[\frac{\partial u_n}{\partial y} + \nu \frac{\partial v_n}{\partial x_n} \right] = 0 \ (n = 1,4) \qquad \text{(D.37)}$$

The displacement equations are obtained from expressions D-4 to D-9, and Fig. D-1.

1. z-direction:

$$w_1 = \{\exp[i\kappa_1 x_1 \cos\alpha_1] + a_1 \exp[-i\kappa_1 x_1 \cos\alpha_1] +$$

$$+ a_1' \exp[-\kappa_1 x_1 (1 + \sin^2\alpha_1)^{1/2}]\}\{\exp[-i\kappa_1 y \sin\alpha_1]\} \qquad \text{(D.38)}$$

$$w_n = \{a_n \exp[-i\kappa_n x_n \cos\alpha_n] + a_n' \exp[-\kappa_n x_n (1+\sin^2\alpha_n)^{1/2}]\} *$$

$$*\{\exp[-i\kappa_n y \sin\alpha_n]\} \qquad \text{(D.39)}$$

(2) x-direction:

$$u_n = b_n(\cos\beta)\{\exp[-i\ell x_n\cos\beta]\}\{\exp[-i\ell y\ \sin\beta]\} +$$

$$+ c_n(\sin\gamma)\{\exp[-it\ x_n\cos\gamma]\}\{\exp[-ity\ \sin\gamma]\} \qquad (D.40)$$

(3) y-direction:

$$v_n = b_n(\sin\beta)\{\exp[-i\ell x_n\cos\beta]\}\{\exp[-i\ell y\ \sin\beta]\} -$$

$$- c_n(\cos\gamma)\{\exp[-it\ x_n\cos\gamma]\}\{\exp[-it\ y\ \sin\gamma]\}\ . \qquad (D.41)$$

At $x_n = 0$, the displacement equations (D-36 to D-39) and their derivatives are (omitting the exponential term on y):

$$u_n\Big|_{x_n = 0} = b_n\cos\beta + c_n\ \sin\gamma \qquad (D.42)$$

$$v_n\Big|_{x_n = 0} = b_n\sin\beta - c_n\cos\gamma \qquad (D.43)$$

$$w_1\Big|_{x_1 = 0} = [1 + a_1 + a_1'] \qquad (D.44)$$

$$w_n\Big|_{x_n = 0} = [a_n + a_n'] \qquad (D.45)$$

$$\left.\frac{\partial u_n}{\partial x_n}\right|_{x_n = 0} = - i\ell\, b_n \cos^2\beta - itc_n \sin\gamma \cos\gamma \tag{D.46}$$

$$\left.\frac{\partial u_n}{\partial y}\right|_{x_n = 0} = - i\ell\, b_n \sin\beta \cos\beta - itc_n \sin^2\gamma \tag{D.47}$$

$$\left.\frac{\partial v_n}{\partial x_n}\right|_{x_n = 0} = - i\ell\, b_n \sin\beta \cos\beta + itc_n \cos^2\gamma \tag{D.48}$$

$$\left.\frac{\partial v_n}{\partial y}\right|_{x_n = 0} = - i\ell\, b_n \sin^2\beta + itc_n \sin\gamma \cos\gamma \tag{D.49}$$

$$\left.\frac{\partial w_1}{\partial x_1}\right|_{x_1 = 0} = i\kappa_1 \cos\alpha_1 - ia_1\kappa_1 \cos\alpha_1 - a_1'\kappa_1 (1+\sin\alpha_1)^{1/2} \tag{D.50}$$

$$\left.\frac{\partial w_n}{\partial x_n}\right|_{x_n = 0} = - ia_n\kappa_n \cos\alpha_n - a_n'\kappa_n (1+\sin^2\alpha_n)^{1/2} \tag{D.51}$$

$$\left.\frac{\partial w_1}{\partial y}\right|_{x_1 = 0} = - i[i+a_1+a_1']\kappa_1 \sin\alpha_1 \qquad (D.52)$$

$$\left.\frac{\partial w_n}{\partial y}\right|_{x_n = 0} = - i[a_n+a_n']\kappa_n \sin\alpha_n \qquad (D.53)$$

$$\left.\frac{\partial^2 w_1}{\partial x_1^2}\right|_{x_1 = 0} = - \kappa_1^2 \cos^2\alpha_1 - a_1\kappa_1^2 \cos^2\alpha_1 +$$

$$+ a_1' \kappa_1^2(1+\sin^2\alpha_1) \qquad (D.54)$$

$$\left.\frac{\partial^2 w_n}{\partial x_n^2}\right|_{x_n = 0} = - a_n\kappa_n^2 \cos^2\alpha_n + a_n'\kappa_n^2 (1+\sin^2\alpha_n) \qquad (D.55)$$

$$\left.\frac{\partial^2 w_1}{\partial y^2}\right|_{x_1 = 0} = - [1+a_1+a_1']\kappa_1^2 \sin^2\alpha_1 \qquad (D.56)$$

$$\left.\frac{\partial^2 w_n}{\partial y^2}\right|_{x_n = 0} = - [a_n+a_n']\kappa_n^2 \sin^2\alpha_n \qquad (D.57)$$

$$\left.\frac{\partial^3 w_1}{\partial x_1^3}\right|_{x_1 = 0} = - i\kappa_1^3 \cos^3\alpha_1 + ia_1\kappa_1^3 \cos^3\alpha_1 -$$

$$- a_1' \kappa_1^3 (1+\sin^2\alpha_1)^{3/2} \qquad \text{(D.58)}$$

$$\left.\frac{\partial^3 w_n}{\partial x_n^3}\right|_{x_n = 0} = i\, a_n\kappa_n^3 \cos^3\alpha_n - a_n'\kappa_n^3 (1+\sin^2\alpha_1)^{3/2} \qquad \text{(D.59)}$$

$$\left.\frac{\partial^3 w_1}{\partial x_1 \partial y^2}\right|_{x_1 = 0} = - i\kappa_1^3 \sin^2\alpha_1 \cos\alpha_1 + ia\kappa^3 1 \sin^2\alpha_1 \cos\alpha_1$$

$$+ a_1'\kappa_1^3 \sin^2\alpha_1 (1+\sin^2\alpha_1)^{1/2} \qquad \text{(D.60)}$$

$$\left.\frac{\partial^3 w_n}{\partial x_n \partial y^2}\right|_{x_n = 0} = i\, a_n\kappa_n^3 \sin^2\alpha_n \cos\alpha_n +$$

$$+ a_n'\kappa_n^3 \sin^2\alpha_n (1+\sin^2\alpha_n)^{1/2} \qquad \text{(D.61)}$$

Substituting expressions (D.42) to (D.61) in the boundary condition equations:

(1) Continuity of linear displacement, (D.21) to (D.29):

(a) $a_1 + a_1' - b_2 \cos\beta - c_2 \sin\gamma = -1$ (D.62)

(b) $a_2 + a_2' + b_1 \cos\beta + c_1 \sin\gamma = 0$ (D.63)

(c) $(b_1 + b_3) \cos\beta + (c_1 + c_3) \sin\gamma = 0$ (D.64)

(d) $(b_2 + b_4) \cos\beta + (c_2 + c_4) \sin\gamma = 0$ (D.65)

(e) $a_2 + a_2' + a_4 + a_4' = 0$ (D.66)

(f) $a_1 + a_1' + a_3 + a_3' = -1$ (D.67)

(g) (h) (i) $(b_1 - b_n) \sin\beta - (c_1 - c_n) \cos\gamma = 0$

$(n = 2,3,4)$ (D.68),(D.69),(D.70)

(2) Continuity of Angular Displacement (D-30) (D-31), (D-32)

$$(j)\ (k)\ (\ell): \quad ia_1 \cos\alpha_1 + a_1' (1+\sin^2\alpha_1) - i\chi_{1n} a_n \cos\alpha_n -$$

$$-\chi_{1n}\, a_n' (1+\sin^2\alpha_n)^{1/2} = i \cos\alpha_1 \qquad (D,71),(D.72),(D.73)$$

where:

$$\chi_{1n} = \left[\frac{h_1}{h_n} \right]^{1/2} \qquad (n = 2,3,4) \qquad (D.74)$$

(3) Sum of Bending Moments (D.34)

$$(m) \sum_{n=1}^{4} \{a_n \psi_n [1-(1-\nu)\sin^2\alpha_n] - a_n' \psi_{1n} [1+(1-\nu)\sin^2\alpha_n]\} =$$

$$= - [1-(1-\nu)\sin^2\alpha_1] \qquad (D.75)$$

where:

$$\psi_{1n} = \frac{D_n \kappa_n^2}{D_1 \kappa_1^2} = \left[\frac{h_n}{h_1} \right]^2 \qquad (n = 2,3,4) \qquad (D.76)$$

4. Sum of Forces (D.35) (D.36) (D.37)

$$(n)\ ia_1(\cos\alpha_1)\ [1+(1-\nu)\sin^2\alpha_1] - a_1'(1+\sin^2\alpha_1)^{1/2}\ [1-(1-\nu)\sin^2\alpha_1] -$$

$$- i\chi_{13}\psi_{13}\ a_3\cos\alpha_3[1+(1-\nu)\sin^2\alpha_3]\ +$$

$$+ a_3'\chi_{13}\psi_{13}(1-\sin^2\alpha_3)^{1/2}\ [1-(1-\nu)\sin^2\alpha_3] +$$

$$+ iF_{12}b_2\ (\cos^2\beta+\nu\sin^2\beta) + iF_{12}c_2(1-\nu)\ \sin\beta\ \cos\beta -$$

$$- iF_{14}b_4\ (\cos^2\beta+\nu\sin^2\beta) - iF_{14}c_4(1-\nu)\ \sin\beta\ \cos\beta =$$

$$= i\ (\cos\alpha_1)\ [1+(1-\nu)\ \sin^2\alpha_1] \qquad (D.77)$$

where:

$$F_{1n} = \frac{Eh_n\ \ell}{D_1(1-\nu^2)\kappa_1^3} = \frac{h_n}{h_1}\left(\frac{2\sqrt{3}\ c_L}{\pi f\ h_1}\right)^{1/2} \quad (n = 2,3,4) \qquad (D.78)$$

$$(o) \quad i\bar{e}_2\chi_{12}\psi_{12}\ (\cos\alpha_2)\ [1+(1-\nu)\sin^2\alpha_2] -$$

$$- a_2'\chi_{12}\psi_{12}(1+\sin^2\alpha_2)^{1/2}\ [1-(1-\nu)\sin^2\alpha_2] -$$

$$- ia_4\chi_{14}\psi_{14}(\cos\alpha_4)\ [1+(1-\nu)\sin^2\alpha_4)] +$$

$$a_4'\chi_{14}\psi_{14}(1+\sin^2\alpha_4)^{1/2}\ [1-(1-\nu)\sin^2\alpha_4] -$$

$$- iF_{11}b_1(\cos^2\beta+\nu\sin^2\beta) - iF_{11}(1-\nu)c_1\sin\beta\cos\gamma +$$

$$+ iF_{13}b_3(\cos^2\beta+\nu\sin^3\beta) + iF_{13}c_3(1-\nu)\sin\beta\cos\beta = 0 \qquad (D.79)$$

$$(k) \quad \sum_{n=1}^{4} \{2h_nb_n\sin\gamma\cos\beta - h_nc_n(1-2\sin^2\gamma)\} = 0 \qquad (D.80)$$

The resulting equations can be written in a matrix form: [A] [X] = [B], where:

$$[X] = \begin{bmatrix} a_1 \\ a_1' \\ b_1 \\ c_1 \\ a_2 \\ a_2' \\ b_2 \\ c_2 \\ a_3 \\ a_3' \\ b_3 \\ c_3 \\ a_4 \\ a_4' \\ b_4 \\ c_4 \end{bmatrix}, \qquad [B] = \begin{bmatrix} -1 \\ 0 \\ 0 \\ i\cos\alpha_1/\chi_{12} \\ -[1-(1-\nu)\sin^2\alpha_1] \\ i\cos\alpha_1[1+(1-\nu)\sin^2\alpha_1] \\ 0 \\ 0 \\ 0 \\ -1 \\ 0 \\ i\cos\alpha_1/\chi_{13} \\ 0 \\ 0 \\ 0 \\ i\cos\alpha_1/\chi_{14} \end{bmatrix}$$

A computer program was developed to set matrix [A] and [B] and to calculate for each angle of incidence, using a library subroutine to solve linear equations with complex coefficients. The amplitude vector was arranged so that the two and three plate problems become particular cases by setting some plate thicknesses as zero, as needed. The order of the matrix is then reduced from 16 to 12 (three plates) or to 8 (two plates). When the thickness of plate 3 is equal to zero, the rows and columns related to this plate and to plate 4 are switched. This is exactly the same approach undertaken by Swift [23] to develop his computer programs.

D.1.2 In-Plane Incidence

The same reference system and procedure were adopted to derive the equations when a longitudinal or a transverse shear incidence wave is considered.

The derivation are not presented herein. Basically, the wave expressions and displacement equations were changed in accordance with the incidence. The same boundary conditions were applied and the same amplitude vector used.

As a result, the [A] matrix for both longitudinal and transverse incidence becomes the same as for the bending incident wave. The difference lies in the [B] vector.

$$[B] = \begin{bmatrix} \text{LONGITUDINAL INCIDENCE} \\ 0 \\ \cos\beta \\ -\sin\beta \\ 0 \\ 0 \\ 0 \\ iF_{11}(\cos^2\beta+\nu\sin^2\beta) \\ 2h_1\sin\gamma\cos\beta \\ \cos\beta \\ 0 \\ -\sin\beta \\ 0 \\ 0 \\ 0 \\ -\sin\beta \\ 0 \end{bmatrix} \quad \begin{bmatrix} \text{TRANSVERSE INCIDENCE} \\ 0 \\ \sin\gamma \\ \cos\gamma \\ 0 \\ 0 \\ 0 \\ iF_{11}(1-\nu)\sin\beta\cos\gamma \\ -h_1(1-2\sin^2\gamma) \\ \sin\gamma \\ 0 \\ \cos\gamma \\ 0 \\ 0 \\ 0 \\ \cos\gamma \\ 0 \end{bmatrix}$$

D-2 Bending Solution

The problem when only flexural transmission is assumed can be considered as a particular case of the three wave fields problem. Its solution can be obtained from the equations derived for bending incidence in the previous paragraph; by making zero the appropriate coefficients and reordering the matrix to use only the applicable equations. However, it is thought to be simpler to have a separate program for the case when bending only is considered (a fourth order problem).

The same coordinate system is used (Fig. D.1). As only flexural waves are present, the energy is transmitted from plate 1 to the others only by bending moment at the joint. We have no displacement in any direction along the joint, which gives four boundary conditions: $w_n = 0 \quad (n = 1,4)$.

The following expressions used in the paragraph (D.1.1) are directly applicable:

(a)	Wave expressions	-- (D-4) to (D-7)
(b)	Bending energy	-- (D-10)
(c)	Transmission coefficients	-- (D-14), (D-17), (D-18)
(d)	Boundary conditions (remaining)	-- (D-30) to (D-32) and (D-34)
(e)	Displacement equations	-- (D-38), (D-39)
(f)	Displacement equations and derivatives at the junction line	-- (D-44), (D-45), (D-50), to (D-57)

The same procedure undertaken in paragraph D.1.1 is followed:

From the continuity of linear displacements:

$$a_1' = -1 - a_1 \qquad \text{(D.81)}$$

$$a_2' = -a_2 \qquad \text{(D.82)}$$

$$a_3' = -a_3 \qquad \text{(D.83)}$$

$$a_4' = -a_4 \qquad \text{(D.84)}$$

By using the above expressions and by applying the remaining boundary conditions, the following results:

1. Continuity of Angular Displacements:

$$[-(1+\sin^2\alpha_1)^{1/2} + i\cos\alpha_1]\frac{a_1}{\chi_{1n}} +$$

$$+ [(1+\sin^2\alpha_n)^{1/2} - i\cos\alpha_n]\, a_n =$$

$$= \frac{1}{\chi_{1n}}[(1+\sin^2\alpha_1)^{1/2} + i\cos\alpha_1] \quad (n = 2,3,4) \quad \text{(D.85), (D.86), D.87)}$$

Equations (D.85), (D.86) and (D.87) are exactly the same as (D.71) (D.72) and (D.73), respectively, when replacing a_1' by $(-1-a_1)$ and a_n' by $(-a_n)$.

2. Sum of Bending Moments:

$$a_1 + \psi_{12}a_2 + \psi_{13}a_3 + \psi_{14}a_4 = -1 \qquad \text{(D.86)}$$

This equation is exactly the same as (D.75), obtained when carrying out the same substitutions as above.

Using matrix notation: [A] [X] = [B],

where

$$[X] = \begin{matrix} a_1 \\ a_2 \\ a_3 \\ a_4 \end{matrix}, \quad [B] = \begin{matrix} -1 \\ [(1+\sin^2\alpha_1)^{1/2} + \cos\alpha_1]/\chi_{12} \\ [(1+\sin^2\alpha_1)^{1/2} + \cos\alpha_1]/\chi_{13} \\ [(1+\sin^2\alpha_1)^{1/2} + \cos\alpha_1]/\chi_{14} \end{matrix}$$

$$[A] = \begin{bmatrix} 1 & \psi_{12} & \psi_{13} & \psi_{14} \\ [-(1-\sin^2\alpha_1)^{1/2} + i\cos\alpha_1]\frac{1}{\chi_{12}} & [(1+\sin^2\alpha_2)^{1/2} - i\cos\alpha_2] & 0 & 0 \\ [-(1+\sin^2\alpha_1)^{1/2} + i\cos\alpha_1]\frac{1}{\chi_{13}} & 0 & [(1+\sin^2\alpha_3)^{1/2} - i\cos\alpha_3] & 0 \\ [-(1+\sin^2\alpha_1)^{1/2} + i\cos\alpha_1]\frac{1}{\chi_{14}} & 0 & 0 & [1+\sin^2\alpha_4)^{1/2} - i\cos\alpha_4 \end{bmatrix}$$